Title

Synthetic Studies Towards Quassinoid Natural Products and Development of a Copper-Catalyzed Double Coupling

Author

Rosen, Rachel

Publication Date

2021

Peer reviewed|Thesis/dissertation

Synthetic Studies Towards Quassinoid Natural Products and Development of a Copper-Catalyzed Double Coupling

By

Rachel Z. Rosen

A dissertation submitted in partial satisfaction of the requirements for the degree of

Doctor of Philosophy

in

Chemistry

in the

Graduate Division

of the

University of California, Berkeley

Committee in Charge:

Prof. Thomas J. Maimone, Chair

Prof. Richmond Sarpong

Prof. Roberto Zoncu

Summer 2021

Abstract

Synthetic Studies Towards Quassinoid Natural Products and Development of a Copper-Catalyzed Double Coupling

By
Rachel Z. Rosen

Doctor of Philosophy in Chemistry

University of California, Berkeley

Professor Thomas J. Maimone, Chair

Innovative carbon-carbon bond forming reactions have been integral to the synthesis of a myriad of complex molecules such as densely functionalized terpene natural products. Key to this effort is the development of novel methodology to generate strategic carbon-carbon bonds to rapidly access complex scaffolds. This dissertation describes a novel approach to the quassinoid natural products and the development of new methodology to help realize this goal. In Chapter 1 we provide an introduction to the quassinoid family of natural products including isolation, structural elucidation, the proposed biosynthesis, biological activity, and previous syntheses. In this chapter, we seek to provide the context with which our synthetic approach is based. Previous total syntheses of quassinoid natural products were hampered by lengthy oxidation sequences following construction of the carbon scaffold. To this end, in Chapter 2, we proposed to leverage the pseudo-symmetry of quassin to construct the carbon scaffold in tandem with the oxidation. To implement this strategy, we developed a novel copper-catalyzed double coupling of epoxy ketones to generate highly diastereo- and regioselective pseudo-symmetric products. We then extended this methodology to couple two different units in a three-component coupling. Finally, to conclude this chapter, the previously developed methodology was applied to the synthesis of the quassinoid core architecture. Having laid the foundation, in Chapter 3, we seek to extend our copper-catalyzed methodology to the construction of quaternary centers and ultimately the full quassinoid carbon skeleton; however, an unexpected rearrangement occured during dioxene cross coupling making a tandem allylic substitution/cross- coupling transformation unfeasible. We therefore surmised that any approach moving forward would need to first generate the quaternary center at the A/B-ring junction prior to dioxene cross-coupling. Accordingly, we first constructed a bicyclic using an ene/condensation/alkylation sequence before elaborating our system with dioxene. Finally, we are able to rapidlyassemble an advanced intermediate containing all the carbons necessary for construction of C19 quassinoids and set the foundation for future work in this area.

Table of Contents

Acknowledgements

Tom, thank you for giving me the amazing opportunity to join your lab. Words cannot express what an incredible experience I have had throughout graduate school. Thank you for all of your mentorship and guidance over the years. You always encouraged me to try the wildest ideas and pushed me to come up with innovative approaches to synthesis. These lessons will forever inform my approach to synthesis. It has been incredible to watch the lab grow and change over the past five years and I hope the lab continues to grow and excel.

Claire, congratulations on your synthesis! It has been a pleasure to grow as a chemist alongside you. I wish you, Christopher, and Julian all the best.

Linus, good luck with finishing your thesis! I wish you all the best in your future endeavors and know that you'll be appreciated addition at Arcus.

Drew and Patti, I had such a wonderful time hanging out with you two while you were still in Berkeley. I know you're both onto bigger and brighter things in Boston, but I miss having another couple to do hot pot with. Thank you for all of the good times and funny memories. Also thank you for the coffee table! Don't worry, I'm taking it with me when I move.

Xirui, I'll never forget all of the wonderful times I had when you brought all of us over for hot pot. Those were some of the most fun times I had during the first couple years of grad school. I wish you all the best in your career and hope you are doing well.

Vasil, it has been a pleasure to see you grow as a chemist. I know it hasn't been all smooth sailing chemistry-wise, but you have become an amazing chemist and friend. Good luck on finishing your synthesis! Ho-hoy!

Matt, thank you for all of the help and guidance during my first couple years of my Ph.D. Working on the quassinoids with you is not a time I'll soon forget.

Kevin, I hope you are doing well at Novartis. I still have the business card you stuck on my hood and it reminds me of all of your shenanigans every time I see it.

Karl, congratulations on getting the new job! You are an amazing chemist, and your synthesis is definitely one for the history books. I wish you all the best, and I hope the new job is everything you dreamed it would be.

Zach and Chi, as the pioneering Maimone students you have undoubtedly shaped the lab into what it is today. Zach, I hope you and Stephanie are doing well and I wish you all the best in your career. Chi, congratulations on your job at Brandeis! I wish you all the best with your career.

Bingqi, you always inspired me with your quite but resolute work ethic. I wish you all the best in your post-doc.

Andre, you have without a doubt made 907 a more exuberant place and it has been a pleasure to see you grow as a chemistry. Good luck finishing your molecule!

Lukas, thank you for all of the hilarious anecdotes and stories. Good luck on your Ph.D, I look forward to seeing what you accomplish.
Paulo, **Danny H**, **Beth**, **Yi**, you have only been in this lab for two years, but it feels like I've known you all for so much longer than that. Paulo, thanks for helping keep me sane during the Covid night shifts and for always making me laugh. You have become a great friend and I wish you all the best with your projects. Danny H., Good luck with your synthesis! You have good chemical insights and I hope you see success in the near future.
Huck, Gong, Michael, Jun, Naifeng, Ken, Martin, Mikiko, thank you for all the valuable experience you have brought to the lab. I know all of you are now onto bigger and better things, so I wish you all the best regain whatever career path you have chosen.
Danny T, thank you for always being there for me. Over the course of my Ph.D. you have made me grow into a better person and a better chemist. Thank you especially for all your love and support throughout my job search process. I was going through some incredibly rough times, but when I needed someone to talk to you were always there to listen.
Mom and Dad, I would not be where I am today without you. Thank you for encouraging me to always do what makes me happy and supporting me throughout graduate school. I know I couldn't have done this without you. I love you bunches and I hope you're proud of the woman I've become.

List of Abbreviations

9-BBN	9-borabicyclo[3.3.1]nonane
[O]	oxidation
Ac	acetyl
AIBN	azobisisobutyronitrile
aq.	aqueous
$BF_3 \bullet OEt_2$	Boron trifluoride diethyl etherate
BINAP	2,2′-bis(diphenylphosphino)-1,1′-binaphthyl
Bn	benzyl
BTPP	*tert*-butyl-imino-tri(pyrrolidino)phosphorane
Bz	benzoyl
CDI	carbonyldiimidazole
CSA	camphorsulfonic acid
d.r.	diastereomeric ratio
dba	dibenzylideneacetone
DBU	1,8-Diazabicyclo[5.4.0]undec-7-ene
DCC	*N,N'*-dicyclohexylcarbodiimide
DCM	dichloromethane
DDQ	2,3-dichloro-5,6-dicyano-1,4-benzoquinone
DIBAL-H	diisobutylaluminum hydride
DIPEA	*N,N*-diisopropylethylamine
DMAP	4-dimethylaminopyridine
DMDO	dimethyldioxirane
DMF	dimethylformamide
DMP	Dess-Martin periodinane
DMPU	N, N′-Dimethylpropyleneurea
DMS	dimethyl sulfide
DMSO	dimethyl sulfoxide
ED_{50}	median effective dose
EDC	1-ethyl-3-(3-dimethylaminopropyl)carbodiimide
ee	enantiomeric excess
EI	electron ionization
ESI	electrospray ionization
Et	ethyl
Glc	glucose
HAT	hydrogen atom transfer
HIV	human immunodeficiency virus
HMDS	hexamethyldisilane
HMPA	hexamethylphosphoric triamide
HRMS	high resolution mass spectrometry
HWE	Horner-Wadsworth-Emmons
Hz	Hertz
*h*v	photoirradiation

IBX	2-iodoxybenzoic acid
IC_{50}	half maximum inhibition concentration
imid	imidazole
i-Pr	isopropyl
IR	infrared
J	coupling constant
KHMDS	potassium bis(trimethylsilyl)amide
L-selectride	lithium tri-*sec*-butylborohydride
LDA	lithiumdiisopropylamide
LHMDS	lithium bis(trimethylsilyl)amide
*m*CPBA	*meta*-chloroperbenzoic acid
Me	methyl
MOM	methoxymethyl
MoOPH	oxodiperoxymolybdenum(pyridine)-(hexamethylphosphoric triamide)
Ms	mesyl (methanesulfonyl)
MS	molecular sieves
MVK	methyl vinyl ketone
NaHMDS	sodium bis(trimethylsilyl)amide
NBS	*N*-bromosuccinimide
n-Bu	butyl
NCS	*N*-chlorosuccinimide
Nf	nonaflyl (nonafluorobutanesulfonyl)
NIS	*N*-iodosuccinimide
NMO	*N*-mehtylmorpholine-*N*-oxide
NMR	nuclear magnetic resonance
nOe	nuclear Overhauser effect
o-tol	*ortho*-tolyl
oct	octyl
PCC	pyridinium chlorochromate
PDC	pyridinium dichromate
Ph	phenyl
Piv	pivaloyl
PMP	*para*-methoxyphenyl
ppm	parts per million
PPTS	pyridinium *para*-toluenesulfonate
py	pyridine
Red-Al	sodium bis(2-methoxyethoxy)alluminum hydride
TBAF	tetrabutylammonium flouride
TBDPS	*tert*-butyldiphenylsilyl
TBHP	*tert*-butylhydroperoxide
TBS	*tert*-butyldimethylsilyl
t-Bu	*tert*-butyl

TES	triethylsilyl
Tf	trifluoromethanesulfonyl
TFA	trifluoroacetic acid
TFAA	trifluoroacetic anhydride
THF	tetrahydrofuran
TIPS	triisopropylsilyl
tiglate	2-methylbut-2-enoate
TLC	thin layer chromatography
TMEDA	Tetramethylethylenediamine
TMS	trimethylsilyl
UV	ultraviolet
Δ	heat
μW	microwave

Chapter 1

An Introduction to the Quassinoid Natural Products

1.1 History and Chemical Structures of the Quassinoid Natural Products

Figure 1.1: *Quassia amara*, a representative species from the Simaroubaceae family of plants from which quassinoids are isolated.

The Amargo (Spanish for bitter) tree, known botanically as *Quassia* amara, is a tropical tree characterized by its short stature and colorful red flowers and berries. Indigenous to several countries throughout South America (Argentina, Brazil, Colombia, Guyana, Peru, Suriname, and Venezuela), *Quassia amara* has been used for centuries as an herbal medicine in the treatment of malaria and as a digestive aid. The first recorded use of the bark of the *Quassia amara* for medicinal purposes is attributed to Surinamese botanist and freedman Graman Quassi in the 18th century, for which the plant genus later received its name.[1]

Given the observed biological activity, the natural product(s) responsible were highly sought after, and in 1835, the extremely bitter and presumed biologically active compound, quassin(**1**), was first isolated as a solid mixture.[2] Further isolation and purification a century later by Clark gave insight into the chemical composition of this species;[3] however, it was not until 1961 that the structure was finally elucidated by Valenta and coworkers[4-5] and subsequently revised by Carman[6-7] giving the structure we associate with quassin today. This marked the beginning of what would become a family of natural products with over 400 known members isolated from *Simaroubaceae* family of plants.[8]

Quassinoids are characterized by their highly oxidized tetracyclic core, typically containing three fused carbocyclic rings (A-, B-, and C-rings) and a fourth γ- or δ-lactone

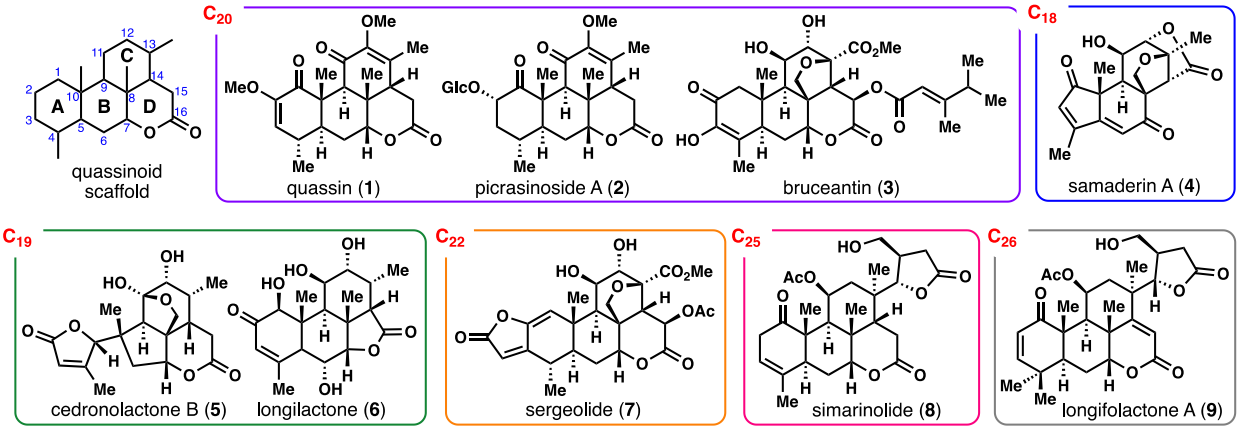

Figure 1.2: General C_{20} quassinoid scaffold (also directly applicable to C_{25} scaffold) and representative examples from each quassinoid subclass.

or lactol (D-ring) (Figure 1.2). Structurally, quassinoids can be further divided into six distinct subclasses based on the number of carbons comprising their core skeleton: C_{26}, C_{25}, C_{22}, C_{20}, C_{19}, and C_{18}. Prominent members from each subclass are depicted in Figure 1.2 to showcase the diversity exhibited throughout this family of natural products with supplementary structural features generating diverse, further complexity. For instance, the C-ring can possess either a C-8 methyl or hydroxymethyl group, the latter of which can form an ether bridge connecting C-8 and C-13 as exemplified in bruceantin (**3**),[9] samandarin A (**4**), and sergeolide (**7**), or a hemiketal bridge as seen in cedronolactone B (**5**). Additional lactones and butenolides are ubiquitous throughout the C_{22} and C_{25} quassinoids and occasionally appear in other subclasses such as the C_{19} quassinoid that contains an A ring butenolide in place of the standard carbocycle (see **5**, Figure 1.2). As secondary metabolites, glycosylation of the quassinoid A-ring alcohols, depicted in picrasinoside A (**2**), is also routine as found with many terpenoids. In addition to the standard oxidation patterns, the C-6 and C-15 positions also frequently contain oxidation that may or may not be esterified (see **6** and **3** respectively, Figure 1.2).[10-11]

To date, there are over 400 isolated and characterized quassinoid compounds; thus, for the purposes of this summation compounds have been organized by both carbon count and isolation source. Although every effort has been made to depict these compounds accurately, structural revisions are common in the field of structural elucidation.

One of the smallest subclasses, the C_{18} quassinoids contain only six known compounds (Figure 1.3, C_{18}). These metabolites were primarily isolated from the species *Eurycoma longifolia* Jack, a tropical plant found primarily in Southeastern Asia and recently discovered in the Philippines. The C_{18} quassinoid subclass is structurally unified by the D-Ring γ-lactone that is appended to the C-Ring through C-11 and C-13. While much of this subclass contains only minor differences in oxidation state, eurycolactone B (**10**) features a C2 chlorination and eurycolactone C (**11**) contains a unique A-ring δ-lactone moiety.[12-15]

The C_{19} subclass contains the second highest number of compounds (Figure 1.3, C_{19}) but this is still only a fraction of the numbers of the C-20 quassinoids. Of the over 50 members found within this subclass, nearly half have been isolated from the same species, *Eurycoma longifolia*.[12, 16-22] Structurally, this subclass is distinguished by several types of A-ring modifications which include: 1) an A-ring butenolide disconnected from the fused core (see **12**, Figure 1.3), and 2) an A-ring γ-lactone connected via a cyclic ether (see **14**). Variable substitution at C-2, C-3, C-6, C-11, C-12, and C-13 also contributes to the wide variety of members present and to the sizable number of C_{19} quassinoids.[11]

The second smallest of the subclasses, the C_{22} quassinoids (Figure 1.3, C_{22}), are comprised of only three known compounds all isolated from *Picrolemma sprucei* Hook (syn. *P. pseudocoffea* Ducke),[23-26] a small tree (or shrub) native to the Amazon region of South America.[27] Initially only two C_{22} quassinoids had been isolated up until 1985;[23-24]

however, two decades later a third compound, neosergeolide (**15**), was discovered containing a unique A-ring butenolide.[25-26]

The C_{25} quassinoids, isolated from a wide range of *Simaroubaceae* species, also comprise a modest collection of compounds from a numbers perspective (Figure 1.3, C_{25}),.[11, 28-30] Distinctive in this grouping is the additional lactone connected to C13 either directly or via an oxidized methylene bridge. The quassinoids odyendane (**18**) and odyendene (**19**), unlike most others in the C_{25} subclass, contain a butenolide moiety in place of the lactone connected at C13.[29] Recently, the unique caged compound perforalactone A (**16**) was isolated from *Harrisonia perforate*. It is believed that this structure is derived from perforalactone B (**17**) via a Bayer-Villager oxidation followed by enzymatic hydrogen atom extraction and subsequent cyclization.[28]

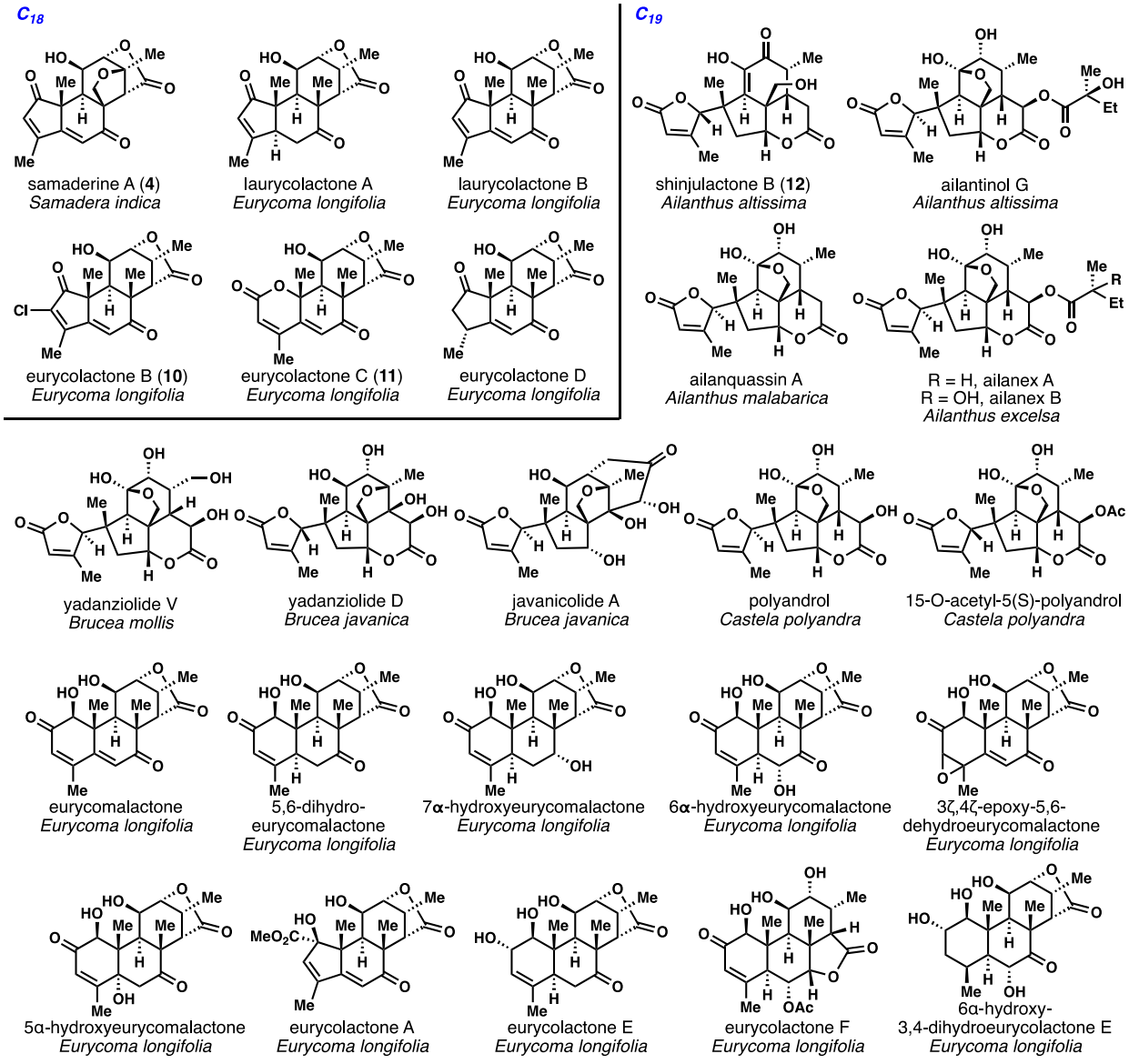

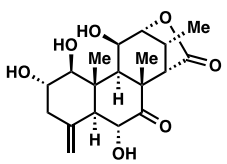

6α-hydroxy-18-dehydro-3-hydroeurycolactone E
Eurycoma longifolia

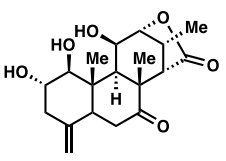

18-dehydro-3-hydroeurycolactone E
Eurycoma longifolia

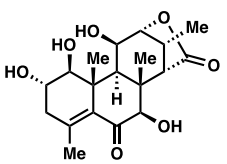

5-dehydro-3-hydro-7β-hydroxy-6-oxoeurycolactone E
Eurycoma longifolia

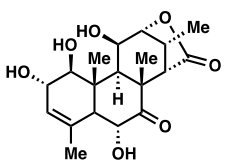

6α-hydroxyeurycolactone E
Eurycoma longifolia

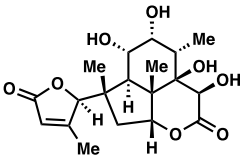

eurylactone A
Eurycoma longifolia

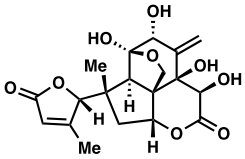

eurylactone B
Eurycoma longifolia

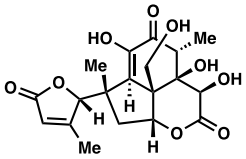

eurylactone E
Eurycoma longifolia

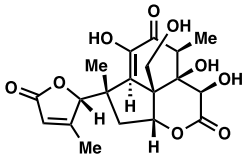

eurylactone F
Eurycoma longifolia

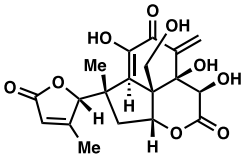

eurylactone G
Eurycoma longifolia

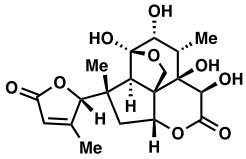

13,21-dihydroeurylactone B
Eurycoma longifolia

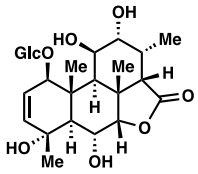

eurycomaoside
Eurycoma longifolia

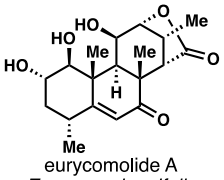

eurycomolide A
Eurycoma longifolia

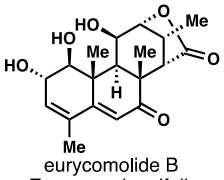

eurycomolide B
Eurycoma longifolia

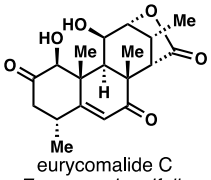

eurycomalide C
Eurycoma longifolia

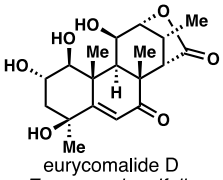

eurycomalide D
Eurycoma longifolia

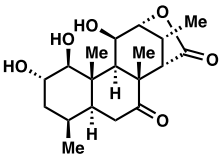

eurycomalide F
Eurycoma longifolia

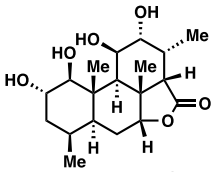

eurycomalide G
Eurycoma longifolia

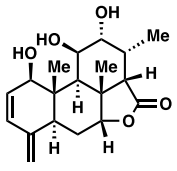

eurycomalide H
Eurycoma longifolia

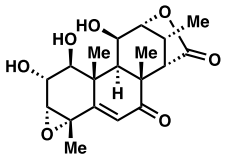

3α,4α-epoxyeurycomalide B
Eurycoma longifolia

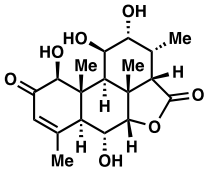

longilactone (**6**)
Eurycoma longifolia

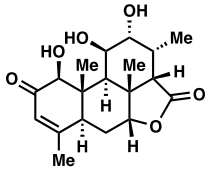

6-dehydrolongilactone
Eurycoma longifolia

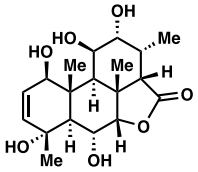

2,3-dehydro-4α-hydroxy-longilactone
Eurycoma longifolia

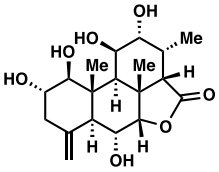

2-dihydro-18-dehydrolongilactone
Eurycoma longifolia

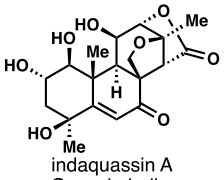

indaquassin A
Quassia indica

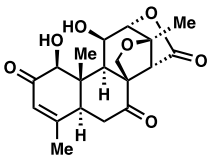

samaderin B
Samadera indica

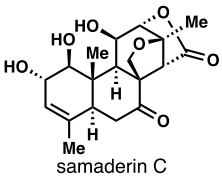

samaderin C
Samadera indica

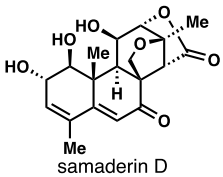

samaderin D
Samadera indica

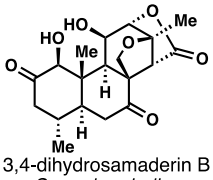

3,4-dihydrosamaderin B
Samadera indica

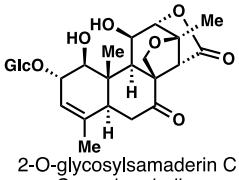

2-O-glycosylsamaderin C
Samadera indica

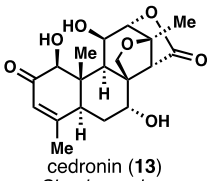

cedronin (**13**)
Simaba cedron

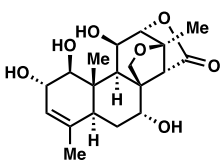

cedronolin
Simaba cedron

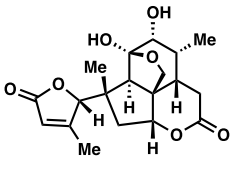

cedronolactone B (**5**)
Simaba cedron

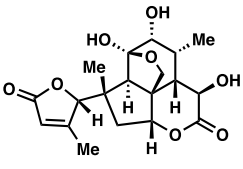

cedronolactone C
Simaba cedron

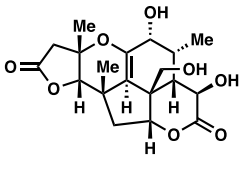

cedronolactone E (**14**)
Simaba cedron

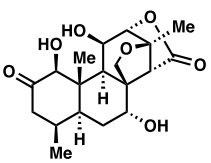

cymosanine
Simaba subcymosa

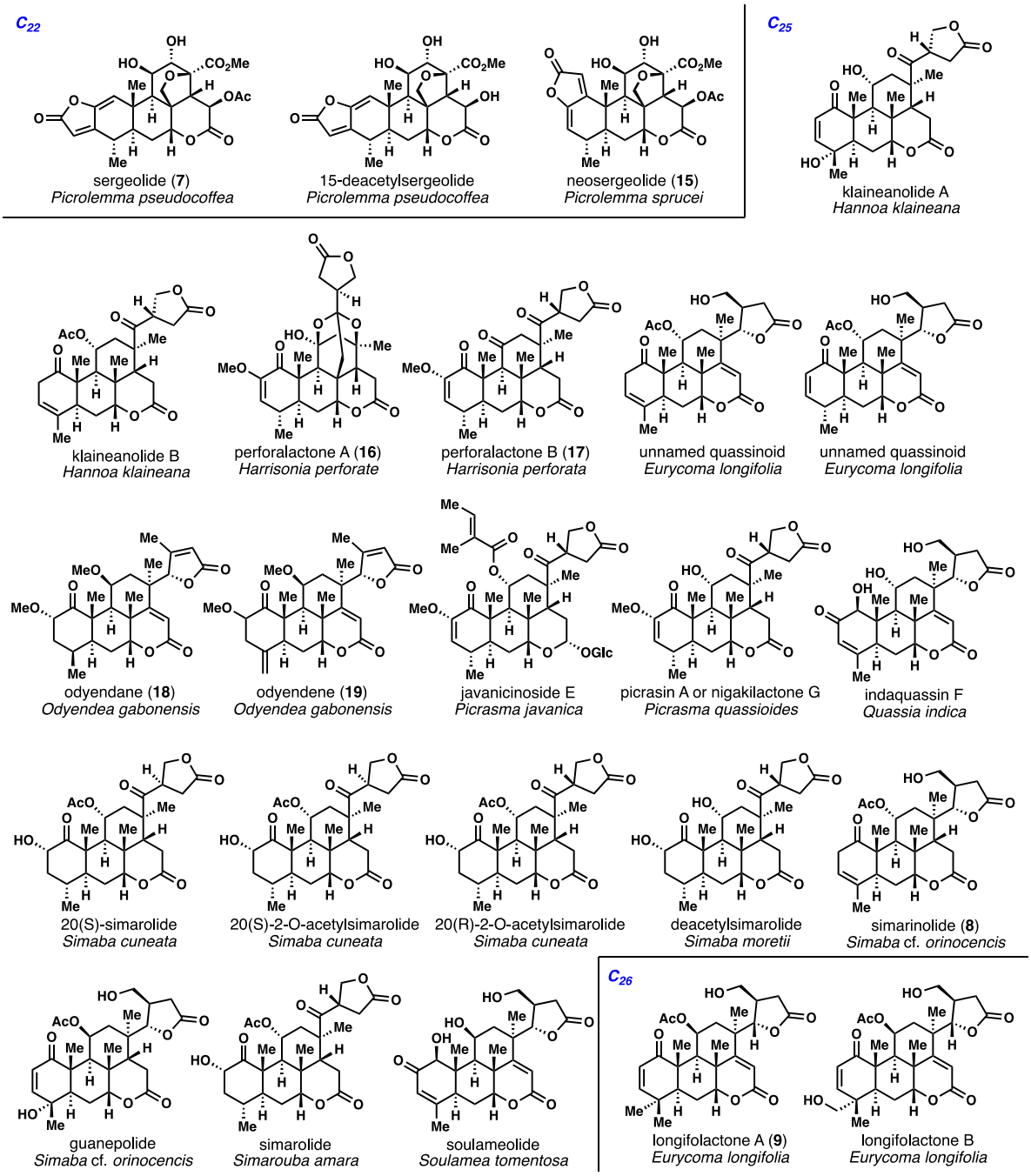

Figure 1.3: List of quassinoid natural products from the C_{18}, C_{19}, C_{22}, C_{25}, and C_{26} subclasses.

The smallest of all currently known subclasses are the C_{26} quassinoids (Figure 1.3, C_{26}). Isolated by Yang and coworkers in 2020 from the root of *Eurycoma longifolia*, these compounds contain a unique alkyl substitution at C4.[30]

The last and most abundant of the subclasses are the C_{20} quassinoids. This abundance resulted in the initial mischaracterization of these compounds as diterpenes; however, as no parent terpene "quassinane" has been isolated, these compounds are more accurately described as degraded triterpene natural products[31] (see Section 1.2

below, quassinoid biosynthesis). Throughout this group, C20 quassinoids contain a number of unifying features the most pronounced of which is the A-ring oxidation pattern with the majority of compounds containing only one of five major A-ring patterns (Figure 1.4 A). Many of the A-ring oxidation patterns contain an α,β-unsaturated ketone in the form of a 1,2-diketone (enol form) or an α-hydroxyenone (A1, A3, A4, A7, A9-12, Figure 4), which is thought to impart some of the biological activity observed throughout this class of natural products (see Section 1.2 below, quassinoid biological activity). While the A-ring has a large variety of oxidation patterns, the C-ring is much more limited in possible configurations with only four major arrangements with few exceptions. To increase the diversity of structures within the C_{20} quassinoids, there is often functionalization (via acylation) of the D-ring C15 oxygen producing a range of ester side chains (figure 1.4 D). Additionally, ester side chains can also be found on C2, C6, and C11 in certain members.[11, 32]

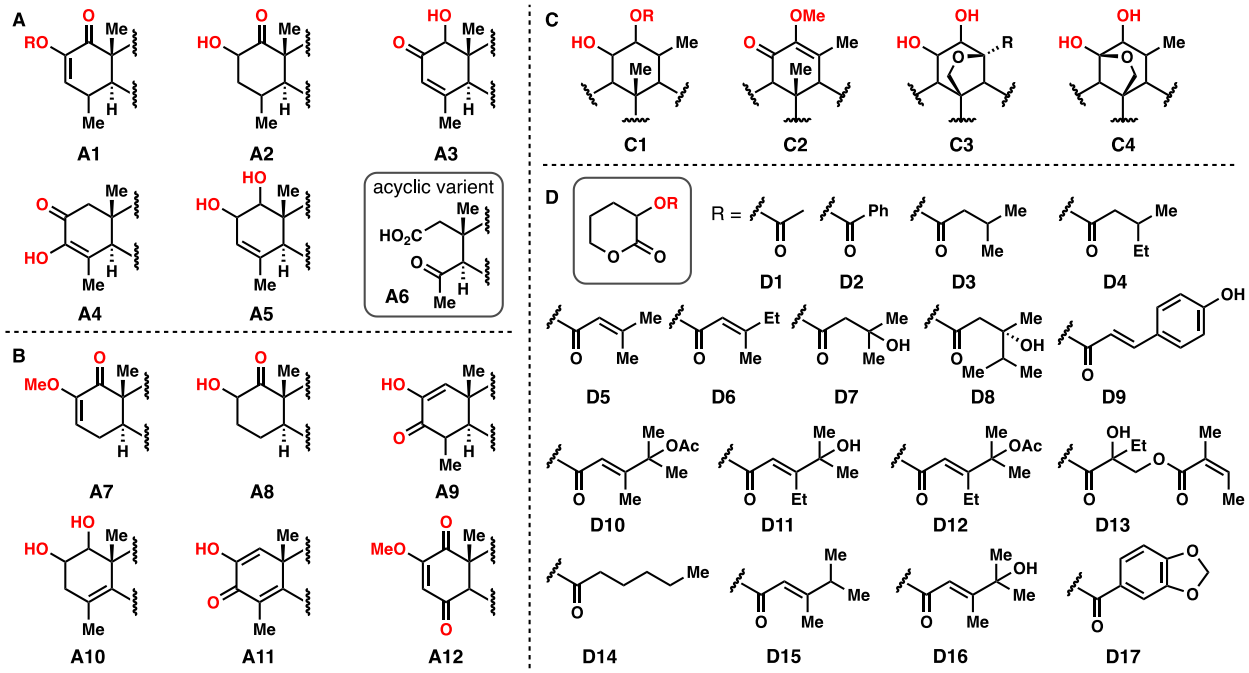

Figure 1.4: (A) Common A-ring oxidation patterns found primarily in the C_{20} and C_{25} quassinoids. Insert: acyclic variant of the A-ring. (B) Uncommon A-ring patterns found in the C_{20} quassinoids. (C) Typical C-ring oxidation patterns. (D) Common ester sidechains, primarily fatty acid derived.

The C_{20} quassinoids have been listed below by isolation source (figure 1.5-1.11). For quassinoids isolated from multiple sources only one has been listed. For the purposes of this summation, redundant compounds have been excluded or both names have been provided under one structure.

Ailanthus altissima

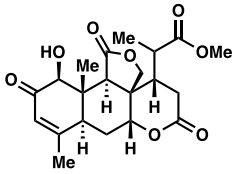
ailantinol A (**20**)
Ailanthus altissima

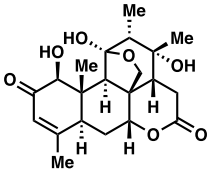
ailantinol B
Ailanthus altissima

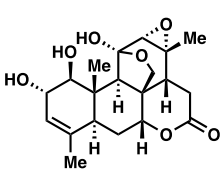
ailantinol C
Ailanthus altissima

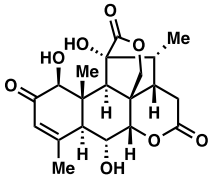
ailantinol D
Ailanthus altissima

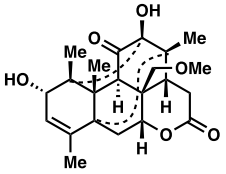
ailantinol E
Ailanthus altissima

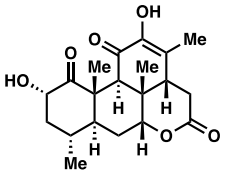
ailantinol F
Ailanthus altissima

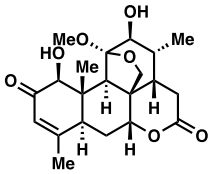
ailantholide
Ailanthus altissima

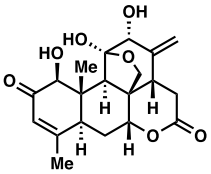
ailanthone
Ailanthus altissima

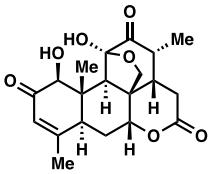
isoailanthone
Ailanthus altissima

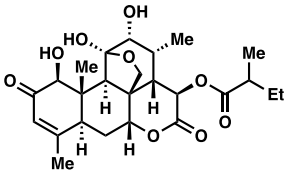
ailanthinone
Ailanthus altissima

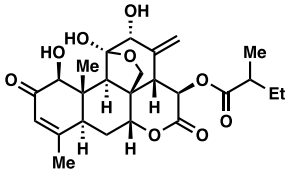
dehydroailanthinone
Ailanthus altissima

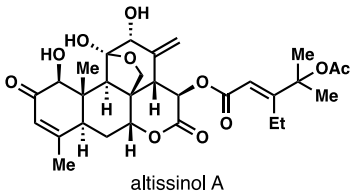
altissinol A
Ailanthus altissima

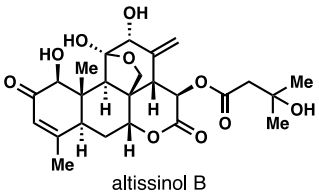
altissinol B
Ailanthus altissima

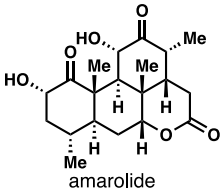
amarolide
Ailanthus altissima

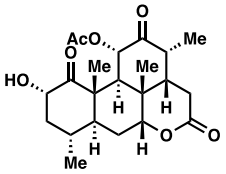
11-acetylamarolide
Ailanthus altissima

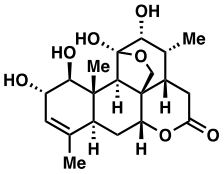
chaparrin
Ailanthus altissima

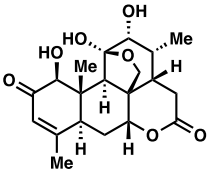
chaparrinone
Ailanthus altissima

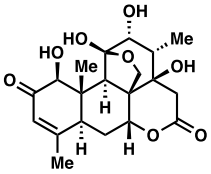
14-hydroxychaparrinone
Ailanthus altissima

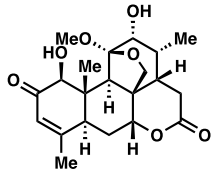
11-O-methylchaparrinone
Ailanthus altissima

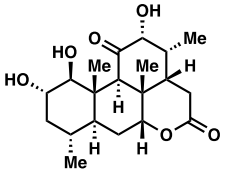
chaparrolide
Ailanthus altissima

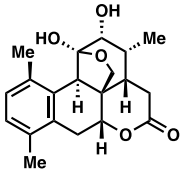
chaparrol
Ailanthus altissima

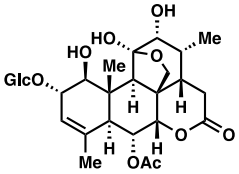
chuglycoside A
Ailanthus altissima

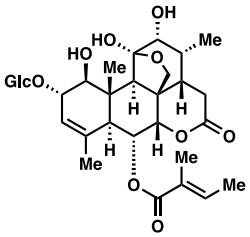
chuglycoside B
Ailanthus altissima

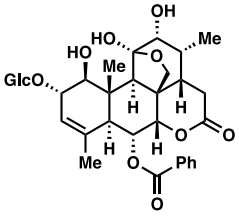
chuglycoside C
Ailanthus altissima

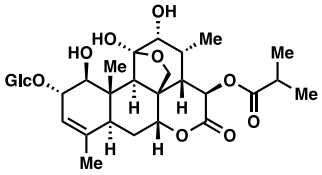
chuglycoside D
Ailanthus altissima

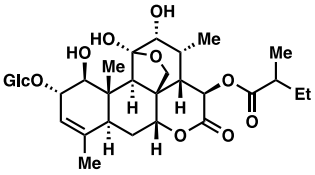
chuglycoside E
Ailanthus altissima

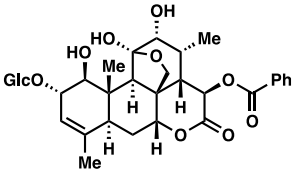
chuglycoside F
Ailanthus altissima

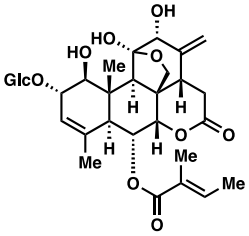
chuglycoside G
Ailanthus altissima

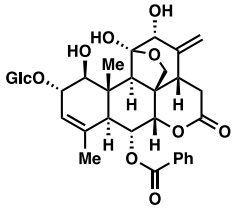

chuglycoside H
Ailanthus altissima

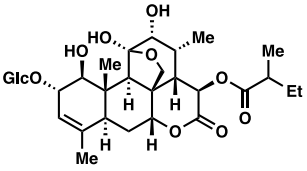

chuglycoside I
Ailanthus altissima

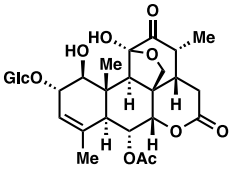

chuglycoside J
Ailanthus altissima

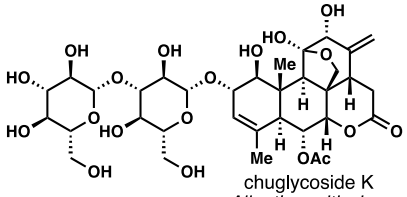

chuglycoside K
Ailanthus altissima

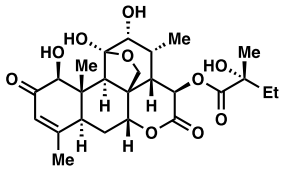

glaucarubinone
Ailanthus altissima

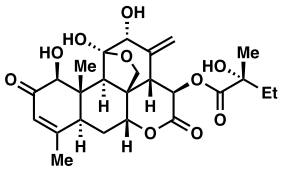

13,18-dehydroglaucarubinone
Ailanthus altissima

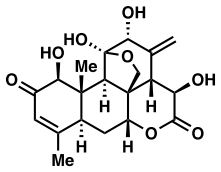

$\Delta^{13(18)}$-glaucarubolone
Ailanthus altissima

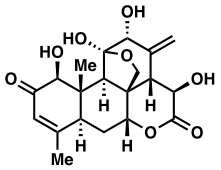

13,18-dehydroglaucarubolone
Ailanthus altissima

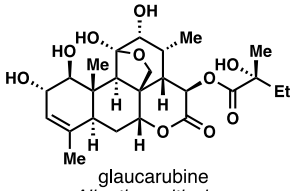

glaucarubine
Ailanthus altissima

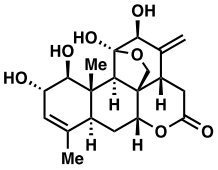

shinjulactone A
Ailanthus altissima

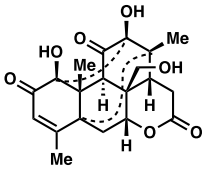

Shinjulactone C
Ailanthus altissima

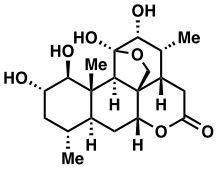

shinjulactone D
Ailanthus altissima

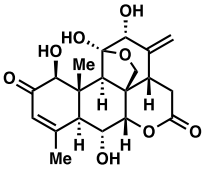

shinjulactone E
Ailanthus altissima

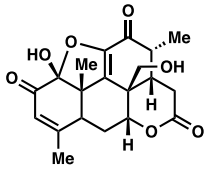

shinjulactone F (**21**)
Ailanthus altissima

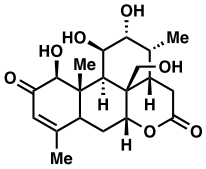

shinjulactone G
Ailanthus altissima

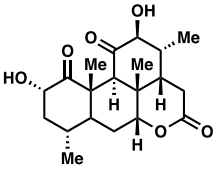

shinjulactone H
Ailanthus altissima

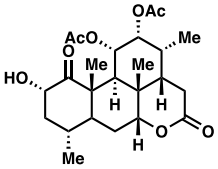

shinjulactone I
Ailanthus altissima

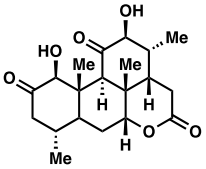

shinjulactone J
Ailanthus altissima

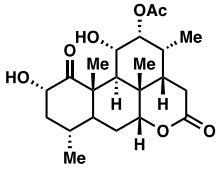

shinjulactone K
Ailanthus altissima

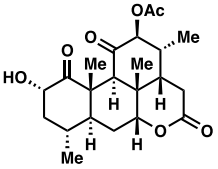

shinjulactone L
Ailanthus altissima

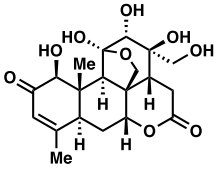

shinjulactone M
Ailanthus altissima

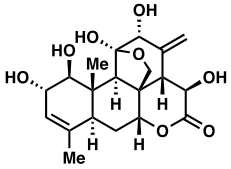

shinjulactone N
Ailanthus altissima

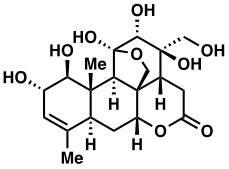

shinjulactone O
Ailanthus altissima

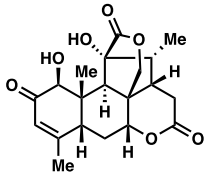

shinjudilactone
Ailanthus altissima

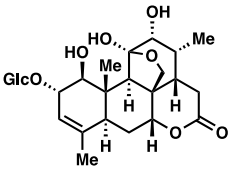

shinjuglycoside A
Ailanthus altissima

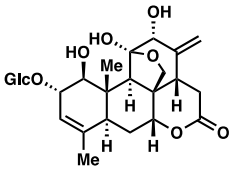

shinjuglycoside B
Ailanthus altissima

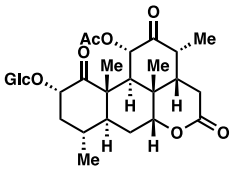

shinjuglycoside C
Ailanthus altissima

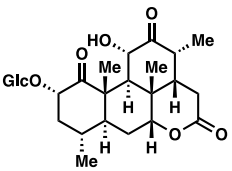

shinjuglycoside D
Ailanthus altissima

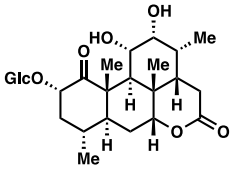

shinjuglycoside E
Ailanthus altissima

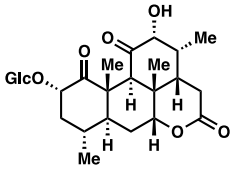

shinjuglycoside F
Ailanthus altissima

Ailanthus excelsa

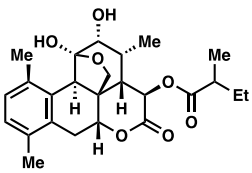

quassinoid A
Ailanthus excelsa

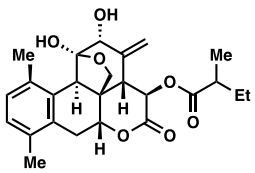

quassinoid B
Ailanthus excelsa

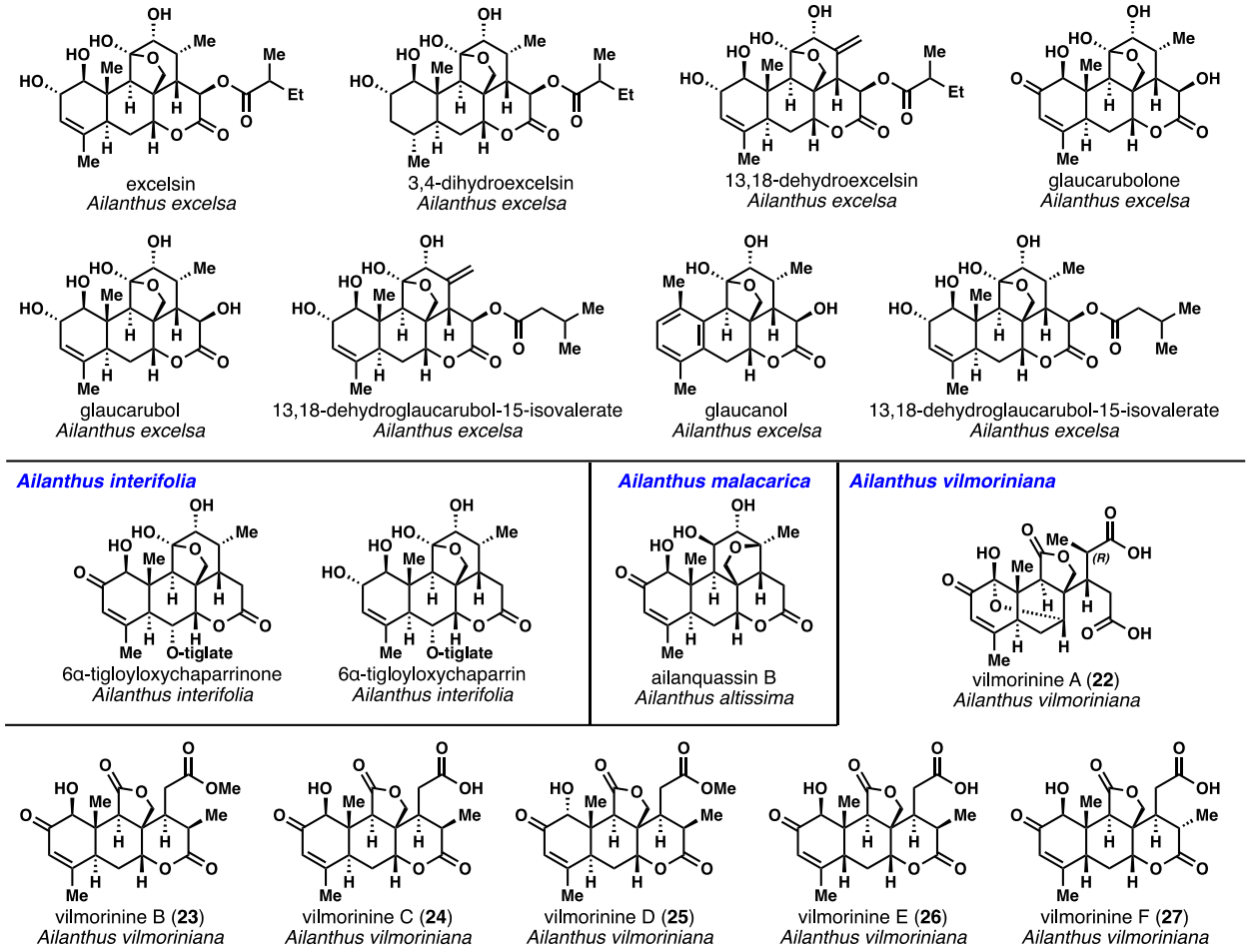

Figure 1.5: Quassinoids isolated from the genus *Ailanthus*

Nearly 80 C_{20} quassinoids have been isolated from the genus *Ailanthus* including several structurally unique compounds (Figure 1.5).[33] Ailantinol A (**20**)[34] and vilmorinines B-F (**22**-**27**) contain a novel dilactone core with a cleaved C-ring.[35] Vilmorinine A (**22**) similarly has a cleaved C-ring, but additionally the D-ring lactone has been cleaved and the hemiketal bridge formed between C1 and C7.[36] Shinjulactone F (**21**) also contains a non-canonical hemiketal connecting the A and C rings through C1 and C11.[37]

The genus *Brucea* also produces a large number of C_{20} quassinoids (Figure 1.6)[38-44] including members such as bruceantin (**3**),[45] javanic acid A (**28**),[44] and yadanziolide A (**29**).[42] The sizeable number of quassinoids isolated from *Brucea* species can be accounted for in the large collection of lipophilic acid ester side chains connected via C15. Within this grouping of molecules, we see the first examples of oxidative cleavage of the A-ring (see **28**).

Brucea antidysenterica

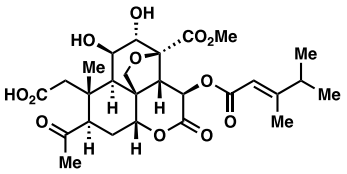

bruceanic acid A
Brucea antidysenterica

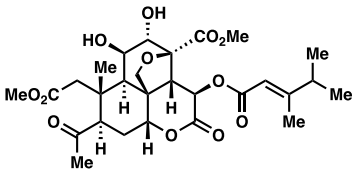

bruceanic acid A methyl ester
Brucea antidysenterica

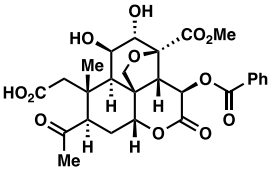

bruceanic acid B
Brucea antidysenterica

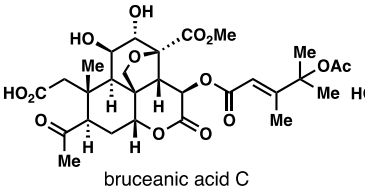

bruceanic acid C
Brucea antidysenterica

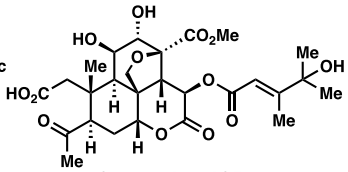

bruceanic acid D
Brucea antidysenterica

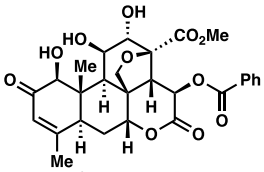

bruceanol A
Brucea antidysenterica

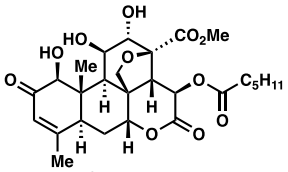

bruceanol B
Brucea antidysenterica

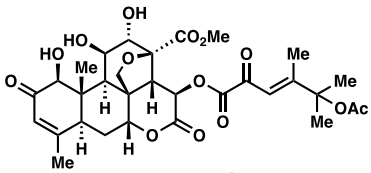

bruceanol C
Brucea antidysenterica

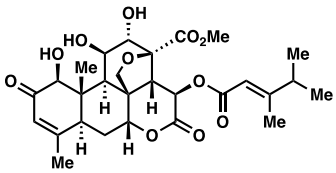

bruceanol D
Brucea antidysenterica

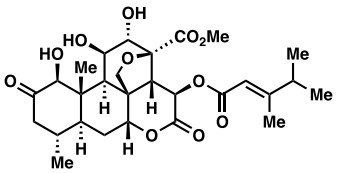

bruceanol E
Brucea antidysenterica

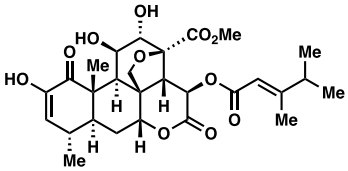

bruceanol F
Brucea antidysenterica

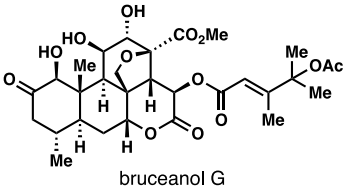

bruceanol G
Brucea antidysenterica

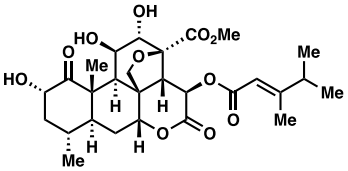

bruceanol H
Brucea antidysenterica

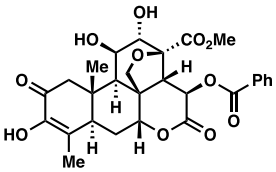

bruceantarin
Brucea antidysenterica

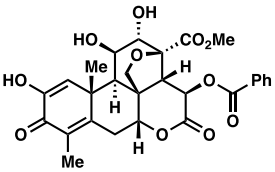

dehydrobruceantarin
Brucea antidysenterica

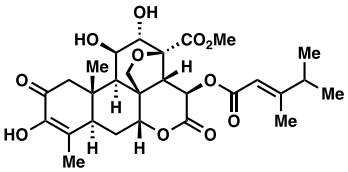

bruceantin (**3**)
Brucea antidysenterica

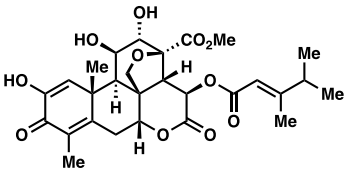

dehydrobruceantin
Brucea antidysenterica

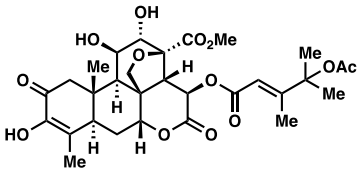

bruceantinol
Brucea antidysenterica

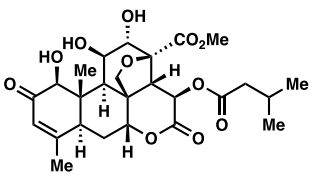

isobruceine A
Brucea antidysenterica

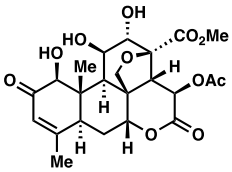

isobruceine B
Brucea antidysenterica

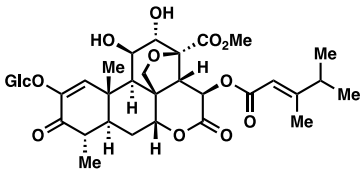

bruceantinoside A
Brucea antidysenterica

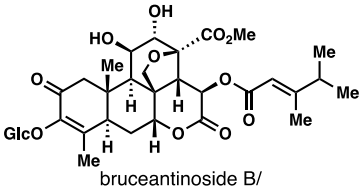

bruceantinoside B/
yadanzioside P
Brucea antidysenterica

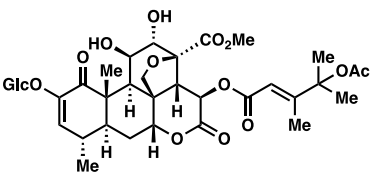

bruceantinoside C
Brucea antidysenterica

Brucea amarissima

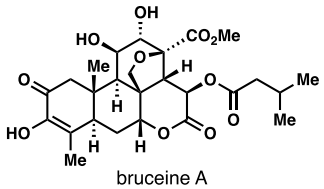
bruceine A
Brucea amarissima

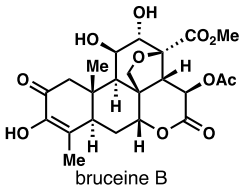
bruceine B
Brucea amarissima

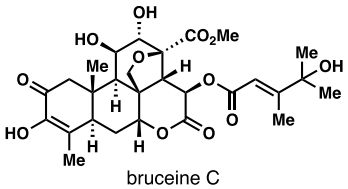
bruceine C
Brucea amarissima

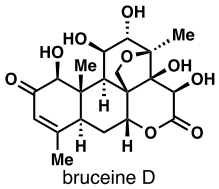
bruceine D
Brucea amarissima

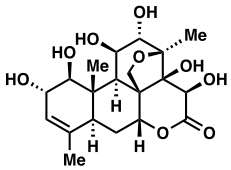
bruceine E
Brucea amarissima

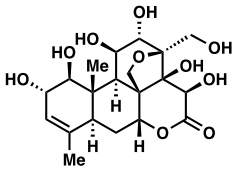
bruceine F
Brucea amarissima

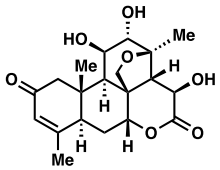
bruceine G
Brucea amarissima

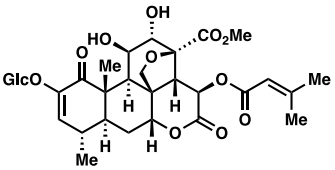
javanicoside I
Brucea amarissima

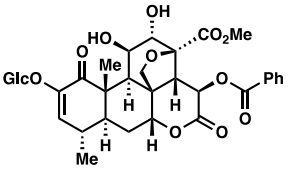
javanicoside J
Brucea amarissima

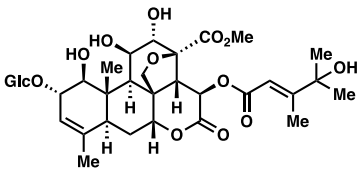
javanicoside K
Brucea amarissima

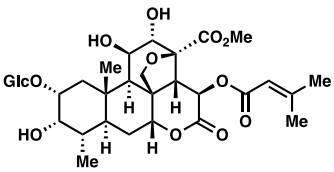
javanicoside K
Brucea amarissima

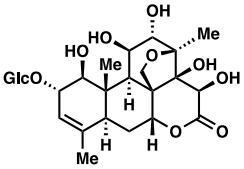
yadanzigan
Brucea amarissima

Brucea javanica

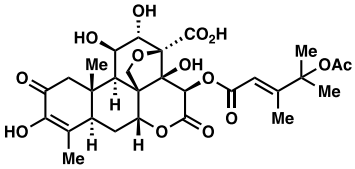
bruceantinol A/B
Brucea javanica

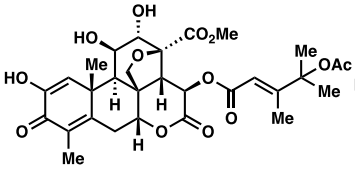
dehydrobruceantinol
Brucea javanica

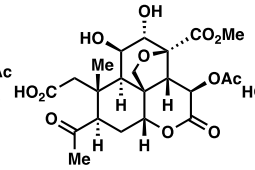
bruceaketolic acid
Brucea javanica

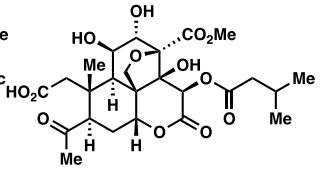
bruceanic acid E
Brucea javanica

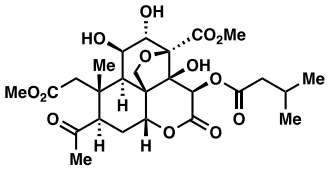
bruceanic acid E methyl ester
Brucea javanica

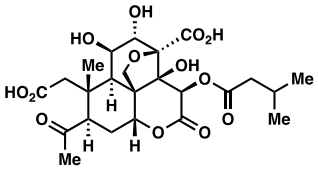
bruceanic acid F
Brucea javanica

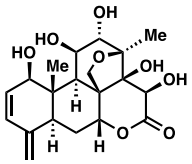
bruceene
Brucea javanica

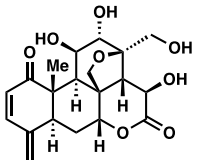
bruceene A
Brucea javanica

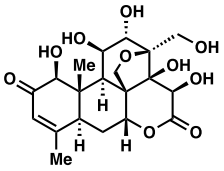
bruceine H/
yadanziolide A
Brucea javanica

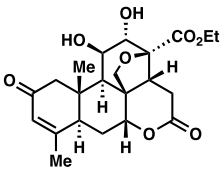
bruceine I
Brucea javanica

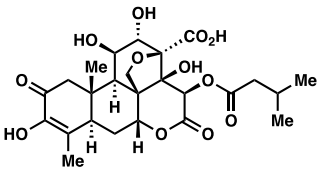
bruceine J
Brucea javanica

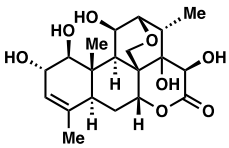
bruceine K
Brucea javanica

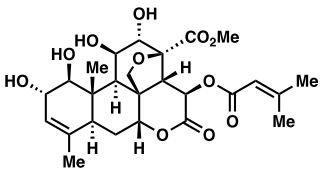

bruceine L
Brucea javanica

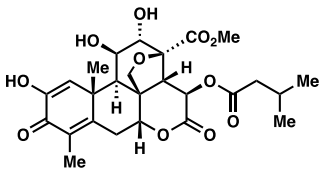

dehydrobruceine A
Brucea javanica

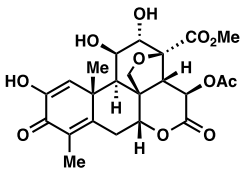

dehydrobruceine B
Brucea javanica

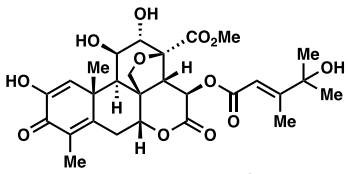

dehydrobruceine C
Brucea javanica

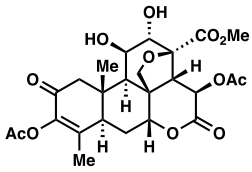

13,15-di-O-acetylbruceolide
Brucea javanica

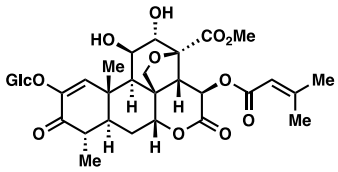

bruceoside A
Brucea javanica

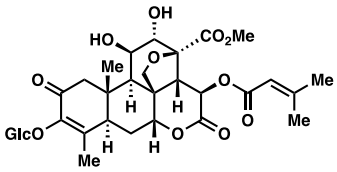

bruceoside B
Brucea javanica

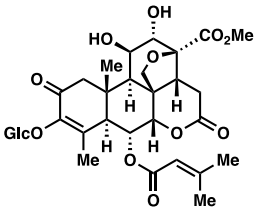

bruceoside C
Brucea javanica

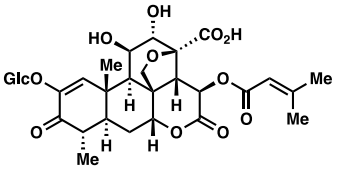

bruceoside D
Brucea javanica

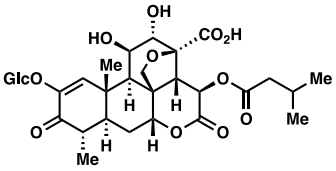

bruceoside E
Brucea javanica

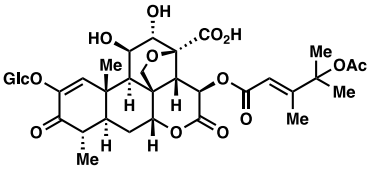

bruceoside F
Brucea javanica

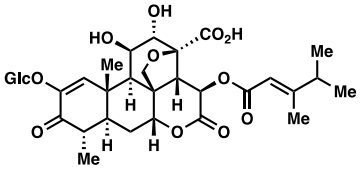

bruceoside G
Brucea javanica

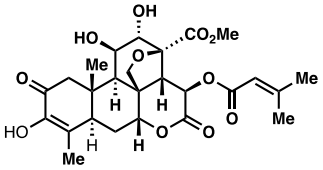

brusatol
Brucea javanica

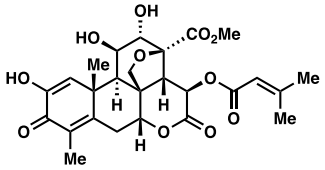

dehydrobrusatol
Brucea javanica

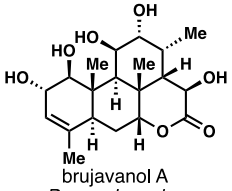

brujavanol A
Brucea javanica

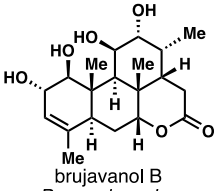

brujavanol B
Brucea javanica

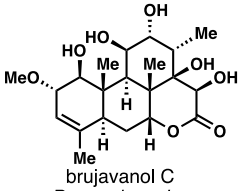

brujavanol C
Brucea javanica

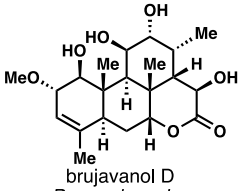

brujavanol D
Brucea javanica

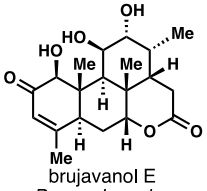

brujavanol E
Brucea javanica

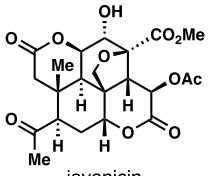

javanicin
Brucea javanica

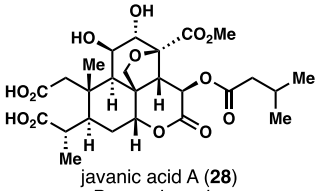

javanic acid A (**28**)
Brucea javanica

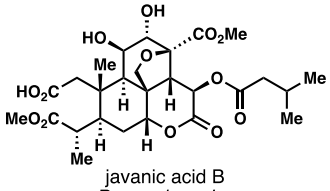

javanic acid B
Brucea javanica

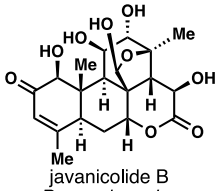

javanicolide B
Brucea javanica

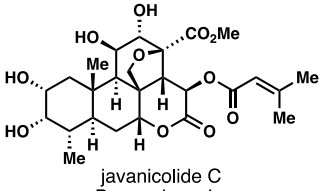

javanicolide C
Brucea javanica

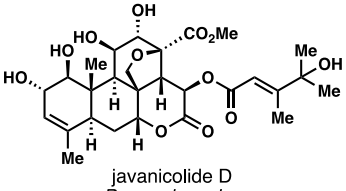

javanicolide D
Brucea javanica

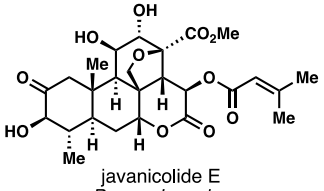

javanicolide E
Brucea javanica

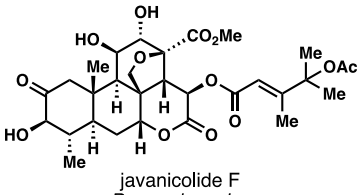

javanicolide F
Brucea javanica

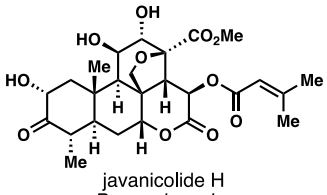

javanicolide H
Brucea javanica

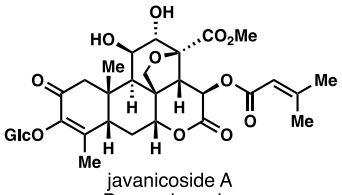

javanicoside A
Brucea javanica

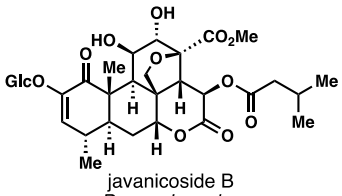

javanicoside B
Brucea javanica

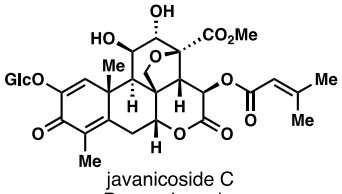

javanicoside C
Brucea javanica

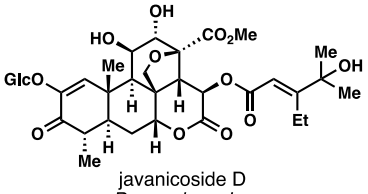

javanicoside D
Brucea javanica

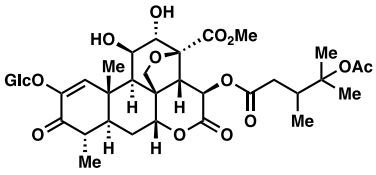

javanicoside E
Brucea javanica

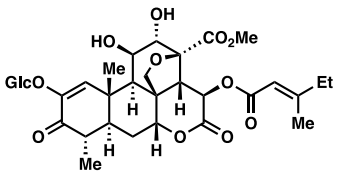

javanicoside F
Brucea javanica

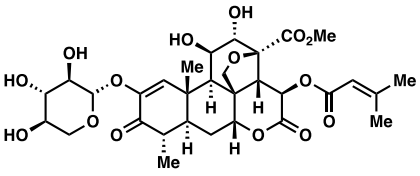

javanicoside G
Brucea javanica

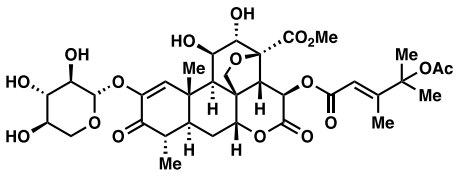

javanicoside H
Brucea javanica

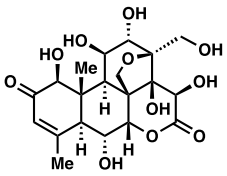

yadanziolide B (**29**)
Brucea javanica

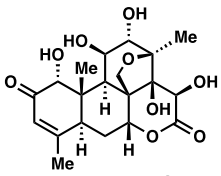

yadanziolide C
Brucea javanica

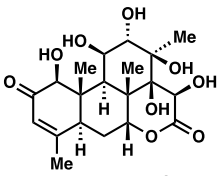

yadanziolide S
Brucea javanica

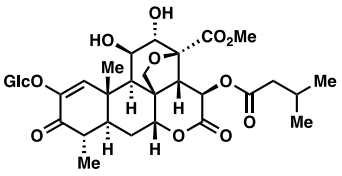

yadanzioside A
Brucea javanica

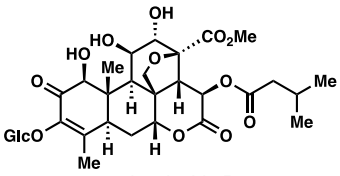

yadanzioside B
Brucea javanica

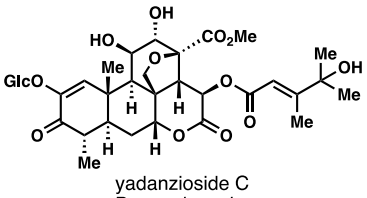

yadanzioside C
Brucea javanica

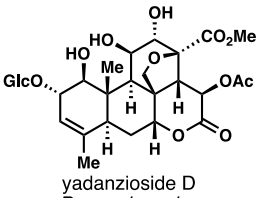

yadanzioside D
Brucea javanica

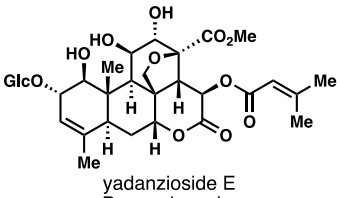

yadanzioside E
Brucea javanica

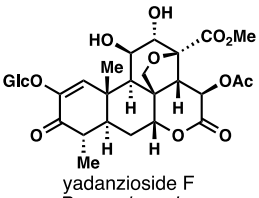

yadanzioside F
Brucea javanica

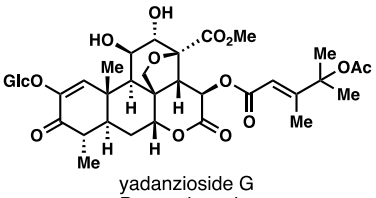

yadanzioside G
Brucea javanica

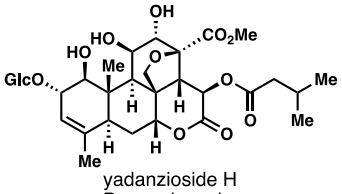

yadanzioside H
Brucea javanica

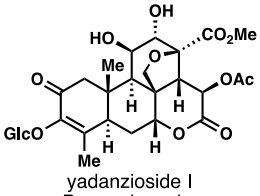

yadanzioside I
Brucea javanica

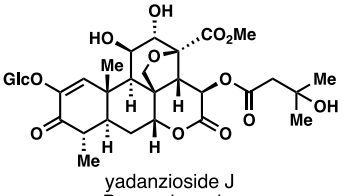

yadanzioside J
Brucea javanica

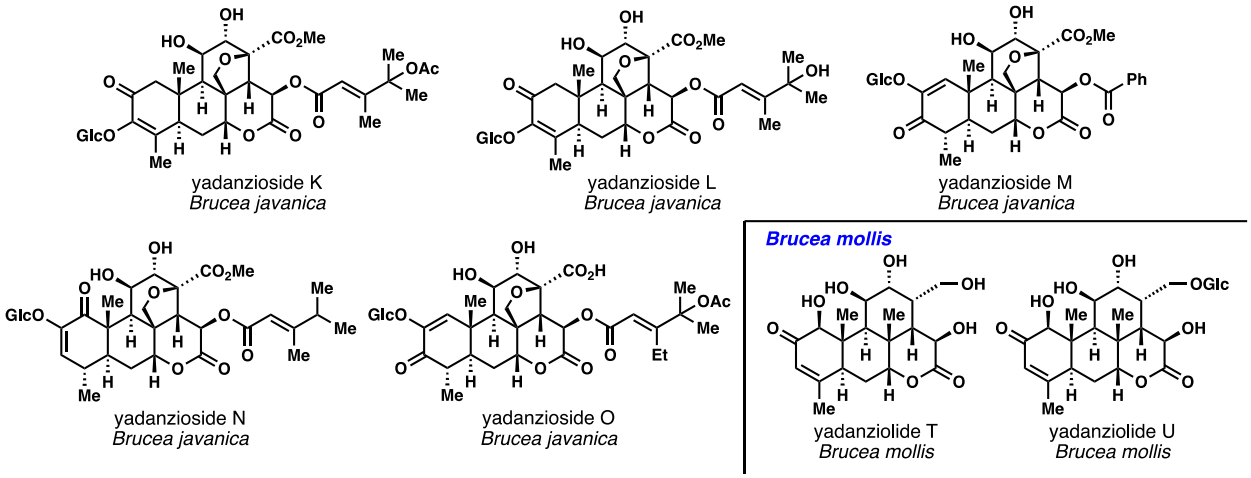

Figure 1.6: Quassinoids isolated from the genus *Brucea*

The genus *Castela* has produced a number of novel structures (Figure 1.7)[11, 46] including peninsularinone (**30**), which contains a highly unique ester appended to the C15 alcohol.[47] Additionally, 11-*O*-*trans*-*p*-coumaroyl amarolide (**31**) contains an exclusive coumaroyl substitution connected to C11 through an ester linkage.[48]

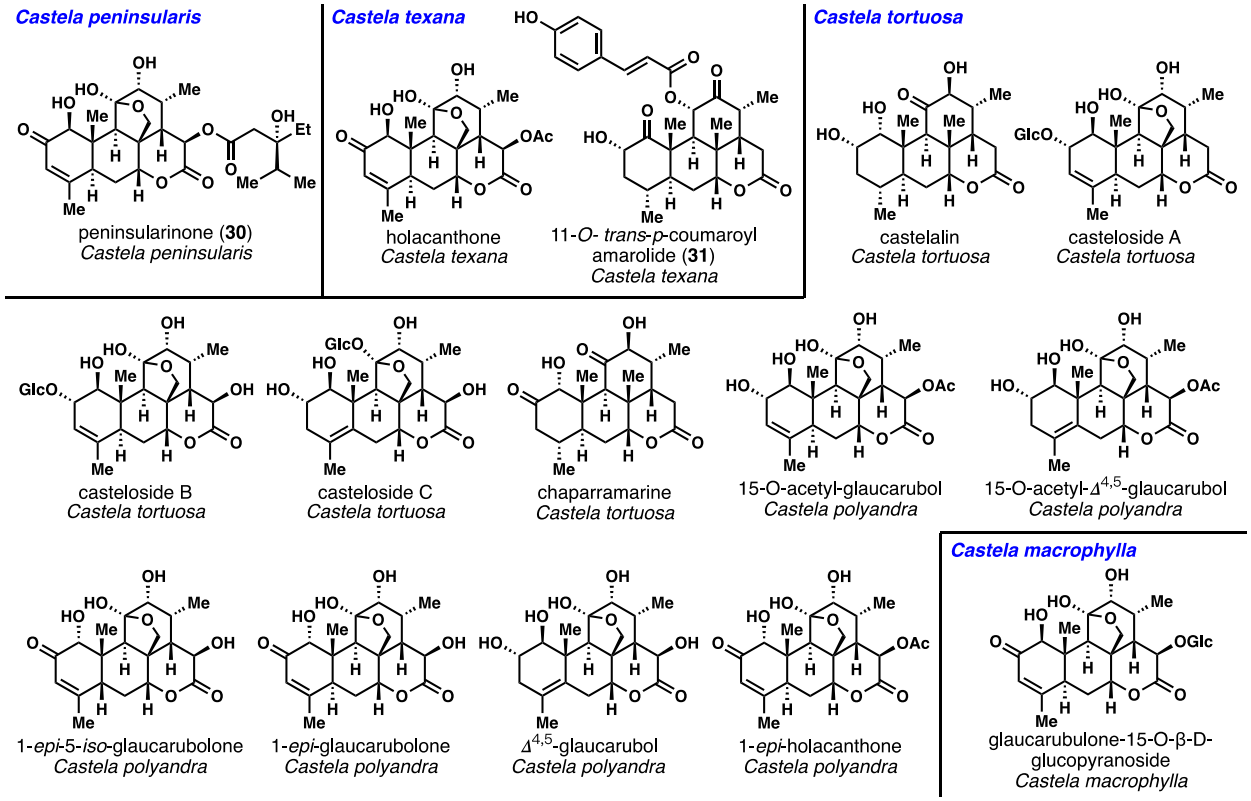

Figure 1.7: Quassinoids isolated from the genus *Castela*.

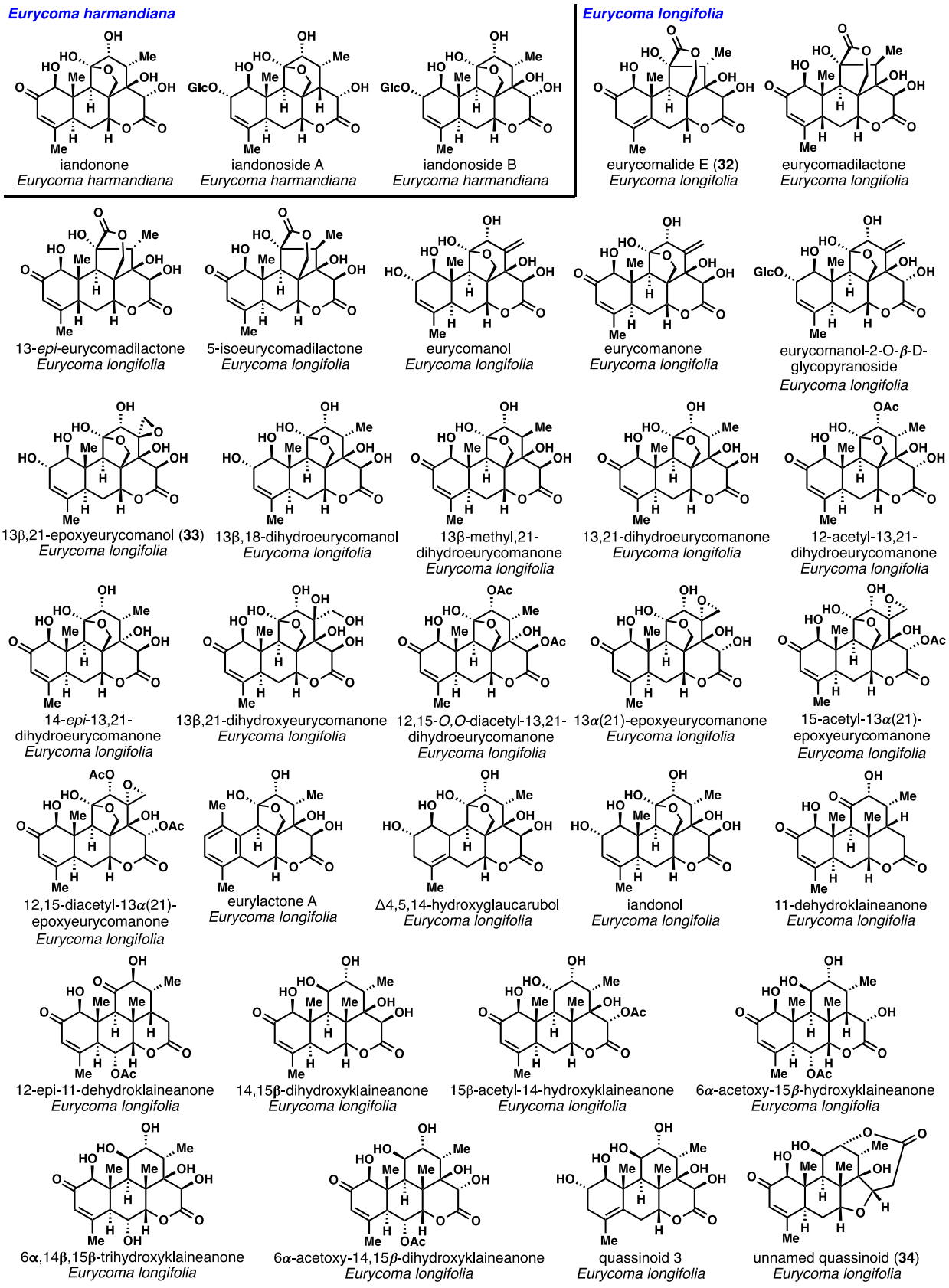

Figure 1.8: Quassinoids isolated from the genus *Eurycoma*.

The genus *Eurycoma* is an abundant source of C_{20} quassinoids (Figure 1.8),[22, 30, 49-50] which, in addition to the large number to the C_{18} and C_{19} quassinoids that arise from this organism, include some members with unusual structures. Similar to the dilactones isolated from *Ailanthus* species, Eurycoma quassinoids contain multiple dilactones, exemplified by eurycomalide E (**32**),[20] but have been discovered with an intact C-ring. Many quassinoids contain oxidation at the C-11 methyl group, most commonly esters and carboxylic acids. Epoxidation as seen in 13β,21-epoxyeurycomanol (**33**) has also been discovered in recent years.[50] Of particular note, from *E. longifolia*, is currently unnamed quassinoid **34**, which contains a unique tetrahydrofuran D-ring and a 7-membered lactone bridging the C and D rings.[30]

Quassinoids have also been isolated from *Hannoa*,[51-53] *Harrisonia*,[54] *Laumoniera*,[55] *Nothospondias*,[56] and *Odyendyea* species[57] (Figure 1.9). Perforaquassins A, B, and C (**35**, **36**, and **37** respectively) were isolated from *Harrisonia Perforata*, which is known to produce liminoid secondary metabolites.

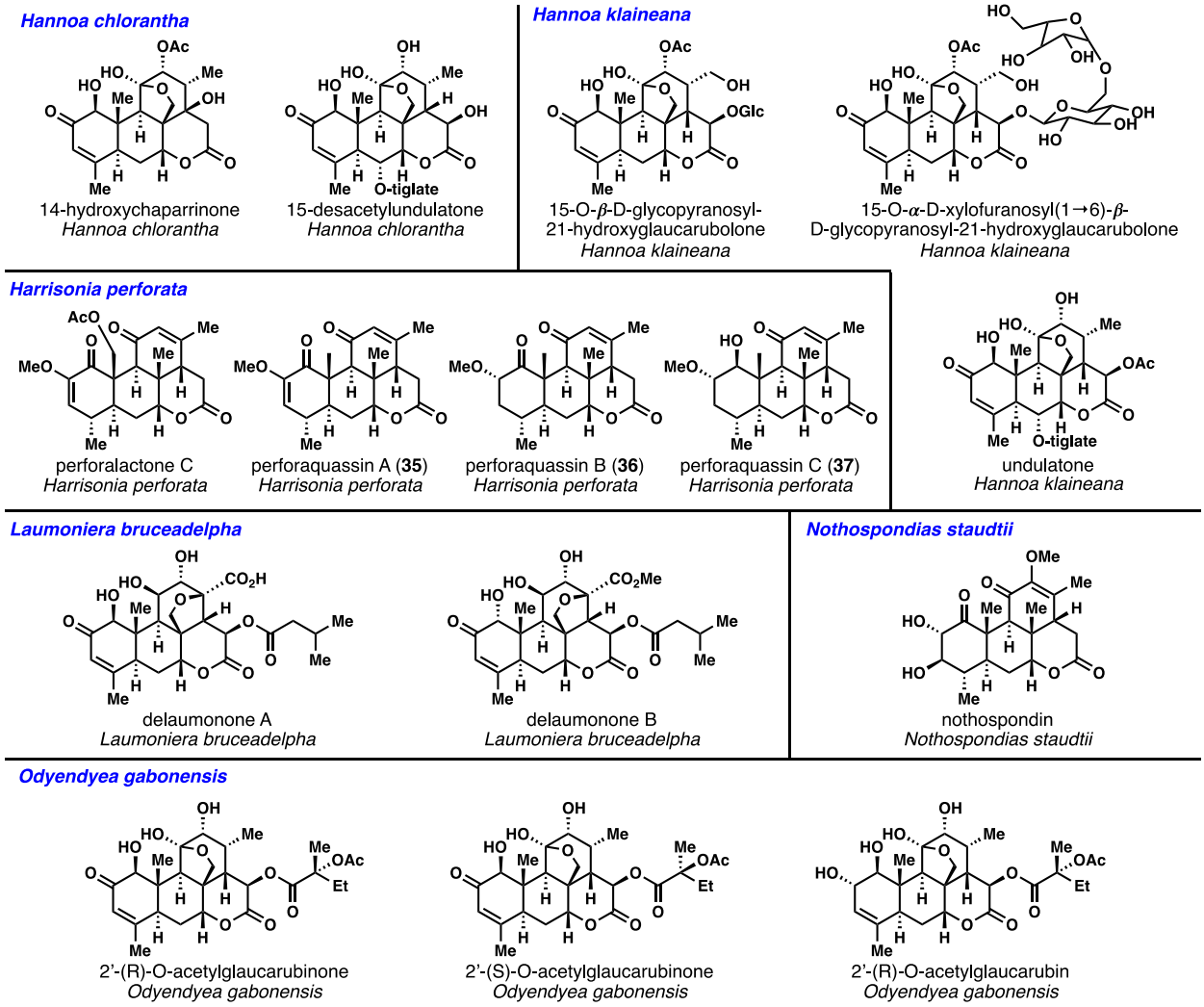

Figure 1.9: Quassinoids from genus *Hannoa*, *Harrisonia, Laumoniera*, *Nothospondias*, and *Odyendyea*.

The genus *Picrasma* has been another abundant source of C_{20} quassinoids (Figure 1.10).[11, 58-60] Picrasinoside C (**38**) contains a novel functionality in the form of a C11/C12 dioxolone. Also isolated from *Picrasma javanica* are the javanicins and related compounds that lack the C-4 methyl group (see javanicin A, **39**).[11]

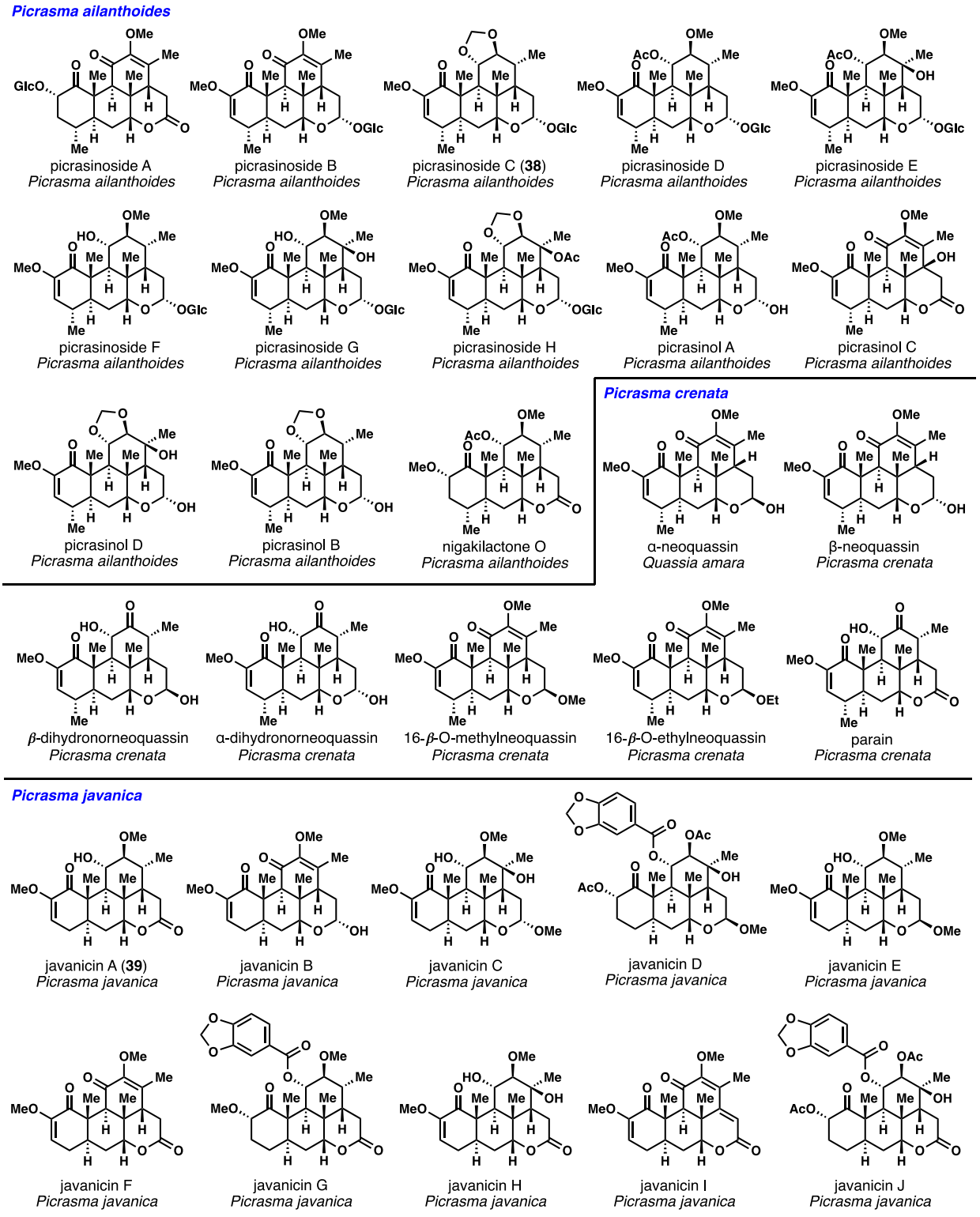

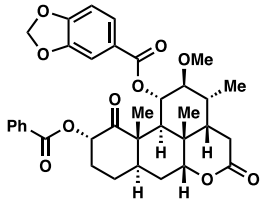

javanicin K
Picrasma javanica

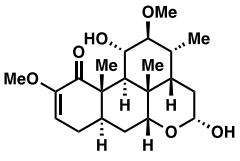

javanicin L
Picrasma javanica

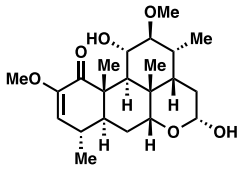

javanicin M
Picrasma javanica

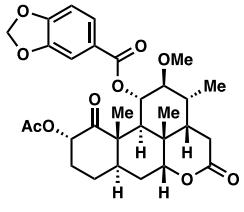

javanicin N
Picrasma javanica

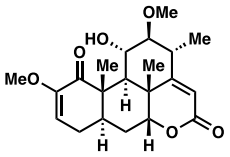

javanicin O
Picrasma javanica

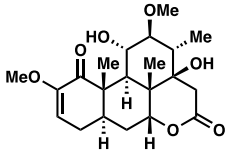

javanicin P
Picrasma javanica

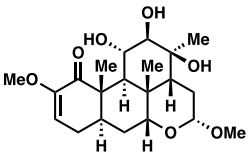

javanicin Q
Picrasma javanica

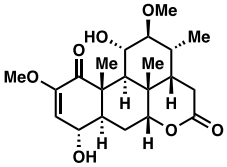

javanicin R
Picrasma javanica

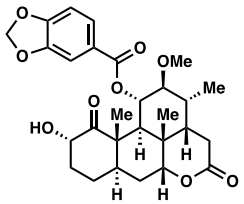

javanicin S
Picrasma javanica

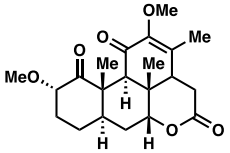

javanicin T
Picrasma javanica

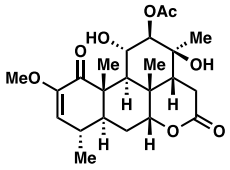

javanicin U
Picrasma javanica

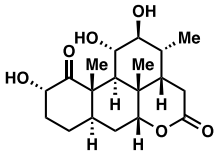

javanicin V
Picrasma javanica

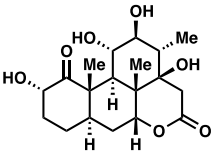

javanicin W
Picrasma javanica

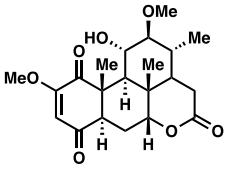

javanicin X
Picrasma javanica

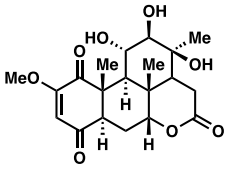

javanicin Y
Picrasma javanica

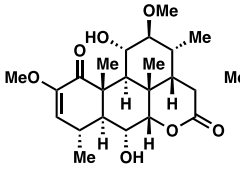

javanicin Z
Picrasma javanica

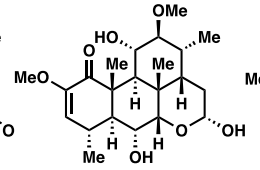

hemiacetaljavanicin
Picrasma javanica

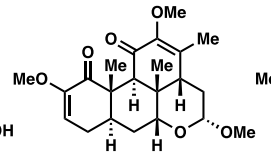

(16R)-methoxyjavanicin B
Picrasma javanica

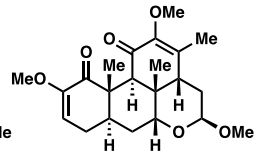

(16S)-methoxyjavanicin B
Picrasma javanica

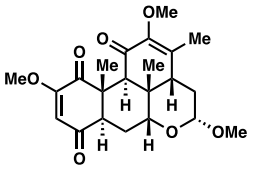

4-keto-(16S)-methoxyjavanicin B
Picrasma javanica

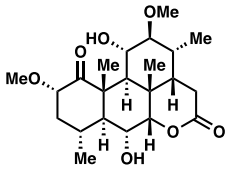

dihydrojavanicin Z
Picrasma javanica

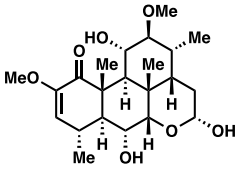

α-hemiacetaljanicin Z
Picrasma javanica

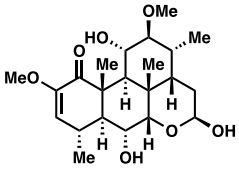

β-hemiacetaljanicin Z
Picrasma javanica

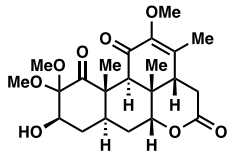

javanicinol A
Picrasma javanica

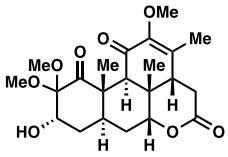

javanicinol B
Picrasma javanica

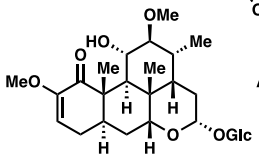

javanicinoside A
Picrasma javanica

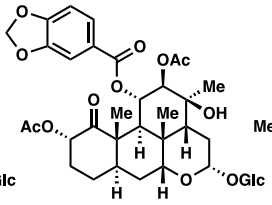

javanicinoside B
Picrasma javanica

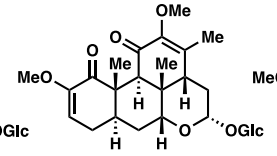

javanicinoside C
Picrasma javanica

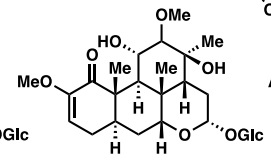

javanicinoside D
Picrasma javanica

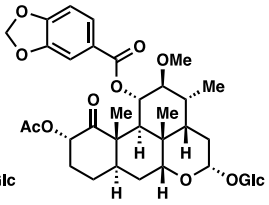

javanicinoside F
Picrasma javanica

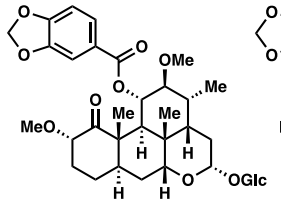

javanicinoside G
Picrasma javanica

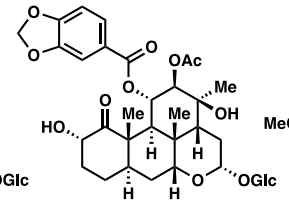

javanicinoside H
Picrasma javanica

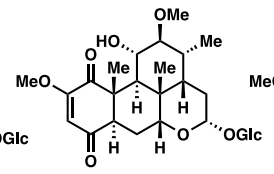

javanicinoside I
Picrasma javanica

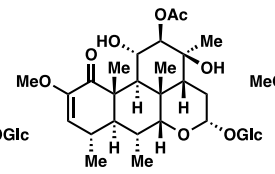

javanicinoside J
Picrasma javanica

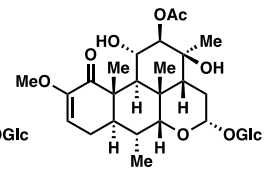

javanicinoside K
Picrasma javanica

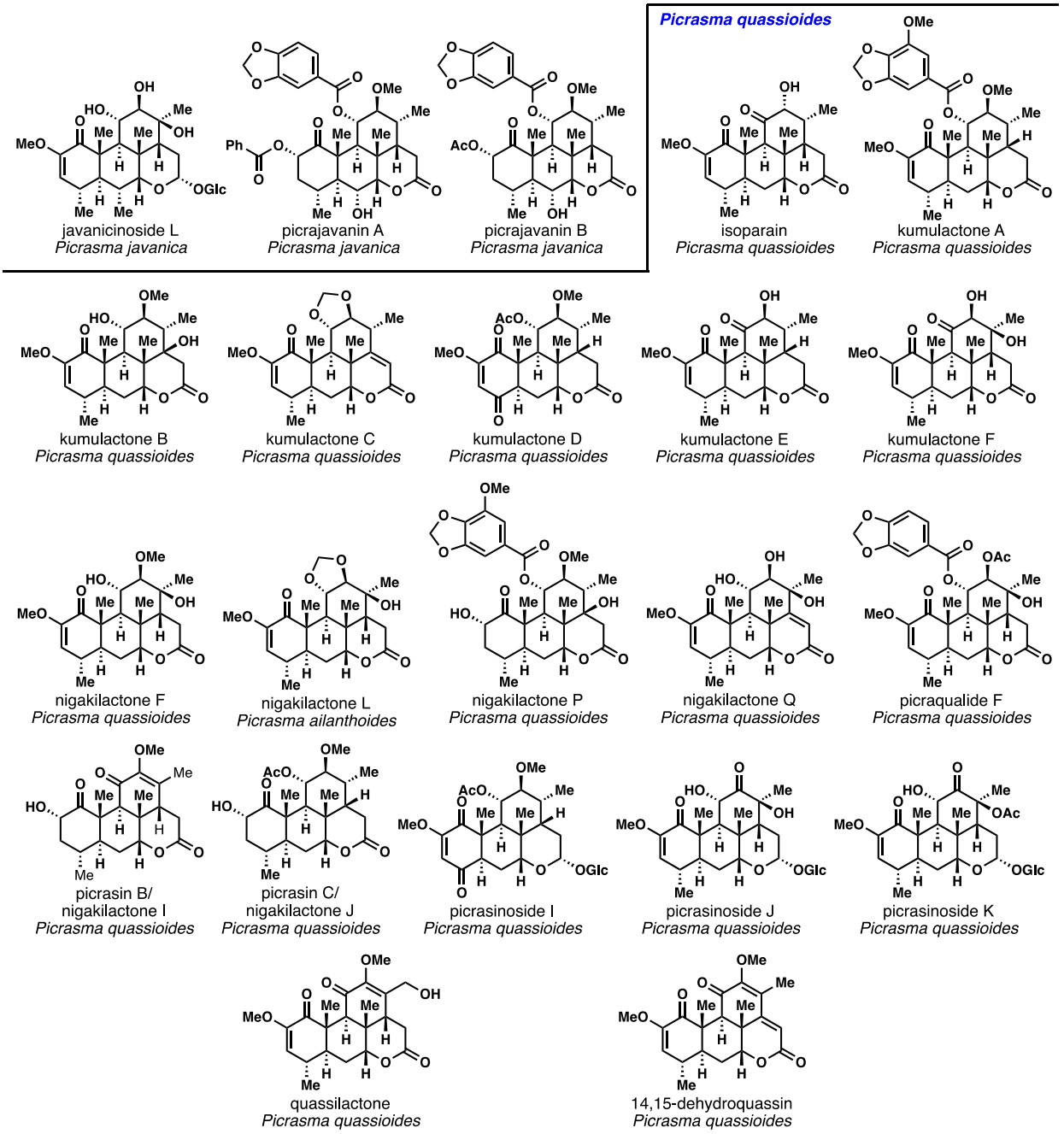

Figure 1.10: Quassinoids isolated from the genus *Picrasma*

The genus *Quassia* contains several exceptional isolates including the flagship member quassin (**1**) itself, novel cyclopropane-containing picrasin K (**40**), and trans-lactonized derivative indaquassin B (**41**). Species from the genera *Simaba* and *Soulamea* have also provided novel quassinoids (Figure 1.11).[11, 32, 61]

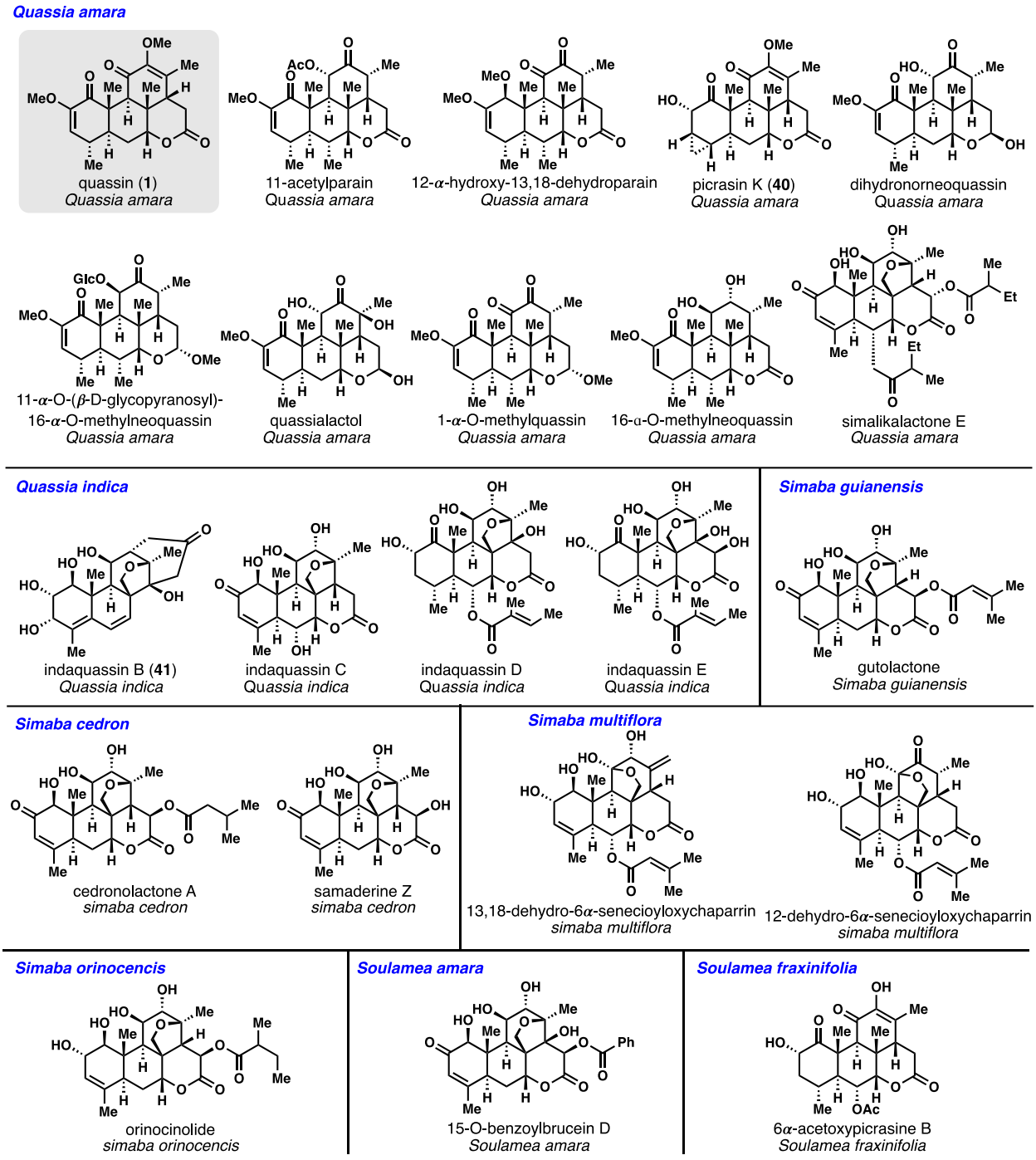

Figure 1.11: Quassinoids isolated for the genus *Quassia*, *Simaba*, and *Soulamea*.

1.2 Proposed Biosynthesis of Quassinoid Natural Products

Biosynthetically, these compounds are thought to be derived from the oxidative degradation of 2,3-oxidosqualene or squalene epoxide (**42**) via 7α-hydroxy apotirucallol (**43**) in a similar fashion to the liminoid family of natural products (Figure 1.12).[32, 62] Further oxidation at C3 and C17 generates lactol **44**, which is thought to undergo trans-

lactonization to arrive at a common tetracyclic core. Cleavage of the C-23/C-24 bond and loss of four carbons then leads to the recently discovered C_{26} quassinoid core (**45**). To arrive at the C_{25} core (**47**), one of the C4 methyl groups must be eliminated. This mysterious demethylation event was originally proposed to occur through a decarboxylative pathway and isolation of the C_{26} scaffold gives credence to this pathway;[30] therefore, from intermediate **45** oxidation and subsequent decarboxylation is thought to give the C_{25} quassinoid skeleton. Cleavage of the C13/C17 bond provides access to the C_{20} skeleton (**48**), which can be converted to the C_{22} (**49**) quassinoids via cyclization of an acetyl group. Alternatively, C_{19} (**50**) quassinoids can be accessed through the C_{20} skeleton via extrusion of C16. The loss of one final carbon and contraction of the A-ring then ultimately gives rise to the the C_{18} class of quassinoids (**51**).[10-11, 63]

Credence was initially given to this hypothesis when, from the same

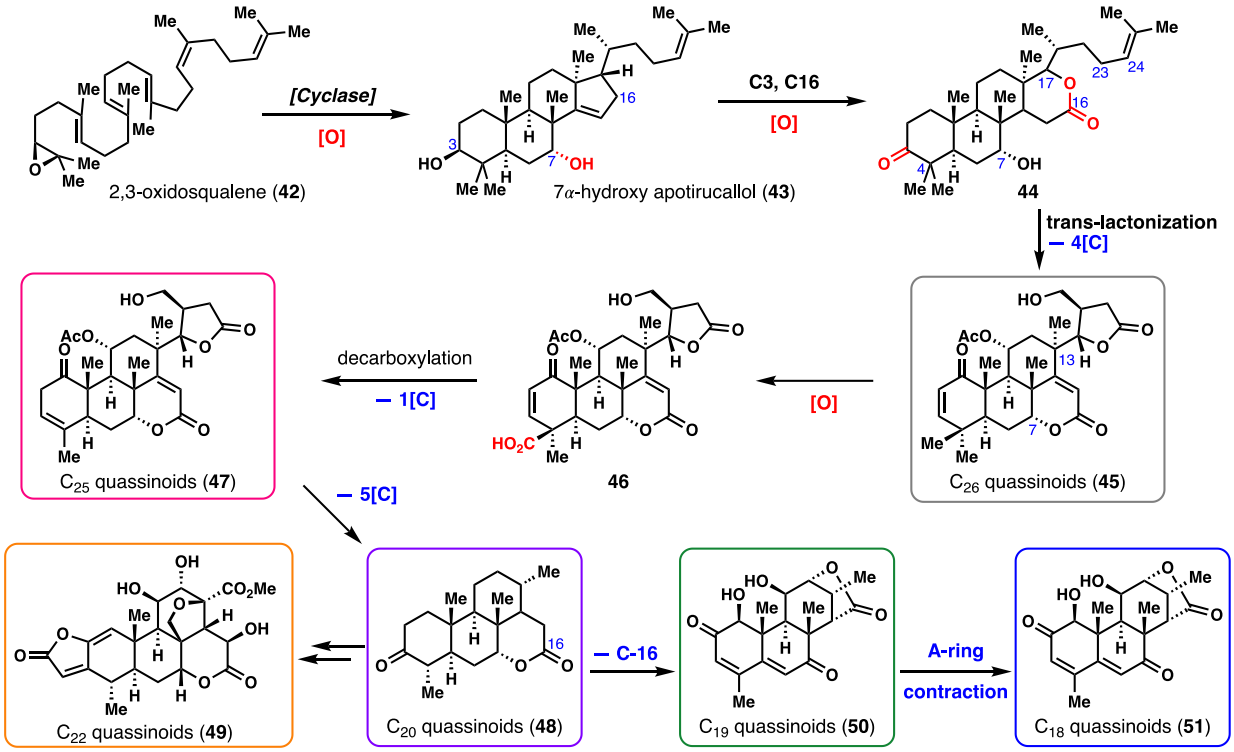

Figure 1.12: Proposed quassinoid biosynthetic pathway

Simaroubaceae species, quassinoids and liminoids were co-isolated (Figure 1.13 A). Liminoid perforin A, a tetranortriterpene, and quassinoids perforaquassin A (**35**), perforaquassin B (**36**), and perfoaquassin C (**37**, Figure 1.12) were all isolated from the bark of *harrisonia perforata*. Perforin A can therefore be thought of as a putative upstream link in the quassinoid biosynthesis.[54] Further support for this biosynthetic pathway was levied by Okogun and coworkers (Figure 1.13 B). In their studies, they subjected the liminoid gedunin to basic conditions, which led to the expulsion of furfural and the generation of a quassinoid-like compound merogedunin. Importantly they were able to

observe trans-lactonization to access the D-ring lactone present in many of the C20 quassinoids. Taken together, these observations give credibility to the proposed quassinoid biosynthetic pathway despite a lack of in-depth enzymological studies.[64]

1.3 Biological Activity of Quassinoid Natural Products

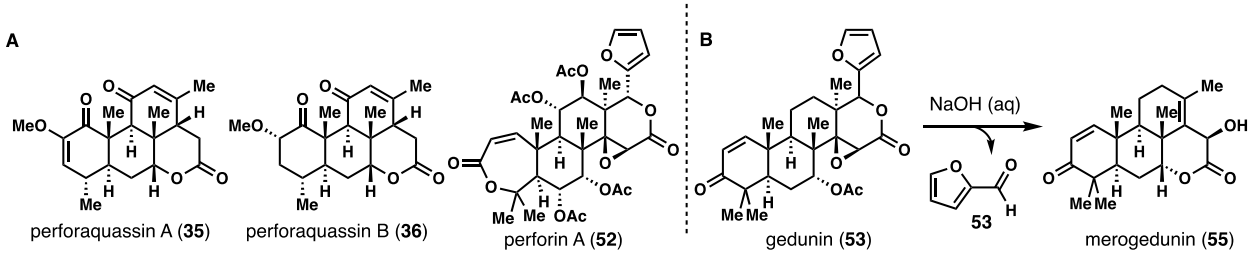

Figure 1.13: Support for biosynthetic pathway. (A) Isolates of *Harrisonia perforate* including liminoid perforin A (**70**) and quassinoids perforaquassins A (**50**) and B (**51**). (B) Putative interconversion between liminoid and quassinoid skeletons via expulsion of furfural (**72**).

A common feature of quassinoid natural products is their extremely bitter taste. Quassin (**1**) specifically is 50 times more bitter than quinine, for which it has earned the moniker bitter principle. These quassinoid bitter principles display a wide range of biological activity including: antimalarial, antiviral, herbicidal, insect antifeedant, insecticidal, larvicidal, antileishmanial, anti-inflammatory, amoebicidal, anticomplement, and anticancer.[32]

Of the myriad biological effects, antimalarial activity is one of the most prominent and longest known effects. Various *Simaroubaceae* have been used as a folk remedy in many parts of the globe for the treatment of malaria. Once such instance is by the “quilombolas” of French Guiana who use the bark of *Simaba cedron*. The compound thought to be primarily responsible for the observed activity against *Plasmodium falciparum* is cedronine (Figure 1.2, **13**, IC_{50} 0.25 µg/mL).[65]

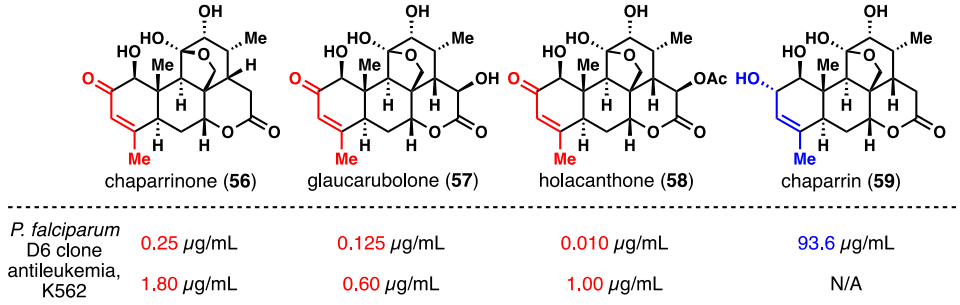

Figure 1.14: Biological activity of chaparrinone (**56**), glaucarubolone (**57**), holacanthone (**58**), and chaparrin (**59**) against *Plasmodium falciparum* and K526 leukemia cells.

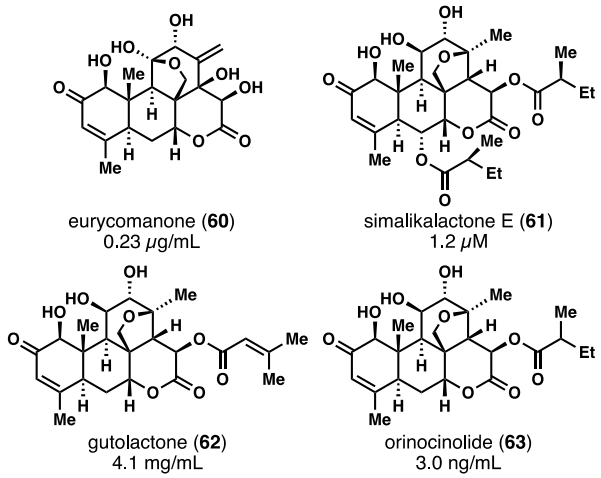

Figure 1.15: Selection of antimalarial quassinoids and their corresponding activites

Many additional quassinoids have shown activity against *Plasmoidum falciparum* as well, including chaparrinone (**56**), glaucarubolone (**57**) and holacanthone (**58**), isolates of *Castela texana* otherwise known as Texan goatbush, that all displayed significant activity against the *p. falciparum* clone D6 (0.25, 0.125, and 0.010 μg/mL) and W2 (0.20, 0.20,and 0.012 μg/mL)(Figure 1.14).[48] Notably chaparrin (**59**), which lacks the A-ring α,β-unsaturated ketone, possesses significantly lower activity against *P. falciparum.* Other *Simaroubaceae* isolates including eurycomanone (**60**, IC_{50} 0.23 μg/mL Gombak A strain.[66] simalikalactone E (**61**, IC_{50} = 1.2 μM, gametocytes),[67] gutolactone (**62**, IC_{50} = 4.1 ng/mL, W-2 strain)[68], and orinocinolide (**63**, IC_{50} = 3.0 ng/mL, W2 clone)[69] also displayed a wide range of activity agains *P*. *falcirarum* types. Particularly notable is isobrucein B (**64**), which boasts the one of the highest activities against *P. falciparum* found to date within the quassinoid family of natural products. With an *in vitro* IC_{50} value of 0.001 μg/mL, isobruceine B (**64**) surpasses both quinine (**65**, 0.06 μg/mL) and chloroquine (**66**, 0.082 μg/mL) in activity against *P. falciparum* (Figure 1.15).[70]

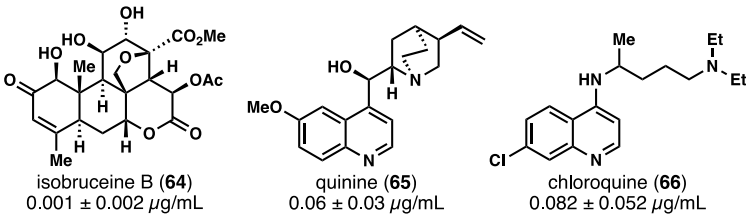

Figure 1.16: Antimalarial activity of isobruceine B (**64**) compared to antimalarial therapeutics quinine (**65**) and chloroqine (**66**).

One of the major drawbacks to a number of the quassinoids as antimalarials is the high cytotoxicity. While this is detrimental to quassinoids as malaria therapeutics, this same feature gives a number of quassinoids their anticancer activity.[32] When antimalarial compounds chaparrinone (**56**), glaucarubolone (**57**), and holacanthone (**58**) were examined they were found to have potent activity against leukemia cells (not selective, 1.00-1.80 μg/mL, Figure 1.14).[48]

In addition to **56**, **57**, **58**, many other quassinoids have been examined for anticancer activity from a variety of *Simaroubaceae* species including but not limited to bruceanol C (**67**, ED_{50} = <0.04μM, KB epidermoid carcinoma),[71] Bruceanol G (**68**, ED_{50} = 0.44, KB nasopharyngeal carcinoma),[72] Bruceine D (**69**, 0.5 μM, nonsmall cell lung cancer H460),[73] 15β-acetyl-14-hydroxyklaineanone (**70**, IC_{50} = 6.6 μg/mL, P-388 murine lymphocytic leukemia) and 6α-acetoxy-14,15β-dihydroxyklaineanone (**71**, IC_{50} = 12.0 μg/mL, P-388 murine lymphocytic leukemia),[22] javanicolide B (**72**, IC_{50} = 8.0 μg/mL, P-388),[74] and

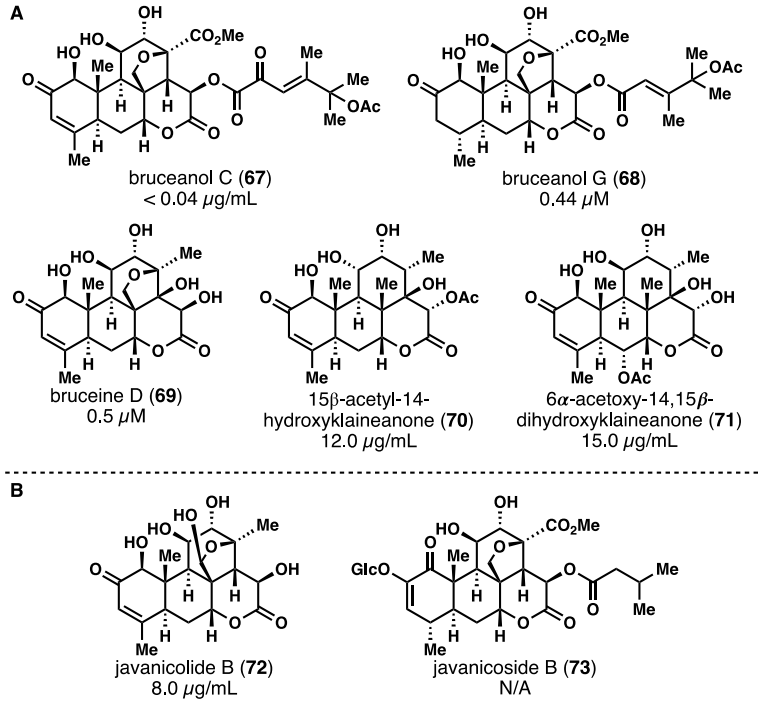

Figure 1.17: (A) Selection of anticancer quassinoids. (B) Comparison of activity between quassinoids (**72**) and quassinoids glycosides (**73**).

javanicoside B (**73**, no activity).[75] Most notably, bruceantin (**3**, Figure 1.2) has been taken through Phase II clinical trials in humans as a treatment for various types of solid tumors.[76]

Given the range and potency of biological activities exhibited by various quassinoids, several studies have been conducted to determine the structure-activity relationship. Dou et al., Wang et al., and Miyake et al. have all associated the presence of the α,β-unsaturated ketone on the quassinoid A-ring with observed cytotoxicity. The presence of the oxomethylene bridge was also connected to higher activity, as cleavage of the bridge between C8 and C11 almost complete ablated the previously observed activity. [22, 48, 77] Additionally, it has been noted that glycosylation can inhibit biological activity for some quassinoids (For example **73**, Figure 1.17 B). Despite these observations, detailed insight into quassinoid cancer targets at the protein-level is greatly lacking.

1.4 Previous Total syntheses of C_{20} Quassinoid Natural Products

Due to both the complex structure and the wide range of biological activities, quassinoids have been the subject of many synthetic ventures. While nature generates quassinoid scaffolds through oxidation and bond cleavage events, synthetically chemists have taken the opposite approach by first building up the carbon skeleton then installing the necessary oxidation. Included below are the relevant syntheses of C_{20} quassinoids.

1.4.1 Grieco's 1980 Synthesis of (±)-Quassin

Quassin, the flagship quassinoid, has been targeted by several research groups with the first successful racemic synthesis achieved by the Grieco group in 1980 (Figure 1.18).[78-79] They employed a key intermolecular Diel-Alder strategy in this synthetic approach. Starting from the Wieland-Miescher ketone (**74**), they first reduced the A-ring

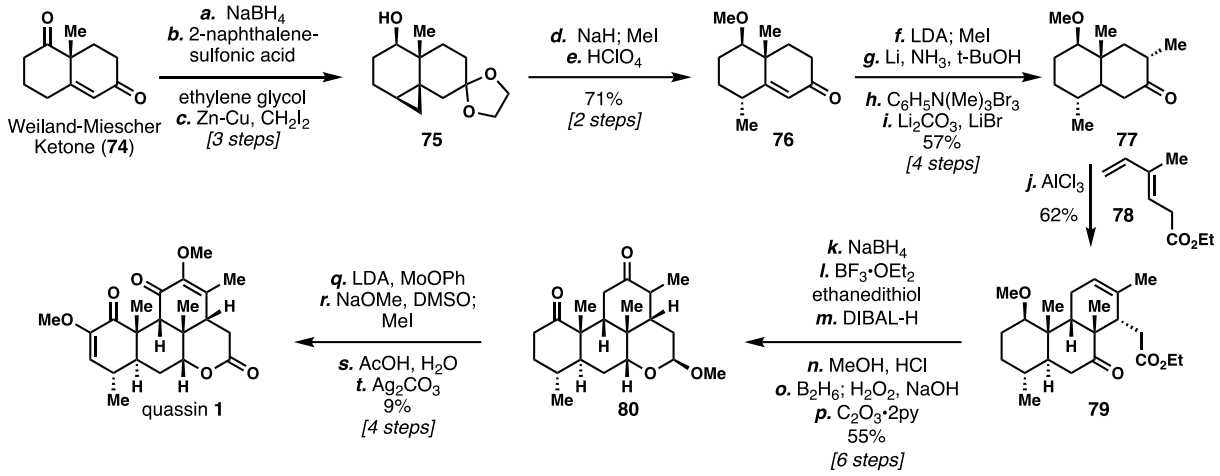

Figure 1.18: Grieco's racemic total synthesis of quassin featuring a key intermolecular Diels-Alder cycloaddition to rapidly access a tricyclic intermediate containing all the carbons necessary for the quassinoid core.

ketone followed by ketalization with concomitant olefin isomerization then cyclopropanation to arrive at intermediate **75**. After protection of the alcohol, the intermediate was treated with perchloric acid resulting in ketal deprotection and E1cB-type elimination of the cyclopropane to install the C4 methyl group (**76**). Alkylation and Birch reduction followed by bromination and subsequent elimination afford key intermediate **77** in only 9 steps. From here cycloaddition with diene **78** gave tricyclic intermediate **79**, thus appending on all of the carbons necessary for the natural product. Through a series of reductions and oxidations they were then able to access protected lactol **80**, which after a-hydroxylation and *O*-alkylation, gave the bisdiosphenol. Finally, selective deprotection of the lactol oxygen and oxidation using Fetizen's conditions gave the natural product in 21 steps from **74**.

1.4.2 Watt's 1990 Synthesis of (+)-Quassin

Drawing inspiration from Grieco's strategy, the Watt group also chose to employ a key intermolecular Diels-Alder based strategy in their approach to the synthesis of quassin (Figure 1.19).[80] Starting again from the Wieland-Miescher ketone , this time in enantiopure form, Watt was able to elaborate to their key Diels-Alder intermediate (**82**) in only 11 steps via bicycle **81**, which was comparable to Grieco's 9-step sequence. Importantly, Watt's intermediate contained additional oxidation at the C8 methyl group as the aldehyde species. While this allowed them to use instead a Danishefsky-type diene (**83**) in their cycloaddition, it also necessitated the later removal of the extraneous oxidation to access **1**. Regardless, the Diels-Alder proceeded smoothly, to give tricyclic compound **84**. Because Watt's diene did not contain the requisite carbons to complete the natural product, they then focused their efforts on appending the necessary carbons. Through a series of manipulations, largely comprising of protecting group interconversion,

they were able to access primary bromide **85** that smoothly underwent a *6-exo* reductive radical cyclization to arrive at tetracycle **86**. From here it took an additional 13 steps to access the correct oxidation pattern present in the quassin, resulting in a 35-step synthesis. While this marked the first enantioselective synthesis of quassin, the strategy suffered from the inability to manipulate oxidation state selectively without the need for extensive protecting group manipulations.

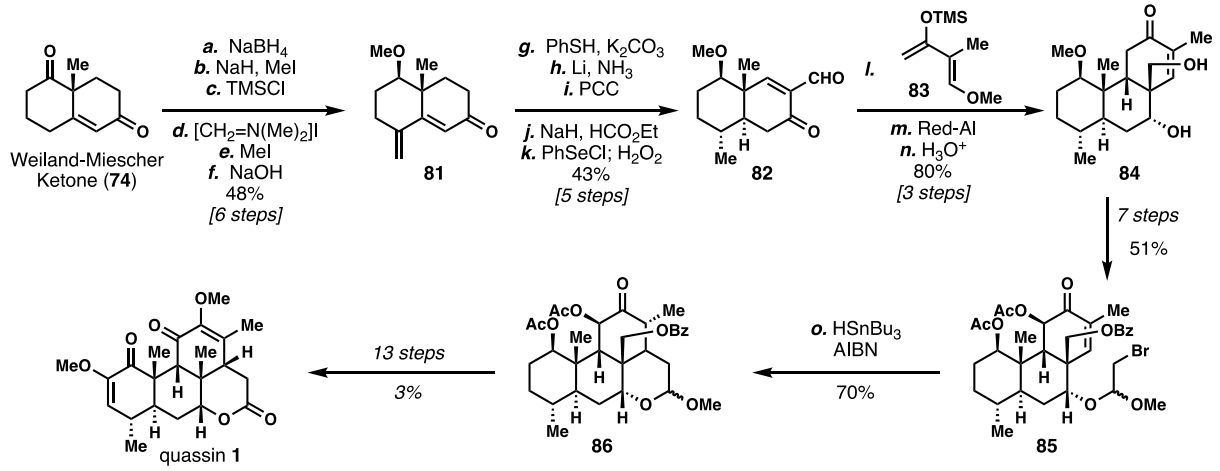

Figure 1.19: Watt's total synthesis of (+)-quassin, enploying a key intermolecular Diels-Alder based strategy with Danishefsky-type diene **83.**

1.4.3 Valenta's 1995 Synthesis of (±)-Quassin

Valenta's effort towards quassin marks a significant departure from the previously employed strategies of both Grieco and Watt. An extended effort of over 16 years, culminated in Valenta's synthesis in 1995 (Figure 1.20);[81-83] however, due to inconsistency in reported yields and conditions, a precise discussion of this route is challenging using typical metrics. Though Valenta's strategy still relies on an intermolecular Diels-Alder, they use a quinone variant involving **87** and **88** to generate a bicyclo[2.2.2]octane system (see **89**) as a mixture of diastereomers. The authors then go on to elaborate this system and append on the carbons necessary to complete the natural product giving highly complex intermediate **90**. At this point, they need to cleave the [2.2.2]-bicycle, which is accomplished with periodic acid to give tetracycle **91** after PtO_2 reduction. Closure of the A-ring and Bayer-Villager oxidation resulted in the quassinoid tetracyclic core (**92**), at which point it takes another 7 steps to manipulate the oxidation state to that found in the natural product **1**. Overall, Valenta was able to achieve the

synthesis of quassin in 32 steps from commercially available materials that was comparable to Watt's in length but utilized a unique and orthogonal strategy.

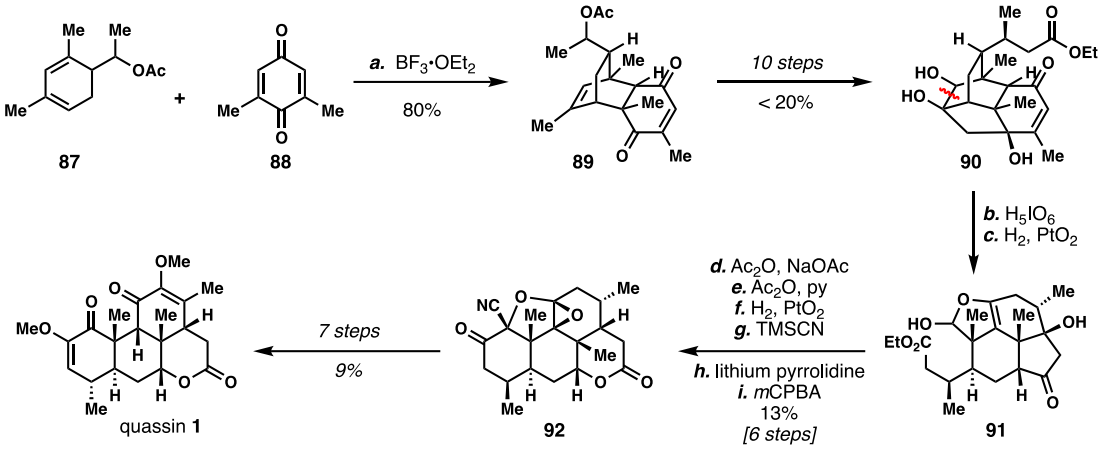

Figure 1.20: Valenta's total synthesis of quassin

1.4.4 Shing's 1998 Synthesis of (+)-Quassin from (+)-Carvone

The most recent synthesis of quassin was achieved by the Shing group in 1998 (Figure 1.21).[84-87] Though their strategy was dissimilar to all of the previous routes, they also sought to employ a Diels-Alder based approach; however, this time an intramolecular variant was employed to create the A-ring. From *(S)*-carvone (**93**), they were able to rapidly synthesize their key Diels-Alder intermediate (**95**) in only three steps. By refluxing intermediate **95** in benzonitrile, they were able to reveal *in-situ* the reactive species via SO_2 extrusion and cyclize to generate tricycle **96**. Unfortunately, due to the low oxidation state of the chosen cycloaddition species, another 13 steps were necessary to construct intermediate **97**, which after intramolecular aldol generates the tetracyclic lactone **98**.

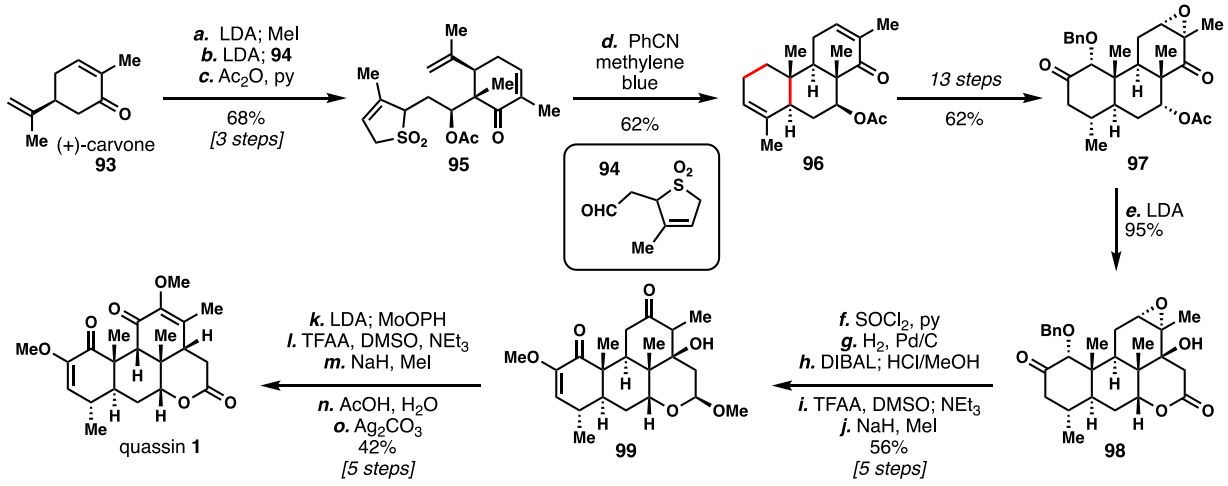

Figure 1.21: Shing's total synthesis of quassin.

Through several protecting group and oxidation state manipulations, they were able to construct **1** in 10 more steps for an overall step count of 28. This strategy, like many of the others also suffered from the inability to construct the carbocyclic core in tandem with the high overall oxidation state of the quassinoids.

1.4.5 Total synthesis of (±)-Amarolide

In addition to quassin, a number of other quassinoid natural products have been synthesized. The racemic total synthesis of amarolide (**108**) was achieved by Hirota et al. in 1987 from previously reported 12β-hydroxy-pricasan-3-one **105** (Figure 1.22).[88-90] The major considerations for this synthesis were: 1) the transposition of the C3 carbonyl to C1, 2) hydroxylation at C2 and C11, and 3) oxidation of the tetrahydropyran to the lactone. To construct key intermediate **105**, they start from 2-methylcyclohexadione (**100**) and

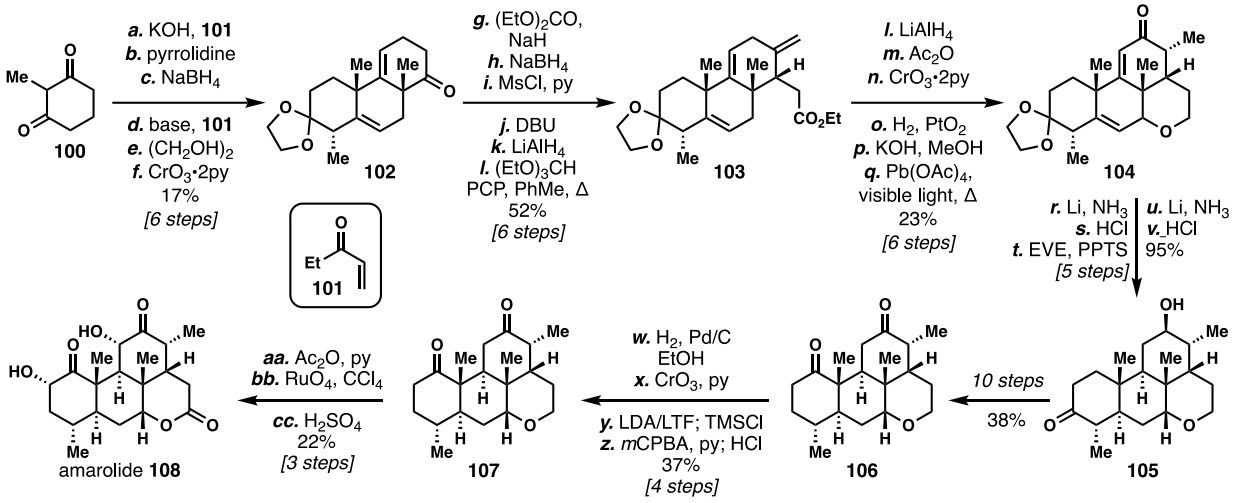

Figure 1.22: Hirota's total synthesis of amarolide

perform a series of Robinson annulations to access tricycle **102**. Alph-alkylation of the ketone followed by a series of reductions and Claisen rearrangement resulted in **103**. After several oxidative manipulations, they were able to achieve the synthesis of tetrahydropyran **104**, which through a series of reductions gave key intermediate **105**. From here, the authors were able to affect their desired A ring carbonyl transposition to access **106** in 10 steps. Generation of the diketone species preceded Rubottom oxidation, which was used to install both C2 and C11 hydroxyl groups resulting in **107**. Finally, acetylation, oxidation, and deprotection gave amarolide (**108**) in 18 steps from **105** or 40 steps from commercially available starting materials.

1.4.6 Total Synthesis of Bruceantin

Since its isolation over 50 years ago, bruceantin **3** has remained a target of synthetic interest due to the highly oxidized, complex scaffold and its known anticancer biological activity. Grieco and coworkers completed the total synthesis of this molecule (figure 1.23)[91] employing tricycle **112**, which had been previously recognized by several synthetic groups as a logical starting point.[92-95] To access this crucial intermediate, they

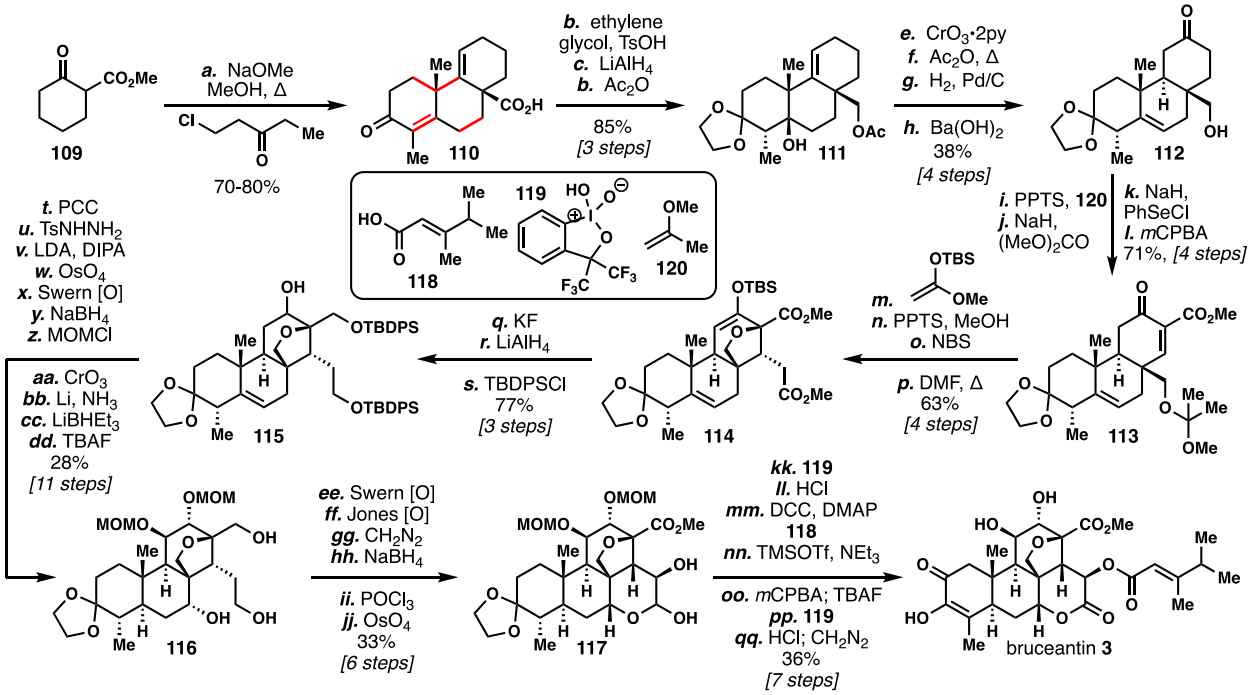

Figure 1.23: Grieco's total synthesis of bruceantin utilizing a double Robinson annulation to rapidly construct a tricyclic intermediate (**110**)

first perform a double Robinson-type annulation on **109** to generate tricycle **110**. From here a series of functional group manipulations, oxidations, and reductions give proposed starting compound **112**. At this stage, after only 8 steps, nearly all of the carbon functionality had been installed (see **114**); therefore, the objective from here was to append on the few remaining carbons and modify the oxidation state to match that of the natural product. Unfortunately, the realization of these goals was far more laborious than anticipated. After only 6 more steps, all of the main scaffold carbons were appended; however, it took Grieco another 35 steps to finally arrive at the natural product highlighting the synthetic challenges this complex quassinoid presents.

1.4.7 Total Synthesis of (±)-Chaparrinone, (±)-Glaucarubolone, (±)-Holacanthone, (±)-Simalikalactone D, and (±)-Shinjulactone C

The quassinoid core architecture is highly conserved throughout this family of natural products. The Grieco group thought to leverage this phenomenon and utilized common synthetic intermediates in their route to chaparrinone (**56**) to gain access to a multitude of natural products including: glaucarbulone (**57**), holacanthone (**58**), simalikalactone D (**130**), and shinjulactone C (**136**).

The synthetic approach to chaparrinone was a combination of Grieco's first Diels-Alder strategy and Watt's oxidized bicyclic intermediate (**82,** Figure 1.24).[96-98] The oxidized intermediate was advantageous for this synthesis, as the natural product contains an hemiketal bridge connecting C8 to C11. In this synthesis, the authors rapidly construct a tricyclic intermediate in only 9 steps from **121**; however, lengthy sequences were required to install the desired oxygenation pattern on the A and C rings. They

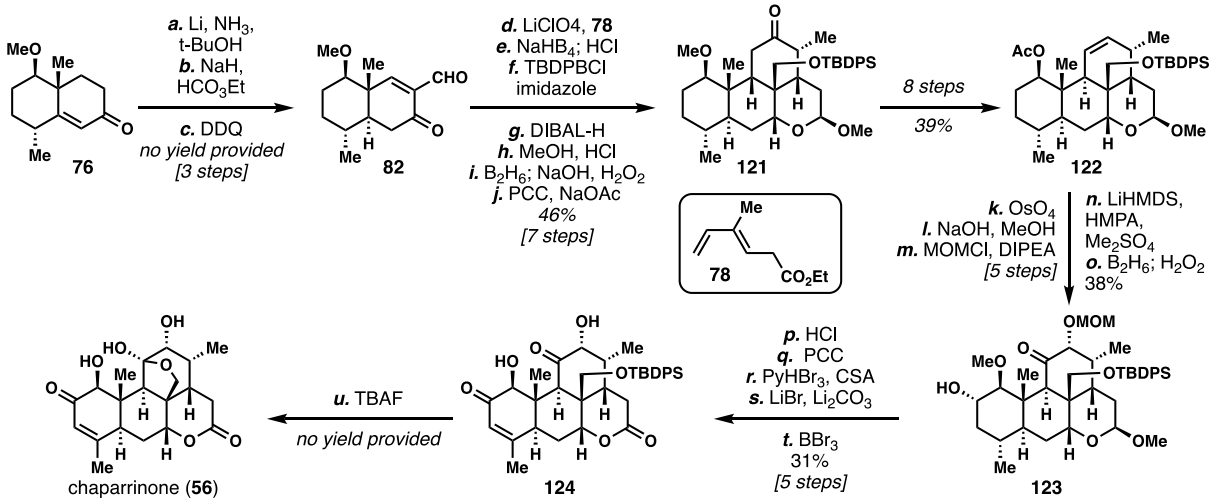

Figure 1.24: Grieco's total synthesis of chaparrinone (**21**) using Watt's oxidized bicycle **82** to gain access to the C8 oxidation state for generation of the hemiketal found in the natural product.

approached the C-ring oxidation first and were able to access key olefin **122** in 8 steps from **121** including a step to epimerize the incorrectly set C9 stereocenter. Through a series of oxidations, including an osmium dihydroxylation and protections they were able to arrive at **123**. Further oxidation was then necessary to oxidize the A-ring ultimately forming α-hydroxy enone **124**. Finally, silyl deprotection of the *tert*-butyldiphenylsilyl (TBDPS) group then directly forged the hemiketal and ultimately chaparrinone (**56**). Overall, this synthesis proceeded in 34 steps from the Wieland-Miesher ketone (**74**) and represents the first synthesis of a quassinoid containing the C8/C11 hemiketal bridge.

Notably, Grieco was also able to intercept advanced intermediate **123** from the chaparrinone syntheses to access both glaucambolone (, Figure 1.25) and holacanthone (**58).**[96, 99] From **123** the remaining challenges in these syntheses are 1) contruction of the C8/C11 hemiketal bridge, 2) incorporation of the 2-oxo-$\Delta^{3,4}$ olefin into the A ring, and 3) incorporation of the C15 hydroxy group. To achieve these goals, a 4-step sequence, which includes installation of the C15 hydroxy via dihydroxylation of an enol ether, gave **125**. Next, the oxidation state of the A-ring was adjusted to give **126**, and finally treatment with BBr_3 and TBAF gave the hemiketal-containing natural product glaucambolone. Finally, by acetylating the C15 hydroxy group of intermediate **126**, **127** can be accessed and ultimately holacanthone.

Similar to Grieco's strategy towards glaucarubolone (**57**) and holacanthone (**58 53**), the Grieco group proposed that by intercepting intermediate **121,** simalikalactone D (**130**, Figure 1.26) could also be accessed.[100] A lengthy 16-step sequence, however, was

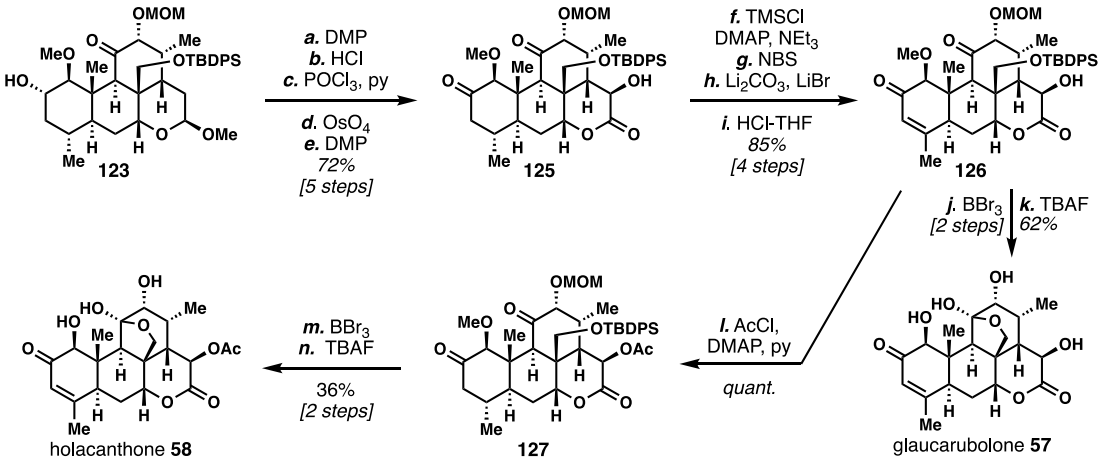

Figure 1.25: Grieco's total synthesis of glaucarubolone (**57**) and holocanthone (**58**) via interception of intermediate **123** from the synthesis of chaparrinone (**55**).

required to manipulate the C-ring oxidation states including construction of the C8/C13 oxomethylene bridge. Nonetheless, with the desired intermediate **128** in hand they were then able to oxidize both the A and D rings in a similar fashion to **57** and **58** to construct intermediate **129**. Finally, installation of the ester side chain and global deprotection gave **130** in 41 steps from the Wieland-Miesher ketone.

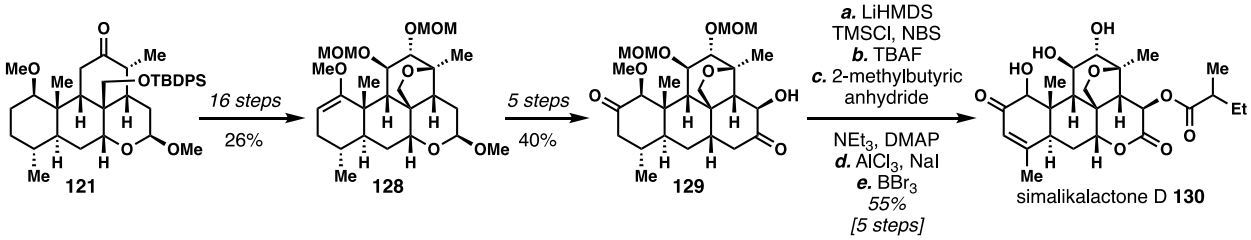

Figure 1.26: Interception of chaparrinone (**55**) intermediate 121 as a route towards the total synthesis of simalikalactone D (**130**)

Similarly, Grieco and co-workers also utilized intermediate **131** from their chaparrinone synthesis in the construction of shinjulactone C (**136**, Figure 1.23).[101] Like previous syntheses, they also manipulate C-ring oxidation first in this synthesis to gain access to intermediate **132**. With the diol on the C-ring protected, the A-ring is then easily oxidized to α-hydroxy enone **133** before performing C-ring oxidation. While accessing the correct oxidation state, the fortuitous formation of the C8/C11 hemiketal (see **134**) served as a protecting group of the C8 hydroxymethyl group allowing for selective manipulation of the C12 hydroxyl. From **134** oxidation at C12 and cleavage of the undesired hemiketal

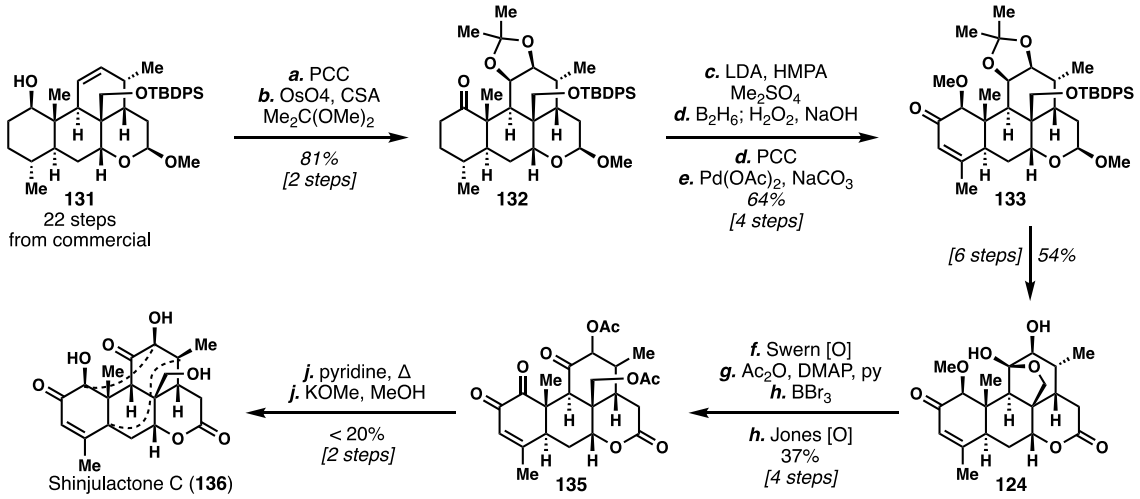

Figure 1.27: Grieco's total synthesis of shinjulactone C (**136**) from common chaparrinone (**55**) intermediate **131**.

provide **135**, which after refluxing in pyridine the C9 stereocenter is inverted and the caged compound shinjulactone C (**136**) is formed after deacetylation. Although this synthesis required 40 steps, they were able to accomplish the synthesis of one of the most synthetically challenging quassinoids **136**.

1.4.8 Total Synthesis of (±)-Klaineanone and (±)-14β,15β-Dihydroxyklaineanone

Similar to Grieco's syntheses that stemmed from chaparrinone (**56**), the Grieco group also intercepted intermediates in their synthesis of quassin (**1**) to access quassinoids klaineanone (**142**, Figure 1.28)[102-103] and 14β,15β-dihydroxyklaineanone (**148**, Figure 1.29).[104] To construct **142**, they started from intermediate **137**, which already contained all of the carbons found in the natural product. All that remained from **137** was to epimerize the C9 stereocenter that was set incorrectly after Diels-Alder cycloaddition to form the C ring and to install the correct oxidation pattern on the A and C rings. Saegusa-Ito oxidation of **137** followed by a series of reductions gave olefin **138** containing a now epimerized C9 stereocenter. Before targeting the oxidation pattern of the A and C rings, they first set the lactone oxidation in a two-step process to arrive at **139**. Since all attempts to elaborate the A ring after installation of the diaxial vicinal diol on the C ring were unsuccessful, they first targeted the A-ring oxidation pattern. Through a series of

oxidations, and a base-catalyzed tautomerization, they were able to access **141**, which was smoothly converted to klaineanone **142** via epoxidation and subsequent epoxide opening.

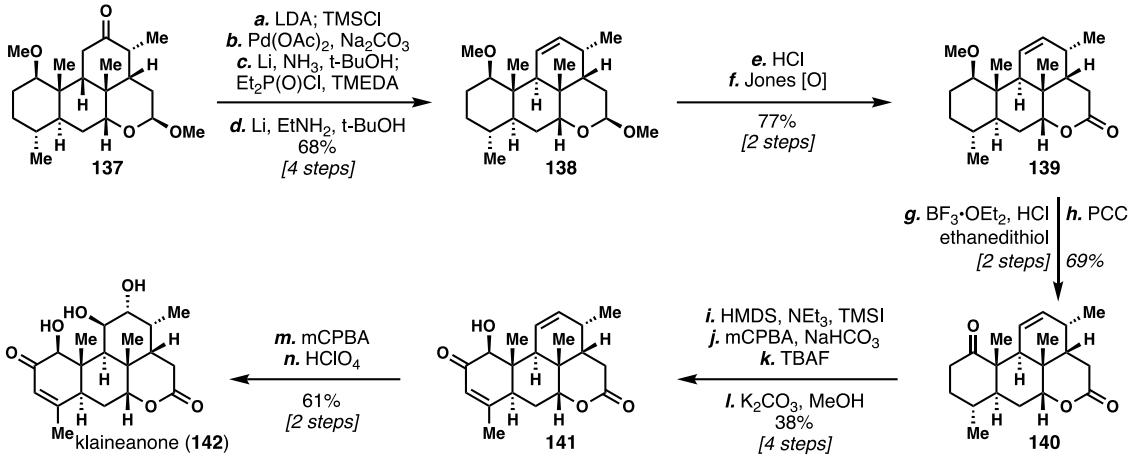

Figure 1.28: Grieco's total synthesis of klaineanone **142** from their quassin (**1**) route intermediate **137**. Elaboration of the A-ring preceded C-ring oxidation to prevent undesired oxidations of the vicinal *trans*-diol moiety.

14β,15β-dihydroxyklaineanone (**148**) can be access in a similar fashion from intermediate **143**, which was also present in the klaineanone (**142**) synthesis. Unlike the previous synthesis, to gain access to **148** Grieco first targeted the C-ring oxidation and protected it prior to oxidation of the A and D rings. From intermediate **143** they first epoxidized and subsequently opened in a similar fashion to the synthesis of klaineanone (**142**) to generate **144**. They then protected the diol as the methoxymethyl ethers (MOM) before α-hydroxylation of the A ring and dihydroxylation of the D ring. The resulting D-ring *syn*-diol **146** was then protected, so they could generate α-bromo ketone **147** which after elimination and global deprotection gave the natural product **148**.

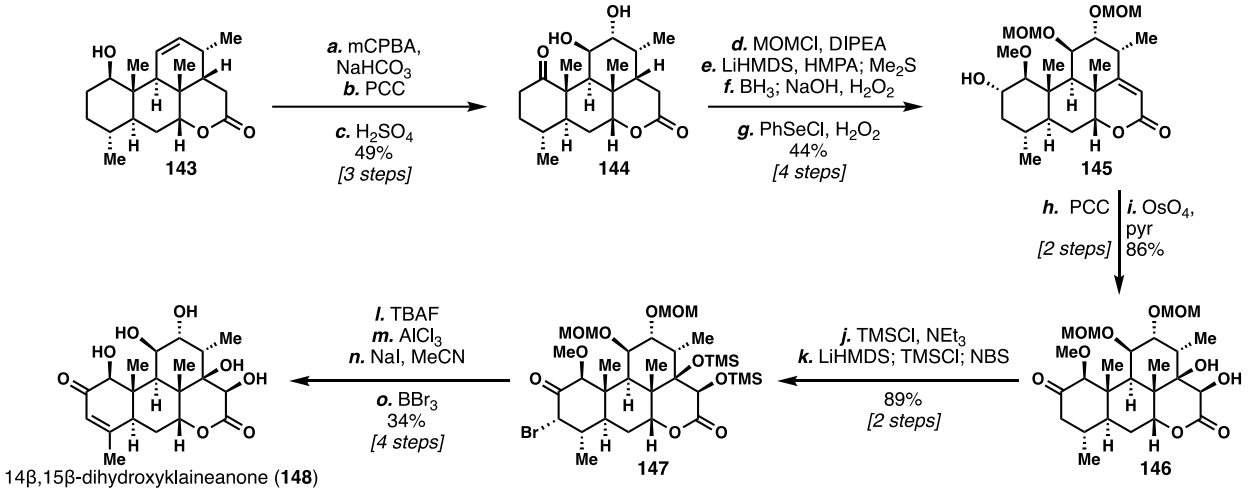

Figure 1.29: Grieco's total synthesis of **148** from previous quassin intermediate **143**. MOM protection of the *trans*-diol allowed for elaboration of the C-ring oxidation pattern prior to A and D ring oxidation.

1.4.9 Total synthesis of (–)-Samaderine Y

Most recently, the quassinoid samaderine Y (**154**, Figure 1.30)[105] has succumb to total synthesis by Shing and coworkers in 2005. Utilizing a similar strategy to their 2000 synthesis of quassin, they identified (+)-carvone as what would become the C ring of their target and employed a similar intramolecular Diels-Alder to construct the ABC ring system. One of the key challenges in this synthesis was construction of the highly oxidized C ring containing the C8/C13 oxomethylene bridge. Unlike in their previous work, Shing

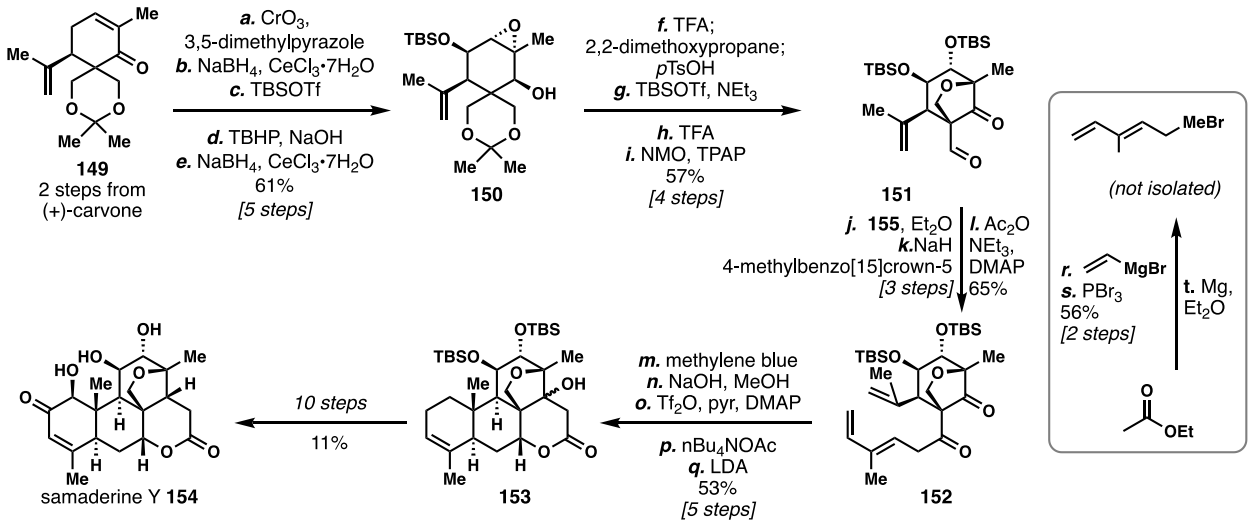

Figure 1.30: Shing's total synthesis of samaderine Y (**154**) from (+)-carvone (**93**) utilizing a key intramolecular Diels-Alder cycloaddition to access the tricyclic core. Insert: synthesis of allylic diene **155**.

chose to incorporate the C-ring oxidation prior to intramolecular Diels-Alder cycloaddition. Starting from **149** (2 steps from (+)-carvone), they performed a series of redox manipulations and protecting group interconversions to arrive at **151** in 9 steps via epoxide intermediate **150** (11 from **93**). They then react their intermediate (**151**) with Grignard reagent **155**, which gave the undesired quaternary methyl addition product. After 1,3-sigmatropic rearrangement, they were finally able to generate key Diels-Alder substrate **152** that cyclized smoothly using their previously employed methylene blue conditions (see Figure 1.17) to afford intermediate **153** after lactonization. Comparable to their quassin synthesis, due to the low oxidation state of their Diels-Alder precursor, it took additional 10 steps to access the natural product (**154**) from their tetracyclic intermediate **153.**

1.5 References

1. Wickens, A., *Libr. J.* **2005,** *130*, 118.
2. Winckler, F. L., *Repert. Pharm.* **1835,** *4*, 85.
3. Clark, E. P., *J. Am. Chem. Soc.* **1937,** *59*, 927.
4. Valenta, Z.; Gray, A. H.; Papadopol, S.; Orr, D. E.; Podesva, C., *Tetrahedron* **1962,** *18*, 1433.

5. Valenta, Z.; Podesva, C.; Papadopol, S., *Tetrahedron* **1961,** *15*, 100.
6. Carman, R. M.; Ward, A. D., *Aust. J. Chem.* **1962,** *15*, 807.
7. Carman, R. M.; Ward, A. D., *Tetrahedron Lett.* **1961,** 10, 317.
8. Duan, Z. K.; Zhang, Z. J.; Dong, S. H.; Wang, Y. X.; Song, S. J.; Huang, X. X., *Phytochemistry* **2021,** *187*, 22.
9. Cuendet, M.; Pezzuto, J. M., *J. Nat. Prod.* **2004,** *67*, 269.
10. Polonsky, J., *Fortschritte der Chemie organischer Naturstoff* **1985,** *47*, 221.
11. Vieira, I. J. C.; Braz-Filho, R., *Stud. Nat. Prod. Chem.* **2006**, 33, 433.
12. Ang, H. H.; Hitotsuyanagi, Y.; Fukaya, H.; Takeya, K., *Phytochemistry* **2002,** *59*, 833.
13. Ang, H. H.; Hitotsuyanagi, Y.; Takeya, K., *Tetrahedron Lett.* **2000,** *41*, 6849.
14. Nguyen-Ngoc-Suong; Bhatnagar, S.; Polonsky, J.; Vuilhorgne, M.; Prange, T.; Pascard, C., *Tetrahedron Lett.* **1982,** *23*, 5159.
15. Wani, M. C.; Taylor, H. L.; Wall, M. E.; McPhail, A. T.; Onan, K. D., *J. Chem. Soc.; Chem. Commun.* **1977**, 295.
16. Chan, K. L.; Iitaka, Y.; Noguchi, H.; Sugiyama, H.; Saito, I.; Sankawa, U., *Phytochemistry* **1992,** *31*, 4295.
17. Itokawa, H.; Qin, X. R.; Morita, H.; Takeya, K., *J. Nat. Prod.* **1993,** *56*, 1766.
18. Kuo, P. C.; Damu, A. G.; Lee, K. H.; Wu, T. S., *Bioorg. Med. Chem.* **2004,** *12*, 537.
19. Morita, H.; Kishi, E.; Takeya, K.; Itokawa, H.; Iitaka, Y., *Phytochemistry* **1993,** *33*, 691.
20. Park, S.; Nhiem, N. X.; Kiem, P. V.; Minh, C. V.; Tai, B. H.; Kim, N.; Yoo, H. H.; Song, J. H.; Ko, H. J.; Kim, S. H., *Bioorg. Med. Chem. Lett.* **2014,** *24*, 3835.
21. Dang, N. H.; Lan, D. T. N.; Minh, N. T. T.; Khanh, N. D.; Trang, D. T.; Cuong, P. V.; Hiep, N. T.; Nam, V. D.; Trung, N. Q.; Dat, N. T., *Nat. Prod. Commun.* **2019,** *14*,1.
22. Miyake, K.; Tezuka, Y.; Awale, S.; Li, F.; Kadota, S., *J. Nat. Prod.* **2009,** *72*, 2135.
23. Moretti, C.; Polonsky, J.; Vuilhorgne, M.; Prange, T., *Tetrahedron Lett.* **1982,** *23*, 647.
24. Polonsky, J.; Bhatnagar, S.; Moretti, C., *J. Nat. Prod.* **1984,** *47*, 994.
25. Vieira, I. J. C.; Rodrigues, E.; Fernandes, J. B.; da Silva, M.; Vieira, P. C., *Magn. Reson. Chem.* **2000,** *38*, 805.
26. Zukerman-Schpector, J.; Pinto, A. D.; Dasilva, J. F. M.; Dasilva, R. B., *Acta Crystallogr. Sect. C-Cryst. Struct. Commun.* **1994,** *50*, 87.
27. Nunomura, R.; Silva, E.; Oliveira, D.; Garcia, A.; Boeloni, J.; Nunomura, S.; Pohlit, A., *Acta Amaz.* **2006,** *35*, 327.
28. Fang, X.; Di, Y. T.; Zhang, Y.; Xu, Z. P.; Lu, Y.; Chen, Q. Q.; Zheng, Q. T.; Hao, X. J., *Angew. Chem. Int. Ed.Int. Edit.* **2015,** *54*, 5592.
29. Forgacs, P.; Provost, J.; Touche, A.; Guenard, D.; Guilhem, J., *Tetrahedron Lett.* **1985,** *26*, 3457.
30. Yang, W. Q.; Shao, X. H.; Deng, F.; Hu, L. J.; Xiong, Y.; Huang, X. J.; Fan, C. L.; Jiang, R. W.; Ye, W. C.; Wang, Y., *J. Nat. Prod.* **2020,** *83*, 1674.
31. Dewick, P. M., *Medicinal Natural Products: A Biosynthetic Approach* **2002**.

32. Boeno, S.; Passos, M.; Felix, M.; Vieira, M.; Junior, A.; Braz-Filho, R.; Vieira, I. J. C., *Stud. Nat. Prod. Chem.* **2021,** *68*, 97.
33. Joshi, B. C.; Sharma, R. P.; Khare, A., *Nat. Prod. Commun.* **2007,** *2*, 869.
34. Kubota, K.; Fukamiya, N.; Hamada, T.; Okano, M.; Tagahara, K.; Lee, K. H., *J. Nat. Prod.* **1996,** *59*, 683.
35. Takeya, K.; Kobata, H.; Ozeki, A.; Morita, H.; Itokawa, H., *J. Nat. Prod.* **1997,** *60*, 642.
36. Takeya, K.; Kobata, H.; Ozeki, A.; Morita, H.; Itokawa, H., *Phytochemistry* **1998,** *48*, 565.
37. Ishibashi, M.; Yoshimura, S.; Tsuyuki, T.; Takahashi, T.; Itai, A.; Iitaka, Y.; Matsushita, K., *Chem. Lett.* **1984,** 13, 555.
38. Chen, H.; Bai, J.; Fang, Z. F.; Yu, S. S.; Ma, S. G.; Xu, S.; Li, Y.; Qu, J.; Ren, J. H.; Li, L.; Si, Y. K.; Chen, X. G., *J. Nat. Prod.* **2011,** *74*, 2438.
39. Chumkaew, P.; Pechwang, J.; Srisawat, T., *J. Nat. Med.* **2017,** *71*, 570.
40. Chumkaew, P.; Phatthiya, A.; Werapun, U.; Srisawat, T., *Chem. Nat. Cmpd.* **2019,** *55*, 471.
41. Liu, J. H.; Jin, H. Z.; Zhang, W. D.; Yan, S. K.; Shen, Y. H., *Chem. Biodivers.* **2009,** *6*, 57.
42. Liu, J. Q.; Wang, C. F.; Li, X. Y.; Chen, J. C.; Li, Y.; Qiu, M. H., *Arch. Pharm. Res.* **2011,** *34*, 1297.
43. Zhan, Y. Z.; Tan, T.; Qian, K.; Yang, S. L.; Feng, Y. L.; Wen, Q., *Nat. Prod. Res.* **2020,** *34*, 1186.
44. Liu, J. H.; Zhao, N.; Zhang, G. J.; Yu, S. S.; Wu, L. J.; Qu, J.; Ma, S. G.; Chen, X. G.; Zhang, T. Q.; Bai, J.; Chen, H.; Fang, Z. F.; Zhao, F.; Tang, W. B., *J. Nat. Prod.* **2012,** *75*, 683.
45. Kupchan, S. M.; Britton, R. W.; Lacadie, J. A.; Ziegler, M. F.; Sigel, C. W., *J. Org. Chem.* **1975,** *40*, 648.
46. Delgoda, R.; Kandagatla, S. K.; Ranor, G.; Brantley, E.; Badal, S.; Francis, S.; Jacobs, H., *Planta Med.* **2015,** *81*, 948.
47. Grieco, P. A.; Moher, E. D.; Seya, M.; Huffman, J. C.; Grieco, H. J., *Phytochemistry* **1994,** *37*, 1451.
48. Dou, J. H.; McChesney, J. D.; Sindelar, R. D.; Goins, D. K.; Walker, L. A., *J. Nat. Prod.* **1996,** *59*, 73.
49. Meng, D. L.; Li, X.; Han, L. F.; Zhang, L. L.; An, W. W.; Li, X., *Fitoterapia* **2014,** *92*, 105.
50. Lahrita, L.; Hirosawa, R.; Kato, E.; Kawabata, J., *Bioorg. Med. Chem.* **2017,** *25*, 4829.
51. Francois, G.; Diakanamwa, C.; Timperman, G.; Bringmann, G.; Steenackers, T.; Atassi, G.; Van Looveren, M.; Holenz, J.; Tassin, J. P.; Assi, L. A.; Vanhaelen-Fastre, R.; Vanhaelen, M., *Int. J. Parasit.* **1998,** *28*, 635.
52. Lumonadio, L.; Vanhaelen, M., *Phytochemistry* **1985,** *24*, 2387.
53. Miralles, J.; Nongonierma, R.; Sagna, C.; Kornprobst, J. M.; Gaydou, E., *Rev. fr. Corps Gras* **1988,** *35*, 13.
54. Kamiuchi, K.; Mitsunaga, K.; Koike, K.; Ouyang, Y.; Ohmoto, T.; Nikaido, T., *Heterocycles* **1996,** *43*, 653.

55. Oshimi, S.; Takasaki, A.; Hirasawa, Y.; Hosoya, T.; Awang, K.; Hadi, A. H. A.; Ekasari, W.; Widyawaruyanti, A.; Morita, H., *Chem. Pharm. Bull.* **2009,** *57*, 867.
56. Diyabalanage, T.; Ratnayake, R.; Wilson, J. A.; Henrich, C. J.; Beutler, J. A.; Colburn, N. H.; McMahon, J. B.; Gustafson, K. R., *Bioorg. Med. Chem. Lett.* **2011,** *21*, 4397.
57. Usami, Y.; Nakagawa-Goto, K.; Lang, J. Y.; Kim, Y.; Lai, C. Y.; Goto, M.; Sakurai, N.; Taniguchi, M.; Akiyama, T.; Morris-Natschke, S. L.; Bastow, K. F.; Cragg, G.; Newman, D. J.; Fujitake, M.; Takeya, K.; Hung, M. C.; Lee, E.; Lee, K. H., *J. Nat. Prod.* **2010,** *73*, 1553.
58. Xu, J.; Xiao, D.; Song, W. W.; Chen, L.; Liu, W. Y.; Xie, N.; Feng, F.; Qu, W., *Fitoterapia* **2016,** *110*, 13.
59. Novello, C. R.; Ferreira, A. G.; Marques, L. C.; Cortez, D. A. G., *Nat. Prod. Res.* **2003,** *17*, 145.
60. Zhao, W. Y.; Song, X. Y.; Zhao, L.; Zou, C. X.; Zhou, W. Y.; Lin, B.; Yao, G. D.; Huang, X. X.; Song, S. J., *J. Nat. Prod.* **2019,** *82*, 714.
61. Cachet, N.; Ho-A-Kwie, F.; Rivaud, M.; Houel, E.; Deharo, E.; Bourdy, G.; Jullian, V., *Phytochem. Lett.* **2012,** *5*, 162.
62. Aarthy, T.; Mulani, F. A.; Pandreka, A.; Kumar, A.; Nandikol, S. S.; Haldar, S.; Thulasiram, H. V., *BMC Plant Biol.* **2018,** *18*, 21.
63. Finefield, J. M.; Sherman, D. H.; Kreitman, M.; Williams, R. M., *Angew. Chem. Int. Ed. Int. Edit.* **2012,** *51*, 4802.
64. Okhale, S. E.; Decatur, J.; Itagaki, Y.; Amupitan, J. O.; Ndukwe, G. I.; Ellestad, G.; Okogun, J. I., *Tetrahedron* **2014,** *70*, 6656.
65. Oliveira, D. R.; Krettli, A. U.; Aguiar, A. C. C.; Leitao, G. G.; Vieira, M. N.; Martins, K. S.; Leitao, S. G., *J. Ethnopharmacol.* **2015,** *173*, 424.
66. Chan, K. L.; Choo, C. Y.; Abdullah, N. R.; Ismail, Z., *J. Ethnopharmacol.* **2004,** *92*, 223.
67. Cachet, N.; Hoakwie, F.; Bertani, S.; Bourdy, G.; Deharo, E.; Stien, D.; Houel, E.; Gornitzka, H.; Fillaux, J.; Chevalley, S.; Valentin, A.; Jullian, V., *Antimicrob. Agents. Chemother.* **2009,** *53*, 4393.
68. Cabral, J. A.; McChesney, J. D.; Milhous, W. K., *J. Nat. Prod.* **1993,** *56*, 1954.
69. Muhammad, I.; Bedir, E.; Khan, S. I.; Tekwani, B. L.; Khan, I. A.; Takamatsu, S.; Pelletier, J.; Walker, L. A., *J. Nat. Prod.* **2004,** *67*, 772.
70. Silva, E. C. C.; Cavalcanti, B. C.; Amorim, R. C. N.; Lucena, J. F.; Quadros, D. S.; Tadei, W. P.; Montenegro, R. C.; Costa-Lotufo, L. V.; Pessoa, C.; Moraes, M. O.; Nunomura, R. C. S.; Nunomura, S. M.; Melo, M. R. S.; de Andrade-Neto, V. F.; Silva, L. F. R.; Vieira, P. P. R.; Pohlit, A. M., *Mem. Inst. Oswaldo Cruz* **2009,** *104*, 48.
71. Fukamiya, N.; Okano, M.; Tagahara, K.; Aratani, T.; Lee, K. H., *J. Nat. Prod.* **1988,** *51*, 349.
72. Imamura, K.; Fukamiya, N.; Nakamura, M.; Okano, M.; Tagahara, K.; Lee, K. H., *J. Nat. Prod.* **1995,** *58*, 1915.
73. Tan, B. Q.; Huang, Y. Y.; Lan, L. H.; Zhang, B.; Ye, L. J.; Yan, W.; Wang, F.; Lin, N. M., *Biomed. Pharmacother.* **2019,** *117*, 5.
74. Kim, I. H.; Suzuki, R.; Hitotsuyanagi, Y.; Takeya, K., *Tetrahedron* **2003,** *59*, 9985.

75. Kim, I. H.; Takashima, S.; Hitotsuyanagi, Y.; Hasuda, T.; Takeya, K., *J. Nat. Prod.* **2004,** *67*, 863.
76. Investigational Drug Branch, C. T. E. P., Division of Cancer Treatment, National Cancer Institute, Bruceantin 1978, Clinical Brochure.
77. Wang, Y.; Wang, W. J.; Su, C.; Zhang, D. M.; Xu, L. P.; He, R. R.; Wang, L.; Zhang, J.; Zhang, X. Q.; Ye, W. C., *Bioorg. Med. Chem. Lett.* **2013,** *23*, 654.
78. Grieco, P. A.; Ferrino, S.; Vidari, G., *J. Am. Chem. Soc.* **1980,** *102*, 7586.
79. Vidari, G.; Ferrino, S.; Grieco, P. A., *J. Am. Chem. Soc.* **1984,** *106*, 3539.
80. Kim, M.; Kawada, K.; Gross, R. S.; Watt, D. S., *J. Org. Chem.* **1990,** *55*, 504.
81. Stojanac, N.; Sood, A.; Stojanac, Z.; Valenta, Z., *Can. J. Chem.; Rev. Can. Chim.* **1975,** *53*, 619.
82. Stojanac, N.; Stojanac, Z.; White, P. S.; Valenta, Z., *Can. J. Chem.; Rev. Can. Chim.* **1979,** *57*, 3346.
83. Stojanac, N.; Valenta, Z., *Can. J. Chem.* **1991,** *69*, 853.
84. Shing, T. K. M.; Tang, Y., *Tetrahedron* **1990,** *46*, 2187.
85. Shing, T. K. M.; Tang, Y., *J. Chem. Soc.; Chem. Commun.* **1992,** 341.
86. Shing, T. K. M.; Jiang, Q.; Mak, T. C. W., *J. Org. Chem.* **1998,** *63*, 2056.
87. Shing, T. K. M.; Jiang, Q., *J. Org. Chem.* **2000,** *65*, 7059.
88. Hirota, H.; Takahashi, T., *J. Synth. Org. Chem. Jpn.* **1987,** *45*, 1199.
89. Hirota, H.; Yokoyama, A.; Miyaji, K.; Nakamura, T.; Igarashi, M.; Takahashi, T., *J. Org. Chem.* **1991,** *56*, 1119.
90. Hirota, H.; Yokoyama, A.; Miyaji, K.; Nakamura, T.; Takahashi, T., *Tetrahedron Lett.* **1987,** *28*, 435.
91. Vanderroest, J. M.; Grieco, P. A., *J. Am. Chem. Soc.* **1993,** *115*, 5841.
92. Kerwin, S. M.; Paul, A. G.; Heathcock, C. H., *J. Org. Chem.* **1987,** *52*, 1686.
93. Sasaki, S.; Grieco, P. A.; Huffman, J. C.; Callant, P.; Imamura, P. M., *J. Org. Chem.* **1985,** *50*, 4880.
94. Snitman, D. L.; Himmelsbach, R. J.; Watt, D. S., *J. Org. Chem.* **1978,** *43*, 4758.
95. Snitman, D. L.; Watt, D. S., *Synth. Commun.* **1978,** *8*, 187.
96. Grieco, P. A.; Collins, J. L.; Moher, E. D.; Fleck, T. J.; Gross, R. S., *J. Am. Chem. Soc.* **1993,** *115*, 6078.
97. Grieco, P. A.; Speake, J. D., *J. Org. Chem.* **1998,** *63*, 5929.
98. Gross, R. S.; Grieco, P. A.; Collins, J. L., *J. Am. Chem. Soc.* **1990,** *112*, 9436.
99. Fleck, T. J.; Grieco, P. A., *Tetrahedron Lett.* **1992,** *33*, 1813.
100. Moher, E. D.; Collins, J. L.; Grieco, P. A., *J. Am. Chem. Soc.* **1992,** *114*, 2764.
101. Collins, J. L.; Grieco, P. A.; Gross, R. S., *J. Org. Chem.* **1990,** *55*, 5816.
102. Grieco, P. A.; Nargund, R. P.; Parker, D. T., *J. Am. Chem. Soc.* **1989,** *111*, 6287.
103. Grieco, P. A.; Parker, D. T.; Nargund, R. P., *J. Am. Chem. Soc.* **1988,** *110*, 5568.
104. Grieco, P. A.; Cowen, S. D.; Mohammadi, F., *Tetrahedron Lett.* **1996,** *37*, 2699.
105. Shing, T. K. M.; Yeung, Y. Y., *Angew. Chem. Int. Ed. Int. Edit.* **2005,** *44*, 7981.

Chapter 2

Development of a Copper-Catalyzed Double Coupling and Application Towards the Quassinoid Core Architecture

2.1 Retrosynthetic Analysis

Upon evaluating quassin (**1**), we and others have noted the pseudo symmetry found within its core architecture. With this consideration in mind, we were particularly inspired by Mandell's synthetic approach wherein they explored the merger of aldehyde **158** and acid chloride **159** to generate pseudo-symmetric compound **160**. They then proposed an ambitious key intramolecular Diels-Alder cycloaddition to construct the final two carbon-carbon bonds and the tetracyclic quassinoid core. It is worth noting that Mandell's chosen bis(orthoquinone) **160** contains all of the requisite carbons for completion of the natural product and is also highly oxidized. This latter feature would make lengthy oxidation sequences after cyclization unnecessary, which was a major contributor to the length of many previous syntheses. Regrettably, their attempts to cyclize were unsuccessful likely due to the inability of their chosen substrate to adopt a reactive confirmation for Diels-Alder cycloaddition and potential electronic mismatching of the diene and dienophile components.[1]

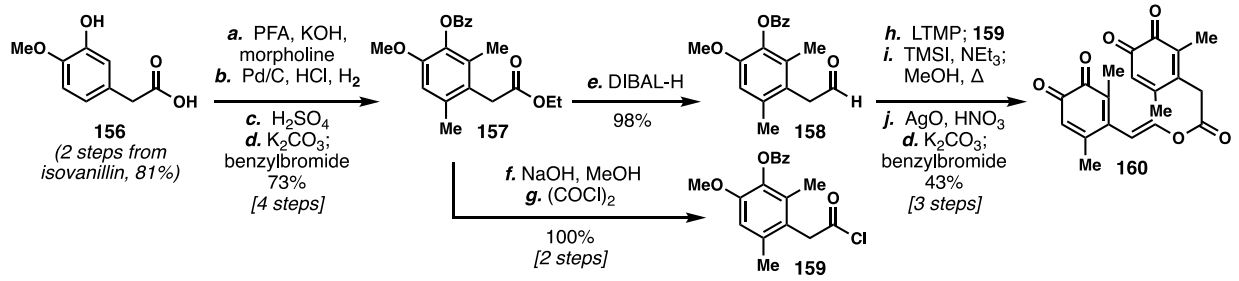

Figure 2.1: Mandell's synthetic approach to the quassinoid core leveraging the latenent symmetry of quassin.

Although Mandell's approach was unsuccessful, it inspired us to use the innate pseudo-symmetry of the quassinoid core in our synthetic strategy. Instead of tethering the A and C rings together and trying to generate the B and D rings simultaneously, we rationalized that we could elaborate the A and C rings from a pre-constructed B-ring (Figure 2.2 A). Since the B-ring remains mostly conserved throughout the quassinoids, we envisioned a transformation to doubly functionalize a B-ring precursor (carvone epoxide, **161**) with two of the same two-carbon units. Specifically, we hoped that this transformation could be accomplished with two oxidized vinyl coupling partners. From our vinylated intermediate (Figure 2.2 C), we then envisioned an intramolecular Diels-Alder reaction could forge the C and D rings simultaneously. A Prins or ene-type reaction could then be used to complete the A ring and the tetracyclic quassinoid core (Figure 2.2 B).

To approach our proposed double coupling, drawing inspiration from the literature, we focused on two transformations, specifically ketone functionalizations. The first was Wender's allylic substitution, or S_N2', of the enolates, enol ethers, and enol phosphates of epoxy ketones with organocuprates (Figure 2.3 A).[2] Notably, Wender attempted to use both organolithium and Grignard reagents in this transformation, but they exclusively gave the expected substitution products. The second transformation guiding our work was McMurry's seminal cross-coupling of vinyl triflates with organocuprates; wherein, without the mediation of other transition metal catalysts, they were able to directly couple cuprates with vinyl triflates (Figure 2.3 B).[3-4] The question we then posed was from the enol triflate of carvone epoxide, could we perform both an allylic substitution and cross-coupling transformation in one pot? Before attempting to answer our primary question, we took into consideration several factors regarding reactivity, regioselectivity, and diastereoselectivity in organometallic S_N2' chemistry. While copper-catalyzed cross-couplings have been observed with a variety of nucleophiles, only lithiates and Grignard reagents have successfully performed cross-couplings with vinyl triflates.[5-11] As for the selectivity, in Wender's studies they were able to exclusively produce the allylic substitution products by using organocuprates;[2] however, several others have faced challenges when trying to select for the S_N2' pathway over the S_N2.[12] As for the diastereoselectivity, there is precedence to favor the *anti*-S_N2' addition products.[13-16] Corey and

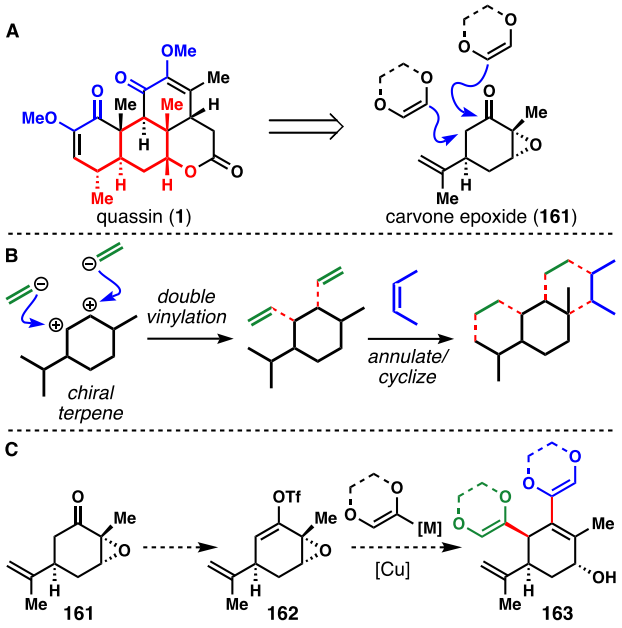

Figure 2.2: (A) Synthetic strategy towards quassin utilizing carvone epoxide as a B-ring precursor. (B) Double vinylation strategy to construct the A and C rings after successive cyclization. (C) Desired novel double coupling strategy to access the quassinoid architecture.

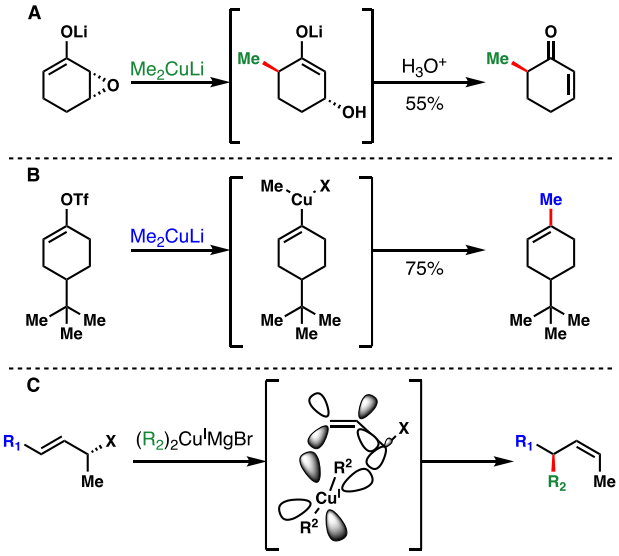

Figure 2.3: (A) Precedence for copper-catalyzed allylic substitution of the enolate of epoxy ketones. (B) Precedence for the copper-catalyzed cross-coupling of vinyl triflates. (C) Proposed mode for *anti*-selectivity of copper-catalyzed allylic substitutions.

others propose a dual coordination of the copper species to both the olefin and the leaving group gives rise to the *anti*-selectivity (Figure 2.3 C).[16] Although this precedent was encouraging, the exact outcomes for our desired transformation were far from obvious, particularly when considering a catalytic system involving unidentified and/or mixed copper-containing species. Moreover, the sterically demanding isopropenyl group also needed to be taken into account in considering possible reagent trajectories in this system.

2.2 Development of a Copper-Catalyzed Double Coupling

At the outset of our work, we chose to explore this transformation using a methyl Grignard nucleophile (MeMgBr) and model substrate **164**. Although for the quassinoid system we wanted to use carvone epoxide, we chose to establish initial reactivity using **164** to exclude potential complications presented by the bulky isopropenyl group. To perform the desired double coupling, from **164**, we first needed to form the vinyl triflate **165**. While small amounts of this triflate **165** could be isolated, the lack of stability made it challenging to access larger quantities for screening reaction conditions. We therefore reasoned that given both reaction conditions for the triflation and proposed double coupling were in THF we could directly attempt the double coupling on the triflate formed *in situ*. Gratifyingly, when we directly tried the double coupling, we isolated our desired cross-coupled/allylic substituted species as a mixture of diastereomers. We theorized that the modest selectivity observed could be due to excess Grignard in solution reacting prior to the cuprate. By running the negative control (no copper catalyst) we were able to observe allylic substitution on our substrate giving credence to this hypothesis.

After our initial success, we then explored the structure of the presumed copper species to try and increase not only yield, but diastereoselectivity. To generate our Gilman-type cuprates, we initially used methyl magnesium bromide; however, we noted in our literature survey that Wender found success when using the corresponding lithiate as a precursor.[2] However, when we attempted to use methyl lithium to access the corresponding cuprate we saw no reactivity. The magnesium chloride and iodides while compatible, were significantly lower yielding than their bromide counterpart. We therefore chose to move forward examining the copper source while using the original methyl magnesium bromide. We were pleased to find that a variety of copper salts were competent in this transformation giving comparable yields (Table 2.1, entries 1-5), but varying selectivities. Notably, though most copper sources gave higher *anti* selectivity as expected, the copper N-heterocyclic carbene (NHC) complex had a slight preference for the *syn* diastereomer (Table 2.1 entry 6). We rationalized this could be due to the very bulky NHC ligand blocking approach from the beta-face (where the methyl group resides) while excess Grignard in solution reacted indiscriminately with the allylic system. After extensive screening of copper sources, we identified that tetrakis(acetonitrile)copper(I)

hexafluorophosphate [Cu(MeCN)$_4$][PF$_6$] (Table 2.1, entry 5) performed the best,[1] giving both the highest yield and selectivity.

Although we could now observe good yields (average of approximately 80% per transformation)[17] and decent selectivity, we wondered if there was a way to further increase the selectivity of our transformation. We first examined TMSCl as an additive, which has found success in copper-mediated conjugate addition reactions;[18] however, no improvements in diastereoselectivity or yield were observed. We then looked into a number of polar additives that could potentially impact the reaction.[19-20] Gratifyingly, we found that when hexamethylphosphoramide (HMPA, Table 2.1, entry 7) was added we could generate our desired double-coupled products as a single diastereomer. Replacement of HMPA with conventional alternatives such as tetramethylenediamine (TMEDA,Tablle 2.1, entry 9) and *N,N*-Dimethylpropyleneurea (DMPU, Table 2.1, entry 8) were also examined but found to be inferior. Lastly, we briefly studied the catalyst loading and identified that adding less than 15 mol% (5 mol% with respect to the Grignard or lithiate) of the copper source caused a steep decline in the yield of the transformation even with extended reaction times.

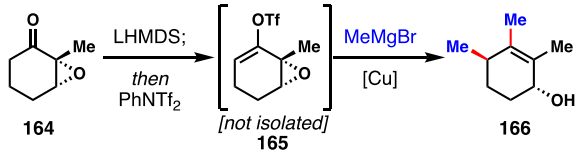

164 165 166

entry	[Cu]	x (mol%)[a]	additive[b]	yield(%)[c]	d.r.[d]
1	CuCl	15	—	43%	3:1
2	CuBr	15	—	42%	3:1
3	CuI	15	—	43%	4:1
4	CuOTf•C_6H_6	15	—	44%	2:1
5	[Cu(MeCN)$_4$]PF$_6$	15	—	43%	7:1
6	(*i*Pr)CuCl	15	—	41%	1:2
7[f]	**[Cu(MeCN)$_4$]PF$_6$**	**15**	**HMPA**	**46%**	**>20:1**
8	[Cu(MeCN)$_4$]PF$_6$	15	DMPU	32%	4:1
9	[Cu(MeCN)$_4$]PF$_6$	15	TMEDA	23%	4:1
10	[Cu(MeCN)$_4$]PF$_6$	15	TMSCl	13%	4:1
11	[Cu(MeCN)$_4$]PF$_6$	15	diglyme	47%	4:1
12	[Cu(MeCN)$_4$]PF$_6$	7.5	HMPA	23%	>20:1
13	[Cu(MeCN)$_4$]PF$_6$	30	HMPA	41%	>20:1

Table 2.1: Standard reaction conditions: epoxide (0.1 mmol, 1.0 equiv), LHMDS (0.1 mmol, 1.0 equiv), PhNTf$_2$ (0.1 mmol, 1.0 equiv), –78 0 ºC, 5 min; then add a solution of MeMgBr (0.3 mmol, 3.0 equiv), [Cu] (X mol%), and additive, 0ºC, 1 hr. [a] mol% with respect to epoxide starting material. [b] Additives included at 5.0 equiv. [c] Isolated yield of **166** after column chromatograpy. [d] Determined by ^{1}HNMR of the crude reaction mixture. [e]Reaction performed using 1.0 mmol of epoxide starting material.

With our reaction suitably optimized, we began our investigation into the scope of this transformation (Figure 2.4). Within the copper-catalyzed coupling literature, one of the challenges has been the use of aryl nucleophiles dues to their lower reactivity compared to their alkyl counterparts.[6-7] However, we found that a wide range of aryl Grignard reagents perform exceptionally well in this transformation. We were pleased to find that both electron-rich and electron-poor aromatic nucleophiles performed well in this transformation (**167**-**173**), giving both high yield and selectivity with a few exceptions. The electron-rich aromatic heterocycles thiophene gave exclusively the allylic substitution product (**186**). Vinyl nucleophiles also performed well in this transformation to give single diastereomers of highly crystalline products (**174**-**175**). We were able to confirm the *anti*-selectivity via X-ray crystallographic analysis of compound **175**. It is important to note that alkyl nucleophiles were much more challenging within this transformation, with the exception of methyl Grignard (**166**), as

they tended to give significantly lower yields likely due to the major competing pathway involving proto de-triflation (see **183**).

Two substrates warrant particular mention at this point. The first is the allyl Grignard product (**177**), which was afforded as a 1:1 *anti*/*syn* mixture of products. We believe this is due to the exceptional nucleophilicity of allyl Grignard as a nucleophile as it is known to react at approximately the diffusion rate limit with certain ketones.[21] The second is the 2,2'-biphenyl product **176** derived from a biphenyl *bis*-Grignard reagent. The inspiration behind this substrate was to investigate whether we could extend this methodology to the construction of carbocyclic rings via annulation. In initial screening,

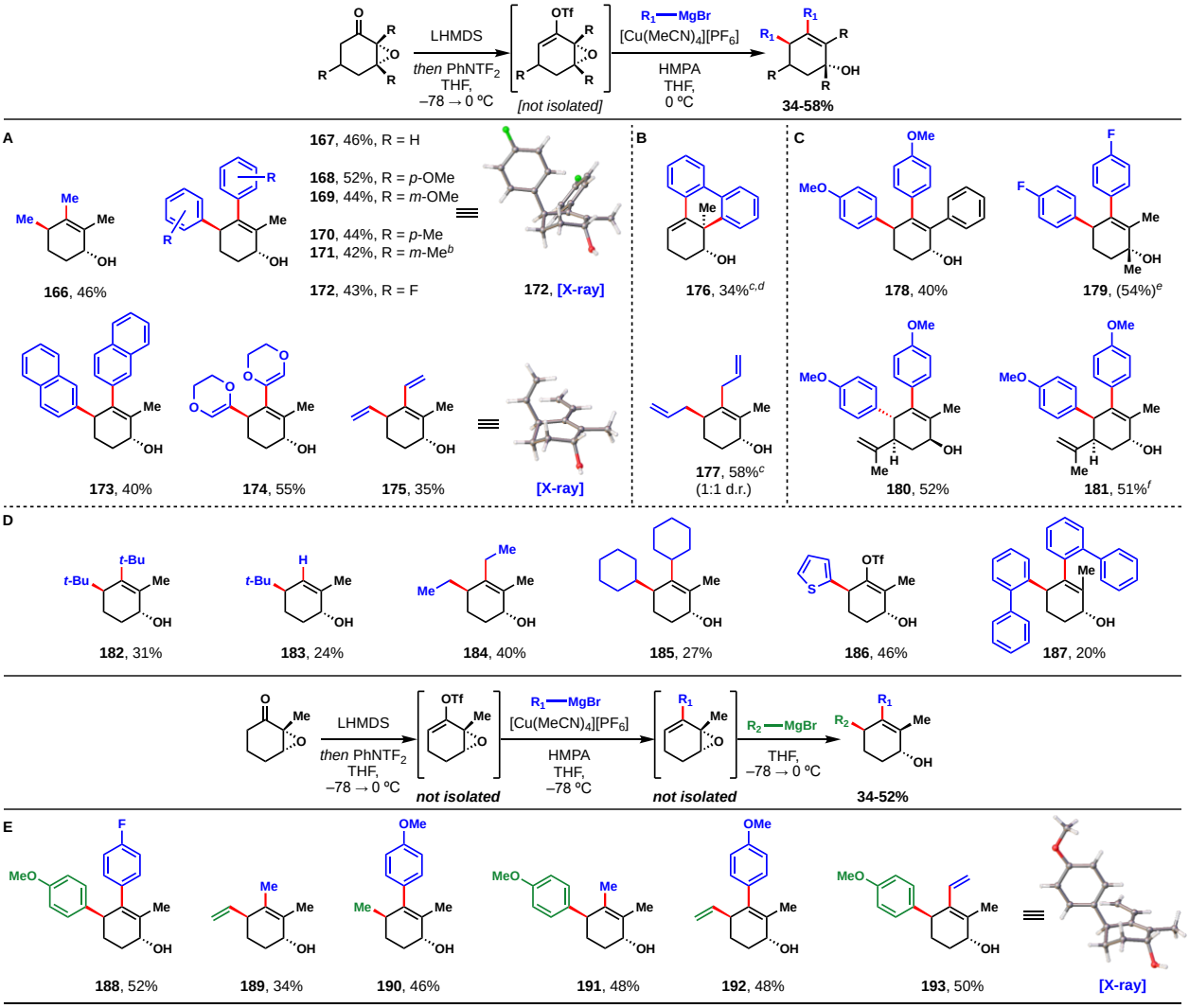

Figure 2.4: Copper-catalyzed double coupling of epoxy ketones and Grignard reagents: (A) Scope with two of the same Grignard reagents. (B) Anomalous products, see main text for further discussion. (C) Use of different epoxides. (D) Problematic substates. (E) Coupling of two different nucleophiles. [a]Reactions were run with 1.0 mmol of epoxide under the optimized conditions. Reported yields are of products isolated as single isomers, except where otherwise indicated. [b]10:1 d.r. [c]CuI used in place of $[Cu(MeCN)_4][PF_6]$ and no HMPA added. [d]2.0 equiv of 2,2'-biphenyldimagnesium bromide used as nucleophile. [e]NMR yield using 1,3,5-trimethoxybenzene as an internal standard. [f]30 mol% loading of $[Cu(MeCN)_4]$ $[PF_6]$ used.

using $[Cu(MeCN)_4][PF_6]$ we observed mono-substitution of two biphenyl units (see **187**) as a mixture with what we believed at the time to be our desired cross-coupled/allylic substitution product. However, when we performed the same reaction using instead copper(I) iodide, we determined that we had instead formed a cross-coupled, S_N2 substituted substrate (**176**) thus forming an all-carbon quaternary center. We theorized that this product likely resulted from a rapid, possibly non-copper catalyzed, intramolecular transformation following an initial SN2' event. Efforts are ongoing to expand this proof-of-concept system to saturated alkyl dinucleophiles.

Further surveying the substrate scope, we next explored alternative epoxide substrates. Gratifyingly, we discovered that a number of more sterically encumbered environments were tolerated in this transformation. Exchanging the 2-methyl group for a phenyl group did not impact reactivity (see **178**). Incorporating substitution at the 3-position, likewise, did not impact the success of the transformation (**179**); however, the tertiary allylic alcohol moiety was extremely acid sensitive and would rapidly decompose upon column chromatography even when using an acid-neutralized stationary phase. We were pleased to note that both diastereomers of carvone epoxide performed well under the reaction conditions (see **180** and **181**). Notably, the *trans*-epoxide (with respect to the isopropenyl group) was able to overcome the inherent steric bias presented by the isopropenyl group to give the *anti*-allylic substitution product selectively.

Having thoroughly explored this transformation to append on two of the same nucleophiles, we wanted to know whether we could differentiate the two transformations thus incorporating two different nucleophilic fragments. To probe the sequence of transformations in our system we slowly titrated in one Grignard species at cryogenic temperatures until we observed complete consumption of the triflate intermediate. The observed product from this experiment was an exclusively cross-coupled species. We then repeated our findings, but now added a second Grignard reagent and allowed the reaction mixture to warm to 0 ºC; under these conditions the second allylic substitution occurred. With this result, we now had the ability to install various functionalities in a modular manner (**188**-**193**). Alkyl, vinyl, and aromatic Grignard nucleophiles were all tolerated in this reaction sequence. We noted, importantly, that it was the order of addition and temperature selection that determined the order of reactivity and not the individual identity of the nucleophile. This is best exemplified by isomeric compounds **190** and **191** and **192** and **193** (confirmed by X-ray crystallography), which were easily accessed through our modified procedure. Having now explored the breadth of this transformation, we went on to apply it to the synthesis of the quassinoid framework.

2.3 Three-Step Synthesis to Tetracyclic Quassinoid Architecture.

To access the quassinoid architecture, we wanted to use a vinyl nucleophile in combination with the *cis* isomer of 6-methyl carvone epoxide and apply our double coupling strategy. While a simple vinyl group could be utilized in this transformation, it lacked much of the high oxidation found in the natural product. We therefore identified dioxene as a potential candidate as it not only contained the desired olefin moiety but also contained additional oxidation on both alkenyl carbons.[22] Thus, we devised a model system using *trans*-carvone epoxide (**161**) to explore this synthetic strategy.

Using our copper methodology, we now combined the enol triflate of carvone epoxide (**162**) with the dioxene nucleophile. Gratifyingly, we found that it performed exceptionally in this reaction sequence giving one of the highest yields observed for this transformation. This product (**163**) was also highly crystalline like the other vinyl substituted products using the model substrate (**174** and **175**, Figure 2.4). We therefore confirmed the *anti*-selectivity using X-ray crystallography.

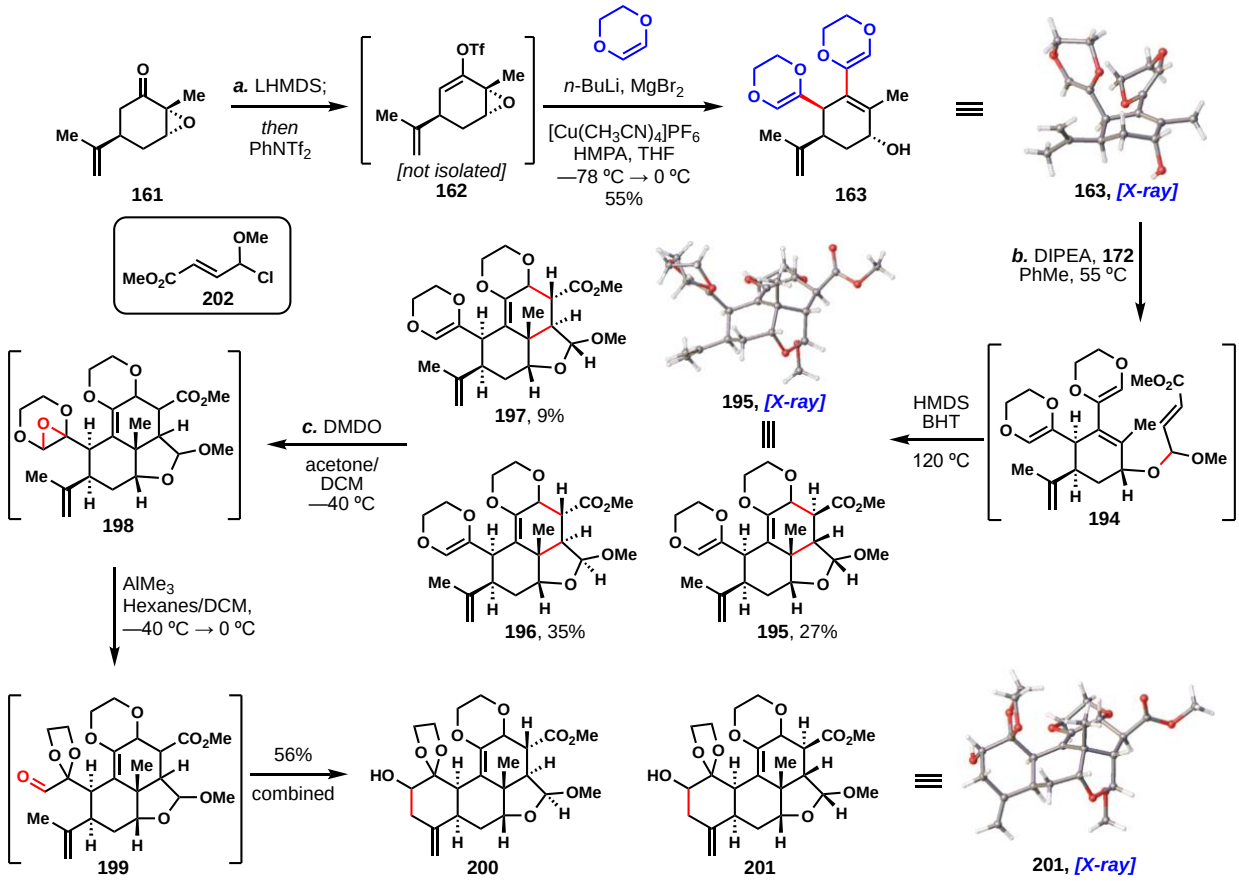

Figure 2.5: 3-Step synthesis of the quassinoid core architecture. Reagents and conditions: (a) LHMDS (1.0 equiv), $PhNTf_2$ (1.0 equiv), THF, 78 / 0 °C, 5 min, then add a solution of CuI (0.35 equiv.) and dioxenyl Grignard (3.5 equiv), THF, 0 °C, 16 h, 58%; (b) DIPEA (4.0 equiv), dienophile (2.0 equiv), PhMe, 23 °C, 12 h, then add PhMe, HMDS, 110 °C, 3d, 71% (Σ of isomers); (c) DMDO (1.0 equiv.) then add $AlMe_3$ (1.5 equiv), DCM/acetone 40 °C / 0 °C, 10 min, 56%.

From this intermediate, we then focused on the construction of the C and D rings, which we thought could arise from an intramolecular Diels-Alder reaction with the dioxene moiety[23-24] tethered through the allylic alcohol. To this end, a number of potential tethers were examined for the use in this transformation. The ideal tether would contain both the correct oxidation state and form an ester linkage when appended onto our intermediate; however, we also needed to consider the electronics and rigidity of the system. We observed during exploration of the copper methodology, that even weak acids (for example silica gel) could catalyze the elimination of the allylic alcohol moiety. This phenomenon was even more pronounced with the dioxene coupling product, as the pendant dioxene oxygen can facilitate the expulsion of the allylic alcohol via an oxocarbenium intermediate. Therefore, ether-linked tethers were more advantageous over their ester counterparts due to the lower propensity for elimination. Of the ether-linked tethers, we eventually discovered that the compound **202** was the best electronic match for this Diels-Alder system. Using the corresponding chloromethyl methyl ether, we alkylated the allylic oxygen to obtain a 1:1 mixture of acetal diastereomers (**194**), which could then be cyclized *in situ* by refluxing the reaction mixture. Interestingly, the acetal stereochemistry had a significant influence on the *endo/exo* Diels-Alder selectivity. The (*S*)-acetal diastereomers, gave exclusively the *endo* cyclization product (**196**); whereas, the (*R*)-acetal preferred the *exo* cyclization (3:1 *exo/endo*, **195**/**197**). The major *exo* cyclization product **195** was confirmed by X-ray crystallography. Since the non-matching stereocenters for each diastereomer would either be ablated or could be epimerized,[25] the two major diastereomers were then taken forward in the synthesis as a mixture.

At this stage, all that remained in the completion of the quassinoid core, was the construction of the A-ring. Previous work by Hanna and coworkers had shown that epoxidized derivatives of substituted dioxenes can rapidly rearrange to give aldehydes under acidic conditions.[26] We thought we could utilize this rearrangement and intercept the aldehyde intermediate to perform an intramolecular ene or Prins-type reaction to assemble the A-ring. Using DMDO, we could selectively epoxidize the desire dioxene olefin (**198**). We could then react the epoxide with Lewis acid *in-situ* to catalyze the rearrangement to the aldehyde (**199**) followed by a subsequent ene reaction. We found that trimethylaluminum worked the best to give mixture of diastereomers **170** and **171**. With the success of our model system and the validation of dioxene as a competent building block in the quassinoid architecture, we then sought to apply our strategy to a pre-alkylated substrate, 6-methyl carvone epoxide, that would generate the critical quaternary center between the A and B rings of quassin (**1**).

2.4 Conclusion

Inspired by the highly oxidized architecture and the myriad biological activities presented throughout the quassinoid family of natural products, we sought construction

of quassin in an efficient manner. To this end, we developed a novel copper-catalyzed double coupling to rapid elaborate cyclic keto epoxides to the corresponding allylic alcohol in one pot. We then elaborated this methodology to a true three-component coupling by differentiating the cross-coupling and allylic substitution transformation to append two different nucleophiles to out keto epoxides in one pot. We then applied our methodology to the construction of the quassinoid core using a model system that does not contain the C10 quaternary methyl group found in the natural product (**1**). In only 3 steps we were able to construct a tetracyclic system resembling that of quassin (**1**) with 7 stereocenters. Key to this efficiency was the using of tandem and cascade processes.

2.5 Distribution of Credit and Acknowledgements

Matt L. Condakes (M.L.C.) initially discovered the copper-catalyzed double coupling reaction and explored a preliminary substrate scope of this transformation with Stephen J. Harwood. Rachel Z. Rosen (R.Z.R.) completed the optimization of the copper-catalyzed double coupling reaction including identification of the optimal copper-catalyst system. R.Z.R performed mechanistic experiments which enabled conditions for the coupling of two different nucleophiles to be developed. M.L.C. and R.Z.R. collaboratively executed and characterized the final substrate scope of the methodology. The route to the full quassinoid architecture was conceptualized by M.L.C. and T.J.M. M.L.C. executed, optimized, and characterized the synthetic route and R.Z.R also executed the copper-catalyzed coupling for the synthetic route.

We are grateful to Hasan Celik for NMR spectroscopic assistance wherein NIH grant GM68933 is acknowledged. Dr. Nick Settineri, Dr. Simon Teat, and Peter Waller are acknowledged for X-ray crystallographic analysis wherein support from NIH Shared Instrument Grant (S10-RR027172) is also acknowledged.

2.6 References

1. Mandell, L.; Lee, D. E.; Courtney, L. F. *J. Org. Chem.* **1982,** *47*, 610.
2. Wender, P. A.; Erhardt, J. M.; Letendre, L. J. *J. Am. Chem. Soc.* **1981,** *103*, 2114.
3. Scott, W. J.; McMurry, J. E., *Accounts Chem. Res.* **1988,** *21*, 47-54.
4. McMurry, J. E.; Scott, W. J., *Tetrahedron Lett.* **1980,** *21*, 4313.
5. Xuan, J.; Zhu, A.; Ma, B. J.; Ding, H. F., *Org. Lett.* **2018,** *20*, 4153.
6. Thapa, S.; Vangala, A. S.; Giri, R., *Synthesis* **2016,** *48*, 504.
7. Thapa, S.; Shrestha, B.; Gurung, S. K.; Giri, R., *Org. Biomol. Chem.* **2015,** *13* , 4816.
8. Thapa, S.; Kafle, A.; Gurung, S. K.; Montoya, A.; Riedel, P.; Giri, R., *Angew. Chem. Int. Ed.* **2015,** *54*, 8236.
9. Karlstrom, A. S. E.; Ronn, M.; Thorarensen, A.; Backvall, J. E., *J. Org. Chem.* **1998,** *63*, 2517.

10. Jonasson, C.; Ronn, M.; Backvall, J. E., *J. Org. Chem.* **2000,** *65* (7), 2122-2126.
11. Hintermann, L.; Xiao, L.; Labonne, A., *Angew. Chem. Int. Ed.* **2008,** *47*, 8246.
12. Kar, A.; Argade, N. P., *Synthesis* **2005,** 18, 2995.
13. Yoshikai, N.; Zhang, S. L.; Nakamura, E., *J. Am. Chem. Soc.* **2008,** *130*, 12862.
14. Yoshikai, N.; Nakamura, E., *Chem. Rev.* **2012,** *112*, 2339.
15. Sheng, W. H.; Wang, M.; Lein, M.; Jiang, L. B.; Wei, W. X.; Wang, J. Y., *Chem.-Eur. J.* **2013,** *19* , 14126.
16. Corey, E. J.; Boaz, N. W., *Tetrahedron Lett.* **1984,** *25*, 3063.
17. Fogg, D. E.; dos Santos, E. N., *Coord. Chem. Rev.* **2004,** *248*, 2365.
18. Lipshutz, B. H.; Hackmann, C., *J. Org. Chem.* **1994,** *59*, 7437.
19. Suzuki, H.; Yoshida, Y.; Osuka, A., *Chem. Lett.* **1982,** 11, 135.
20. Tsuruya, S.; Kawamura, T.; Yonezawa, T., *J Polym. Sci, Part A: Polym. Chem.* **1971,** *9*, 1659.
21. Read, J. A.; Woerpel, K. A., *J. Org. Chem.* **2017,** *82*, 2300.
22. Kravina, A. G.; Carreira, E. M., *Angew. Chem.Int. Ed.* **2018,** *57*, 13159.
23. Blanchotcourtois, V.; Fetizon, M.; Hanna, I., *Tetrahedron Lett.* **1992,** *33*, 5061.
24. Fetizon, M.; Goulaouic, P.; Hanna, I.; Prange, T., *J. Org. Chem.* **1988,** *53*, 5672.
25. Valenta, Z.; Podesva, C.; Papadopol, S., *Tetrahedron* **1961,** *15*, 100.
26. Baylon, C.; Hanna, I., *Tetrahedron Lett.* **1995,** *36*, 6475.

Supporting Information for

Chapter 2

Development of a Copper-Catalyzed Double Coupling and Applications Towards the Quassinoid Core Architecture

SI2.1 General Procedures:

All reactions were performed in flame- or oven-dried glassware under a positive pressure of nitrogen or argon, unless otherwise noted. Air- and moisture-sensitive liquids were transferred via syringe. Volatile solvents were removed under reduced pressure rotary evaporation below 35 °C. Analytical and preparative thin-layer chromatography (TLC) were performed using glass plates pre-coated with silica gel (250 μm thickness, 10 μm particle size, Millipore Sigma) impregnated with a fluorescent indicator (254 nm). TLC plates were visualized by exposure to ultraviolet light (UV) and then were stained by submersion in an ethanolic anisaldehyde solution, followed by brief heating on a hot plate. Flash column chromatography was performed employing silica gel purchased from Fisher (60 Å, 230-400 mesh, 40-63 μm).

Anhydrous tetrahydrofuran (THF), diethyl ether (Et_2O), toluene (PhMe), and dichloromethane (DCM) were obtained by passing these previously degassed solvents through activated alumina columns. Hexamethylphosphoramide (HMPA) was distilled over calcium hydride and stored under inert atmosphere. Though commercially available, *cis*-carvone epoxide could also be prepared according to the literature procedure.[1] Additional epoxide substrates were prepared following established literature protocols,[2] with the exception of 2,3-epoxy-2-methyl-cyclohexanone, which is uncharacterized in the literature. Dimethyldioxirane (DMDO) was prepared according to the *Organic Synthesis* procedure.[3] Lithium bis(trimethylsilyl)amide was purchased as a 1.0 M solution in THF from Millipore Sigma and used as received. N-Phenyl-bis(trifluoromethanesulfonamide) was purchased from Oakwood Chemicals and used as received. Grignard reagents were purchased from Millipore Sigma and used as received, except where otherwise indicated. $[Cu(MeCN)_4][PF_6]$ was purchased from Millipore Sigma and used as received. All other solvents and reagents, including additional copper sources, were purchased at the highest commercial grade and used as received, without additional purification.

Proton nuclear magnetic resonance (^{1}H NMR) spectra and carbon nuclear magnetic resonance (^{13}C NMR) spectra were recorded on Bruker DRX 500 (500 MHz/126 MHz), Bruker AV 500 (500 MHz/126 MHz), Bruker AV 600 (600 MHz/151 MHz), or Bruker AV 700 (700 MHz/176 MHz) spectrometers at 23 °C. Fluorine nuclear magnetic resonance (^{1}F NMR) spectra were recorded on a Bruker AVQ 400 (376 MHz) spectrometer at 23 ºC. Proton chemical shifts are expressed as parts per million (ppm, δ scale) and are referenced to residual protium in the NMR solvent ($CHCl_3$: δ 7.26, C_6D_5H: δ 7.16, CD_2HOD: δ 3.31). Carbon chemical shifts are expressed as parts per million (ppm, δ scale) and are referenced to the carbon resonance of the NMR solvent ($CDCl_3$: δ 77.16, C_6D_6: 128.06, CD_3OD: δ 49.00). Fluorine chemical shifts are expressed as parts per million (ppm, δ scale) and are not additionally referenced. Data are represented as follows: chemical shift, multiplicity (s = singlet, d = doublet, t = triplet, q = quartet, m = multiplet, br = broad), coupling constant (*J*) in Hertz (Hz), and integration. Infrared (IR) spectra were recorded on a Bruker Alpha FT-IR spectrometer as thin films and are reported in frequency of absorption (cm^{-1}). Optical rotations were recorded on a Perkin Elmer polarimeter, model 241. High-resolution mass spectra were obtained at the QB3/Chemistry Mass Spectrometry Facility at University of California, Berkeley using a Thermo LTQ-FT mass spectrometer, and at the Lawrence Berkeley National Laboratory Catalysis Center using a Perkin Elmer AxION 2 TOF mass spectrometer. X-ray diffraction

data for compounds were collected at the Small Molecule X-ray Crystallography Facility (CheXray) at University of California, Berkeley using a Bruker MicroSTAR-H APEX II QUAZAR X-ray source.

Standard Procedure for the Cu-catalyzed double coupling reaction between epoxy ketones and Grignard reagents employing a single nucleophile.

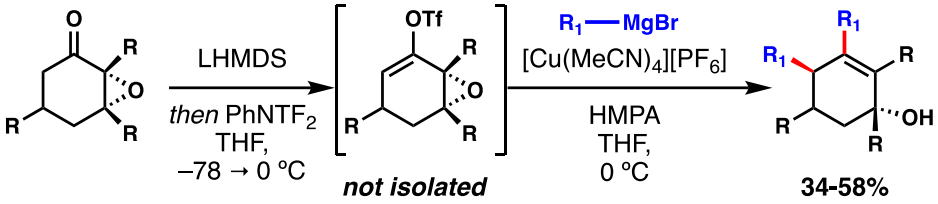

A solution of epoxy ketone (1.0 mmol, 1.0 equiv) in THF (2 mL) was cooled to –78 ºC. LHMDS (1.0 M in THF, 1.0 mL, 1.0 mmol, 1.0 equiv) was added dropwise and the resulting solution was stirred for 10 min. *N*-Phenyl-bis(trifluoromethanesulfonamide) (357 mg, 1.0 mmol, 1.0 equiv) was then added as a solid and the solution was warmed to 0 ºC and stirred for 10 min. In a separate flask, at 23 ºC, $[Cu(MeCN)_4][PF_6]$ (55 mg, 0.15 mmol, 0.15 equiv) was suspended in THF (1 mL). The desired Grignard reagent (typically 1.0 M in THF, 3.0 mL, 3.0 mmol, 3.0 equiv) was added dropwise to the suspension, followed by HMPA (0.87 mL, 5.0 mmol, 5.0 equiv). The mixture was stirred until homogeneous and cooled to 0 ºC. The so-prepared cuprate solution was then directly added to the enol triflate solution and the reaction mixture was stirred at 0 ºC until product formation was complete (typically 1-2 h). The reaction mixture was diluted with Et_2O:hexanes (1:1, 20 mL) and quenched with a 9:1 saturated aqueous ammonium chloride:saturated aqueous ammonium hydroxide solution (5 mL). The biphasic suspension was stirred vigorously until the aqueous layer had turned a deep blue. The layers were separated and the organic layer was further washed with water (2 x 10 mL) and brine (10 mL), dried over Na_2SO_4, filtered, and concentrated. The crude residue was purified by silica gel chromatography, and due to the instability of products to acid, chromatographic eluents were buffered with triethylamine (typically 27→47% Et_2O in hexanes + 3% Et_3N). Residence time of the compounds on the column was likewise minimized. Products were afforded as solid, single isomers, except where otherwise indicated.

Standard Procedure for the Cu-catalyzed double coupling reaction between epoxy ketones and Grignard reagents employing two different nucleophiles.

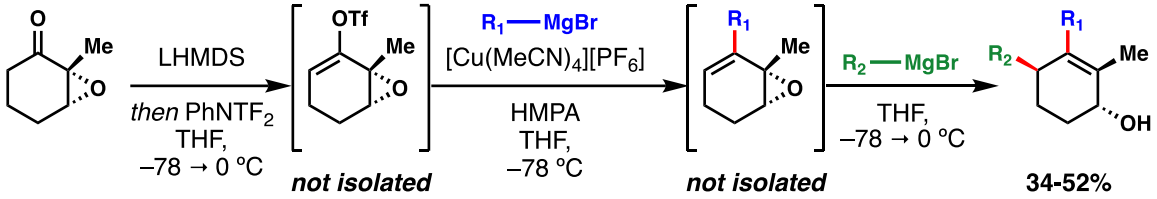

A solution of epoxy ketone (1.0 mmol, 1.0 equiv) in THF (2 mL) was cooled to –78 ºC. LHMDS (1.0 M in THF, 1.0 mL, 1.0 mmol, 1.0 equiv) was added dropwise and the resulting solution was stirred for 10 min. N-Phenyl-bis(trifluoromethanesulfonamide) (1.0 mmol, 1.0 equiv) was then added as a solid and the solution was warmed to 0 ºC and stirred for 10 min before being re-cooled to –78 ºC. In a separate flask, at 23 ºC, $[Cu(MeCN)_4][PF_6]$ (55 mg, 0.15 mmol, 0.15 equiv) was suspended in THF (1 mL). The desired Grignard reagent for cross-coupling (typically 1.0 M in THF, 2.0 mL, 2.0 mmol, 2.0 equiv) was added dropwise to the suspension, followed by HMPA (0.87 mL, 5.0 mmol, 5.0 equiv). The mixture was stirred until homogeneous, cooled briefly to 0 ºC, and then added dropwise to the enol triflate solution. Conversion to the cross-coupled product was carefully monitored and addition was stopped when full conversion was observed (typically when only 80-90% of the solution – or *ca*. 1.6-1.8 equiv of Grignard reagent – had been added). At the end of addition, the reaction was stirred for 1 h at –78 ºC. The desired Grignard reagent for allylic substitution (typically 1.0 M in THF, 2.0 mL, 2.0 mmol, 2.0 equiv) was then added dropwise. The solution was allowed to warm to 0 ºC and was stirred at that temperature for a further hour, or until complete conversion to product. The reaction mixture was diluted with Et_2O:hexanes (1:1, 20 mL) and quenched with a 9:1 saturated aqueous ammonium chloride:saturated aqueous ammonium hydroxide solution (5 mL). The biphasic suspension was stirred vigorously until the aqueous layer had turned a deep blue. The layers were separated and the organic layer was further washed with water (2 x 10 mL) and brine (10 mL), dried over Na_2SO_4, filtered, and concentrated. The crude residue was purified by silica gel chromatography (typically 27→47% Et_2O in hexanes + 3% Et_3N). Products were afforded as solid, single isomers, except where otherwise indicated.

Products from coupling two of the same nucleophiles:

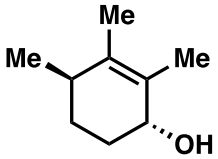

Substrate 166: The standard procedure was followed with 2,3-epoxy-2-methyl-cyclohexanone (126 mg, 1.0 mmol, 1.0 equiv) and MeMgBr (3.0 M in Et_2O diluted with THF to 1.0 M, 3.0 mL, 3.0 mmol, 3.0 equiv) to afford **166** (62 mg, 0.44 mmol, 44%) as a white solid (> 20:1 d.r.). ^{1}H NMR (700 MHz, $CDCl_3$) δ 3.89 (d, *J* = 5.5 Hz, 1H), 2.09 – 2.03 (m, 1H), 1.90 – 1.82 (m, 2H), 1.73 (s, 3H), 1.64 (s, 3H), 1.64 – 1.60 (m, 1H), 1.36 (d, *J* = 5.5 Hz, 1H), 1.35 – 1.31 (m, 1H), 0.98 (d, *J* = 7.1 Hz, 3H); ^{13}C NMR (176 MHz, $CDCl_3$) δ 135.6, 127.4, 69.6, 34.7, 28.2, 25.7, 18.5, 18.0, 16.9; IR (thin film) ν_{max}: 3349, 2923, 2853, 1668, 1462 cm^{-1}; HRMS (EI) calcd for $C_9H_{16}O$: 140.1201, found: 140.1203.

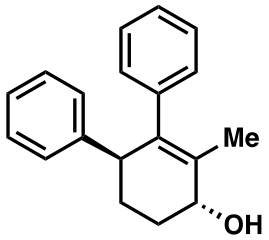

Substrate 167: Magnesium turnings (112 mg, 4.8 mmol, 4.8 equiv) were suspended in THF (3.0 mL) and a drop of 1,2-dibromoethane (< 10 µL) was added. Separately, bromobenzene (0.42 mL, 4.0 mmol, 4.0 equiv) was dissolved in THF (1.0 mL) and then added dropwise to the magnesium suspension. After Grignard initiation, addition was slowed so as to maintain a gentle reflux. Upon completion of addition, the resulting grey solution was stirred at room temperature for a further hour. The so-prepared phenylmagnesium bromide solution was used in the coupling step without further purification (1.0 M assumed). The standard procedure was followed with 2,3-epoxy-2-methyl-cyclohexanone (126 mg, 1.0 mmol, 1.0 equiv) and phenylmagnesium bromide (1.0 M in THF, 3.0 mL, 3.0 mmol, 3.0 equiv) to afford **167** (122 mg, 0.46 mmol, 46%) as a white solid (> 20:1 d.r.). ^{1}H NMR (700 MHz, $CDCl_3$) δ 7.20 (dd, *J* = 8.5, 7.0 Hz, 2H), 7.18 (dd, *J* = 8.5, 7.0 Hz, 2H), 7.13 (dd, *J* = 8.5, 1.3 Hz, 2H), 7.11 (tt, *J* = 7.0, 1.3 Hz, 1H), 7.10 (tt, J = 7.0, 1.3 Hz, 1H), 7.06 (dd, *J* = 8.4, 1.3 Hz, 2H), 4.25 – 4.23 (m, 1H), 3.78 (dq, *J* = 5.8, 1.5 Hz, 1H), 2.36 – 2.30 (m, 1H), 1.96 – 1.89 (m, 1H), 1.81 (d, *J* = 1.5 Hz, 3H), 1.74 – 1.69 (m, 2H), 1.67 (br s, 1H); ^{13}C NMR (151 MHz, $CDCl_3$) δ 143.2, 142.3, 137.7, 133.4, 128.9 (4C), 128.1 (2C), 127.9 (2C), 126.4, 126.1, 68.7, 46.9, 27.3, 27.3, 18.1; IR (thin film) ν_{max}: 3146, 2937, 1601, 619 cm^{-1}; HRMS (EI) calcd for $C_{19}H_{20}O$: 264.1514, found: 264.1518.

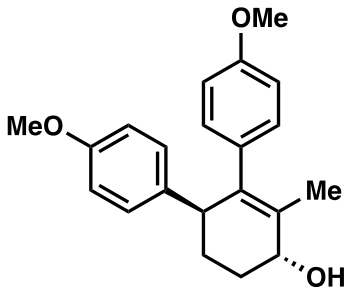

Substrate 168: The standard procedure was followed with 2,3-epoxy-2-methyl-cyclohexanone (126 mg, 1.0 mmol, 1.0 equiv) and 4-methoxyphenylmagnesium bromide (0.5 M in THF, 6.0 mL, 3.0 mmol, 3.0 equiv) to afford **168** (168 mg, 0.52 mmol, 52%) as a white solid (> 20:1 d.r.). ^{1}H NMR (600 MHz, $CDCl_3$) δ 7.03 (d, *J* = 8.1 Hz, 2H), 6.98 (d, *J* = 8.1 Hz, 2H), 6.75 (d, *J* = 8.1 Hz, 2H), 6.72 (d, *J* = 8.1 Hz, 2H), 4.20 (br s, 1H), 3.74 (s, 3H), 3.72 (s, 3H), 3.72 – 3.69 (m, 1H), 2.28 (td, *J* = 13.4, 5.6 Hz, 1H), 1.88 (tdd, *J* = 13.4, 3.4, 2.9 Hz, 1H), 1.81 (s, 3H), 1.72 – 1.62 (m, 3H); ^{13}C NMR (151 MHz, $CDCl_3$) δ 158.0, 157.9, 137.5, 135.4, 134.7, 133.0, 129.9 (2C), 129.8 (2C), 113.5 (2C), 113.3 (2C), 68.7, 55.3, 55.2, 46.1, 27.3, 27.1, 18.2; IR (thin film) ν_{max}: 3352, 2930, 1607, 1508, 1240 cm^{-1}; HRMS (ESI) calcd for $C_{21}H_{24}O_3Na$ $[M+Na]^+$: 347.1623, found: 347.1628.

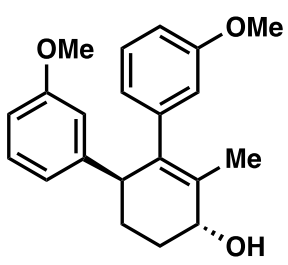

Substrate 169: Magnesium turnings (112 mg, 4.8 mmol, 4.9 equiv) were suspended in THF (3.0 mL) and a drop of 1,2-dibromoethane (< 10 µL) was added. Separately, 3-bromoanisole (0.51 mL, 4.0 mmol 4.0 equiv) was dissolved in THF (1.0 mL) and then added dropwise to the magnesium suspension. After Grignard initiation, addition was slowed so as to maintain a gentle reflux. Upon completion of addition, the resulting grey solution was stirred at room temperature for a further hour. The so-prepared 3-methoxyphenylmagnesium bromide solution was used in the coupling step without further purification (1.0 M assumed). The standard procedure was followed with 2,3-epoxy-2-methyl-cyclohexanone (126 mg, 1.0 mmol, 1.0 equiv) and 3-methoxyphenyl-magnesium bromide (1.0 M in THF, 3.0 mL, 3.0 mmol, 3.0 equiv) to afford **169** (142 mg, 0.44 mmol, 44%) as a white solid (> 20:1 d.r.). ^{1}H NMR (700 MHz, $CDCl_3$) δ 7.13 (t, *J* = 7.9 Hz, 1H), 7.10 (t, *J* = 7.9 Hz, 1H), 6.74 (dt, *J* = 7.9, 1.5 Hz, 1H), 6.68 (t, *J* = 2.1 Hz, 1H), 6.66 (dd, J = 7.9, 2.1 Hz, 1H), 6.66 (dd, J = 7.9 2.1 Hz, 1H), 6.66 (ddd, J = 7.9, 2.5, 1.5 Hz, 1H), 6.61 (dd, *J* = 2.5, 1.5 Hz, 1H), 4.21 (br d, *J* = 5.8 Hz, 1H), 3.75 (s, 3H), 3.73 (br dq, J = 5.1, 1.5 Hz, 1H), 3.70 (s, 3H), 2.34 – 2.26 (m, 1H), 1.97 – 1.89 (m, 1H), 1.81 (d, *J* = 1.5 Hz, 3H), 1.73 – 1.68 (m, 2H), 1.65 (d, *J* = 5.8 Hz, 1H); ^{13}C NMR (151 MHz, $CDCl_3$) δ 159.5, 159.2, 145.0, 143.7, 137.6, 133.5, 129.0, 128.8, 121.5, 121.5, 115.2, 114.8, 111.8, 111.0, 68.7, 55.3, 55.2, 46.8, 27.3, 27.2, 18.2; IR (thin film) ν_{max}: 3247, 2938, 1604, 1575, 1480, 1048 cm^{-1}; HRMS (ESI) calcd for $C_{21}H_{24}O_3Na$ $[M+Na]^+$: 347.1618, found: 347.1615.

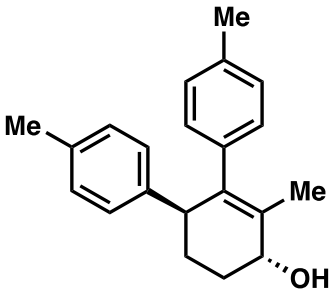

Substrate 170: Magnesium turnings (112 mg, 4.8 mmol, 4.9 equiv) were suspended in THF (3.0 mL) and a drop of 1,2-dibromoethane (< 10 µL) was added. Separately, 4-bromotoluene (0.49 mL, 4.0 mmol 4.0 equiv) was dissolved in THF (1.0 mL) and then added dropwise to the magnesium suspension. After Grignard initiation, addition was slowed so as to maintain a gentle reflux. Upon completion of addition, the resulting grey solution was stirred at room temperature for a further hour. The so-prepared 4-tolylmagnesium bromide solution was used in the coupling step without further purification (1.0 M assumed). The standard procedure was followed with 2,3-epoxy-2-methyl-cyclohexanone (126 mg, 1.0 mmol, 1.0 equiv) and 4-tolylmagnesium bromide (1.0 M in THF, 3.0 mL, 3.0 mmol, 3.0 equiv) to afford **170** (116 mg, 0.44 mmol, 44%) as a white solid (> 20:1 d.r.). ^{1}H NMR (600 MHz, $CDCl_3$) δ 7.02 (s, 4H), 6.99 (d, *J* = 8.0 Hz, 2H), 6.96 (d, *J* = 8.0 Hz, 2H), 4.20 (dd, *J* = 4.4, 2.4 Hz, 1H), 3.74 (dq, *J* = 5.7, 1.4 Hz, 1H), 2.30 (dddd, *J* = 15.2, 12.9, 5.7, 2.4 Hz, 1H), 2.26 (s, 3H), 2.24 (s, 3H), 1.88 (tt, *J* = 15.2, 13.9, 4.4 Hz, 1H), 1.81 (d, *J* = 1.4 Hz, 3H), 1.71 – 1.64 (m, 2H), 1.63 (s, 1H); ^{13}C NMR (151 MHz, $CDCl_3$) δ 140.2, 139.4, 137.7, 135.9, 135.5, 133.0, 128.82 (2C), 128.79 (2C), 128.77 (2C), 128.6 (2C), 68.7, 46.4, 27.3, 27.1, 21.2, 21.1, 18.3; IR (thin film) ν_{max}: 3265, 2937 1511, 814 cm^{-1}; HRMS (EI) calcd for $C_{21}H_{24}O$: 292.1827, found: 292.1823.

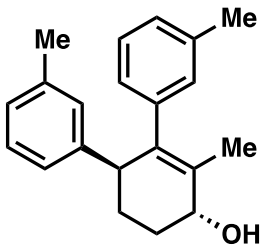

Substrate 171: Magnesium turnings (112 mg, 4.8 mmol, 4.8 equiv) were suspended in THF (3.0 mL) and a drop of 1,2-dibromoethane (< 10 µL) was added. Separately, 3-bromotoluene (0.49 mL, 4.0 mmol 4.0 equiv) was dissolved in THF (1.0 mL) and then added dropwise to the magnesium suspension. After Grignard initiation, addition was slowed so as to maintain a gentle reflux. Upon completion of addition, the resulting grey solution was stirred at room temperature for a further hour. The so-prepared 3-tolylmagnesium bromide solution was used in the coupling step without further purification (1.0 M assumed). The standard procedure was followed with 2,3-epoxy-2-methyl-cyclohexanone (126 mg, 1.0 mmol, 1.0 equiv) and 3-tolylmagnesium bromide (1.0 M in THF, 3.0 mL, 3.0 mmol, 3.0 equiv) to afford **171** (110 mg, 0.42 mmol, 42%) as a white solid (10:1 d.r., major reported). ^{1}H NMR (600 MHz, $CDCl_3$) δ 7.10 (t, *J* = 7.6 Hz, 1H), 7.07 (t, *J* = 7.7 Hz, 1H), 6.98 – 6.89 (m, 5H), 6.85 (d, *J* = 7.6 Hz, 1H), 4.22 (s, 1H), 3.74 (d, *J* = 5.6 Hz, 1H), 2.34 – 2.24 (m, 1H), 2.28 (s, 3H), 2.26 (s, 3H), 1.91 (td, *J* = 13.1, 5.6 Hz, 1H), 1.81 (s, 3H), 1.73 – 1.65 (m, 3H); ^{13}C NMR (176 MHz, $CDCl_3$) δ 143.1, 142.3, 137.8, 137.6, 137.3, 133.1, 129.8, 129.6, 127.8, 127.7, 127.1, 126.8, 126.0, 125.9, 68.7, 46.7, 27.2, 27.1, 21.6, 21.6, 18.2. IR (thin film) ν_{max}: 3170, 2934, 1604, 1484 cm^{-1}; HRMS (ESI) calcd for $C_{21}H_{24}ONa$ $[M+Na]^+$: 315.1719, found: 315.1720.

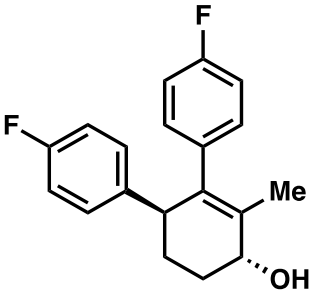

Substrate 172: The standard procedure was followed with 2,3-epoxy-2-methyl-cyclohexanone (126 mg, 1.0 mmol, 1.0 equiv) and 4-fluorophenylmagnesium bromide (1.0 M in THF, 3.0 mL, 3.0 mmol, 3.0 equiv) to afford **172** (128 mg, 0.43 mmol, 43%) as a white solid (> 20:1 d.r.). ^{1}H NMR (500 MHz, $CDCl_3$) δ 7.06 (dd, *J* = 8.5, 5.6 Hz, 2H), 7.00 (dd, *J* = 8.5, 5.6 Hz, 2H), 6.88 (t, *J* = 8.5 Hz, 2H), 6.87 (t, *J* = 8.5 Hz, 2H), 4.23 (dt, *J* = 4.7, 3.0 Hz, 1H), 3.72 (tq, *J* = 3.0, 1.6 Hz, 1H), 2.31 (tdd, *J* = 13.2, 5.7, 3.0 Hz, 1H), 1.88 (dddd, *J* = 14.0, 13.2, 5.0, 3.0 Hz, 1H), 1.79 (d, *J* = 1.6 Hz, 3H), 1.76 (d, *J* = 4.7 Hz, 1H), 1.71 (ddt, *J* = 14.0, 5.7, 3.0 Hz, 1H), 1.66 (ddt, *J* = 13.2, 5.0, 3.0 Hz, 1H); ^{13}C NMR (126 MHz, $CDCl_3$) δ 161.42 (d, J = 245 Hz, 1H), 161.39 (d, J = 242 Hz, 1H), 138.7 (d, *J* = 3.2 Hz), 137.8 (d, *J* = 3.5 Hz), 136.6, 134.1, 130.4 (d, *J* = 7.7 Hz, 2C), 130.1 (d, *J* = 7.9 Hz, 2C), 115.0 (d, J = 21 Hz, 2C), 114.9 (d, J = 21 Hz, 2C), 68.4, 46.2, 27.2, 18.1; ^{19}F NMR (376 MHz, $CDCl_3$) δ –115.30 (tt, *J* = 8.5, 5.6 Hz), –116.38 (tt, *J* = 8.5, 5.6 Hz); IR (thin film) ν_{max}: 3333, 2934, 1602, 1505 cm^{-1}; HRMS (EI) calcd for $C_{19}H_{18}OF_2$: 300.1326, found: 300.1326.

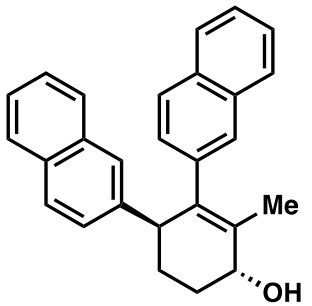

Substrate 173: Magnesium turnings (80 mg, 3.3 mmol, 1.1 equiv) were suspended in THF (3.0 mL) and a crystal of iodine (< 10 mg) was added. The magnesium suspension was heated at 65 ºC. Separately, 2-bromonaphthalene (620 mg, 3.0 mmol 1.0 equiv) was dissolved in THF (3.0 mL) and then added dropwise to the heated magnesium suspension. Upon completion of addition, the resulting brown-grey solution was heated at 65 ºC for a further hour. The so-prepared 2-naphthylmagnesium bromide solution

was used in the coupling step without further purification (0.5 M assumed). The standard procedure was followed with 2,3-epoxy-2-methyl-cyclohexanone (126 mg, 1.0 mmol, 1.0 equiv) and 2-naphthylmagnesium bromide (0.5 M in THF, 6.0 mL, 3.0 mmol, 3.0 equiv) to afford **173** (147 mg, 0.40 mmol, 40%) as a white solid (> 20:1 d.r.). ^{1}H NMR (700 MHz, $CDCl_3$) δ 7.77 (d, *J* = 8.2 Hz, 1H), 7.75 (d, *J* = 8.2 Hz, 1H), 7.73 – 7.70 (m, 3H), 7.66 (d, *J* = 8.2 Hz, 1H), 7.63 (s, 2H), 7.43 (t, *J* = 7.2 Hz, 1H), 7.41 – 7.34 (m, 4H), 7.31 (d, *J* = 8.2 Hz, 1H), 4.36 (dd *J* = 3.7, 3.0 Hz, 1H), 4.11 (d, *J* = 3.0 Hz, 1H), 2.48 (dddd, *J* = 13.9, 13.3, 5.7, 3.0 Hz, 1H), 2.03 (tdd, *J* = 13.9, 3.7, 3.0 Hz, 1H), 1.94 (d, *J* = 1.8 Hz, 3H), 1.86 (dq, *J* = 13.3, 3.0 Hz, 1H), 1.86 (br s, 1H), 1.79 (ddt, *J* = 13.9, 5.7, 3.0 Hz, 1H); ^{13}C NMR (176 MHz, $CDCl_3$) δ 140.7, 139.8, 137.5, 134.2, 133.3, 133.2, 132.2, 132.1, 127.9, 127.8, 127.7, 127.61, 127.59, 127.56 (2C, overlapping), 127.5, 127.4, 127.2, 125.89, 125.87, 125.6, 125.3, 68.7, 47.0, 27.22, 27.20, 18.3; IR (thin film) ν_{max}: 3357, 2933, 1629, 1598, 745 cm^{-1}; HRMS (EI) calcd for $C_{27}H_{24}O$: 364.1827, found: 364.1829.

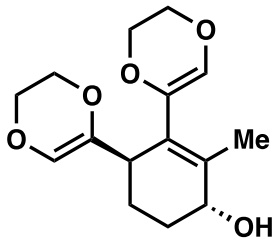

Substrate 174: Dioxene (0.65 M in THF, 5.1 mL, 3.3 mmol, 3.3 equiv) was cooled to 0 ºC. *n*BuLi (2.6 M in hexanes, 1.2 mL, 3.0 mmol, 3.0 equiv) was added and the pale yellow solution was stirred at 0 ºC for 1 h. Anhydrous $MgBr_2$ (550 mg, 3.0 mmol, 3.0 equiv) was added and the solution was allowed to warm to room temperature over 30 min. The so-prepared dioxenemagnesium bromide solution was used in the coupling step without further purification. The standard procedure was followed with 2,3-epoxy-2-methyl-cyclohexanone (126 mg, 1.0 mmol, 1.0 equiv) and dioxene-magnesium bromide (*ca.* 6.5 mL, 3.0 equiv) to afford **174** (153 mg, 0.55 mmol, 55%) as a white solid (> 20:1 d.r.). ^{1}H NMR (700 MHz, $CDCl_3$) δ 5.94 (s, 1H), 5.77 (s, 1H), 4.11 (ddd, *J* = 10.0, 7.5, 3.6 Hz, 1H), 4.08 – 4.01 (m, 5H), 3.99 (dt, *J* = 10.9, 3.8 Hz, 1H), 3.96 (t, *J* = 3.8 Hz, 2H), 2.84 (tq, *J* = 5.3, 1.7 Hz, 1H), 1.99 (ddt, *J* = 18.0, 10.1, 4.5 Hz, 1H), 1.94 (d, *J* = 1.7 Hz, 3H), 1.84 – 1.76 (m, 2H), 1.68 – 1.63 (m, 1H), 1.45 (s, 1H); ^{13}C NMR (151 MHz, $CDCl_3$) δ 138.4, 137.6, 135.1, 128.5, 126.6, 123.7, 68.7, 64.8, 64.6, 64.4, 64.1, 39.3, 28.9, 22.6, 18.3; IR (thin film) ν_{max}: 3338, 2937, 1718, 1660, 1145, 919 cm^{-1}; HRMS (ESI) calcd for $C_{15}H_{20}O_5Na$ $[M+Na]^+$: 303.1203, found: 303.1201.

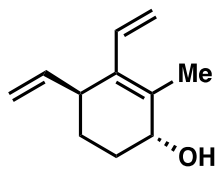

Substrate 175: The standard procedure was followed with 2,3-epoxy-2-methyl-cyclohexanone (126 mg, 1.0 mmol, 1.0 equiv) and vinylmagnesium bromide (1.0 M in THF, 3.0 mL, 3.0 mmol, 3.0 equiv) to afford **175** (56 mg, 0.35 mmol, 35%) as a white solid (> 20:1 d.r.). ^{1}H NMR (700 MHz, $CDCl_3$) δ 6.67 (dd, *J* = 17.5, 11.2 Hz, 1H), 5.78 (ddd, *J* = 17.3, 10.3, 6.2 Hz, 1H), 5.22 (dd, *J* = 17.5, 1.4 Hz, 1H), 5.13 (dd, *J* = 11.2, 1.4 Hz, 1H), 5.04 (dt, *J* = 10.3, 1.6 Hz, 1H), 4.89 (dt, *J* = 17.3, 1.6 Hz, 1H), 3.98 (t, *J* = 2.3 Hz, 1H), 3.16 (dtt, *J* = 6.1, 2.4, 1.6 Hz, 1H), 1.95 (br s, 3H), 1.90 (dddd, *J* = 14.6, 12.1, 4.8, 2.3 Hz, 1H), 1.84 (dddd, *J* = 14.3, 13.7, 4.3, 2.4 Hz, 1H), 1.69 (ddt, *J* = 13.7, 4.8, 2.3 Hz, 1H), 1.59 (br s, 1H), 1.58 (ddt, *J* = 12.1, 4.3, 2.3 Hz, 1H); ^{13}C NMR (151 MHz, $CDCl_3$) δ 140.5, 134.3, 133.9, 133.1, 115.5, 115.3, 69.5, 37.7, 27.0, 23.3, 17.3; IR (thin film) ν_{max}: 3161, 2924, 1636, 1418 cm^{-1}; HRMS (EI) calcd for $C_{11}H_{16}O$: 164.1201, found: 164.1200.

Anomalous products:

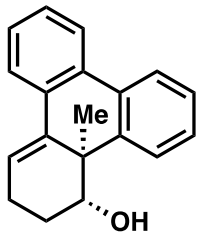

Substrate 176: This compound was prepared in a departure from the standard procedure in the following ways: copper(I) iodide was used in place of tetrakis(acetonitrile)copper(I) hexafluorophosphate, and no HMPA was added. Magnesium turnings (115 mg, 4.8 mmol, 4.8 equiv) were ground in a mortar and pestle then transferred to a 2-neck round bottom flask equipped with a reflux condenser. The apparatus was flame dried and its contents were placed under an argon atmosphere. THF (6.0 mL) was added followed by 3 drops of 1,2-dibromoethane (*ca*. 30 µL). Separately, 2,2'-dibromobiphenyl (624 mg, 2.0 mmol, 2.0 equiv) was dissolved in THF (2.0 mL) and then added dropwise to the magnesium suspension. After Grignard initiation, a vigorous reflux was maintained throughout addition. Upon completion of addition, the resulting solution was heated at 60 ºC for 4 h. The reaction mixture was cooled to room temperature and a wide-bore needle was used to transfer the resulting Grignard solution (transfer quantitated with 2 x 1.0 mL THF rinses). Special care was taken to ensure all solids (excepting small flakes of residual magnesium metal) were transferred to the copper suspension. This modified standard procedure was then followed with 2,3-epoxy-2-methyl-cyclohexanone (126 mg, 1.0 mmol, 1.0 equiv) and the presumed 2,2'-biphenyldimagnesium bromide reagent (0.25 M in THF, 10 mL, 2.0 equiv) to afford **176** (91 mg, 34 mmol, 34%) as a foamy solid (> 20:1 d.r., > 20:1 S_N2:S_N2'). ^{1}H NMR (600 MHz, $CDCl_3$) δ 8.13 – 8.08 (m, 1H), 7.78 – 7.70 (m, 2H), 7.41 (dd, *J* = 7.6, 1.4 Hz, 1H), 7.34 (td, *J* = 7.6, 1.4 Hz, 1H), 7.31 – 7.26 (m, 3H), 5.99 (dd, *J* = 5.8, 2.4 Hz, 1H), 4.46 (dt, *J* = 9.8, 4.4 Hz, 1H), 2.45 – 2.37 (m, 1H), 2.33 – 2.25 (m, 1H), 1.99 – 1.91 (m, 2H), 1.64 (d, *J* = 4.4 Hz, 1H), 1.23 (s, 3H); ^{13}C NMR (151 MHz, $CDCl_3$) δ 145.3, 140.5, 135.7, 132.8, 132.6, 128.5, 128.1, 128.0, 127.0, 126.6, 126.4, 124.2, 123.7, 123.1, 74.0, 43.8, 30.3, 25.3, 21.2; IR (thin film) ν_{max}: 3379, 3062, 2932, 1445, 1405, 751 cm^{-1}; HRMS (EI) calcd for $C_{19}H_{18}O$: 262.1358, found: 262.1358.

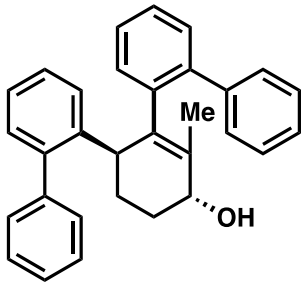

Substrate 187: This compound was prepared in a departure from the standard procedure in the following ways: copper(I) iodide was used in place of tetrakis(acetonitrile)copper(I) hexafluorophosphate, and no HMPA was added. Magnesium turnings (115 mg, 4.8 mmol, 4.8 equiv) were ground in a mortar and pestle then transferred to a 2-neck round bottom flask equipped with a reflux condenser. The apparatus was flame dried and its contents were placed under an argon atmosphere. THF (6.0 mL) was added followed by 3 drops of 1,2-dibromoethane (*ca*. 30 µL). Separately, 2,2'-dibromobiphenyl (624 mg, 2.0 mmol, 2.0 equiv) was dissolved in THF (2.0 mL) and then added dropwise to the magnesium suspension. After Grignard initiation, a vigorous reflux was maintained throughout addition. Upon completion of addition, the resulting solution was heated at 60 ºC for 4 h. The reaction mixture was cooled to room temperature and a wide-bore needle was used to transfer the resulting Grignard solution (transfer quantitated with 2 x 1.0 mL THF rinses). Special care was taken to ensure all solids (excepting small flakes of residual magnesium metal) were transferred to the copper suspension. The standard procedure was then followed with 2,3-epoxy-2-methyl-cyclohexanone (126 mg, 1.0 mmol, 1.0 equiv) and the presumed 2,2'-

biphenyldimagnesium bromide reagent (0.25 M in THF, 10 mL, 2.0 equiv) to afford **187** (nmr yield: 21 mmol 20%) as 1:1 mixture with **176** (> 20:1 d.r., > 20:1 d.r. respectively). ^{1}H NMR (600 MHz, $CDCl_3$) δ 8.13 – 8.09 (m, 1H)*, 7.78 – 7.70 (m, 2H)*, 7.41 (dd, *J* = 7.6, 1.4 Hz, 1H)*, 7.37 (dd, *J* = 8.1, 1.3 Hz, 2H), 7.34 (td, *J* = 7.6, 1.4 Hz, 1H)*, 7.32 – 7.27 (m, 7H)**, 7.21 – 7.14 (m, 6H), 7.06 (ddd, *J* = 7.6, 5.6, 3.2 Hz, 1H), 7.02 (dd, *J* = 7.5, 1.5 Hz, 1H), 6.97 – 6.93 (m, 2H), 6.79 (d, *J* = 7.2 Hz, 2H), 6.76 – 6.72 (m, 1H), 5.99 (dd, *J* = 5.8, 2.4 Hz, 1H)*, 4.46 (dt, *J* = 9.8, 4.4 Hz, 1H)*, 4.13 (dt, *J* = 9.8, 4.4 Hz, 1H), 3.26 (d, *J* = 6.0 Hz, 1H), 2.45 – 2.37 (m, 1H)*, 2.33 – 2.25 (m, 1H)*, 1.99 – 1.91 (m, 3H)**, 1.80 (d, *J* = 1.4 Hz, 3H), 1.71 (d, *J* = 6.5 Hz, 1H), 1.64 (d, *J* = 4.4 Hz, 1H)*, 1.50 (dq, *J* = 14.2, 3.6 Hz, 1H), 1.35 (tdd, *J* = 13.5, 6.3, 3.4 Hz, 1H),1.23 (s, 3H)*. ^{13}C NMR (151 MHz, $CDCl_3$) δ 145.3*, 142.5, 141.8, 141.4, 140.6, 140.5*, 140.0, 137.9, 135.7*, 134.3, 132.8*, 132.6*, 130.4, 129.9, 129.7, 129.2, 129.0, 128.7, 128.5*, 128.1*, 128.0*, 127.6*, 126.9, 126.7, 126.6*, 126.6, 126.4*, 125.9, 124.2*, 123.7*, 123.1*, 73.9*, 68.7, 43.8*, 41.4, 30.3*, 26.8, 25.3, 24.9, 21.2*, 18.5. HRMS (EI) calcd for $C_{19}H_{18}O$: 416.2140, found: 416.2140.
Note: Compound 185 was isolated as an inseparable mixture of 176 and 185. The peaks corresponding to only 176 are reported above.
* indicates peaks corresponding only to compound **176**
** indicates overlapping peaks for **176** and **187**

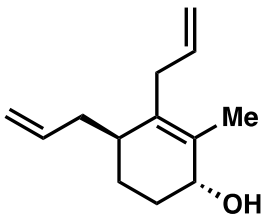

Substrate 177: This compound was prepared in a departure from the standard procedure in the following ways: copper(I) iodide was used at 35 mol% loading in place of tetrakis(acetonitrile)copper(I) hexafluorophosphate, and no HMPA was added. This modified standard procedure was followed with 2,3-epoxy-2-methyl-cyclohexanone (126 mg, 1.0 mmol, 1.0 equiv) and allylmagnesium bromide (1.0 M in Et_2O, 3.0 mL, 3.0 mmol, 3.0 equiv) to afford **177** (107 mg, 0.56 mmol, 56%) as mixture of diastereomers (~1:1 d.r. as judged by ^{1}H NMR analysis). To characterize this mixture as a single compound, the crude residue was quickly passed through a plug of silica gel (eluting with 97% Et_2O + 3% Et_3N) and then immediately oxidized to ketone **SI-1**.

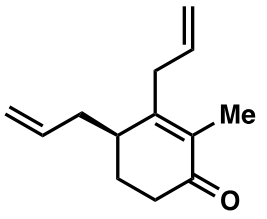

Ketone SI2-1: PCC (299 mg, 1.4 mmol, 3.0 equiv) was added to **177** (~1:1 d.r., 89 mg, 0.46 mmol, 1.0 equiv) dissolved in DCM (4.6 mL) and the solution was stirred for 12 h. The reaction mixture was diluted with EtOAc (5 mL) and filtered through celite. The organic phase was quenched with saturated *aq*. $NaHCO_3$ (10 mL) and the layers were separated. The aqueous layer was extracted with EtOAc (2 x 5 mL). The combined organic layer was dried over Na_2SO_4, filtered, and concentrated. The crude residue was purified by silica gel chromatography (25% Et_2O in hexanes) to afford ketone **SI-1** (84 mg, 0.44 mmol, 96%) as a single compound. ^{1}H NMR (600 MHz, $CDCl_3$) δ 5.82 – 5.72 (m, 2H), 5.13 – 5.05 (m, 4H), 3.15 (ddt, *J* = 14.9, 5.7, 1.8 Hz, 1H), 2.90 (dd, *J* = 14.9, 6.9 Hz, 1H), 2.52 (ddd, *J* = 17.5, 12.8, 5.9 Hz, 1H), 2.41 – 2.36 (m, 2H), 2.33 (dt, *J* = 17.5, 4.1 Hz, 1H), 2.18 (ddd, *J* = 14.9, 11.0, 8.0 Hz, 1H), 2.01 – 1.91 (m, 2H), 1.77 (br s, 3H); ^{13}C NMR (151 MHz, $CDCl_3$) δ 199.2, 158.5, 136.8, 133.4, 132.2, 117.1, 116.9, 38.6, 38.0, 35.4, 33.1, 25.4, 11.0; IR (thin film) ν_{max}: 2925, 1662, 1448, 911 cm^{-1}; HRMS (EI) calcd for $C_{13}H_{18}O$: 190.1358, found: 190.1356.

Coupling with *tert*-butylmagnesium chloride: The standard procedure was followed with 2,3-epoxy-2-methyl-cyclohexanone (126 mg, 1.0 mmol, 1.0 equiv) and *tert*-butylmagnesium chloride (1.0 M in THF, 3.0 mL, 3.0 mmol, 3.0 equiv) to afford **182** (69 mg, 0.31 mmol, 31%) as a white solid (> 20:1 d.r.) and **183** (40 mg, 0.24 mmol, 24%).

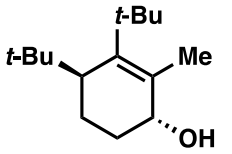

Substrate 182: ^{1}H NMR (600 MHz, C_6D_6) δ 3.84-3.79 (m, 1H), 2.29 (t, *J* = 4.0 Hz, 1H), 2.10 (tt, *J* = 13.4, 6.9 Hz, 1H), 1.95 (s, 3H), 1.65(ddd, *J* = 13.3, 6.6, 3.5 Hz, 1H), 1.47 (ddd, *J* = 13.6, 6.4, 2.9 Hz, 1H), 1.40 (dq, *J* = 13.3, 6.6, 5.9 Hz, 1H), 1.22 (s, 9H), 0.88 (s, 9H; ^{13}C NMR (151 MHz, C_6D_6) δ 144.3, 134.3, 70.1, 43.0, 35.9, 35.5,31.9, 31.3, 30.2, 23.7, 20.0 cm^{-1}; HRMS (EI) calcd for $C_{15}H_{27}O$ [M-H]: 223.2069, found: 223.2099

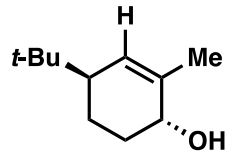

Substrate 183: ^{1}H NMR (600 MHz, C_6D_6) δ 5.50 (dd, *J* = 3.4, 1.8 Hz, 1H) 4.11-1.06 (m, 1H), 2.16 (dtd, *J* = 10.1, 5.5, 2.6 Hz, 1H), 1.87 (ddt, *J* = 10.5, 5.3, 2.6 Hz, 1H), 1.78 (s, 3H), 1.43 (tdd, *J* = 12.3, 7.4, 2.5 Hz, 1H), 1.31-1.25 (m, 1H), 0.86 (s, 9H; ^{13}C NMR (151 MHz, C_6D_6) δ 137.1, 127.1, 70.39, 46.5, 33.7, 33.1, 27.4, 23.2,19.7 cm^{1}; HRMS (EI) calcd for $C_{11}H_{19}OK$ [M+K]$^{+}$: 206.1073, found: 206.1071

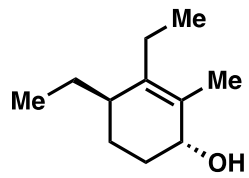

Substrate 184: The standard procedure was followed with 2,3-epoxy-2-methyl-cyclohexanone (126 mg, 1.0 mmol, 1.0 equiv) and ethylmagnesium bromide (1.0 M in THF, 3.0 mL, 3.0 mmol, 3.0 equiv) to afford **184** (56 mg, 0.35 mmol, 40%) as a clear oil (~1:1 d.r.). ^{1}H NMR (600 MHz, $CDCl_3$) δ 3.97 (q, *J* = 6.2 Hz, 1H), 3.87 – 3.82 (m, 1H), 2.15 (dqd, *J* = 12.7, 7.5, 5.1 Hz, 2H), 2.00 – 1.83 (m, 3H), 1.83 – 1.75 (m, 1H), 1.75 (d, *J* = 1.4 Hz, 3H), 1.74 (d, *J* = 1.7 Hz, 3H), 1.70 – 1.55 (m, 5H), 1.54 – 1.45 (m, 1H), 1.36 (d, *J* = 7.1 Hz, 1H), 1.30 (d, *J* = 6.6 Hz, 1H), 1.29 – 1.22 (m, 1H), 1.17 (ddq, *J* = 14.3, 10.5, 7.2 Hz, 1H), 0.95 (dt, *J* = 9.4, 7.6 Hz, 5H), 0.90 (q, *J* = 7.3 Hz, 5H).; ^{13}C NMR (101 MHz, $CDCl_3$) δ 141.03, 140.43, 128.56, 127.37, 70.89, 69.30, 39.10, 39.04, 29.60, 27.63, 25.31, 24.47, 23.78, 23.75, 23.09, 20.49, 16.31, 15.78, 13.11, 12.90, 12.82, 12.10.; HRMS (EI) calcd for $C_{11}H_{19}OK$ [M+K]$^{+}$: 206.1073, found: 206.1073

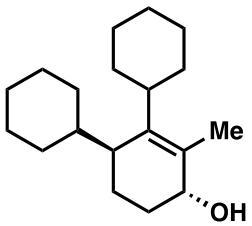

Substrate 185: Magnesium turnings (170 mg, 7 mmol, 7.0 equiv) were suspended in THF (10.0 mL) and a drop of 1,2-dibromoethane (< 10 µL) was added. Separately, cyclohexyl bromide (0.43 mL, 3.5 mmol 3.5 equiv) was dissolved in THF (4.0 mL) and then added dropwise to the magnesium suspension. After Grignard initiation, addition was slowed so as to maintain a gentle reflux. Upon completion of addition, the resulting grey solution was stirred at room temperature for a further hour. The so-prepared cyclohexylmagnesium bromide solution was used in the coupling step without further purification (0.25 M assumed). The standard procedure was followed with 2,3-epoxy-2-methyl-cyclohexanone (126 mg, 1.0 mmol, 1.0 equiv) and cyclohexylmagnesium bromide (0.25 M in THF, 12 mL, 3.0 mmol, 3.0 equiv) to afford **185** (81 mg, 0.29 mmol, 29%) as a white solid (> 20:1 d.r.). ^{1}H NMR (600 MHz, $CDCl_3$) δ 3.87 (t, *J* = 3.4 Hz, 1H), 2.26 (tt, *J* = 12.3, 3.4 Hz, 1H), 2.01 (br s, 1H), 1.83 (d, *J* = 1.6 Hz, 3H), 1.82 – 1.75 (m, 4H), 1.74 – 1.63 (m, 5H), 1.62 – 1.54 (m, 4H), 1.52 –

1.44 (m, 3H), 1.41 – 1.32 (m, 2H), 1.32 – 1.22 (m, 4H), 1.18 (tt, *J* = 12.9, 3.3 Hz, 1H), 1.14 – 1.04 (m, 2H), 0.97 (qd, *J* = 12.1, 3.4 Hz, 1H); ^{13}C NMR (151 MHz, $CDCl_3$) δ 140.5, 130.0, 70.1, 43.1, 41.6, 41.3, 32.6, 32.3, 30.1, 29.9, 29.4, 27.8, 27.7, 27.6, 27.4, 27.0, 26.6, 19.0, 17.7; IR (thin film) ν_{max}: 3314, 2924, 2873, 1444 cm^{-1}; HRMS (EI) calcd for $C_{19}H_{32}O$: 276.2453, found: 276.2450.

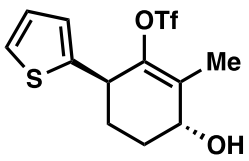

Substrate 186: Thiopene (0.65 M in THF, 5.1 mL, 3.3 mmol, 3.3 equiv) was cooled to 0 ºC. *n*BuLi (2.6 M in hexanes, 1.2 mL, 3.0 mmol, 3.0 equiv) was added and the pale-yellow solution was stirred at 0 ºC for 1 h. Anhydrous $MgBr_2$ (550 mg, 3.0 mmol, 3.0 equiv) was added and the solution was allowed to warm to room temperature over 30 min. The so-prepared thiophenemagnesium bromide solution was used in the coupling step without further purification. The standard procedure was followed with 2,3-epoxy-2-methyl-cyclohexanone (126 mg, 1.0 mmol, 1.0 equiv) and thiophene-magnesium bromide (*ca.* 6.5 mL, 3.0 equiv) to afford **186** (153 mg, 0.55 mmol, 55%) as a white solid (> 20:1 d.r.). ^{1}H NMR (500 MHz, $CDCl_3$) δ 7.14 (d, *J* = 5.1 Hz, 1H), 6.87 (dd, *J* = 5.1, 3.5 Hz, 1H), 6.77 (d, *J* = 3.5 Hz, 2H), 4.21 (t, *J* = 4.5 Hz, 1H), 4.03 (d, *J* = 5.6 Hz, 1H), 2.30 (dddd, *J* = 14.0, 11.5, 5.9, 3.0 Hz, 1H), 2.00 – 1.94 (m, 2H), 1.93 (br s, 3H), 1.77 (ddt, *J* = 13.8, 7.2, 3.8 Hz, 1H), 1.66 (ddt, *J* = 14.1, 7.0, 3.6 Hz, 1H). ^{13}C NMR (126 MHz, $CDCl_3$) δ 146.42, 142.86, 130.74, 126.69, 125.70, 124.49, 69.44, 39.38, 28.77, 27.98, 14.78.

Products with an alternative epoxide starting material:

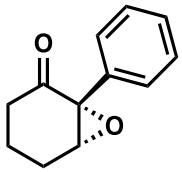

Epoxide SI2-2: 2-phenyl-cyclohexenone (473 mg, 2.75 mmol, 1.0 equiv) was dissolved in EtOH (3.8 mL) at rt. Separately H_2O_2 (50wt% in H_2O, 0.11 mL, 3.9 mmol, 1.4 equiv) was diluted with H_2O (0.29 mL) and then added dropwise to the former solution. An aqueous solution of NaOH (5.0 M, 20 µL, 0.93 mmol, 0.34 equiv) was then added dropwise and the reaction mixture was stirred for 1 h. Brine (5 mL was added) followed by DCM (10 mL). The layers were separated and the aqueous layer was futher extracted with DCM (2 x 5 mL). The combined organic phases were dried over Na_2SO_4, filtered and concentrated. The crude residue was purified by column chromatography (30% Et_2O in hexanes) to afford **SI-3** (333 mg, 1.77 mmol, 64%) as a clear, colorless oil. ^{1}H NMR (700 MHz, C_6D_6) δ 7.42 (dd, *J* = 7.7, 1.3 Hz, 2H), 7.16 (t, *J* = 7.7 Hz, 2H), 7.10 (tt, *J* = 7.7, 1.3 Hz, 1H), 2.94 (t, *J* = 2.1 Hz, 1H), 2.35 (dt, *J* = 16.6, 5.2 Hz, 1H), 1.72 (ddd, *J* = 16.6, 10.9, 5.6 Hz, 1H), 1.64 (dtd, *J* = 15.2, 4.9, 2.1 Hz, 1H), 1.55 (dddd, *J* = 13.4, 10.9, 10.2, 5.2, 4.9 Hz, 1H), 1.26 (dddd, *J* = 15.2, 10.2, 5.5, 2.1 Hz, 1H), 1.08 (ddddd, *J* = 13.4, 5.8, 5.6, 5.5, 4.9 Hz, 1H); ^{13}C NMR (176 MHz, C_6D_6) δ 202.8, 135.3, 128.3, 128.2 (2C), 127.6 (2C), 64.7, 62.5, 37.8, 23.5, 18.1; IR (thin film) ν_{max}: 2951, 1709, 1498 cm^{-1}; HRMS (EI) calcd for $C_{12}H_{12}O_2$: 188.0837, found: 188.0837.

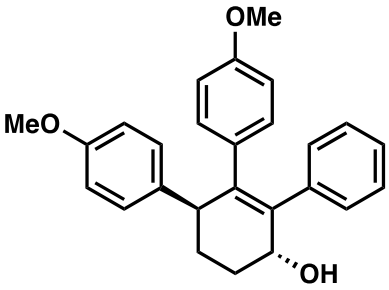

Substrate 178: The standard procedure was followed with 2,3-epoxy-2-phenyl-cyclohexanone (188 mg, 1.0 mmol, 1.0 equiv) and 4-methoxyphenylmagnesium bromide (0.5 M in THF, 6.0 mL, 3.0 mmol, 3.0 equiv) to afford **178** (154 mg, 0.40 mmol, 40%) as a white solid. ^{1}H NMR (700 MHz, C_6D_6) δ 7.18 (dd, *J* = 7.7, 0.9 Hz, 2H), 7.08 (d, *J* = 8.6 Hz, 2H), 7.03 (tt, *J* = 7.7, 0.9 Hz, 2H), 6.94 (tt, *J* = 7.7, 0.9 Hz, 1H), 6.94 (d, *J* = 8.6 Hz, 2H), 6.73 (d, *J* = 8.7 Hz, 2H), 6.43 (d, *J* = 8.8 Hz, 2H), 4.63 (t, *J* = 4.5, 3.0 Hz, 1H), 4.02 (dd, *J* = 5.8, 3.0 Hz, 1H), 3.24 (s, 3H), 3.02 (s, 3H), 2.55 (tdd, *J* = 13.2, 5.8, 3.0 Hz, 1H), 2.01 (dddd, *J* = 13.6, 13.2, 4.5, 3.1 Hz, 1H), 1.89 (ddt, *J* = 13.6, 5.4, 3.0 Hz, 1H), 1.76 (ddt, *J* = 13.2, 5.4, 3.0 Hz, 1H); ^{13}C NMR (176 MHz, C_6D_6) δ 158.5, 158.4, 141.8, 139.9, 139.6, 135.4, 134.2, 131.1 (2C), 130.5 (2C), 130.0 (2C), 128.37 (2C), 128.35, 126.7, 114.0 (2C), 113.4 (2C), 68.2, 54.7, 54.3, 46.1, 27.7, 26.9; IR (thin film) ν_{max}: 3332, 2970, 1467, 1379, 950 cm^{-1}; HRMS (EI) calcd for $C_{26}H_{26}O_3$: 386.1882, found: 386.1884.

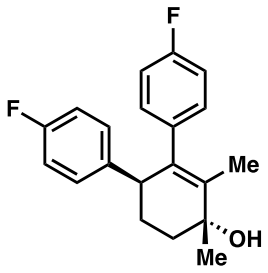

Substrate 179: The standard procedure was followed with 2,3-epoxy-2,3-dimethyl-cyclohexanone (140 mg, 1.0 mmol, 1.0 equiv) and 4-fluorophenylmagnesium bromide (1.0 M in THF, 3.0 mL, 3.0 mmol, 3.0 equiv) to afford **179**. **179** was unstable to purification by silica gel chromatography, even with buffered eluent; yield was assessed by NMR of the crude reaction mixture with 1,3,5-trimethoxybenzene as an internal standard and determined to be 54% (> 20:1 d.r.). An analytic sample could be isolated by preparatory TLC (50% Et_2O in hexanes) with minimal decomposition. ^{1}H NMR (700 MHz,

C_6D_6) δ 6.75 – 6.72 (m, 4H), 6.69 – 6.63 (m, 4H), 3.43 (ddq, *J* = 4.1, 3.0, 1.7 Hz, 1H), 2.06 (dddd, *J* = 13.2, 11.9, 5.8, 3.0 Hz, 1H), 1.67 (ddd, *J* = 13.6, 11.9, 4.1 Hz, 1H), 1.62 (d, *J* = 1.7 Hz, 3H), 1.54 (ddd, *J* = 13.6, 5.8, 3.0 Hz, 1H), 1.48 (dddd, *J* = 13.2, 6.8, 4.1, 3.0 Hz, 1H), 1.29 (s, 3H), 1.08 (br s, 1H); ^{13}C NMR (176 MHz, C_6D_6) δ 161.79 (d, *J* = 244 Hz), 161.75 (d, *J* = 245 Hz), 139.3 (d, *J* = 3.2 Hz), 138.6 (d, *J* = 3.7 Hz), 137.7, 135.5, 130.7 (d, *J* = 7.7 Hz, 2C), 130.2 (d, *J* = 7.7 Hz, 2C), 128.4, 128.0, 115.1 (d, *J* = 21.5 Hz, 2C), 115.0 (d, *J* = 21.3 Hz, 2C), 69.8, 47.2, 35.3, 29.0, 28.2, 14.7; IR (thin film) ν_{max}: 3381, 2933, 1601, 1504, 1367 cm^{-1}; HRMS (EI) calcd for $C_{20}H_{20}OF_2$: 314.1482, found: 314.1483.

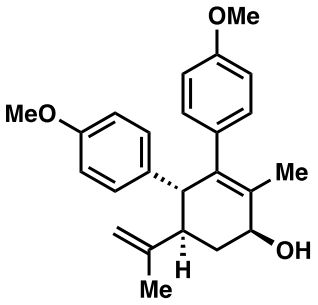

Substrate 180: The standard procedure was followed with *trans*-carvone epoxide (166 mg, 1.0 mmol, 1.0 equiv) and 4-methoxyphenylmagnesium bromide (0.5 M in THF, 6.0 mL, 3.0 mmol, 3.0 equiv) to afford **180** (189 mg, 0.52 mmol, 52%) as a white solid (> 20:1 d.r.). $[\alpha]_D^{23}$ = +143 (*c* 0.8, C_6H_6); ^{1}H NMR (700 MHz, $CDCl_3$) δ 6.96 (d, *J* = 8.3 Hz, 2H), 6.90 (d, *J* = 8.3 Hz, 2H), 6.71 (d, *J* = 8.3 Hz, 2H), 6.70 (d, *J* = 8.3 Hz, 2H), 4.90 (s, 1H), 4.84 (s, 1H), 4.23 (ddd, *J* = 9.4, 6.0, 4.8 Hz, 1H), 3.74 (d, *J* = 4.8 Hz, 1H), 3.73 (s, 3H), 3.72 (s, 3H), 2.42 (dt, *J* = 6.0, 4.8 Hz, 1H), 2.10 (dt, *J* = 13.7, 4.8 Hz, 1H), 2.03 (dt, *J* = 13.7, 6.0 Hz, 1H), 1.98 (d, *J* = 9.4 Hz, 1H), 1.81 (s, 3H), 1.77 (s, 3H); ^{13}C NMR (151 MHz, $CDCl_3$) δ 157.92, 157.89, 150.1, 135.73, 135.71, 134.6, 133.5, 123.0 (2C), 129.9 (2C), 113.5 (2C), 113.3 (2C), 111.3, 70.4, 55.3, 55.2, 50.8, 47.4, 33.2, 21.9, 17.2; IR (thin film) ν_{max}: 3371, 2931, 1643, 1509, 1241 cm^{-1}; HRMS (ESI) calcd for $C_{24}H_{28}O_3Na$ $[M+Na]^+$: 387.1931, found: 387.1928.

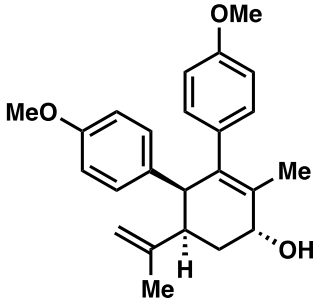

Substrate 181: This compound was prepared in a departure from the standard procedure in the following way: $[Cu(MeCN)_4][PF_6]$ was used at 0.30 mol% loading. This modified standard procedure was followed with *cis*-carvone epoxide (166 mg, 1.0 mmol, 1.0 equiv) and 4-methoxyphenylmagnesium bromide (0.5 M in THF, 6.0 mL, 3.0 mmol, 3.0 equiv) to afford **181** (186 mg, 0.51 mmol, 51%) as a white solid (> 20:1 d.r.). $[\alpha]_D^{23}$ = –96.3 (*c* 0.3, C_6D_6); ^{1}H NMR (700 MHz, $CDCl_3$) δ 6.93 (d, *J* = 8.7 Hz, 2H), 6.80 (d, *J* = 8.7 Hz, 1H), 6.65 (d, *J* = 8.7 Hz, 3H), 4.72 (q, *J* = 1.6 Hz, 1H), 4.68 (d, *J* = 1.1 Hz, 1H), 4.19 (t, *J* = 4.7 Hz, 1H), 3.71 (s, 6H), 3.54 (d, *J* = 7.8 Hz, 1H), 2.68 (ddd, *J* = 10.4, 7.8, 3.5 Hz, 1H), 2.00 (ddd, *J* = 13.7, 10.4, 4.7 Hz, 1H), 1.91 (dt, *J* = 13.7, 4.7, 3.5 Hz, 1H), 1.71 (d, *J* = 1.8 Hz, 3H), 1.70 (br s, 1H), 1.66 (s, 3H); ^{13}C NMR (151 MHz, $CDCl_3$) δ 157.70, 157.67, 147.4, 138.1, 135.6, 134.2, 131.9, 130.0 (2C), 129.9 (2C), 113.3 (2C), 113.1 (2C), 111.3, 69.8, 55.19, 55.16, 51.3, 45.7, 34.9, 21.2, 18.7; IR ν_{max}: 3361, 2932, 1646, 1508 cm^{-1}; HRMS (ESI) calcd for $C_{24}H_{28}O_3Na$ $[M+Na]^+$: 387.1931, found: 387.1928.

Products from coupling two different nucleophiles:

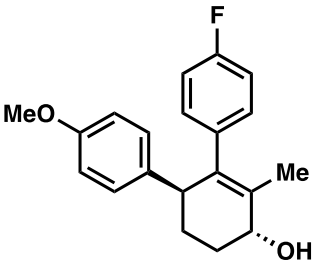

Substrate 188: The standard procedure was followed with 2,3-epoxy-2-methyl-cyclohexanone (126 mg, 1.0 mmol, 1.0 equiv) and 4-fluorophenylmagnesium bromide (1.0 M in THF, 2.0 mL, 2.0 mmol, 2.0 euqiv) followed by 4-methoxyphenylmagnesium bromide (0.5 M in THF, 4.0 mL, 2.0 mmol, 2.0 equiv) to afford **20** (163 mg, 0.52 mmol, 52%) as a white foam (this product was isolated as a ~15:1 inseparable mixture with byproduct **X**). ^{1}H NMR (700 MHz, $CDCl_3$) δ 7.03 (d, *J* = 8.7 Hz, 2H), 7.02 (dd, *J* = 8.4, 5.6 Hz, 2H), 6.87 (dd, *J* = 9.4, 8.4 Hz, 2H), 6.77 (d, *J* = 8.7 Hz, 2H), 4.23 (t, *J* = 3.0 Hz, 1H), 3.74 (s, 3H), 3.69 (tq, *J* = 3.0, 2.0 Hz, 1H), 2.31 (tdd, *J* = 13.4, 5.8, 3.0 Hz, 1H), 2.06 (s, 1H), 1.93 (tdd, *J* = 13.4, 5.0, 3.0 Hz, 1H), 1.80 (d, *J* = 2.0 Hz, 3H), 1.71 (ddt, *J* = 13.4, 5.8, 3.0 Hz, 1H), 1.68 (ddt, *J* = 13.4, 5.0, 3.0 Hz, 1H); ^{13}C NMR (176 MHz, $CDCl_3$) δ 161.3 (d, *J* = 244.9 Hz), 157.9, 138.1 (d, *J* = 3.2 Hz), 137.0, 135.0, 133.6, 130.3 (d, *J* = 7.7 Hz, 2C), 129.6 (2C), 114.7 (d, *J* = 21.1 Hz, 2C), 113.5 (2C), 68.5, 55.2, 46.1, 27.3, 27.2, 18.1; IR (thin film) ν_{max}: 3355, 2934, 1602, 1582, 1442 cm^{-1}; HRMS (EI) calcd for $C_{20}H_{21}OF$: 312.1526, found: 312.1529.

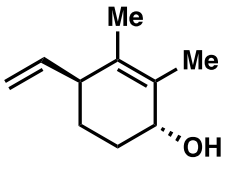

Substrate 189: The standard procedure was followed with 2,3-epoxy-2-methyl-cyclohexanone (126 mg, 1.0 mmol, 1.0 equiv) and methylmagnesium bromide (3.0 M in Et_2O diluted with THF to 1.0 M, 2.0 mL, 2.0 mmol, 2.0 euqiv) followed by vinylmagnesium bromide (1.0 M in THF, 2.0 mL, 2.0 mmol, 2.0 equiv) to afford **21** (46 mg, 0.34 mmol, 34%) as a white solid (> 20:1 d.r.). ^{1}H NMR (400 MHz, $CDCl_3$) δ 5.71 (ddd, *J* = 17.0, 10.2, 7.7 Hz, 1H), 5.02 (ddd, *J* = 10.2, 2.0, 0.9 Hz, 1H), 4.94 (ddd, *J* = 17.0, 2.0, 1.2 Hz, 1H), 3.92 (br s, 1H), 2.62 (br s, 1H), 1.95 – 1.81 (m, 2H), 1.78 (s, 3H), 1.66 – 1.62 (m, 1H), 1.61 (s, 3H), 1.52 – 1.43 (m, 1H); ^{13}C NMR (151 MHz, $CDCl_3$) δ 140.2, 131.9, 129.4, 115.1, 69.3, 44.9, 28.0, 23.8, 18.4, 17.0; IR (thin film) ν_{max}: 3773, 2931, 1443 cm^{-1}; HRMS (EI) calcd for $C_{10}H_{16}O$: 152.1201, found: 152.1199.

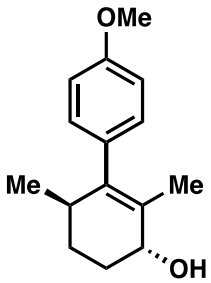

Substrate 190: The standard procedure was followed with 2,3-epoxy-2-methyl-cyclohexanone (126 mg, 1.0 mmol, 1.0 equiv) and methylmagnesium bromide (1.0 M in Et_2O diluted with THF to 1.0 M, 2.0 mL, 2.0 mmol, 2.0 euqiv) followed by 4-methoxyphenylmagnesium bromide (1.0 M in THF, 2.0 mL, 2.0 mmol, 2.0 equiv) to afford **190** (107 mg, 0.46 mmol, 46%) as a white solid (> 20:1 d.r.). ^{1}H NMR (600 MHz, $CDCl_3$) δ 6.95 – 6.91 (m, 2H), 6.81 – 6.77 (m, 2H), 4.00 (t, *J* = 3.9 Hz, 1H), 3.74 (s, 3H), 2.39 (s, 1H), 1.96 (tdd, *J* = 12.9, 5.6, 2.9 Hz, 1H), 1.87 (tdd, *J* = 13.1, 4.4, 3.0 Hz, 1H), 1.72 – 1.65 (m, 1H), 1.56 (d, *J* = 1.6 Hz, 3H), 1.42 (ddt, *J* = 12.9, 5.8, 3.0 Hz, 1H), 0.74 (d, *J* = 7.1 Hz, 3H). ^{13}C NMR (126 MHz, $CDCl_3$) δ 158.02, 141.36, 134.80, 129.88, 129.65, 113.35, 68.87, 55.20, 34.55, 27.88, 25.51, 18.58, 17.75. HRMS (EI) calcd for $C_{15}H_{20}O$: 232.1463, found: 232.1466.

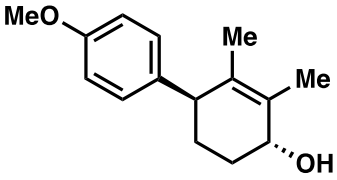

Substrate 191: The standard procedure was followed with 2,3-epoxy-2-methyl-cyclohexanone (126 mg, 1.0 mmol, 1.0 equiv) and methylmagnesium bromide (1.0 M in Et_2O diluted with THF to 1.0 M, 2.0 mL, 2.0 mmol, 2.0 euqiv) followed by 4-methoxyphenylmagnesium bromide (1.0 M in THF, 2.0 mL, 2.0 mmol, 2.0 equiv) to afford **191** (111 mg, 0.48 mmol, 48%) as a white solid (> 20:1 d.r.). ^{1}H NMR (700 MHz, $CDCl_3$) δ 7.01 (d, *J* = 8.6 Hz, 2H), 6.83 (d, *J* = 8.6 Hz, 2H), 4.04 (dd, J = 3.6, 2.9 Hz, 1H), 3.79 (s, 3H), 3.26 (t, *J* = 4.3 Hz, 1H), 2.12 (tdd, *J* = 13.2, 5.9, 2.9 Hz, 1H), 1.75 (tt, *J* = 13.5, 3.6 Hz, 1H), 1.59 – 1.50 (m, 3H), 1.54 (s, 3H); ^{13}C NMR (176 MHz, $CDCl_3$) δ 158.0, 136.2, 132.3, 130.5, 129.5 (2C), 113.7 (2C), 69.3, 55.3, 46.0, 27.6, 27.3, 18.9, 16.9; IR (thin film) ν_{max}: 3429, 2935, 1610, 1509, 830 cm^{-1}; HRMS (EI) calcd for $C_{15}H_{20}O$: 232.1463, found: 232.1466.

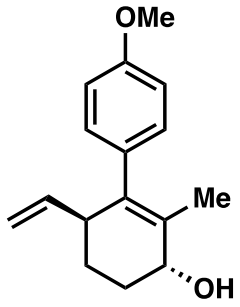

Substrate 192: The standard procedure was followed with 2,3-epoxy-2-methyl-cyclohexanone (126 mg, 1.0 mmol, 1.0 equiv) and 4-methoxyphenylmagnesium bromide (1.0 M in THF, 2.0 mL, 2.0 mmol, 2.0 equiv) followed by vinylmagnesium bromide (1.0 M in THF, 2.0 mL, 2.0 mmol, 2.0 euqiv) to afford **192** (117 mg, 0.48 mmol, 48%) as a white solid (> 20:1 d.r.). ^{1}H NMR (700 MHz, $CDCl_3$) δ 7.02 (d, *J* = 8.6 Hz, 2H), 6.84 (d, *J* = 8.6 Hz, 2H), 5.65 (ddd, *J* = 17.4, 10.3, 7.3 Hz, 1H), 4.88 (dd, *J* = 10.3, 1.7 Hz, 1H), 4.80 (dt, *J* = 17.4, 1.7 Hz, 1H), 4.09 (dt, *J* = 6.4, 2.9 Hz, 1H), 3.09 – 3.04 (m, 1H), 2.07 (dddd, *J* = 13.5, 13.1, 5.5, 2.9 Hz, 1H), 1.94 (tt, *J* = 13.7, 3.3 Hz, 1H), 1.77 (ddt, *J* = 13.7, 5.5, 2.9 Hz, 1H), 1.70 (d, *J* = 1.6 Hz, 3H), 1.66 (dddd, *J* = 13.1, 5.5, 3.3, 2.9 Hz, 1H), 1.57 (d, *J* = 6.4 Hz, 1H); ^{13}C NMR (176 MHz, $CDCl_3$) δ 158.1, 139.3, 137.7, 134.6, 131.8, 130.1 (2C), 115.3, 113.3 (2C), 68.7, 55.3, 44.4, 27.8, 23.7, 18.2; IR (thin film) ν_{max}: 3352, 2933, 1607, 1509, 1242 cm^{-1}; HRMS (EI) calcd for $C_{16}H_{20}O_2$: 244.1463, found: 244.1460.

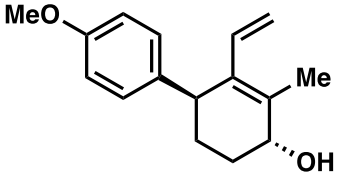

Substrate 193: The standard procedure was followed with 2,3-epoxy-2-methyl-cyclohexanone (126 mg, 1.0 mmol, 1.0 equiv) and vinylmagnesium bromide (1.0 M in THF, 2.0 mL, 2.0 mmol, 2.0 euqiv) followed by 4-methoxyphenyl-magnesium bromide (1.0 M in THF, 2.0 mL, 2.0 mmol, 2.0 equiv) to afford **193** (122 mg, 0.50 mmol, 50%) as a white solid (> 20:1 d.r.). ^{1}H NMR (700 MHz, $CDCl_3$) δ 7.01 (d, *J* = 8.6 Hz, 1H), 6.81 (d, *J* = 8.6 Hz, 1H), 6.70 (dd, *J* = 17.5, 11.1 Hz, 1H), 5.01 (dd, *J* = 11.1, 1.3 Hz, 1H), 4.97 (dd, *J* = 17.5, 1.3 Hz, 1H), 4.09 (t, *J* = 5.2 Hz, 1H), 3.77 (s, 3H), 3.75 (d, *J* = 5.5 Hz, 1H), 2.18 – 2.09 (m, 1H), 2.06 (d, *J* = 1.3 Hz, 3H), 1.73 – 1.66 (m, 1H), 1.62 (br s, 1H), 1.61 – 1.57 (m, 2H); ^{13}C NMR (176 MHz, $CDCl_3$) δ 157.9, 136.4, 135.2, 133.8, 133.2, 129.1 (2C), 116.1, 113.7 (2C), 69.6, 55.3, 39.5, 26.6, 26.5, 17.3; IR (thin film) ν_{max}: 3445, 2932, 1611, 1510, 1251 cm^{-1}; HRMS (EI) calcd for $C_{16}H_{20}O_2$: 244.1463, found: 244.1460.

Synthetic studies on the quassinoid core architecture:

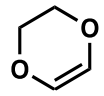

Dioxene (SI2-3): Although commercially available, dioxene can also be prepared in a rapid, economical fashion from readily accessible starting materials. Described here is a modification of known literature protocols[4] to produce dioxene on large scale. Dioxane (85 mL, 1.0 mol, 1.0 equiv) was placed in a 500 mL flask and a reflux condenser was attached. In addition to the inlet tubing at the top of the condenser providing a positive pressure of nitrogen, outlet tubing to a beaker containing 4 M NaOH (1000 mL) was connected. Sulfuryl chloride (162 mL, 2.0 mol, 2.0 equiv) was added dropwise over 30 min. After this addition was completed, the cooling bath was removed and the resulting pale yellow solution was heated at 40 ºC for 16 h. The solution was then heated at 65 ºC for 4 h at which point it gradually turned colorless. The solution was cooled to room temperature and argon was sparged through to displace any trace acidic gas. The crude product was concentrated under reduced pressure and the resulting *trans*-2,3-dichloro-1,4-dioxane was used immediately in the next step without further purification. This highly sensitive intermediate gradually decomposes over time and is best used fresh for subsequent chemistry.

Magnesium metal (36 g, 1.5 mol, 1.5 equiv) was suspended in THF (250 mL). The so-prepared crude *trans*-2,3-dichloro-1,4-dioxane (1.0 mol assumed, 1.0 equiv) was added neat to that suspension dropwise. After Grignard initiation, addition was continued to maintain a steady reflux. The resulting suspension was heated at 65 ºC for 4 h. The grey suspension was cooled to room temperature and filtered through Celite. Additional THF (*ca.* 200 mL) was used to wash the filter cake and quantitate transfer. The crude solution was directly distilled (100 ºC, house vacuum) into a flask cooled to –78 ºC. Dioxene was found to readily azeotrope with THF and so purified dioxene was afforded as a solution in THF (0.65 M, 28 g, 330 mmol, 33% over two steps, as judged by ^{1}H NMR analysis).

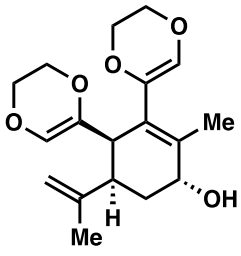

Diene 163: Carvone epoxide (332 mg, 2.0 mmol 1.0 equiv) was dissolved in THF (4.0 mL) and cooled to –78 ºC. LHMDS (1.0 M in THF, 2.0 mL, 2.0 mmol, 1.0 equiv) was added dropwise and the resulting solution was briefly warmed to 0 ºC (< 5 min) before being cooled back to –78 ºC. N-Phenyl-bis(trifluoromethanesulfonamide) (750 mg, 2.1 mmol, 1.05 equiv) was added as a solid and the reaction mixture was warmed to 0 ºC. In a separate flask, dioxene (0.65 M in THF, 12.3 mL, 8.0 mmol, 4.0 equiv) was cooled to 0 ºC. *n*-BuLi (2.5 M in hexanes, 3.0 mL, 7.4 mmol, 3.7 equiv) was added and the pale yellow solution was stirred for 1 h. In another separate flask, $[Cu(MeCN)_4][PF_6]$ (55 mg, 0.15 mmol, 0.15 equiv) was combined with anhydrous $MgBr_2$ (1.3 g, 7.0 mmol, 3.5 equiv). To this mixture of solids was rapidly added the dioxene-lithium solution followed by HMPA (0.87 mL, 5.0 mmol, 5.0 equiv). The cloudy suspension was stirred at 0 ºC for 30 min before being added dropwise to the enol triflate at –78 ºC. A wide-bore needle was used and care was taken during this operation to ensure all solids were transferred along with the solution. The reaction mixture was allowed to warm to 0 ºC slowly over 3 h then was stirred for an addition 1h at this temperature. The reaction mixture was diluted with EtOAc (50 mL) and quenched with a 9:1 saturated aqueous ammonium chloride:saturated aqueous ammonium hydroxide solution (10 mL). The biphasic suspension was stirred vigorously until the

aqueous layer had turned a deep blue. The layers were separated and the organic layer was further washed with water (2 x 10 mL) and brine (10 mL), dried over Na_2SO_4, filtered, and concentrated. The crude residue was purified by silica gel chromatography (27 → 37% Et_2O in hexanes + 3% Et_3N) to afford diene **163** (179 mg, 56 mmol, 55%) as a white solid. $[\alpha]_D^{23}$ = +176 (*c* 1.0, C_6D_6); ^{1}H NMR (700 MHz, $CDCl_3$) δ 5.94 (s, 1H), 5.73 (s, 1H), 4.82 (br s, 1H), 4.66 (br s, 1H), 4.16 – 4.11 (m, 2H), 4.08 – 4.00 (m, 3H), 3.92 – 3.85 (m, 4H), 2.94 (dq, *J* = 5.8, 1.6 Hz, 1H), 2.46 (ddd, *J* = 13.7, 5.8, 2.4 Hz, 1H), 2.18 (td, *J* = 13.7, 4.2 Hz, 1H), 1.98 (d, *J* = 1.6 Hz, 3H), 1.78 (br s, 3H), 1.73 (dt, *J* = 13.7, 2.4 Hz, 1H), 1.58 (br s, 1H). ^{13}C NMR (176 MHz, $CDCl_3$) δ 147.5, 136.3, 135.7, 134.5, 129.6, 126.9, 124.4, 109.9, 69.2, 64.6, 64.5, 64.4, 64.0, 42.0, 38.3, 32.5, 22.9, 19.1; IR (thin film) ν_{max}: 3419, 3034, 1673, 1478, 1143 cm^{-1}; HRMS (ESI): calcd for $C_{18}H_{25}O_5$ $[M+H]^+$: 321.1657, found: 321.1654.

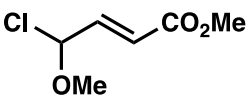

Dienophile 202: (*E*)-4,4-dimethoxybut-2-enoic acid methyl ester (480 mg, 3.0 mmol, 1.0 equiv)[5] and acetyl chloride (430 µL, 6.0 mmol, 2.0 equiv) were combined with a crystal of iodine (8 mg, 0.03 mmol, 0.01 equiv). The mixture was stirred at rt for 6 h. The crude residue was directly concentrated and then azeotroped from benzene (3 x 5 mL). The dienophile was used immediately in the next step without further purification (*ca.* 480 mg, near quantitative mass recovery). This crude product typically contained *ca.* 5% recovered starting material and *ca*. 5% (2E)-4-oxo-2-butenoic acid, along with some decomposition products; a purity of 80% was conservatively assumed by ^{1}H NMR analysis for the subsequent step. Tabulated ^{1}H and ^{13}C NMR data of this unpurified material were obtained: ^{1}H NMR (600 MHz, C_6D_6) δ 7.00 (dd, *J* = 15.6, 4.7 Hz, 1H), 6.11 (dd, *J* = 15.6, 1.3 Hz, 1H), 5.34 (ddq, *J* = 4.7, 1.3, 1.1 Hz, 1H), 3.30 (s, 3H), 2.97 (d, *J* = 1.1 Hz, 3H); ^{13}C NMR (151 MHz, C_6D_6) δ 165.6, 142.6, 122.4, 95.3, 57.2, 51.4.

Diels-Alder Reaction: Diene **163** (320 mg, 1.0 mmol, 1.0 equiv) was dissolved in PhMe (10 mL) and *N,N*-diisopropylethylamine (0.67 mL, 4.0 mmol, 4.0 equiv) was added at room temperature. Dienophile **202** (crude from previous operation, 328 mg, 2.0 mmol, 2.0 equiv) was dissolved in PhMe (5 mL) and added dropwise to the solution. The reaction mixture was stirred at room temperature for 12 h and then diluted with further PhMe (10 mL) and HMDS (2.5 mL). A reflux condenser was attached and the solution was heated at 110 ºC for 3 d. The reaction mixture was cooled to room temperature and concentrated. The crude residue was directly purified by silica gel chromatography (7 → 47% Et_2O in hexanes + 3% Et_3N; products are very sensitive to acid) to afford the desired product as a mixture of diastereomers (~1.3:1 d.r. as judged by ^{1}H NMR analysis, 279 mg, 0.62 mmol, 62%). A small amount of additional diastereomers was isolated as well (~11:1 d.r., 40 mg, 0.09 mmol, 9%). The two major diastereomers were used in subsequent chemistry as a mixture but could be separated by very careful preparatory TLC (2% THF in DCM). The two additional diastereomers could not be separated from each other; in this case, only the primary component of that mixture is reported.

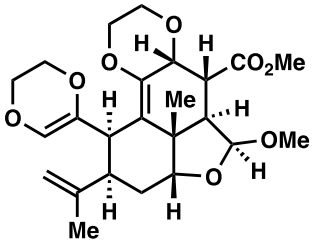

Diels-Alder Product 195: $[\alpha]_D^{23}$ = +6.7 (*c* 0.7, C_6D_6); ^{1}H NMR (600 MHz, C_6D_6) δ 6.03 (s, 1H), 5.53 (d, *J* = 4.5 Hz, 1H), 4.93 (br s, 1H), 4.89 (br s, 1H), 4.46 (dd, *J* = 8.0, 5.3 Hz, 1H), 4.38 (d, *J* = 7.7 Hz, 1H), 3.79 (dd, *J* = 13.2, 7.7 Hz, 1H), 3.71 (d, *J* = 5.4 Hz, 1H), 3.50 (s, 3H), 3.48 – 3.30 (m, 8H), 3.28 (s, 3H), 2.83 (dd, *J* = 13.2, 4.5 Hz, 1H), 2.48 (ddd, *J* = 14.6, 9.7, 8.0 Hz, 1H), 2.35 (ddd, *J* = 9.7, 7.7, 5.4 Hz, 1H), 1.85 (ddd, *J* = 14.6, 7.7, 5.3 Hz, 1H), 1.71 (br s, 3H), 1.52 (s, 3H); ^{13}C NMR (176 MHz, C_6D_6) δ 171.1, 146.8, 143.6, 136.4, 131.0, 128.4, 124.6, 111.1, 104.3, 82.2, 71.2, 68.2, 66.8, 64.0, 63.6, 55.0, 51.4, 51.1, 43.2, 42.7, 42.1, 36.9, 31.4, 26.4, 23.1; IR (thin film) vmax: 2978, 1745, 1671, 1096 cm^{-1}; HRMS (ESI): calcd for $C_{24}H_{33}O_8$ $[M+H]^+$: 449.2175, found: 449.2180.

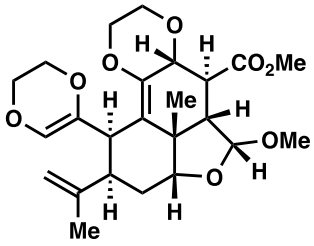

Diels-Alder Product 196: $[\alpha]_D^{23}$ = –66.4 (*c* 1.2, C_6D_6); ^{1}H NMR (600 MHz, $CDCl_3$) δ 5.88 (s, 1H), 4.84 (d, *J* = 6.1 Hz, 1H), 4.84 (br s, 1H), 4.74 (br s, 1H), 4.66 (dd, *J* = 7.3, 1.1 Hz, 1H), 3.98 – 3.84 (m, 8H), 3.80 (dt, *J* = 11.7, 2.5 Hz, 1H), 3.76 (s, 3H), 3.48 (d, *J* = 5.3 Hz, 1H), 3.34 (s, 3H), 3.16 (dd, *J* = 7.3, 3.6 Hz, 1H), 2.42 – 2.36 (m, 3H), 1.87 – 1.81 (m, 1H), 1.80 (br s, 3H), 1.15 (s, 3H); ^{13}C NMR (151 MHz, $CDCl_3$) δ 175.7, 147.6, 143.2, 138.4, 123.8, 115.7, 109.9, 104.8, 83.6, 68.7, 66.0, 64.4, 64.1, 63.8, 56.0, 52.5, 51.9, 45.2, 40.8, 38.0, 35.2, 27.8, 24.1, 23.0; IR (thin film) ν_{max}: 2956, 1736, 1671, 1646, 1091 cm^{-1}; HRMS (ESI): calcd for $C_{24}H_{32}O_8Na$ $[M+Na]^+$: 471.1995, found: 471.1999.

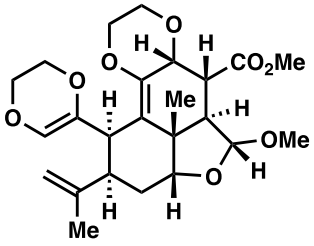

Diels-Alder Product 197: Afforded as a ~11:1 mixture of diastereomers; major reported. $[\alpha]_D^{23}$ = –17.7 (*c* 1.1, C_6D_6); ^{1}H NMR (700 MHz, C_6D_6) δ 6.02 (s, 1H), 4.94 (d, *J* = 8.1 Hz, 1H), 4.90 – 4.85 (m, 1H), 4.83 – 4.79 (m, 1H), 4.37 (d, *J* = 9.1 Hz, 1H), 4.37 (t, *J* = 8.0 Hz, 1H), 3.75 (d, *J* = 6.7 Hz, 1H), 3.59 (s, 3H), 3.53 – 3.50 (m, 1H), 3.48 (dd, *J* = 12.8, 9.1 Hz, 1H), 3.45 (s, 3H), 3.43 – 3.40 (m, 2H), 3.39 – 3.36 (m, 2H), 3.33 – 3.28 (m, 3H), 3.00 (dd, *J* = 12.8, 8.1 Hz, 1H), 2.49 (q, *J* = 9.7, 6.7 Hz, 1H), 2.41 (dt, *J* = 14.4, 8.0, 6.7 Hz, 1H), 2.02 (ddd, *J* = 14.4, 9.7, 8.0 Hz, 1H), 1.67 – 1.64 (m, 3H), 1.08 (s, 3H); ^{13}C NMR (176 MHz, C_6D_6) δ 170.1, 147.2, 142.3, 136.5, 125.7, 124.5, 111.0, 106.7, 80.9, 68.9, 66.5, 65.8, 64.0, 63.6, 55.4, 51.3, 49.8, 44.2, 43.2, 42.9, 36.3, 31.7, 23.3, 22.3; IR (thin film) ν_{max}: 2965, 1740, 1565, 1435, 1137 cm^{-1}; HRMS (ESI): calcd for $C_{24}H_{32}O_8Na$ $[M+Na]^+$: 471.1995, found: 471.2000.

Oxidation/Ene Reaction: The purified mixture of Diels-Alder products **195** and **196** (~1.3:1 d.r., 200 mg, 0.45 mmol, 1.0 equiv) was dissolved in DCM (7.5 mL) and cooled to –40 ºC. Freshly prepared and titrated DMDO (0.06 M in acetone, 7.5 mL, 0.45 mmol, 1.0 equiv) was then added dropwise. At the conclusion of the addition (< 5 min), the reaction mixture was further diluted with DCM (7.5 mL) and $AlMe_3$ (2.0 M in hexanes, 330 µL, 0.67 mmol, 1.5 equiv) was added dropwise. The resulting solution was allowed to warm to 0 ºC over 5 min before H_2O (20 µL) was added. An aqueous solution of NaOH (3 M, 20 µL) was added followed by additional H_2O (50 µL). When no further bubbling was observed,

$MgSO_4$ was added and the suspension was warmed to room temperature and stirred for 15 min. The mixture was filtered through celite, the residue was concentrated, and the crude product was purified by column chromatography (47→ 97% EtOAc in hexanes + 3% Et_3N) to afford quassin architectures **SI-7** and **27** (~1.3:1 d.r. as judged by ^1H NMR analysis, 116 mg, 0.25 mmol, 57%). These diastereomers could be separated by careful preparatory TLC (7% THF in DCM) and were subsequently characterized as single compounds:

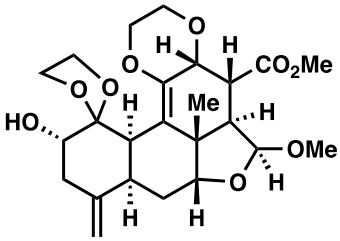

Quassin Architecture 200: $[\alpha]_D^{23}$ = +79.4 (*c* 0.8, CD_3OD); ^1H NMR (700 MHz, CD_3OD) δ 5.00 (d, *J* = 4.4 Hz, 1H), 4.85 (t, *J* = 2.0 Hz, 1H), 4.76 (t, *J* = 2.0 Hz, 1H), 4.41 (d, *J* = 7.7 Hz, 1H), 4.07 (dd, *J* = 8.6, 2.7 Hz, 1H), 4.03 (td, *J* = 7.1, 3.4 Hz, 1H), 3.97 (td, *J* = 7.1, 3.4 Hz, 1H), 3.92 (dt, *J* = 8.2, 7.1 Hz, 1H), 3.88 – 3.81 (m, 2H), 3.79 – 3.75 (m, 1H), 3.73 (dt, *J* = 8.2, 7.1 Hz, 1H), 3.70 – 3.68 (m, 1H), 3.68 (s, 3H), 3.67 (d, *J* = 5.4 Hz, 1H), 3.67 (dd, *J* = 3.8, 3.1 Hz, 1H), 3.49 (dd, *J* = 13.4, 7.8 Hz, 1H), 3.26 (s, 3H), 2.77 (ddt, *J* = 14.6, 3.8, 2.0 Hz, 1H), 2.51 (dt, *J* = 12.0, 7.5, 5.4 Hz, 1H), 2.38 (ddd, *J* = 15.0, 12.0, 8.6 Hz, 1H), 2.31 (dd, *J* = 13.3, 4.4 Hz, 1H), 2.26 (dd, *J* = 14.6, 3.1 Hz, 1H), 1.55 (ddd, *J* = 15.0, 7.5, 2.7 Hz, 1H), 1.22 (s, 3H); ^{13}C NMR (176 MHz, CD_3OD) δ 173.3, 147.2, 147.1, 129.1, 112.3, 110.6, 105.1, 82.9, 71.7, 70.0, 69.4, 67.7, 66.3, 65.1, 55.4, 53.0, 52.1, 43.3, 42.2, 41.7, 37.0, 36.0, 32.7, 27.8; IR (thin film) ν_{max}: 3488, 2954, 1742, 1653, 1437 cm^{-1}; HRMS (ESI) calcd for $C_{24}H_{32}O_9Na$ $[M+Na]^+$: 487.1944, found: 487.1947.

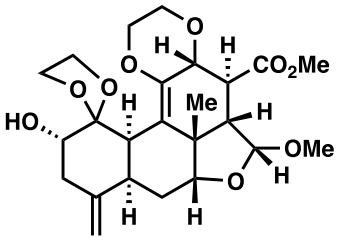

Quassin Architecture 201: $[\alpha]_D^{23}$ = –41.8 (*c* 1.0, CD_3OD); ^1H NMR (700 MHz, CD_3OD) δ 4.82 (t, *J* = 2.2 Hz, 1H), 4.81 (d, *J* = 5.6 Hz, 1H), 4.73 (t, *J* = 2.2 Hz, 1H), 4.67 (dd, *J* = 7.5, 1.1 Hz, 1H), 3.98 – 3.91 (m, 3H), 3.88 – 3.82 (m, 3H), 3.79 – 3.75 (m, 2H), 3.75 (s, 3H), 3.71 – 3.67 (m, 2H), 3.61 (t, *J* = 3.1 Hz, 1H), 3.35 (s, 3H), 3.09 (dd, *J* = 7.5, 3.4 Hz, 1H), 2.71 (ddt, *J* = 14.3, 3.1, 2.2 Hz, 1H), 2.66 (ddd, *J* = 13.8, 6.1, 3.1 Hz, 1H), 2.50 (td, *J* = 13.8, 2.9 Hz, 1H), 2.39 (dd, *J* = 5.6, 3.4 Hz, 1H), 2.27 (dt, *J* = 14.3, 3.1, 1.4 Hz, 1H), 1.49 (dtd, *J* = 13.8, 3.1, 1.3 Hz, 1H), 1.16 (s, 3H); ^{13}C NMR (176 MHz, CD_3OD) δ 176.9, 148.3, 146.4, 112.8, 112.0, 111.9, 106.3, 85.3, 71.2, 69.9, 66.6, 66.0, 65.3, 64.8, 55.9, 54.0, 52.8, 46.4, 41.6, 39.0, 36.6, 36.4, 30.9, 25.5; IR (thin film) ν_{max}: 3451, 2919, 1735, 1652, 1436 cm^{-1}; HRMS (ESI) calcd for $C_{24}H_{32}O_9Na$ $[M+Na]^+$: 487.1944, found: 487.1951.

References:

(1) L. Wang, H. Wang, Y. Li, P. Tang, *Angew. Chem. Int. Ed*. **2005**, *54*, 5732.
(2) (a) P. Kraft, C. Berthold, *Synthesis* **2008**, *4*, 543; (b) C. E. Harding, S. L. King, *J. Org. Chem.* **1992**, *57*, 883; (c) Q. Wang, Q. Huang, B. Chen. J. Lu, H. Wang, X. She, X. Pan, *Angew. Chem. Int. Ed.* **2006**, *45*, 3651.
(3) D. F. Taber, P. W., DeMatteo, R. A. Hassan, *Org. Synth.* **2013**, *90*, 350.
(4) R. I. Meltzer, A. D. Lewis, A. Fischman, *J. Org. Chem.* **1959**, *24*, 1763.
(5) L.-L. Shen, H.-S. Mun, J.-H. Jeong, *Eur. J. Org. Chem.* **2010**, 6895.

X-Ray Crystallographic Data for Substrate 172

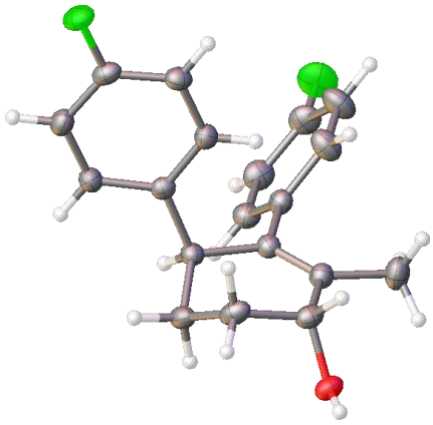

A colorless prism 0.20 x 0.18 x 0.07 mm in size was mounted on a Cryoloop with Paratone oil. Data were collected in a nitrogen gas stream at 100(2) K using ω scans. Crystal-to-detector distance was 60 mm and exposure time was 5 seconds per frame using a scan width of 2.0°. Data collection was 100% complete to 79.1° in θ. A total of 41015 reflections were collected covering the indices, -33<=*h* <=33, -34<=*k* <=31, -13<=*l* <=14. 3304 reflections were found to be symmetry independent, with an R_{int} of 0.0417. Indexing and unit cell refinement indicated a rhombohedral, trigonal lattice. The space group was found to be R-3 (No. 148). The data were integrated using the Bruker SAINT software program and scaled using the SADABS software program. Solution by iterative methods (SHELXT-2014) produced a complete heavy-atom phasing model consistentwith the proposed structure. All non-hydrogen atoms were refined anisotropically by full-matrix least-squares (SHELXL-2016). All hydrogen atoms were placed using a riding model. Their po- sitions were constrained relative to their parent atom using the appropriate HFIX command in SHELXL-2016.

Table SI2.1.1: Crystal data and structure refinement for 172.

Identification code	**179**
Empirical formula	$C_{19}H_{18}F_2O$
Formula weight	300.33
Temperature (K)	100(2)
Crystal system	trigonal
Space group	R-3
a (Å)	26.8452(2)
b (Å)	26.8452(2)
c (Å)	11.23090(10)
α (°)	90
β (°)	90
γ (°)	120
Volume ($Å^3$)	7009.36(12)
Z	18
ρ_{calc} (g/cm_3)	1.281
μ (mm^{-1})	0.776
F(000)	2844.0
Crystal size (mm^3)	0.2 × 0.18 × 0.07
Radiation	CuKα (λ = 1.54184)
2Θ range for data collection (°)	6.586 to 158.188
Index ranges	$-33 \leq h \leq 33$, $-34 \leq k \leq 31$, $-13 \leq l \leq 14$
Reflections collected	41015
Independent reflections	3304 [R_{int} = 0.0417, R_{sigma} = 0.0142]
Data/restraints/parameters	3304/0/204
Goodness-of-fit on F^2	1.059
Final R indexes [I>=2σ (I)]	R_1 = 0.0447, wR_2 = 0.1205
Final R indexes [all data]	R_1 = 0.0463, wR_2 = 0.1217
Largest diff. peak/hole (e $Å^{-3}$)	1.07/-0.23

Table SI2.1.2: Fractional Atomic Coordinates ($\times 10^4$) and Equivalent Isotropic Displacement Parameters (Å2×103) for 172. Ueq is defined as 1/3 of the trace of the orthogonalized Uij tensor.

Atom	*x*	*y*	*z*	U(eq)
F2	4706.2(4)	5311.7(4)	-416.8(7)	34.2(2)
O1	3904.0(4)	6112.5(5)	6525.9(9)	28.7(2)
F1	3457.0(5)	2749.2(4)	5482.4(11)	49.8(3)
C14	3826.5(6)	5108.6(5)	2722.8(12)	21.7(3)
C8	3681.7(6)	4376.3(6)	5088.5(12)	24.3(3)
C7	3768.2(6)	4969.4(6)	4958.9(12)	22.9(3)
C15	4398.1(6)	5237.3(6)	2729.5(12)	24.5(3)
C19	3559.1(6)	5043.9(6)	1621.0(12)	26.0(3)
C2	4073.9(6)	5388.1(6)	5752.5(12)	25.5(3)
C6	3497.8(6)	5067.9(6)	3860.3(12)	22.6(3)
C17	4415.8(6)	5238.9(6)	620.1(12)	26.5(3)
C16	4698.1(6)	5302.0(6)	1677.7(13)	26.9(3)
C18	3853.3(6)	5110.5(6)	562.4(13)	28.5(3)
C9	3131.9(6)	3891.6(6)	5062.5(13)	28.1(3)
C5	3437.9(6)	5604.9(6)	4001.9(12)	27.8(3)
C3	4194.7(6)	5997.7(6)	5581.0(12)	26.7(3)
C4	4013.7(7)	6109.8(6)	4373.3(13)	30.1(3)
C10	3051.9(7)	3343.2(6)	5200.1(15)	34.0(3)
C11	3528.2(7)	3283.7(6)	5343.0(15)	35.0(3)
C13	4147.7(7)	4289.9(7)	5224.7(15)	34.6(3)
C1	4317.6(7)	5303.0(7)	6893.1(14)	36.0(4)
C12	4079.2(7)	3746.1(7)	5350.1(17)	39.8(4)

Table SI2.1.3: Anisotropic Displacement Parameters ($Å^2 \times 10^3$) for **172**. The anisotropic dis-placement factor exponent takes the form:$-2\pi^2[h^2a^{*2}U_{11}+2hka^*b^*U_{12}+\ldots]$

Atom	U_{11}	U_{22}	U_{33}	U_{23}	U_{13}	U_{12}
F2	41.7(5)	38.7(5)	25.3(4)	3.5(3)	10.4(4)	22.4(4)
O1	29.8(5)	27.8(5)	25.3(5)	-4.4(4)	3.9(4)	12.0(4)
F1	61.3(7)	25.7(5)	66.1(7)	3.3(4)	2.0(5)	24.4(5)
C14	23.3(6)	17.7(6)	23.1(6)	0.3(5)	1.8(5)	9.6(5)
C8	26.6(7)	23.8(6)	21.6(6)	1.7(5)	0.6(5)	11.9(5)
C7	21.9(6)	23.5(6)	22.3(6)	2.5(5)	2.1(5)	10.7(5)
C15	24.0(6)	24.7(6)	23.7(7)	-1.3(5)	-1.9(5)	11.4(5)
C19	24.2(7)	29.2(7)	25.9(7)	-1.3(5)	-2.0(5)	14.3(6)
C2	24.9(6)	26.5(7)	23.5(6)	0.7(5)	0.1(5)	11.5(5)
C6	21.1(6)	24.2(6)	22.4(6)	1.0(5)	0.8(5)	11.3(5)
C17	33.3(7)	23.3(6)	23.6(7)	2.2(5)	7.6(5)	14.7(6)
C16	23.0(6)	27.4(7)	30.1(7)	-1.0(5)	2.9(5)	12.5(5)
C18	34.1(7)	31.4(7)	22.5(7)	-1.3(5)	-2.9(5)	18.2(6)
C9	25.9(7)	28.8(7)	29.0(7)	1.2(5)	2.6(5)	13.3(6)
C5	35.7(7)	34.6(7)	22.1(6)	2.2(5)	3.0(5)	24.3(6)
C3	25.6(7)	24.5(7)	26.9(7)	-1.6(5)	4.8(5)	10.3(5)
C4	42.2(8)	24.1(7)	26.4(7)	2.6(5)	8.2(6)	18.4(6)
C10	29.6(7)	24.9(7)	38.2(8)	-0.9(6)	2.2(6)	6.8(6)
C11	45.2(9)	23.1(7)	38.8(8)	2.7(6)	2.2(7)	18.6(7)
C13	25.8(7)	27.1(7)	48.1(9)	5.7(6)	-1.5(6)	11.2(6)
C1	41.6(9)	34.6(8)	30.0(8)	-3.7(6)	-9.9(6)	17.7(7)
C12	34.6(8)	34.4(8)	57.0(11)	5.3(7)	-2.0(7)	22.1(7)

Table SI2.1.4: Bond Lengths for **172**.

Atom	Atom	Length (Å)	Atom	Atom	Length (Å)
F2	C17	1.3601(15)	C19	C18	1.389(2)
O1	C3	1.4389(16)	C2	C3	1.5132(19)
F1	C11	1.3586(17)	C2	C1	1.507(2)
C14	C15	1.3941(18)	C6	C5	1.5366(18)
C14	C19	1.3972(19)	C17	C16	1.373(2)
C14	C6	1.5253(18)	C17	C18	1.372(2)
C8	C7	1.4968(18)	C9	C10	1.386(2)
C8	C9	1.3972(19)	C5	C4	1.518(2)
C8	C13	1.390(2)	C3	C4	1.521(2)
C7	C2	1.3449(19)	C10	C11	1.375(2)
C7	C6	1.5203(18)	C11	C12	1.376(2)
C15	C16	1.3908(19)	C13	C12	1.384(2)

Table SI2.1.5: Bond Angles for **172**.

Atom	Atom	Atom	Angle (˚)	Atom	Atom	Atom	Angle (˚)
C15	C14	C19	117.97(12)	F2	C17	C16	118.79(13)
C15	C14	C6	122.61(12)	F2	C17	C18	118.38(13)
C19	C14	C6	119.33(12)	C18	C17	C16	122.82(13)
C9	C8	C7	121.23(12)	C17	C16	C15	118.04(13)
C13	C8	C7	120.95(12)	C17	C18	C19	118.39(13)
C13	C8	C9	117.82(13)	C10	C9	C8	121.15(14)
C8	C7	C6	115.49(11)	C4	C5	C6	109.19(11)
C2	C7	C8	121.99(12)	O1	C3	C2	106.97(11)
C2	C7	C6	122.50(12)	O1	C3	C4	110.74(12)
C16	C15	C14	121.54(13)	C2	C3	C4	114.25(11)
C18	C19	C14	121.23(13)	C5	C4	C3	110.59(11)
C7	C2	C3	122.05(12)	C11	C10	C9	118.51(14)
C7	C2	C1	124.50(13)	F1	C11	C10	119.23(14)
C1	C2	C3	113.43(12)	F1	C11	C12	118.18(14)
C14	C6	C5	110.35(11)	C10	C11	C12	122.59(14)
C7	C6	C14	112.49(11)	C12	C13	C8	122.07(14)
C7	C6	C5	111.24(11)	C11	C12	C13	117.84(14)

Table SI2.1.6: Hydrogen Atom Coordinates (Å×10^4) and Isotropic Displacement Parameters (Å^2×10^3) for **172**.

Atom	*x*	*y*	*z*	U(eq)
H15	4587.1	5281.93	3469.94	29
H19	3168.72	4952.72	1595.58	31
H6	3101.59	4728.98	3776.96	27
H16	5086.77	5387.4	1690.59	32
H18	3669.6	5068.14	-183.87	34
H9	2807.13	3938.64	4948.4	34
H5A	3313.52	5692.61	3238.7	33
H5B	3143.66	5534.2	4612.33	33
H3	4617.69	6264.16	5674.47	32
H4A	3984.32	6462.67	4414.11	36
H4B	4308.74	6171.85	3771.47	36
H10	2676.49	3015.83	5195.9	41
H13	4525.12	4614.27	5231.85	41
H1A	4129.25	4891.6	7078.94	54
H1B	4250.16	5505.96	7542.48	54
H1C	4732.06	5456.03	6799.58	54
H12	4402.08	3693.85	5438.22	48
H1	4071(9)	6511(10)	6653(19)	54(6)

X-Ray Crystallographic Data for Substrate 175

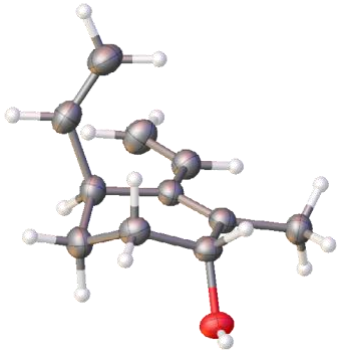

A colorless needle 0.24 x 0.06 x 0.05 mm in size was mounted on a Cryoloop with Paratone oil. Data were collected in a nitrogen gas stream at 100(2) K using ω scans. Crystal-to-detector distance was 60 mm and exposure time was 5 seconds per frame using a scan width of 2.0°. Data collection was 100% complete to 79.1° in θ. A total of 10823 reflections were collected covering the indices, -28<=*h*<=14, -28<=*k*<=27, -9<=*l*<=9. 2055 reflections were found to be symmetry independent, with an R_{int} of 0.0386. Indexing and unit cell refinement indicated a body centered, tetragonal lattice. The space group was found to be $I4_1/a$ (No. 88). The data were integrated using the Bruker SAINT software program and scaled using the SADABS software program. Solution by iterative methods (SHELXT-2014) produced a complete heavy-atom phasing model consistent with the proposed structure. All non-hydrogen atoms were refined anisotropically by full-matrix least-squares (SHELXL-2016). All hydrogen atoms were placed using a riding model. Their positions were constrained relative to their parent atom using the appropriate HFIX command in SHELXL-2016.

Table SI2.2.1: Crystal data and structure refinement for **175**.

Identification code	**175**
Empirical formula	$C_{11}H_{16}O$
Formula weight	164.24
Temperature (K)	100(2)
Crystal system	tetragonal
Space group	$I4_1/a$
a (Å)	22.7253(4)
b (Å)	22.7253(4)
c (Å)	7.5782(2)
α (°)	90
β (°)	90
γ (°)	90
Volume ($Å^3$)	3913.68(17)
Z	16
ρ_{calc} (g/cm_3)	1.115
μ (mm^{-1})	0.533
F(000)	1440.0
Crystal size (mm^3)	0.24 × 0.06 × 0.05
Radiation	CuKα (λ = 1.54184)
2Θ range for data collection (°)	7.78 to 158.146
Index ranges	$-28 \leq h \leq 14$, $-28 \leq k \leq 27$, $-9 \leq l \leq 9$
Reflections collected	10823
Independent reflections	2055 [R_{int} = 0.0386, R_{sigma} = 0.0215]
Data/restraints/parameters	2055/0/173
Goodness-of-fit on F^2	1.081
Final R indexes [I>=2σ (I)]	R_1 = 0.0529, wR_2 = 0.1395
Final R indexes [all data]	R_1 = 0.0579, wR_2 = 0.1431
Largest diff. peak/hole (e $Å^{-3}$)	0.22/-0.18

Table SI2.2.2: Fractional Atomic Coordinates ($\times 10^4$) and Equivalent Isotropic Displacement Parameters ($Å^2 \times 10^3$) for **175**. U_{eq} is defined as 1/3 of the trace of the orthogonalized U_{ij} tensor.

Atom	***x***	***y***	***z***	**U(eq)**
O1	2139.1(5)	4573.3(5)	3787.1(16)	33.7(3)
C9	1648.5(7)	3358.2(7)	5843(2)	29.2(4)
C2	1563.1(7)	3938.6(7)	5556(2)	29.1(4)
C3	1622.6(7)	4208.7(7)	3739(2)	30.0(4)
C6	1835.0(7)	2941.2(7)	4375(2)	32.2(4)
C10	1579.2(7)	3107.6(7)	7620(2)	33.9(4)
C1	1424.5(8)	4379.6(8)	6981(2)	34.2(4)
C4	1671.8(8)	3764.3(8)	2259(2)	33.8(4)
C7	1352.6(8)	2535.0(8)	3743(2)	38.2(4)
C5	2092.6(8)	3275.9(8)	2794(2)	35.9(4)
C11	1659.0(9)	2550.2(8)	8087(3)	42.7(5)
C8	791.7(9)	2564.4(9)	4127(3)	46.6(5)

Table SI2.2.3: Anisotropic Displacement Parameters ($Å^2 \times 10^3$) for **175**. The anisotropic dis-placement factor exponent takes the form:$-2\pi^2[h^2a^{*2}U_{11}+2hka^*b^*U_{12}+\ldots]$.

Atom	U_{11}	U_{22}	U_{33}	U_{23}	U_{13}	U_{12}
O1	32.6(6)	33.7(6)	34.7(7)	7.0(5)	-4.5(5)	-6.4(4)
C9	26.1(7)	30.7(8)	31.0(8)	-2.8(6)	-0.2(6)	-0.1(6)
C2	25.0(7)	31.4(8)	30.9(8)	-0.7(6)	0.4(6)	-0.5(6)
C3	26.3(7)	30.4(8)	33.4(8)	0.9(6)	-2.4(6)	-1.4(6)
C6	34.3(8)	28.6(8)	33.7(9)	-2.2(7)	-1.4(7)	3.8(6)
C10	35.7(8)	33.8(8)	32.2(9)	-0.3(7)	0.9(7)	-1.0(6)
C1	36.9(9)	30.7(8)	35.1(9)	-3.3(7)	2.2(7)	1.4(7)
C4	37.2(9)	36.2(9)	28.0(8)	2.3(7)	-0.3(7)	-4.1(7)
C7	47.6(10)	29.0(8)	38.0(10)	-2.3(7)	-3.9(8)	-0.8(7)
C5	36.8(9)	37.4(9)	33.4(9)	-6.7(7)	4.6(7)	1.8(7)
C11	54.6(11)	35.5(9)	37.9(10)	4.8(8)	-1.3(8)	-2.4(8)
C8	44.6(10)	39.4(10)	55.7(12)	-3.6(9)	-5.1(9)	-7.5(8)

Table SI2.2.4: Bond Lengths for **175**.

Atom	Atom	Length (Å)	Atom	Atom	Length (Å)
O1	C3	1.4373(18)	C3	C4	1.513(2)
C9	C2	1.351(2)	C6	C7	1.511(2)
C9	C6	1.522(2)	C6	C5	1.535(2)
C9	C10	1.470(2)	C10	C11	1.328(2)
C2	C3	1.513(2)	C4	C5	1.520(2)
C2	C1	1.506(2)	C7	C8	1.309(3)

Table SI2.2.5: Bond Angles for **175**.

Atom	Atom	Atom	Angle (˚)	Atom	Atom	Atom	Angle (˚)
C2	C9	C6	122.01(15)	C2	C3	C4	114.22(14)
C2	C9	C10	120.68(15)	C9	C6	C5	111.63(14)
C10	C9	C6	117.29(14)	C7	C6	C9	114.20(14)
C9	C2	C3	121.99(15)	C7	C6	C5	109.40(14)
C9	C2	C1	124.35(15)	C11	C10	C9	126.80(17)
C1	C2	C3	113.63(14)	C3	C4	C5	109.65(14)
O1	C3	C2	106.50(13)	C8	C7	C6	127.22(17)
O1	C3	C4	110.05(13)	C4	C5	C6	109.26(14)

Table SI2.2.6: Hydrogen Atom Coordinates (Å×10^4) and Isotropic Displacement Parameters (Å^2×10^3) for **175**.

Atom	*x*	*y*	*z*	U(eq)
H1	2115(10)	4837(11)	2950(40)	55(7)
H11A	1590(10)	2414(10)	9360(30)	53(6)
H11B	1777(10)	2240(11)	7220(40)	57(7)
H8A	622(10)	2883(11)	4920(30)	58(7)
H8B	488(12)	2276(11)	3650(30)	62(7)
H3	1266(9)	4473(9)	3520(30)	36(5)
H4A	1267(9)	3597(8)	2020(30)	34(5)
H6	2164(8)	2695(8)	4900(30)	35(5)
H4B	1801(9)	3966(9)	1190(30)	39(5)
H5A	2496(10)	3446(9)	3160(30)	46(6)
H1A	1766(12)	4470(12)	7700(40)	72(8)
H5B	2168(8)	3000(9)	1800(30)	33(5)
H10	1467(9)	3374(9)	8570(30)	37(5)
H1B	1081(11)	4270(11)	7730(40)	62(7)
H7	1502(10)	2212(10)	2910(30)	49(6)
H1C	1334(13)	4757(13)	6500(40)	81(9)

X-Ray Crystallographic Data for Substrate 193

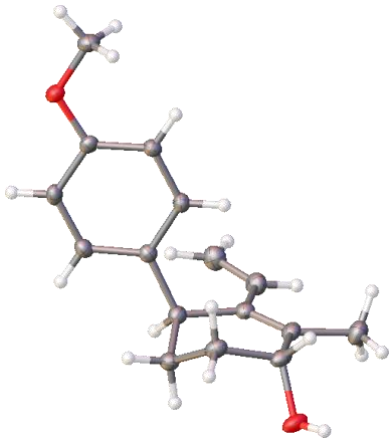

A colorless prism 0.22 x 0.22 x 0.05 mm in size was mounted on a Cryoloop with Paratone oil. Data were collected in a nitrogen gas stream at 100(2) K using ω scans. Crystal-to-detector distance was 60 mm and exposure time was 5 seconds per frame using a scan width of 2.0°. Data collection was 97% complete to 74.5° in θ. A total of 8543 reflections were collected covering the indices, -6<=*h*<=6, -9<=*k*<=7, -39<=*l*<=39. 2588 reflections were found to be symmetry independent, with an R_{int} of 0.0288. Indexing and unit cell refinement indicated a primitive, orthorhombic lattice. The space group was found to be $P2_12_12_1$ (No. 19). The data were integrated using the Bruker SAINT software program and scaled using the SADABS software program. Solution by iterative methods (SHELXT-2014) produced a complete heavy-atom phasing model consistent with the proposed structure. All non-hydrogen atoms were refined anisotropically by full-matrix least-squares (SHELXL-2016). All hydrogen atoms were placed using a riding model. Their positions were constrained relative to their parent atom using the appropriate HFIX command in SHELXL-2016.

Although racemic starting material was used to prepare this crystal, spontaneous resolution appears to have occurred. Due to this unexpected outcome, identifying anomalous dispersion was not prioritized during data collection and thus insufficient data exists to definitively assign the absolute stereochemistry of the crystal. It has been rendered here in the enantiomer that corresponds to how the structure was depicted in the main text.

Table SI2.3.1: Crystal data and structure refinement for **193**.

Identification code	**193**
Empirical formula	$C_{16}H_{20}O_2$
Formula weight	244.32
Temperature (K)	100(2)
Crystal system	orthorhombic
Space group	$P2_12_12_1$
a (Å)	5.52630(10)
b (Å)	7.5880(2)
c (Å)	31.5641(6)
α (°)	90
β (°)	90
γ (°)	90
Volume ($Å^3$)	1323.60(5)
Z	4
ρ_{calc} (g/cm_3)	1.226
μ (mm^{-1})	0.622
F(000)	528.0
Crystal size (mm^3)	0.22 × 0.22 × 0.05
Radiation	CuKα (λ = 1.54184)
2Θ range for data collection (°)	11.214 to 148.98
Index ranges	$-6 \leq h \leq 6$, $-9 \leq k \leq 7$, $-39 \leq l \leq 39$
Reflections collected	8543
Independent reflections	2588 [R_{int} = 0.0288, R_{sigma} = 0.0177]
Data/restraints/parameters	2588/0/177
Goodness-of-fit on F^2	1.069
Final R indexes [I>=2σ (I)]	R_1 = 0.0330, wR_2 = 0.0866
Final R indexes [all data]	R_1 = 0.0334, wR_2 = 0.0869
Largest diff. peak/hole (e $Å^{-3}$)	0.20/-0.20
Flack parameter	0.32(9)

Table SI2.3.2: Fractional Atomic Coordinates ($\times 10^4$) and Equivalent Isotropic Displacement Parameters ($Å^2 \times 10^3$) for **193**. U_{eq} is defined as 1/3 of the trace of the orthogonalized U_{ij} tensor.

Atom	*x*	*y*	*z*	U(eq)
O2	1794(2)	6540.2(16)	7924.5(4)	20.9(3)
O1	448(3)	7688(2)	5139.8(4)	27.6(3)
C13	2178(3)	6437(2)	7495.1(5)	17.2(3)
C11	1301(3)	5520(2)	6782.1(5)	18.0(3)
C12	717(3)	5526(2)	7214.4(5)	18.2(3)
C15	4756(3)	7314(2)	6919.8(5)	19.0(3)
C14	4213(3)	7336(2)	7347.1(5)	18.9(3)
C10	3309(3)	6411(2)	6628.0(5)	17.1(3)
C16	-354(3)	5741(2)	8082.8(5)	22.9(4)
C3	2928(3)	5013(2)	5888.4(5)	18.9(4)
C4	1121(3)	5253(2)	5608.2(5)	21.1(4)
C9	3936(3)	6516(2)	6157.5(5)	18.7(4)
C8	3202(3)	8323(2)	5977.1(5)	21.4(4)
C7	495(3)	8354(2)	5891.8(5)	22.4(4)
C6	-160(3)	7003(2)	5555.3(5)	21.6(4)
C1	5779(4)	2875(3)	6222.9(6)	28.0(4)
C5	181(4)	3849(3)	5313.1(6)	28.2(4)
C2	4100(3)	3290(2)	5938.6(6)	24.8(4)

Table SI2.3.3: Anisotropic Displacement Parameters ($Å^2 \times 10^3$) for **193**. The anisotropic dis-placement factor exponent takes the form:$-2\pi^2[h^2a^{*2}U_{11}+2hka^*b^*U_{12}+\ldots]$.

Atom	U_{11}	U_{22}	U_{33}	U_{23}	U_{13}	U_{12}
O2	25.0(6)	22.7(6)	15.1(5)	0.5(5)	-0.4(5)	-3.1(5)
O1	26.0(7)	41.5(8)	15.2(6)	5.9(5)	0.7(5)	3.2(6)
C13	19.3(8)	16.8(7)	15.5(7)	1.9(6)	-1.6(6)	2.4(7)
C11	17.3(8)	18.2(7)	18.6(7)	-1.7(6)	-1.5(6)	-1.6(7)
C12	17.8(8)	18.2(7)	18.5(7)	1.3(6)	1.1(6)	-2.4(7)
C15	15.6(8)	19.1(7)	22.4(8)	1.1(6)	0.3(7)	-2.0(7)
C14	17.3(8)	19.0(7)	20.3(8)	-1.1(6)	-4.8(7)	-1.1(7)
C10	16.3(8)	17.1(7)	17.9(7)	0.0(6)	0.0(6)	0.8(7)
C16	24.6(9)	25.8(8)	18.2(7)	2.4(7)	3.5(7)	-0.2(8)
C3	18.9(8)	22.2(8)	15.5(7)	-0.8(6)	3.7(7)	-1.2(7)
C4	20.4(8)	27.4(9)	15.5(7)	-2.0(7)	2.2(7)	-1.8(7)
C9	15.8(7)	22.3(8)	17.9(7)	-0.4(7)	1.0(6)	-1.6(7)
C8	25.0(9)	20.8(8)	18.5(8)	1.0(7)	1.9(7)	-3.3(7)
C7	25.2(9)	23.9(8)	18.1(7)	2.1(7)	1.2(7)	3.2(8)
C6	17.9(8)	31.9(9)	14.9(7)	2.1(7)	2.3(6)	1.5(7)
C1	27.3(10)	24.4(9)	32.5(9)	-1.0(8)	-1.0(8)	1.9(8)
C5	29.2(10)	33.2(10)	22.2(8)	-5.1(8)	-3.7(8)	-0.2(8)
C2	27.1(9)	22.9(8)	24.3(8)	-4.3(7)	0.7(7)	0.3(8)

Table SI2.3.4: Bond Lengths for **193**.

Atom	Atom	Length (Å)	Atom	Atom	Length (Å)
O2	C13	1.3743(19)	C3	C4	1.346(2)
O2	C16	1.423(2)	C3	C9	1.527(2)
O1	C6	1.450(2)	C3	C2	1.468(2)
C13	C12	1.384(2)	C4	C6	1.514(2)
C13	C14	1.396(2)	C4	C5	1.508(2)
C11	C12	1.402(2)	C9	C8	1.539(2)
C11	C10	1.388(2)	C8	C7	1.520(3)
C15	C14	1.382(2)	C7	C6	1.519(2)
C15	C10	1.399(2)	C1	C2	1.329(3)
C10	C9	1.527(2)			

Table SI2.3.5: Bond Angles for **193**.

Atom	Atom	Atom	Angle (°)	Atom	Atom	Atom	Angle (°)
C13	O2	C16	116.79(13)	C2	C3	C9	116.36(15)
O2	C13	C12	124.74(15)	C3	C4	C6	122.55(16)
O2	C13	C14	115.26(14)	C3	C4	C5	124.46(17)
C12	C13	C14	120.00(15)	C5	C4	C6	112.98(15)
C10	C11	C12	121.58(16)	C10	C9	C3	114.77(14)
C13	C12	C11	119.36(16)	C10	C9	C8	110.27(13)
C14	C15	C10	121.65(16)	C3	C9	C8	111.30(13)
C15	C14	C13	119.70(16)	C7	C8	C9	109.81(15)
C11	C10	C15	117.70(15)	C6	C7	C8	110.35(15)
C11	C10	C9	123.23(15)	O1	C6	C4	107.81(14)
C15	C10	C9	119.01(14)	O1	C6	C7	109.61(15)
C4	C3	C9	122.33(16)	C4	C6	C7	113.76(14)
C4	C3	C2	121.26(17)	C1	C2	C3	126.33(18)

Table SI2.3.6: Hydrogen Atom Coordinates (Å×10^4) and Isotropic Displacement Parameters (Å^2×10^3) for **193**.

Atom	*x*	*y*	*z*	U(eq)
H11	319.64	4903.17	6594.18	22
H12	-639.44	4922.97	7311.5	22
H15	6117.03	7913.55	6823.83	23
H14	5199.06	7947.68	7535.2	23
H16A	-1731.63	6213.76	7936.72	34
H16B	-499.1	5978.24	8380.45	34
H16C	-278.03	4490.41	8038.04	34
H9	5703.24	6446.56	6137.26	22
H8A	3616.43	9242.85	6177.8	26
H8B	4076.54	8544.44	5716.09	26
H7A	-375.73	8093.92	6151.22	27
H7B	19.15	9519.46	5797.1	27
H6	-1909.02	6797.36	5566.26	26
H5A	1489.57	3397.83	5145.11	42
H5B	-1029.6	4345.74	5130.56	42
H5C	-517.15	2908.42	5475.86	42
H2	3621.13	2402.75	5753.48	30
H1	-810(70)	7790(50)	4995(11)	72(10)
H1A	6390(50)	1700(30)	6232(7)	32(6)
H1B	6420(50)	3700(30)	6438(8)	37(6)

X-Ray Crystallographic Data for Substrate 163

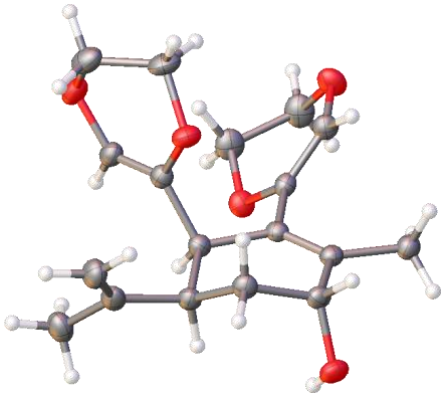

A colorless prism 0.16 x 0.13 x 0.05 mm in size was mounted on a Cryoloop with Paratone oil. Data were collected in a nitrogen gas stream at 100(2) K using ω scans. Crystal-to-detector distance was 60 mm and exposure time was 5 seconds per frame using a scan width of 2.0°. Data collection was 99% complete to 68.3° in θ. A total of 20223 reflections were collected covering the indices, -9<=*h*<=9, -7<=*k*<=7, -18<=*l*<=19. 2984 reflections were found to be symmetry independent, with an R_{int} of 0.0352. Indexing and unit cell refinement indicated a primitive, monoclinic lattice. The space group was found to be $P2_1$ (No. 4). The data were integrated using the Bruker SAINT software program and scaled using the SADABS software program. Solution by iterative methods (SHELXT-2014) produced a complete heavy-atom phasing model consistent with the proposed structure. All non-hydrogen atoms were refined anisotropically by full-matrix least-squares (SHELXL-2014). All hydrogen atoms were placed using a riding model. Their positions were constrained relative to their parent atom using the appropriate HFIX command in SHELXL-2014. Absolute stereochemistry was unambiguously determined from the diffraction data.

Table SI2.4.1: Crystal data and structure refinement for 163.

Identification code	163
Empirical formula	$C_{18}H_{24}O_5$
Formula weight	320.39
Temperature (K)	99.97
Crystal system	monoclinic
Space group	$P2_1$
a (Å)	8.0320(3)
b (Å)	6.3518(2)
c (Å)	16.1371(6)
α (°)	90
β (°)	93.7797(15)
γ (°)	90
Volume ($Å^3$)	821.49(5)
Z	2
ρ_{calc} (g/cm_3)	1.2951
μ (mm^{-1})	0.768
F(000)	345.2
Crystal size (mm^3)	0.16× 0.13× 0.05
Radiation	Cu Kα (λ = 1.54178)
2Θ range for data collection (°5).4	8 to 136.56
Index ranges	$-9 \le h \le 9$, $-7 \le k \le 7$, $-18 \le l \le 19$
Reflections collected	20223
Independent reflections	2984 [R_{int} = 0.0352, R_{sigma} = 0.0192]
Data/restraints/parameters	2984/1/297
Goodness-of-fit on F^2	1.096
Final R indexes [I>=2σ (I)]	R_1 = 0.0243, wR_2 = 0.0616
Final R indexes [all data]	R_1 = 0.0249, wR_2 = 0.0620
Largest diff. peak/hole (e $Å^{-3}$) 0.	3/-0.12
Flack parameter	0.02(11)

Table SI2.4.2: Fractional Atomic Coordinates ($\times 10^4$) and Equivalent Isotropic Displacement Parameters ($Å^2 \times 10^3$) for **163**. U_{eq} is defined as 1/3 of the trace of the orthogonalized U_{ij} tensor.

Atom	*x*	*y*	*z*	U(eq)
O1	-2348.9(11)	-217.9(14)	3233.7(6)	26.7(2)
O2	-7451.1(11)	-860.9(14)	1044.1(6)	28.1(2)
O3	-2480.9(11)	4804.0(14)	1581.5(6)	25.1(2)
O4	-941.7(11)	3337.3(15)	4135.2(6)	30.9(2)
O5	456.6(12)	2965.6(14)	974.2(6)	30.1(2)
C6	-3794.2(14)	1429.3(18)	1641.2(7)	19.5(2)
C7	-6284.3(16)	1141(2)	3629.5(8)	27.4(3)
C8	-4374.1(15)	2035.6(19)	2492.8(8)	20.3(2)
C9	-2942.5(15)	1816(2)	3133.5(7)	21.4(3)
C10	-2331.4(16)	2669.7(18)	1418.6(7)	20.1(3)
C11	-939.0(15)	1845(2)	1157.6(8)	24.0(3)
C12	-4030.0(16)	-641(2)	301.7(8)	24.6(3)
C13	-4487.6(14)	-107(2)	1165.2(7)	20.6(2)
C14	-2258.7(15)	3459(2)	3539.3(8)	24.9(3)
C15	-6165.3(18)	-429(2)	4171.2(9)	32.8(3)
C16	-5878.5(15)	-1445(2)	1470.2(8)	22.9(3)
C17	-712.3(17)	-239(2)	3650.4(9)	32.4(3)
C18	-650.5(19)	1210(3)	4392.5(9)	34.3(3)
C19	-5992.5(15)	875(2)	2712.5(8)	22.8(3)
C20	-5966.9(16)	-1388(2)	2408.8(8)	23.6(3)
C21	-875.6(19)	5781(2)	1680.6(9)	31.3(3)
C22	137(2)	5199(2)	960.6(10)	34.5(3)
C23	-6715.1(19)	3323(2)	3884.7(10)	33.8(3)

Table SI2.4.3: Anisotropic Displacement Parameters ($Å^2 \times 10^3$) for **163**. The anisotropic dis-placement factor exponent takes the form:$-2\pi^2[h^2a^{*2}U_{11}+2hka^*b^*U_{12}+\ldots]$.

Atom	U_{11}	U_{22}	U_{33}	U_{12}	U_{13}	U_{23}
O1	21.9(4)	26.4(5)	30.8(5)	-0.9(4)	-4.4(4)	3.3(4)
O2	21.4(4)	29.7(5)	32.4(5)	-4.2(4)	-4.9(4)	-1.8(4)
O3	28.3(4)	18.5(4)	28.9(5)	-3.0(4)	3.8(4)	0.4(4)
O4	27.2(5)	40.7(6)	24.3(4)	-7.2(4)	-3.7(4)	-3.6(4)
O5	23.8(4)	29.3(5)	38.2(5)	-6.6(4)	9.9(4)	-1.3(4)
C6	18.0(5)	19.9(6)	20.5(6)	1.6(5)	1.0(4)	2.3(5)
C7	19.1(6)	36.9(8)	26.8(7)	-5.0(5)	5.2(5)	-5.1(6)
C8	20.0(6)	18.7(6)	22.1(6)	-0.7(5)	1.8(5)	-0.6(5)
C9	20.8(6)	23.4(6)	20.2(6)	-2.6(5)	3.4(5)	0.9(5)
C10	24.4(6)	17.5(6)	18.1(5)	-1.4(5)	-0.8(5)	0.5(5)
C11	23.2(6)	22.8(6)	26.2(6)	-4.2(5)	3.2(5)	0.4(5)
C12	25.6(6)	25.6(7)	22.5(6)	-0.7(5)	0.3(5)	-1.6(5)
C13	19.2(6)	20.2(6)	22.2(6)	1.1(5)	-0.4(5)	0.8(5)
C14	22.4(6)	31.8(7)	20.6(6)	-2.9(5)	1.5(5)	-0.8(5)
C15	33.7(7)	42.1(9)	23.2(7)	-1.4(7)	6.1(6)	-1.0(6)
C16	20.3(6)	22.4(6)	25.8(6)	-3.1(5)	-0.6(5)	-2.7(5)
C17	23.6(6)	36.7(8)	35.6(7)	0.9(6)	-7.1(6)	6.6(7)
C18	28.5(7)	47.8(9)	26.1(7)	-4.6(6)	-2.8(6)	7.2(6)
C19	18.6(6)	26.9(6)	22.9(6)	-1.9(5)	2.7(5)	-1.1(5)
C20	21.7(6)	24.2(6)	25.1(6)	-4.8(5)	3.5(5)	0.9(5)
C21	34.1(7)	24.7(6)	35.6(8)	-10.5(6)	5.8(6)	-0.8(6)
C22	38.0(8)	31.0(8)	35.5(8)	-11.6(6)	9.4(6)	1.3(6)
C23	32.5(7)	37.0(8)	33.1(8)	-3.4(7)	10.8(6)	-6.3(6)

Table SI2.4.1.4: Bond Lengths for **163**.

Atom	Atom	Length (Å)	Atom	Atom	Length (Å)
O1	C9	1.3830(15)	C7	C19	1.5227(17)
O1	C17	1.4366(16)	C7	C23	1.493(2)
O2	C16	1.4460(15)	C8	C9	1.5013(16)
O3	C10	1.3876(15)	C8	C19	1.5555(16)
O3	C21	1.4304(17)	C9	C14	1.3312(19)
O4	C14	1.3840(15)	C10	C11	1.3283(18)
O4	C18	1.4286(19)	C12	C13	1.5031(16)
O5	C11	1.3763(15)	C13	C16	1.5114(16)
O5	C22	1.4415(18)	C16	C20	1.5214(17)
C6	C8	1.5291(16)	C17	C18	1.508(2)
C6	C10	1.4785(17)	C19	C20	1.5193(18)
C6	C13	1.3403(17)	C21	C22	1.508(2)
C7	C15	1.325(2)			

Table SI2.4.5: Bond Angles for **163**.

Atom	Atom	Atom	Angle (°)	Atom	Atom	Atom	Angle (°)
C17	O1	C9	111.16(10)	C11	C10	C6	124.48(11)
C21	O3	C10	110.88(11)	C10	C11	O5	125.39(11)
C18	O4	C14	110.97(10)	C12	C13	C6	125.29(11)
C22	O5	C11	111.44(10)	C16	C13	C6	120.72(11)
C10	C6	C8	112.22(10)	C16	C13	C12	113.97(10)
C13	C6	C8	123.97(10)	C9	C14	O4	124.72(13)
C13	C6	C10	123.76(11)	C13	C16	O2	110.02(10)
C19	C7	C15	123.26(13)	C20	C16	O2	111.75(10)
C23	C7	C15	121.64(13)	C20	C16	C13	113.26(10)
C23	C7	C19	115.10(12)	C18	C17	O1	110.32(12)
C9	C8	C6	109.31(9)	C17	C18	O4	110.49(11)
C19	C8	C6	113.21(10)	C8	C19	C7	110.70(10)
C19	C8	C9	114.37(10)	C20	C19	C7	115.12(11)
C8	C9	O1	114.18(10)	C20	C19	C8	110.21(10)
C14	C9	O1	123.16(11)	C19	C20	C16	110.25(10)
C14	C9	C8	122.58(12)	C22	C21	O3	109.61(12)
C6	C10	O3	113.23(10)	C21	C22	O5	109.51(12)
C11	C10	O3	122.03(11)				

Table SI2.4.6: Hydrogen Atom Coordinates (Å×10^4) and Isotropic Displacement Parameters (Å^2×10^3) for **163**.

Atom	*x*	*y*	*z*	U(eq)
H2	-7569(11)	452(3)	1064(10)	42.2(3)
H11	-903.6(15)	360(2)	1092.2(8)	28.8(3)
H17a	-500(20)	-1710(30)	3813(11)	38(4)
H8	-4623(18)	3490(30)	2476(9)	23(3)
H12a	-5030(20)	-860(30)	-56(10)	26(3)
H21a	-1037(19)	7290(30)	1691(10)	27(4)
H14	-2630(18)	4970(30)	3433(9)	22(3)
H19	-6900(17)	1620(20)	2405(8)	16(3)
H12b	-3380(20)	-1970(30)	322(11)	37(4)
H15a	-5890(20)	-1940(30)	4017(12)	44(5)
H22a	1240(20)	5900(30)	1007(10)	33(4)
H15b	-6330(20)	-140(30)	4738(11)	33(4)
H23a	-7750(20)	3740(30)	3583(10)	32(4)
H18a	-1520(20)	830(30)	4754(11)	36(4)
H16	-5673(16)	-2910(20)	1324(8)	15(3)
H20a	-7024(19)	-2160(20)	2552(9)	22(4)
H23b	-5920(20)	4380(30)	3738(11)	43(5)
H23c	-6810(20)	3480(30)	4474(12)	45(5)
H18b	430(20)	1160(30)	4703(10)	33(4)
H20b	-5042(19)	-2140(20)	2648(9)	20(4)
H17b	110(20)	250(20)	3216(10)	30(4)
H22b	-440(20)	5550(30)	432(11)	39(5)
H21b	-260(20)	5280(20)	2220(10)	30(4)
H12c	-3390(20)	540(30)	77(10)	29(4)

X-Ray Crystallographic Data for Diels Alder Adduct 195

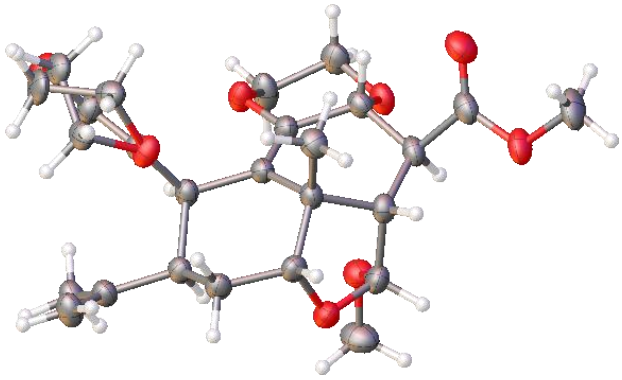

A colorless prism 0.22 x 0.11 x 0.04 mm in size was mounted on a Cryoloop with Paratone oil. Data were collected in a nitrogen gas stream at 100(2) K using ω scans. Crystal-to-detector distance was 60 mm and exposure time was 5 seconds per frame using a scan width of 2.0°. Data collection was 100% complete to 74.5° in θ. A total of 22974 reflections were collected covering the indices, -9<=*h*<=9, -25<=*k*<=25, -10<=*l*<=10. 4646 reflections were found to be symmetry independent, with an R_{int} of 0.0521. Indexing and unit cell refinement indicated a primitive, monoclinic lattice. The space group was found to be $P2_1$ (No. 4). The data were integrated using the Bruker SAINT software program and scaled using the SADABS software program. Solution by iterative methods (SHELXT-2014) produced a complete heavy-atom phasing model consistent with the proposed structure. All non-hydrogen atoms were refined anisotropically by full-matrix least-squares (SHELXL-2016). All hydrogen atoms were placed using a riding model. Their positions were constrained relative to their parent atom using the appropriate HFIX command in SHELXL-2016. Absolute stereochemistry was unambiguously determined from the diffraction data.

Table SI2.5.1: Crystal data and structure refinement for **195**.

Identification code	**195**
Empirical formula	$C_{24}H_{32}O_8$
Formula weight	448.49
Temperature (K)	100(2)
Crystal system	monoclinic
Space group	$P2_1$
a (Å)	7.47360(10)
b (Å)	20.0163(2)
c (Å)	8.26160(10)
α (°)	90
β (°)	113.345(2)
γ (°)	90
Volume (Å^3)	1134.71(3)
Z	2
ρ_{calc} (g/cm$_3$)	1.313
μ (mm^{-1})	0.813
F(000)	480.0
Crystal size (mm^3)	0.220 × 0.100 × 0.040
Radiation	CuKα (λ = 1.54184)
2Θ range for data collection (°)	8.836 to 148.972
Index ranges	$-9 \leq h \leq 9$, $-25 \leq k \leq 25$, $-10 \leq l \leq 10$
Reflections collected	22974
Independent reflections	4646 [R_{int} = 0.0521, R_{sigma} = 0.0291]
Data/restraints/parameters	4646/1/312
Goodness-of-fit on F^2	1.102
Final R indexes [I>=2σ (I)]	R_1 = 0.0396, wR_2 = 0.1091
Final R indexes [all data]	R_1 = 0.0408, wR_2 = 0.1098
Largest diff. peak/hole (e Å^{-3})	0.20/-0.17
Flack parameter	-0.04(10)

Table SI2.5.2: Fractional Atomic Coordinates ($\times 10^4$) and Equivalent Isotropic Displacement Parameters ($Å^2 \times 10^3$) for **195**. U_{eq} is defined as 1/3 of the trace of the orthogonalized U_{ij} tensor.

Atom	*x*	*y*	*z*	U(eq)
C1	11350(5)	2772.2(18)	10359(5)	50.5(8)
C2	8252(4)	3241.2(12)	8809(4)	34.3(5)
C3	6577(3)	3617.7(12)	8978(3)	30.6(5)
C4	4803(4)	3618.2(12)	7207(3)	30.2(5)
C5	1816(4)	3055.0(13)	5816(4)	38.8(6)
C6	745(4)	3707.2(13)	5543(4)	41.7(6)
C7	3756(3)	4279.4(12)	6698(3)	28.2(4)
C8	4544(3)	4873.3(11)	7300(3)	26.8(4)
C9	6680(3)	4908.8(12)	8551(3)	28.6(5)
C10	7974(4)	4949.1(13)	7506(4)	35.0(5)
C11	7231(3)	4309.3(12)	9820(3)	31.0(5)
C12	6487(4)	4508.9(13)	11226(3)	34.6(5)
C13	3910(6)	4385.6(17)	12158(5)	51.8(8)
C14	7079(3)	5478.6(12)	9892(3)	31.7(5)
C15	5967(4)	6120.4(12)	9216(3)	30.7(5)
C16	3780(3)	5996.7(11)	8292(3)	28.4(5)
C17	2557(4)	6626.6(12)	7742(3)	30.6(5)
C18	3275(4)	7221.4(14)	7649(4)	40.2(6)
C19	425(4)	6535.3(13)	7312(4)	37.8(6)
C20	3313(3)	5505.4(11)	6715(3)	27.5(5)
C21	3356(3)	5844.7(11)	5098(3)	29.3(5)
C22	1802(4)	5871.4(13)	3584(3)	35.4(5)
C23A	3342(18)	6660(5)	2461(15)	44(2)
C24A	5232(9)	6329(3)	3638(7)	36.6(18)
C23B	3603(15)	6427(5)	2345(13)	35.5(17)
C24B	4733(8)	6699(3)	4109(7)	33.1(16)
O1	9679(3)	3128.8(11)	10390(3)	41.4(5)
O2	8349(3)	3065.8(12)	7447(3)	47.8(5)
O3	3561(3)	3094.1(9)	7353(2)	34.6(4)
O4	1924(3)	4243.9(9)	5354(2)	34.3(4)
O5	4584(3)	4280.0(10)	10793(2)	38.3(4)
O6	6584(3)	5217.8(9)	11299(2)	36.0(4)
O7	1739(3)	6200.1(11)	2090(2)	42.6(5)
O8	5095(3)	6150.7(9)	5334(2)	34.9(4)

Table SI2.5.3: Anisotropic Displacement Parameters ($Å^2 \times 10^3$) for **195**. The anisotropic dis-placement factor exponent takes the form:$-2\pi^2[h^2a^{*2}U_{11}+2hka^*b^*U_{12}+\ldots]$.

Atom	U_{11}	U_{22}	U_{33}	U_{23}	U_{13}	U_{12}
C1	39.9(14)	49.2(17)	68(2)	20.3(15)	27.2(14)	20.7(13)
C2	35.8(12)	25.3(12)	45.8(14)	7.2(10)	20.6(11)	5.2(9)
C3	31.3(11)	24.8(11)	38.6(12)	7.1(10)	16.9(10)	6.6(9)
C4	34.6(11)	22.6(11)	34.1(11)	0.4(9)	14.4(10)	2.0(9)
C5	43.0(13)	23.4(12)	43.0(13)	-3.1(10)	9.6(11)	-3.7(10)
C6	35.6(13)	23.1(12)	54.5(16)	1.7(11)	5.1(12)	-2.8(10)
C7	32.0(10)	24.5(10)	26.9(10)	2.4(9)	10.2(9)	2.5(9)
C8	30.4(11)	23.3(10)	25.9(9)	1.5(8)	10.5(8)	2.2(9)
C9	29.4(11)	23.6(11)	30.2(10)	1.6(9)	8.8(9)	3.1(8)
C10	34.8(11)	31.0(12)	41.0(12)	1.3(10)	17.1(10)	-0.3(10)
C11	28.9(10)	28.5(11)	32.7(11)	4.9(9)	9.0(9)	4.6(9)
C12	38.6(12)	32.0(12)	28.7(12)	5.7(9)	8.4(10)	5.9(10)
C13	68(2)	47.2(18)	53.9(17)	-3.7(14)	39.3(16)	-2.1(14)
C14	29.9(11)	32.0(12)	27.8(11)	-1.1(9)	5.9(9)	0.9(9)
C15	33.3(11)	24.5(11)	30.1(11)	-3.0(8)	8.0(9)	-2.5(9)
C16	32.0(11)	21.9(11)	28.9(10)	1.0(8)	9.6(8)	0.5(9)
C17	33.6(12)	24.2(10)	31.6(11)	-1.1(9)	10.2(10)	2.0(9)
C18	37.8(13)	25.7(12)	49.6(15)	0.1(11)	9.2(11)	0.3(10)
C19	36.3(13)	28.3(13)	47.0(14)	2.9(10)	14.7(11)	4.9(9)
C20	28.8(11)	20.8(10)	29.1(11)	1.1(8)	7.3(9)	-1.2(8)
C21	33.3(11)	21.2(10)	31.3(11)	0.7(9)	10.5(9)	-1.8(9)
C22	39.8(13)	29.9(12)	30.7(11)	3.4(10)	7.9(10)	-2.1(10)
C23A	61(5)	23(5)	41(4)	15(4)	12(3)	7(4)
C24A	52(3)	28(3)	34(3)	1(2)	21(2)	-4(2)
C23B	48(4)	22(4)	36(3)	11(4)	16(3)	1(3)
C24B	44(3)	21(3)	37(3)	8(2)	20(2)	3.3(19)
O1	34.9(9)	41.0(10)	51.1(11)	14.5(9)	19.9(8)	15.1(8)
O2	47.9(11)	47.9(12)	53.2(12)	-0.5(10)	26.1(10)	12.2(10)
O3	37.1(9)	21.6(8)	42.3(10)	2.7(7)	12.8(8)	0.8(7)
O4	35.4(8)	22.5(8)	34.6(8)	0.7(7)	2.6(7)	-1.3(7)
O5	44.6(10)	38.1(10)	36.9(9)	2.0(8)	21.2(8)	2.1(8)
O6	44.7(10)	32.2(9)	28.4(8)	1.5(7)	11.5(7)	4.8(7)
O7	46.4(11)	45.3(11)	27.6(8)	7.8(8)	5.5(7)	-3.7(8)
O8	36.5(9)	30.7(9)	32.5(9)	7.2(7)	8.5(7)	-6.1(7)

Table SI2.5.4: Bond Lengths for **195**.

Atom	Atom	Length (Å)	Atom	Atom	Length (Å)
C1	O1	1.447(3)	C12	O6	1.421(3)
C2	O2	1.208(3)	C13	O5	1.422(3)
C2	O1	1.338(3)	C14	O6	1.450(3)
C2	C3	1.514(3)	C14	C15	1.512(3)
C3	C4	1.536(3)	C15	C16	1.526(3)
C3	C11	1.540(4)	C16	C17	1.517(3)
C4	O3	1.437(3)	C16	C20	1.558(3)
C4	C7	1.510(3)	C17	C18	1.321(4)
C5	O3	1.417(3)	C17	C19	1.500(4)
C5	C6	1.501(4)	C20	C21	1.510(3)
C6	O4	1.437(3)	C21	C22	1.328(3)
C7	C8	1.332(3)	C21	O8	1.379(3)
C7	O4	1.381(3)	C22	O7	1.383(3)
C8	C9	1.521(3)	C23A	O7	1.444(13)
C8	C20	1.526(3)	C23A	C24A	1.514(13)
C9	C10	1.533(3)	C24A	O8	1.488(5)
C9	C14	1.534(3)	C23B	O7	1.400(10)
C9	C11	1.538(3)	C23B	C24B	1.469(12)
C11	C12	1.526(3)	C24B	O8	1.444(5)
C12	O5	1.399(3)			

Table SI2.5.5: Bond Angles for **195**.

Atom	Atom	Atom	Angle (˚)	Atom	Atom	Atom	Angle (˚)
O2	C2	O1	122.8(2)	O6	C14	C9	105.83(19)
O2	C2	C3	126.0(2)	C15	C14	C9	116.36(19)
O1	C2	C3	111.2(2)	C14	C15	C16	111.7(2)
C2	C3	C4	110.2(2)	C17	C16	C15	114.5(2)
C2	C3	C11	111.3(2)	C17	C16	C20	111.44(18)
C4	C3	C11	115.44(19)	C15	C16	C20	111.18(19)
O3	C4	C7	112.5(2)	C18	C17	C19	120.9(2)
O3	C4	C3	105.17(19)	C18	C17	C16	123.8(2)
C7	C4	C3	114.96(19)	C19	C17	C16	115.3(2)
O3	C5	C6	109.5(2)	C21	C20	C8	115.6(2)
O4	C6	C5	110.7(2)	C21	C20	C16	112.32(18)
C8	C7	O4	119.8(2)	C8	C20	C16	110.57(18)
C8	C7	C4	125.1(2)	C22	C21	O8	122.6(2)
O4	C7	C4	114.7(2)	C22	C21	C20	122.3(2)
C7	C8	C9	119.0(2)	O8	C21	C20	115.07(19)
C7	C8	C20	120.0(2)	C21	C22	O7	124.6(2)
C9	C8	C20	121.0(2)	O7	C23A	C24A	110.0(7)
C8	C9	C10	110.23(19)	O8	C24A	C23A	108.3(6)
C8	C9	C14	112.14(19)	O7	C23B	C24B	114.6(7)
C10	C9	C14	112.4(2)	O8	C24B	C23B	106.8(5)
C8	C9	C11	110.6(2)	C2	O1	C1	115.2(2)
C10	C9	C11	111.5(2)	C5	O3	C4	111.15(19)
C14	C9	C11	99.50(18)	C7	O4	C6	113.97(19)
C12	C11	C9	103.56(19)	C12	O5	C13	113.1(2)
C12	C11	C3	115.7(2)	C12	O6	C14	110.48(19)
C9	C11	C3	116.23(19)	C22	O7	C23B	109.9(4)
O5	C12	O6	111.5(2)	C22	O7	C23A	112.4(5)
O5	C12	C11	111.1(2)	C21	O8	C24B	109.5(3)
O6	C12	C11	105.4(2)	C21	O8	C24A	112.7(3)
O6	C14	C15	108.9(2)				

Table SI2.5.6: Hydrogen Atom Coordinates ($Å \times 10^4$) and Isotropic Displacement Parameters ($Å^2 \times 10^3$) for **195**.

Atom	*x*	*y*	*z*	U(eq)
H1A	10926	2343	9758	76
H1B	12287	2694	11570	76
H1C	11968	3038	9727	76
H3	6187	3357	9818	37
H4	5261	3490	6265	36
H5A	987	2690	5942	47
H5B	2124	2956	4781	47
H6A	-479	3679	4473	50
H6B	400	3797	6563	50
H10A	7776	4550	6769	52
H10B	9344	4976	8325	52
H10C	7629	5347	6755	52
H11	8686	4300	10406	37
H12	7366	4319	12391	42
H13A	4862	4206	13269	78
H13B	2657	4158	11858	78
H13C	3744	4866	12290	78
H14	8505	5581	10384	38
H15A	6441	6335	8380	37
H15B	6218	6430	10216	37
H16	3378	5766	9169	34
H18A	2438	7599	7305	48
H18B	4628	7272	7926	48
H19A	-221	6972	7088	57
H19B	255	6320	8306	57
H19C	-153	6255	6259	57
H20	1933	5361	6389	33
H22	654	5649	3523	42
H23A	3119	7063	3051	53
H23B	3424	6801	1344	53
H24A	5454	5922	3062	44
H24B	6338	6638	3856	44
H23C	3474	6778	1460	43
H23D	4341	6052	2126	43
H24C	5979	6888	4164	40
H24D	3990	7056	4395	40

Table SI2.5.7:. Atomic Occupancy for **195**.

Atom	***Occupancy***	**Atom**	***Occupancy***	**Atom**	***Occupancy***
C23A	0.488(11)	H23A	0.488(11)	H23B	0.488(11)
C23B	0.512(11)	H23C	0.512(11)	H23D	0.512(11)
C24A	0.488(11)	H24A	0.488(11)	H24B	0.488(11)
C24B	0.512(11)	H24C	0.512(11)	H24D	0.512(11)

X-Ray Crystallographic Data for Quassin Architecture 201

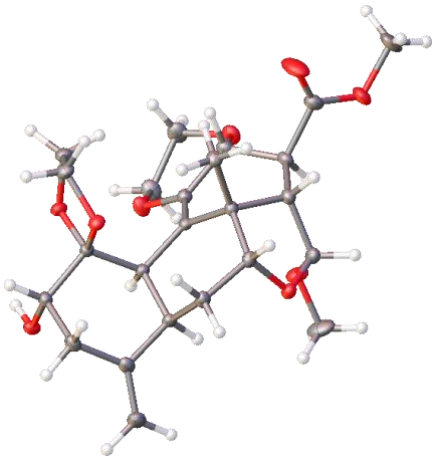

A colorless block 0.38 x 0.24 x 0.15 mm in size was mounted on a Cryoloop with Paratone oil. Data were collected in a nitrogen gas stream at 100(2) K using ω scans. Crystal-to-detector distance was 60 mm and exposure time was 5 seconds per frame using a scan width of 2.0°. Data collection was 100% complete to 28.3° in θ. A total of 82913 reflections were collected covering the indices, -14<=*h*<=14, -10<=*k*<=10, -17<=*l*<=17. 5843 reflections were found to be symmetry independent, with an R_{int} of 0.0378. Indexing and unit cell refinement indicated a primitive, monoclinic lattice. The space group was found to be $P2_1$ (No. 4). The data were integrated using the Bruker SAINT software program and scaled using the SADABS software program. Solution by iterative methods (SHELXT-2014) produced a complete heavy-atom phasing model consistent with the proposed structure. All non-hydrogen atoms were refined anisotropically by full-matrix least-squares (SHELXL-2016). All hydrogen atoms were placed using a riding model. Their positions were constrained relative to their parent atom using the appropriate HFIX command in SHELXL-2016. Absolute stereochemistry was unambiguously determined from the diffraction data.

Table SI2.6.1: Crystal data and structure refinement for **201**.

Identification code	**201**
Empirical formula	$C_{24}H_{32}O_9$
Formula weight	464.49
Temperature (K)	100(2)
Crystal system	monoclinic
Space group	$P2_1$
a (Å)	11.1125(4)
b (Å)	8.0779(3)
c (Å)	13.1558(5)
α (°)	90
β (°)	98.011(2)
γ (°)	90
Volume ($Å^3$)	1169.41(8)
Z	2
ρ_{calc} (g/cm_3)	1.319
μ (mm^{-1})	0.101
F(000)	496.0
Crystal size (mm^3)	0.380 × 0.240 × 0.150
Radiation	MoKα (λ = 0.71073)
2Θ range for data collection (°)	3.126 to 56.662
Index ranges	$-14 \leq h \leq 14$, $-10 \leq k \leq 10$, $-17 \leq l \leq 17$
Reflections collected	82913
Independent reflections	5843 [R_{int} = 0.0378, R_{sigma} = 0.0181]
Data/restraints/parameters	5843/1/313
Goodness-of-fit on F^2	1.064
Final R indexes [I>=2σ (I)]	R_1 = 0.0305, wR_2 = 0.0805
Final R indexes [all data]	R_1 = 0.0321, wR_2 = 0.0821
Largest diff. peak/hole (e $Å^{-3}$)	0.30/-0.20
Flack parameter	-0.08(16)

Table SI2.6.2: Fractional Atomic Coordinates ($\times 10^4$) and Equivalent Isotropic Displacement Parameters ($Å^2 \times 10^3$) for **201**. U_{eq} is defined as 1/3 of the trace of the orthogonalized U_{ij} tensor.

Atom	*x*	*y*	*z*	U(eq)
C1	11777.7(18)	674(3)	1990.8(19)	32.2(5)
C2	10174.1(15)	2443(2)	2275.4(14)	20.3(4)
C3	8965.5(15)	3201(2)	1829.1(13)	15.7(3)
C4	9077.8(15)	5095(2)	1888.4(13)	16.0(3)
C5	9635.1(17)	7292(2)	879.9(15)	23.3(4)
C6	8338.3(17)	7840(3)	642.6(14)	22.7(4)
C7	7874.2(14)	5950(2)	1941.1(12)	13.9(3)
C8	7073.0(14)	5365(2)	2524.4(12)	12.1(3)
C9	7353.4(14)	3712(2)	3069.2(12)	13.4(3)
C10	8133.0(16)	3908(2)	4128.2(13)	16.9(3)
C11	7944.3(14)	2493(2)	2381.3(12)	14.7(3)
C12	6866.1(15)	1798(2)	1650.0(13)	17.3(3)
C13	5724.1(19)	2086(3)	6.6(15)	33.2(5)
C14	6193.7(15)	2739(2)	3179.2(12)	14.7(3)
C15	5116.1(15)	3733(2)	3412.7(13)	15.3(3)
C16	4810.1(14)	5111(2)	2615.9(13)	13.5(3)
C17	5903.7(14)	6302(2)	2605.9(12)	12.1(3)
C18	5993.5(14)	7583(2)	3481.1(12)	12.8(3)
C19	7287.1(16)	7827(2)	5013.4(13)	20.1(4)
C20	7906.3(15)	8523(2)	4153.7(14)	18.8(3)
C21	4777.4(15)	8501(2)	3486.9(12)	14.8(3)
C22	3789.1(15)	7253(2)	3640.9(13)	17.5(3)
C23	3656.1(15)	6002(2)	2784.4(13)	16.4(3)
C24	2596.7(16)	5675(3)	2219.9(16)	24.2(4)
O1	10618.3(12)	1437.4(18)	1612.2(11)	24.8(3)
O2	10669.1(14)	2698(3)	3129.8(12)	40.4(4)
O3	9647.8(11)	5543.9(17)	1019.6(10)	20.7(3)
O4	7692.3(11)	7487.5(16)	1491.8(10)	18.8(3)
O5	6673.9(11)	2722.3(18)	742.9(9)	21.7(3)
O6	5847.1(11)	1933.1(16)	2195.5(9)	16.3(2)
O7	6332.1(11)	6844.7(16)	4465.1(9)	15.7(2)
O8	6903.2(10)	8797.7(15)	3361.7(9)	15.8(2)
O9	4398.4(11)	9318.3(16)	2543.9(10)	17.2(3)

Table SI2.6.3: Anisotropic Displacement Parameters ($Å^2 \times 10^3$) for **201**. The anisotropic dis-placement factor exponent takes the form:$-2\pi^2[h^2a^{*2}U_{11}+2hka^*b^*U_{12}+\ldots]$.

Atom	U_{11}	U_{22}	U_{33}	U_{23}	U_{13}	U_{12}
C1	17.8(9)	27.5(10)	50.8(13)	6.1(10)	2.8(8)	11.3(8)
C2	14.1(7)	22.7(9)	23.7(9)	2.4(7)	1.3(6)	1.9(7)
C3	12.7(7)	19.0(8)	15.2(7)	-0.3(6)	1.1(6)	3.9(6)
C4	13.7(7)	19.0(8)	15.6(7)	1.0(6)	3.0(6)	0.5(6)
C5	21.9(8)	22.8(10)	27.7(9)	4.8(8)	12.2(7)	-1.9(7)
C6	26.1(9)	23.4(10)	20.7(8)	7.1(7)	10.3(7)	2.2(7)
C7	14.6(7)	13.7(8)	13.2(7)	0.2(6)	0.7(6)	0.7(6)
C8	11.7(7)	12.4(8)	11.6(7)	-1.9(6)	-0.7(5)	0.6(6)
C9	14.4(7)	12.4(7)	13.3(7)	-0.2(6)	1.7(5)	1.2(6)
C10	18.9(8)	18.2(9)	12.7(7)	0.9(6)	-0.9(6)	1.6(6)
C11	15.3(7)	14.7(8)	13.9(7)	0.0(6)	1.3(6)	2.4(6)
C12	16.2(8)	17.0(8)	19.1(8)	-4.1(7)	3.1(6)	0.1(6)
C13	26.9(10)	50.9(14)	19.6(9)	-7.9(9)	-4.9(7)	-10.0(9)
C14	17.8(7)	13.0(8)	13.3(7)	0.2(6)	2.5(6)	-0.9(6)
C15	16.2(7)	13.3(8)	17.1(7)	1.1(6)	4.7(6)	-1.4(6)
C16	11.7(7)	13.5(8)	15.4(7)	0.2(6)	1.7(6)	-1.5(6)
C17	11.2(7)	12.9(7)	12.1(7)	-0.1(6)	0.9(5)	-0.3(6)
C18	13.4(7)	11.9(7)	13.0(7)	0.5(6)	1.8(5)	-0.7(6)
C19	19.7(8)	22.7(9)	16.3(8)	-3.2(7)	-2.5(6)	-1.2(7)
C20	13.9(7)	20.0(9)	21.1(8)	-2.0(7)	-2.6(6)	-0.8(7)
C21	14.9(7)	13.3(8)	16.2(7)	-0.8(6)	2.1(6)	1.8(6)
C22	15.1(7)	18.1(9)	20.3(8)	0.7(7)	6.0(6)	2.0(6)
C23	13.6(7)	14.9(8)	21.3(8)	3.6(7)	5.0(6)	-0.7(6)
C24	15.5(8)	22.0(9)	34.3(10)	-1.9(8)	1.1(7)	-1.4(7)
O1	17.4(6)	24.6(7)	31.9(7)	0.1(6)	2.3(5)	9.5(5)
O2	27.5(7)	61.4(12)	28.4(8)	-6.0(8)	-9.8(6)	19.2(8)
O3	19.7(6)	22.0(7)	22.6(6)	1.8(5)	10.1(5)	1.1(5)
O4	20.2(6)	16.6(6)	21.7(6)	5.6(5)	9.8(5)	2.2(5)
O5	18.9(6)	31.0(7)	13.9(6)	-1.5(5)	-2.1(4)	-5.4(6)
O6	16.0(6)	15.7(6)	17.3(6)	-3.5(5)	2.5(4)	-1.5(5)
O7	18.0(6)	17.0(6)	11.5(5)	-0.1(5)	-0.6(4)	-1.2(5)
O8	13.3(5)	15.2(6)	17.9(6)	0.1(5)	-0.8(4)	-2.6(5)
O9	13.5(5)	15.3(6)	22.1(6)	3.6(5)	-0.3(5)	-0.3(5)

Table SI2.6.4: Bond Lengths for **201**.

Atom	Atom	Length (Å)	Atom	Atom	Length (Å)
C1	O1	1.452(2)	C12	O5	1.399(2)
C2	O2	1.198(2)	C12	O6	1.427(2)
C2	O1	1.336(2)	C13	O5	1.425(2)
C2	C3	1.517(2)	C14	O6	1.452(2)
C3	C4	1.536(3)	C14	C15	1.508(2)
C3	C11	1.540(2)	C15	C16	1.534(2)
C4	O3	1.429(2)	C16	C23	1.514(2)
C4	C7	1.515(2)	C16	C17	1.552(2)
C5	O3	1.424(2)	C17	C18	1.541(2)
C5	C6	1.498(3)	C18	O7	1.4275(19)
C6	O4	1.438(2)	C18	O8	1.4328(19)
C7	C8	1.340(2)	C18	C21	1.542(2)
C7	O4	1.378(2)	C19	O7	1.436(2)
C8	C17	1.520(2)	C19	C20	1.512(3)
C8	C9	1.527(2)	C20	O8	1.433(2)
C9	C14	1.533(2)	C21	O9	1.416(2)
C9	C10	1.543(2)	C21	C22	1.525(2)
C9	C11	1.544(2)	C22	C23	1.505(2)
C11	C12	1.535(2)	C23	C24	1.328(3)

Table SI2.6.5: Bond Angles for **201**.

Atom	Atom	Atom	Angle (˚)	Atom	Atom	Atom	Angle (˚)
O2	C2	O1	123.62(17)	C15	C14	C9	116.62(14)
O2	C2	C3	124.03(18)	C14	C15	C16	110.71(13)
O1	C2	C3	112.34(15)	C23	C16	C15	110.89(13)
C2	C3	C4	108.70(15)	C23	C16	C17	112.75(14)
C2	C3	C11	109.79(14)	C15	C16	C17	110.89(13)
C4	C3	C11	113.93(14)	C8	C17	C18	114.84(13)
O3	C4	C7	114.42(14)	C8	C17	C16	111.70(13)
O3	C4	C3	104.72(14)	C18	C17	C16	112.30(12)
C7	C4	C3	112.97(14)	O7	C18	O8	106.55(12)
O3	C5	C6	108.18(16)	O7	C18	C17	112.23(13)
O4	C6	C5	110.45(14)	O8	C18	C17	110.55(12)
C8	C7	O4	119.59(14)	O7	C18	C21	108.47(12)
C8	C7	C4	121.79(15)	O8	C18	C21	107.67(13)
O4	C7	C4	117.95(14)	C17	C18	C21	111.16(12)
C7	C8	C17	120.50(15)	O7	C19	C20	102.20(13)
C7	C8	C9	117.94(14)	O8	C20	C19	102.26(13)
C17	C8	C9	121.52(13)	O9	C21	C22	107.02(13)
C8	C9	C14	111.91(13)	O9	C21	C18	111.93(13)
C8	C9	C10	112.72(14)	C22	C21	C18	109.29(14)
C14	C9	C10	109.93(13)	C23	C22	C21	109.98(13)
C8	C9	C11	110.99(13)	C24	C23	C22	122.63(16)
C14	C9	C11	99.22(13)	C24	C23	C16	121.77(17)
C10	C9	C11	111.32(13)	C22	C23	C16	115.59(14)
C12	C11	C3	113.72(13)	C2	O1	C1	115.16(16)
C12	C11	C9	104.01(13)	C5	O3	C4	110.95(14)
C3	C11	C9	116.18(14)	C7	O4	C6	116.89(14)
O5	C12	O6	110.55(14)	C12	O5	C13	113.46(15)
O5	C12	C11	110.66(14)	C12	O6	C14	110.62(12)
O6	C12	C11	105.17(13)	C18	O7	C19	107.91(13)
O6	C14	C15	107.50(13)	C18	O8	C20	107.68(13)
O6	C14	C9	105.53(12)				

Table SI2.6.6: Hydrogen Atom Coordinates (Å×10^4) and Isotropic Displacement Parameters (Å^2×10^3) for **201**.

Atom	*x*	*y*	*z*	U(eq)
H1A	12027	-48	1459	48
H1B	11697	18	2604	48
H1C	12392	1537	2165	48
H3	8794	2880	1089	19
H4	9643	5383	2523	19
H5A	10086	7591	308	28
H5B	10030	7844	1511	28
H6A	8309	9044	500	27
H6B	7943	7259	22	27
H10A	8880	4511	4050	25
H10B	8341	2812	4420	25
H10C	7673	4526	4587	25
H11	8298	1561	2827	18
H12	7015	611	1492	21
H13A	5728	2662	-649	50
H13B	4940	2261	251	50
H13C	5851	899	-89	50
H14	6387	1874	3721	18
H15A	5301	4228	4105	18
H15B	4405	2994	3409	18
H16	4655	4572	1926	16
H17	5725	6953	1956	15
H19A	7852	7138	5485	24
H19B	6956	8720	5409	24
H20A	8335	9571	4361	23
H20B	8492	7723	3932	23
H21	4861	9326	4059	18
H22A	4004	6681	4307	21
H22B	3008	7836	3653	21
H9	4900(30)	10030(40)	2440(20)	34(7)
H24A	1830(20)	6300(40)	2337(19)	31(7)
H24B	2510(20)	4890(40)	1640(20)	33(7)

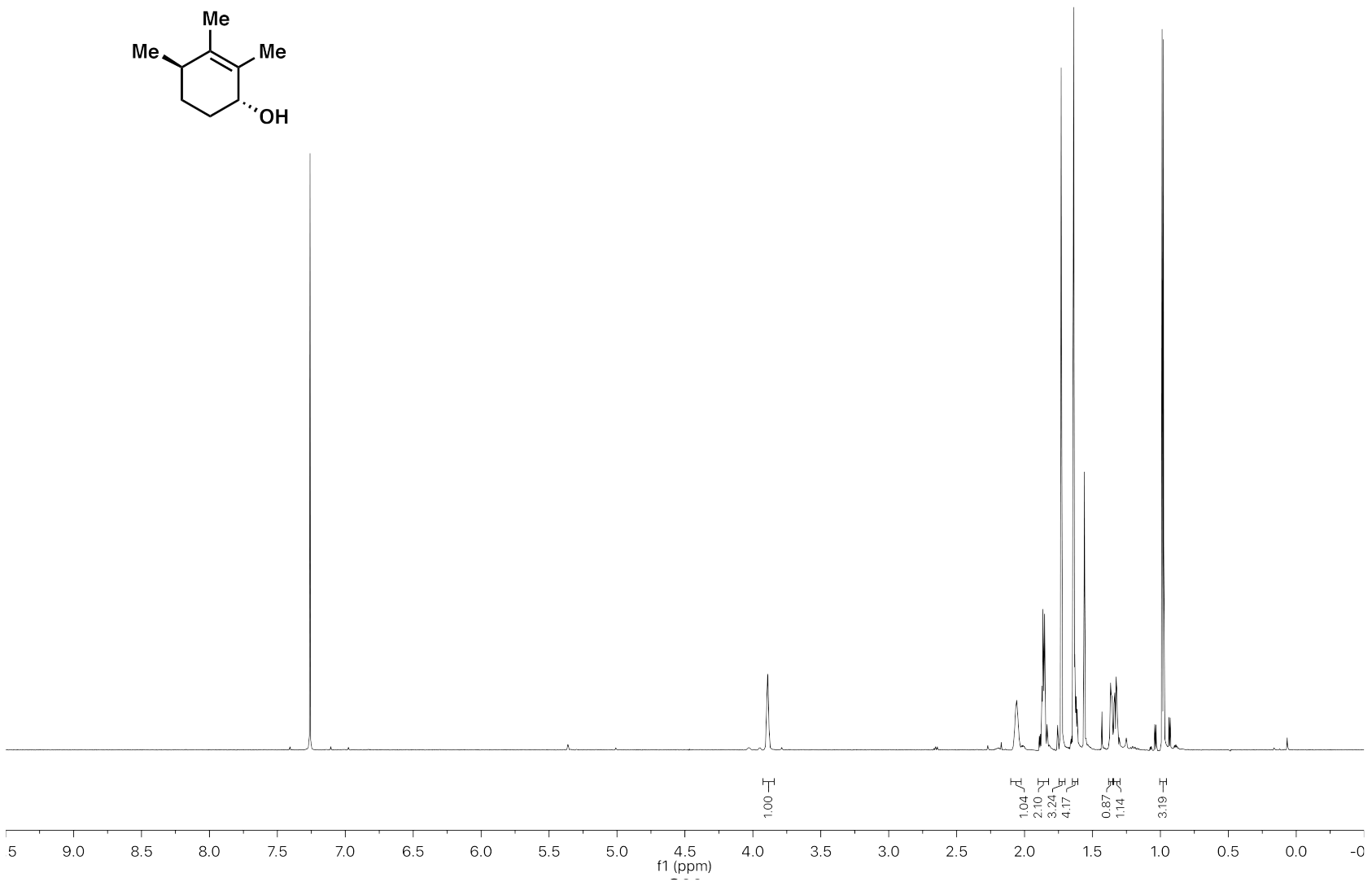
Me
Me
Me
OH
1.00
1.04
2.10
3.24
4.17
0.87
1.14
3.19
f1 (ppm)

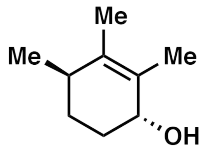
Me
Me
Me
OH

210
200
190
180
170
160
150
140
130
120
110
100
90
80
70
60
50
40
30
20
10
f1 (ppm)

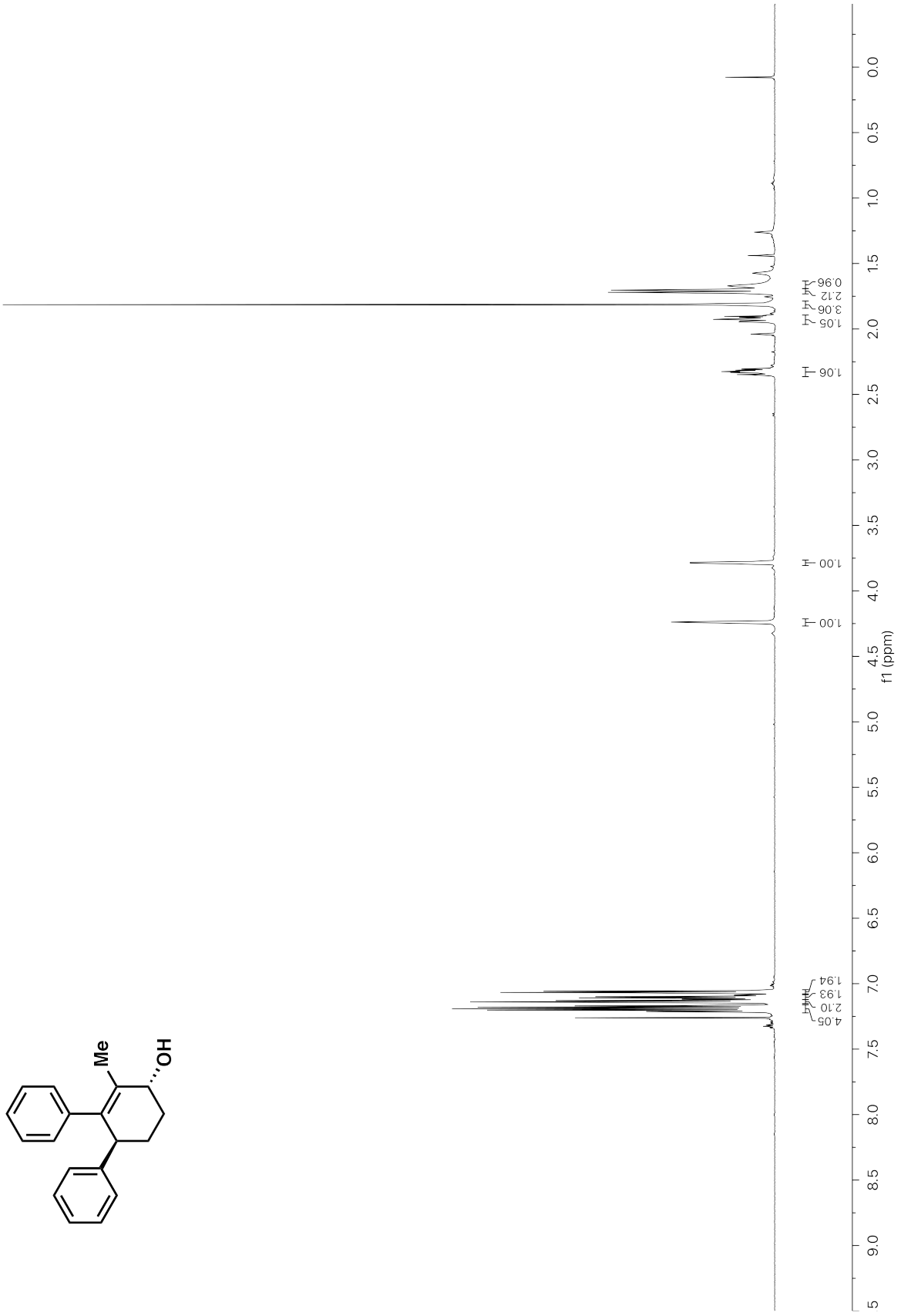
Me
OH
4.05
2.10
1.93
1.94
1.00
1.00
1.06
1.05
3.06
2.12
0.96
f1 (ppm)

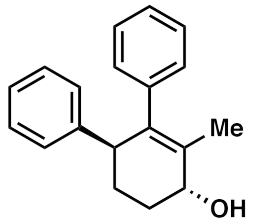
Me
OH

210
200
190
180
170
160
150
140
130
120
110
100
90
80
70
60
50
40
30
20
10
f1 (ppm)

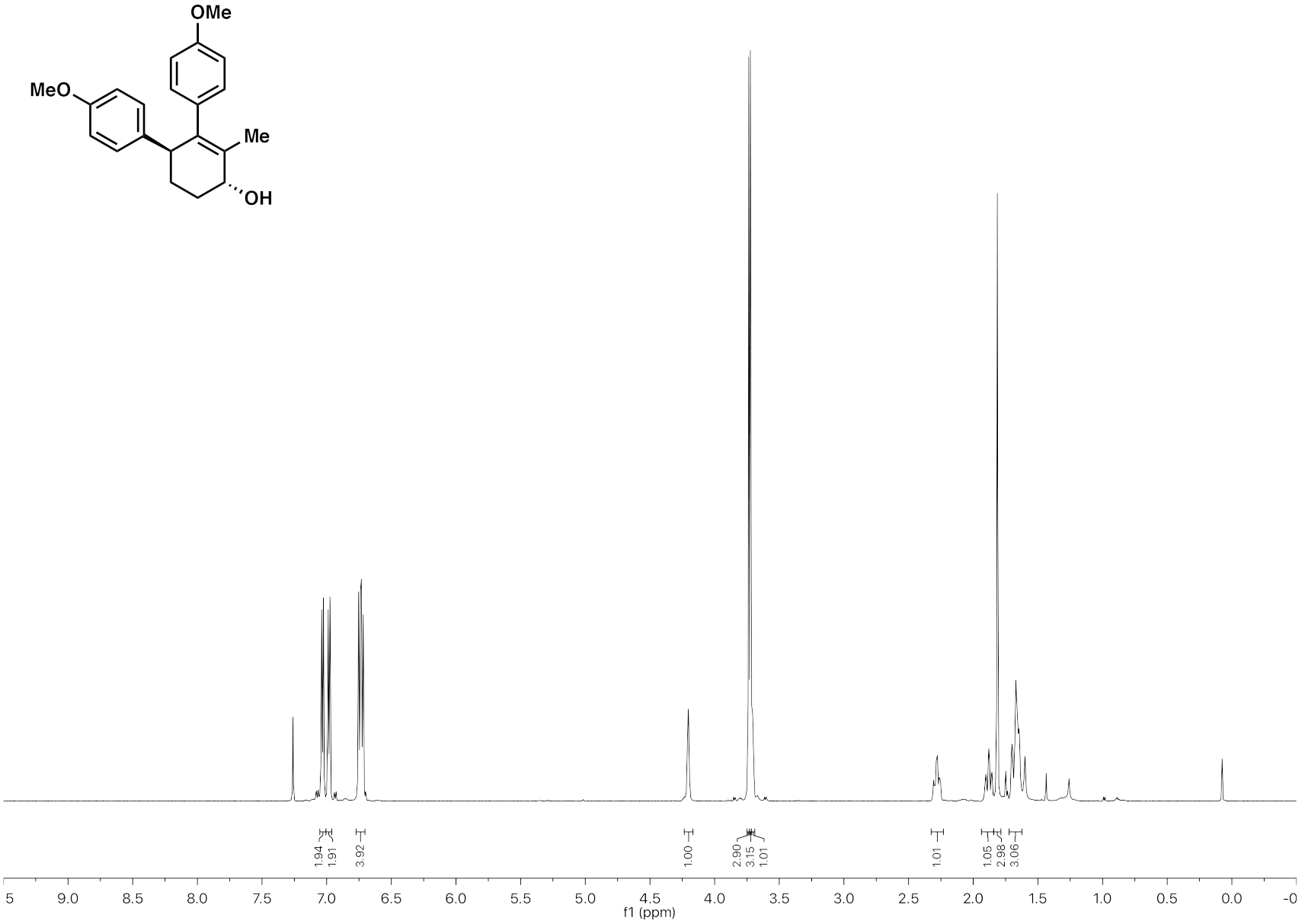
OMe
MeO
Me
OH
1.94
1.91
3.92
1.00
2.90
3.15
1.01
1.01
1.05
2.98
3.06
9.0
8.5
8.0
7.5
7.0
6.5
6.0
5.5
5.0
4.5
4.0
3.5
3.0
2.5
2.0
1.5
1.0
0.5
0.0
f1 (ppm)

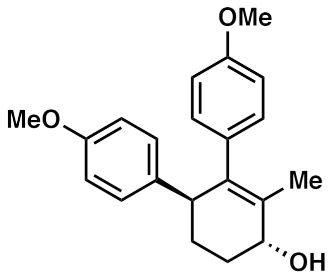
OMe
MeO
Me
OH

210
200
190
180
170
160
150
140
130
120
110
100
90
80
70
60
50
40
30
20
10
f1 (ppm)

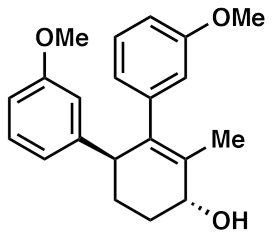
OMe
OMe
Me
OH

0.96
0.96
0.97
1.01
2.77
0.93
1.00
2.93
1.08
2.85
0.99
1.00
2.92
1.99
0.91
9.0
8.5
8.0
7.5
7.0
6.5
6.0
5.5
5.0
4.5
4.0
3.5
3.0
2.5
2.0
1.5
1.0
0.5
0.0
f1 (ppm)

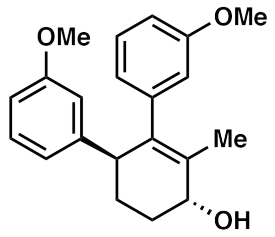
OMe
OMe
Me
OH

210
200
190
180
170
160
150
140
130
120
110
100
90
80
70
60
50
40
30
20
10
f1 (ppm)

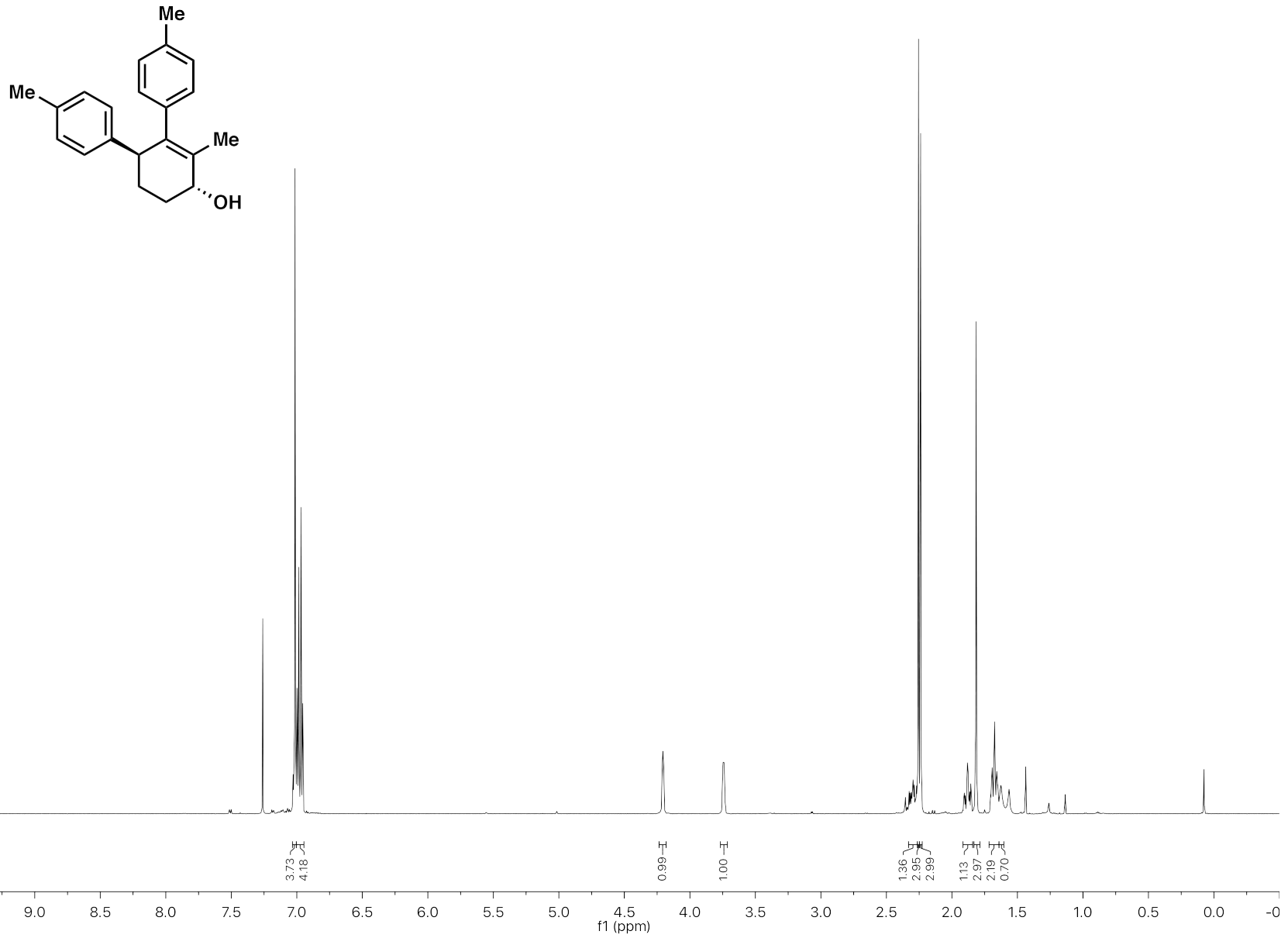
Me
Me
Me
OH
3.73
4.18
0.99
1.00
1.36
2.95
2.99
1.13
2.97
2.19
0.70
5
9.0
8.5
8.0
7.5
7.0
6.5
6.0
5.5
5.0
4.5
4.0
3.5
3.0
2.5
2.0
1.5
1.0
0.5
0.0
-0
f1 (ppm)

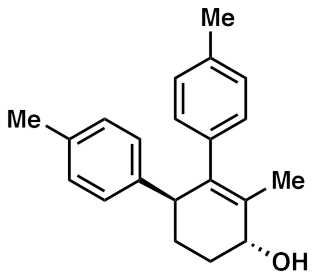
Me
Me
Me
OH

210
200
190
180
170
160
150
140
130
120
110
100
90
80
70
60
50
40
30
20
10
f1 (ppm)

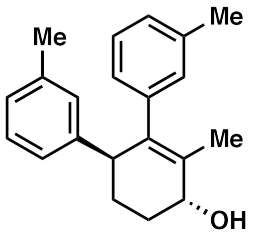
Me
Me
Me
OH

1.01
1.06
4.90
0.95
0.10
1.00
0.98
1.02
3.04
2.84
1.17
2.92
3.04
9.0
8.5
8.0
7.5
7.0
6.5
6.0
5.5
5.0
4.5
4.0
3.5
3.0
2.5
2.0
1.5
1.0
f1 (ppm)

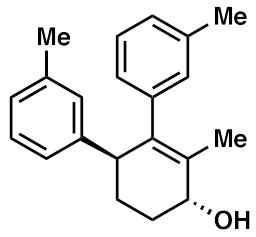
Me
Me
Me
OH

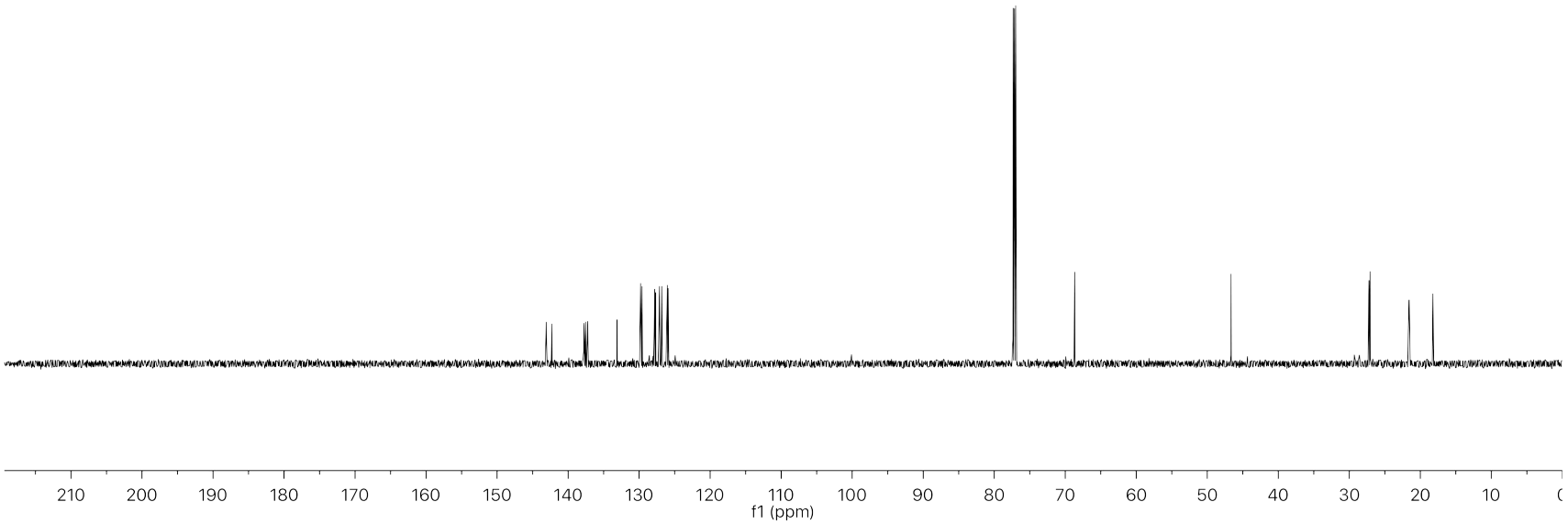
210
200
190
180
170
160
150
140
130
120
110
100
90
80
70
60
50
40
30
20
10
f1 (ppm)

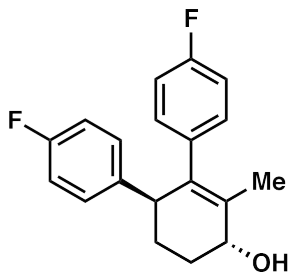
F
F
Me
OH

1.98
2.00
3.83
1.00
0.98
1.01
1.06
2.87
1.00
1.07
1.07
9.0
8.5
8.0
7.5
7.0
6.5
6.0
5.5
5.0
4.5
4.0
3.5
3.0
2.5
2.0
1.5
1.0
0.5
0.0
-0
f1 (ppm)

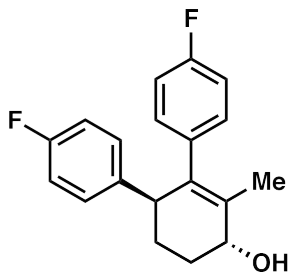
F
F
Me
OH

210
200
190
180
170
160
150
140
130
120
110
100
90
80
70
60
50
40
30
20
10
f1 (ppm)

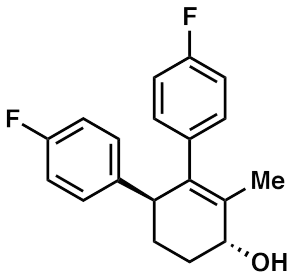
F
F
Me
OH

1.00
0.89
8.0
-108.5
-109.0
-109.5
-110.0
-110.5
-111.0
-111.5
-112.0
-112.5
-113.0
-113.5
-114.0
-114.5
-115.0
-115.5
-116.0
-116.5
-117.0
-117.5
f1 (ppm)

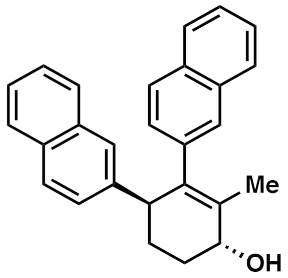
Me
OH

1.02
1.01
2.91
1.00
1.93
1.01
3.88
0.98
1.00
1.00
1.02
1.10
3.05
1.92
1.14
5
9.0
8.5
8.0
7.5
7.0
6.5
6.0
5.5
5.0
4.5
4.0
3.5
3.0
2.5
2.0
1.5
1.0
0.5
0.0
-0
f1 (ppm)

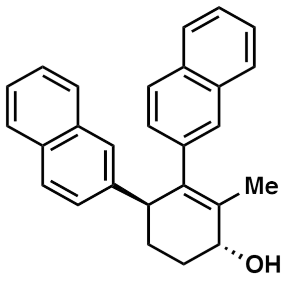
Me
OH

210
200
190
180
170
160
150
140
130
120
110
100
90
80
70
60
50
40
30
20
10
f1 (ppm)

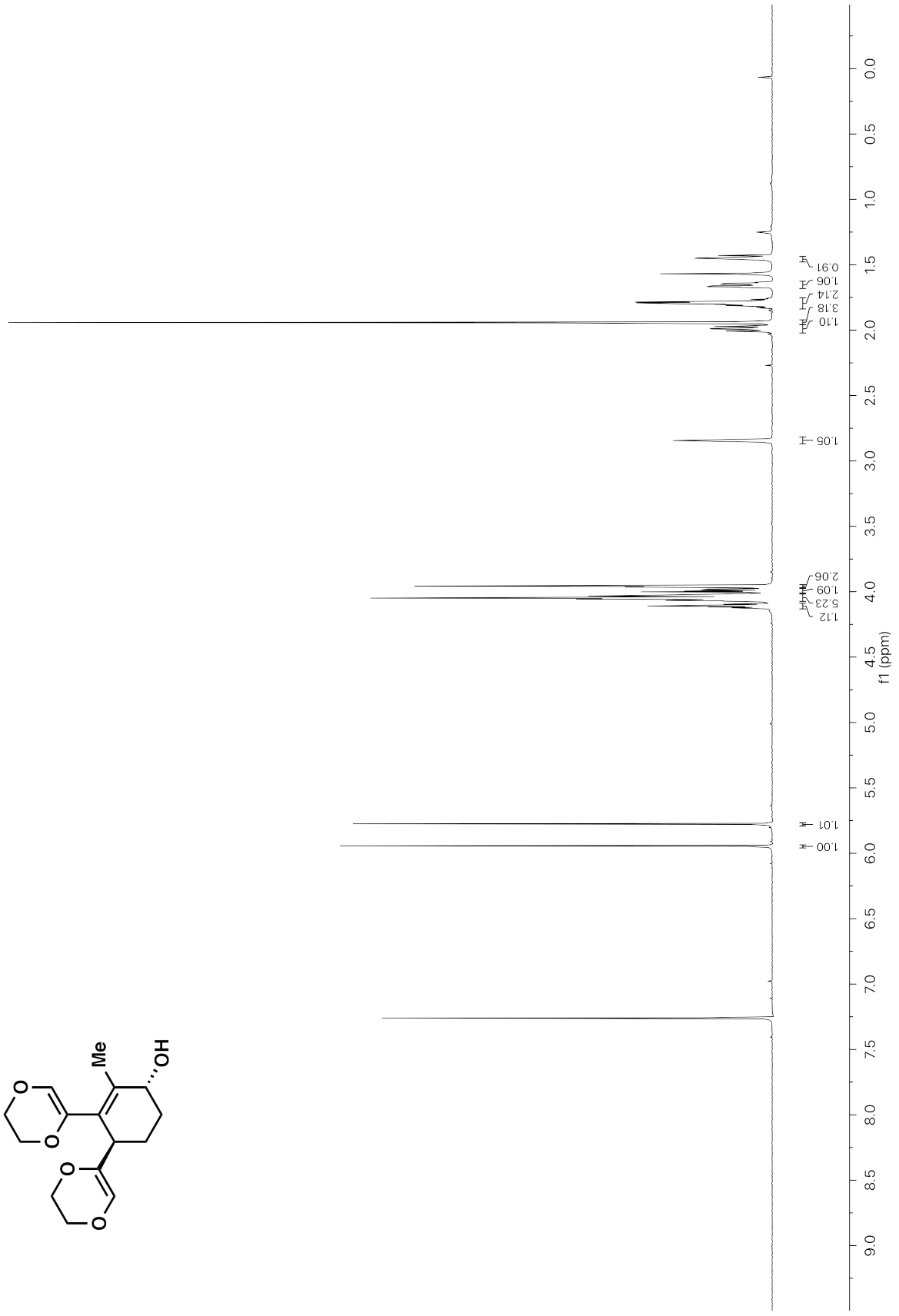
Me
OH
O
O
O
O
1.00
1.01
1.05
1.12
5.23
1.09
2.06
1.10
3.18
2.14
1.06
0.91
f1 (ppm)

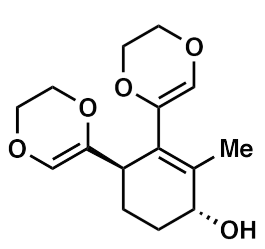
O
O
O
O
Me
OH

210
200
190
180
170
160
150
140
130
120
110
100
90
80
70
60
50
40
30
20
10
f1 (ppm)

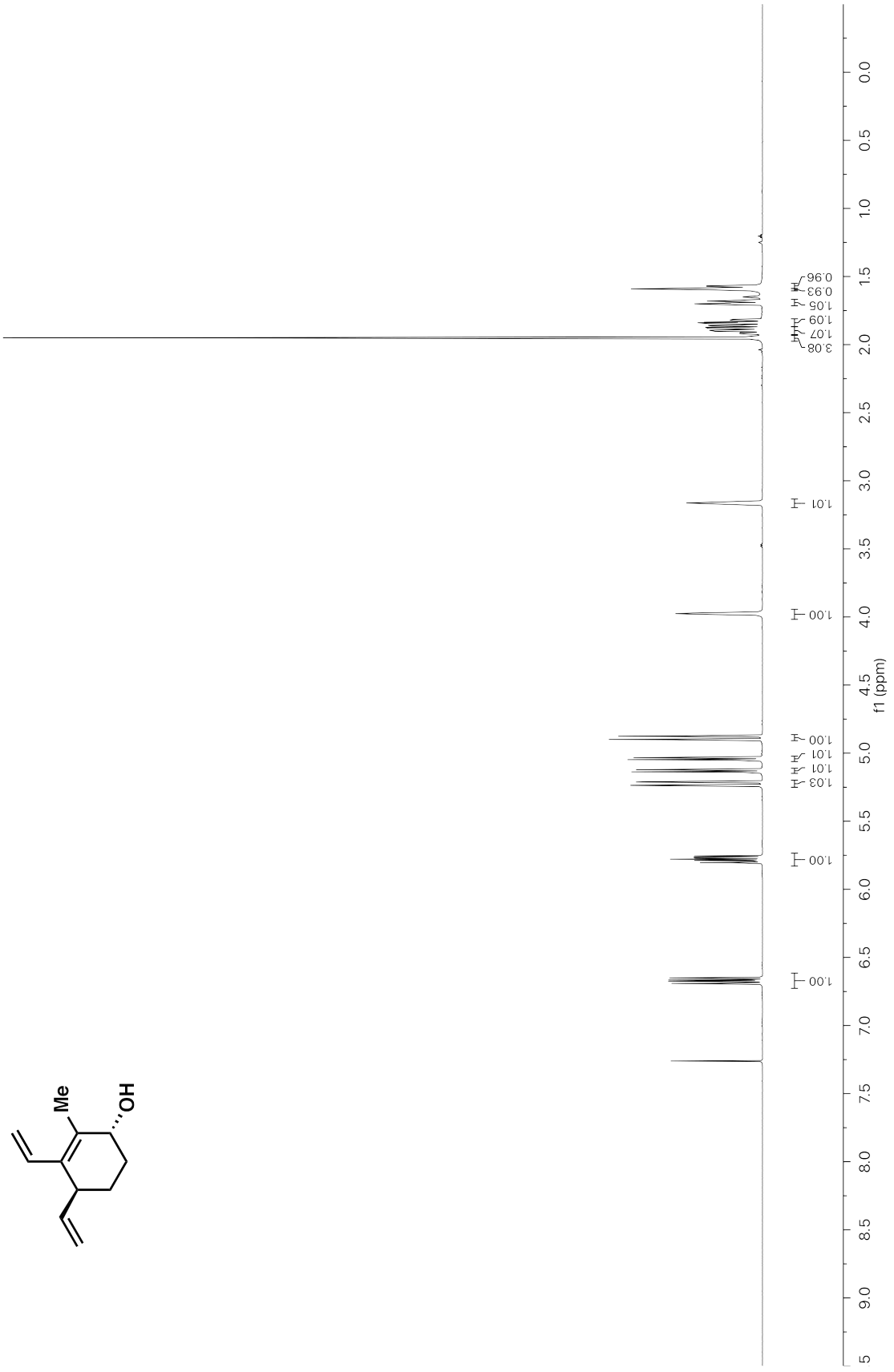
Me
OH
3.08
1.07
1.09
1.05
0.93
0.96
1.01
1.00
1.00
1.01
1.01
1.01
1.03
1.00
1.00
0.0
0.5
1.0
1.5
2.0
2.5
3.0
3.5
4.0
4.5
5.0
5.5
6.0
6.5
7.0
7.5
8.0
8.5
9.0
5
f1 (ppm)

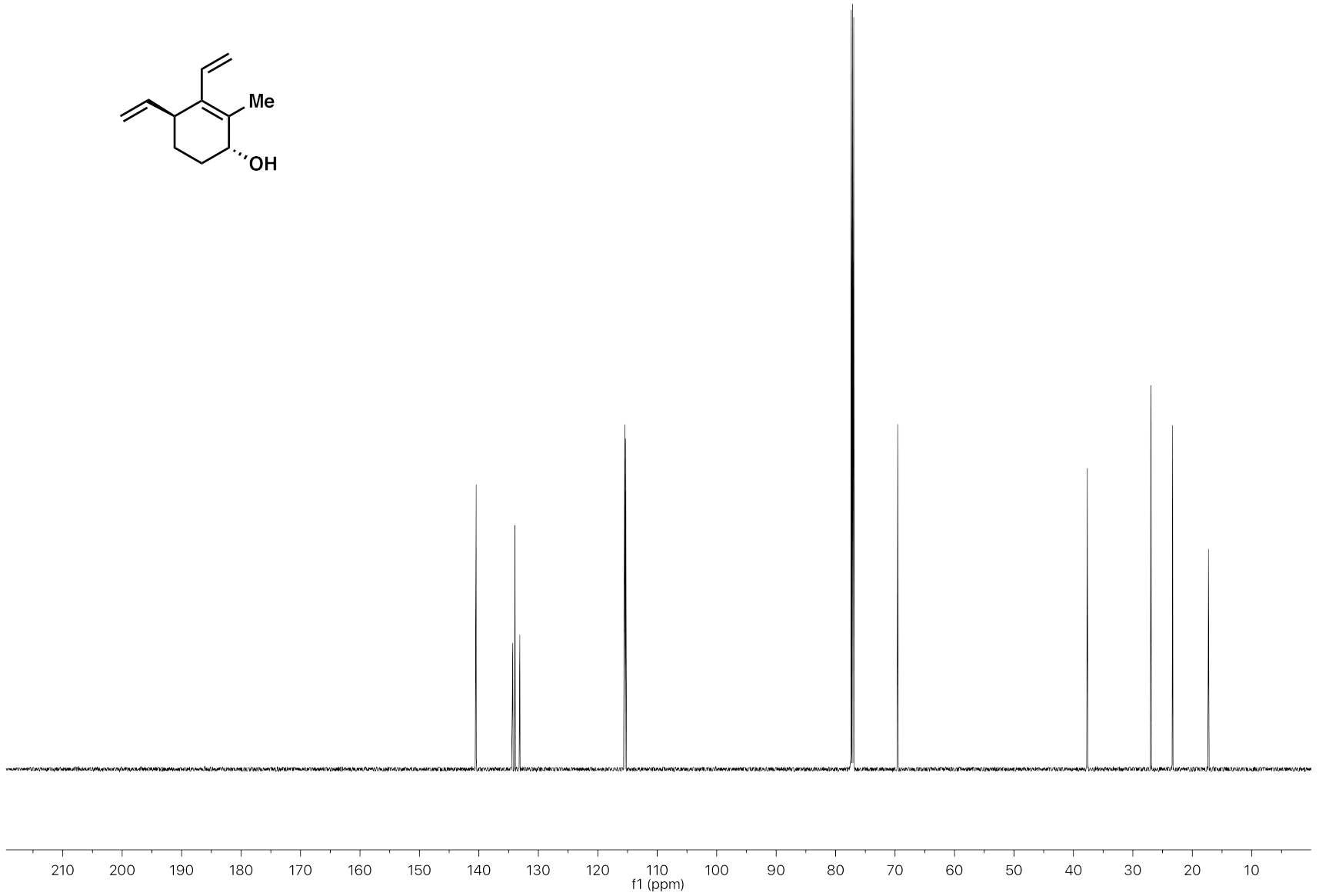
Me
OH
210
200
190
180
170
160
150
140
130
120
110
100
90
80
70
60
50
40
30
20
10
f1 (ppm)

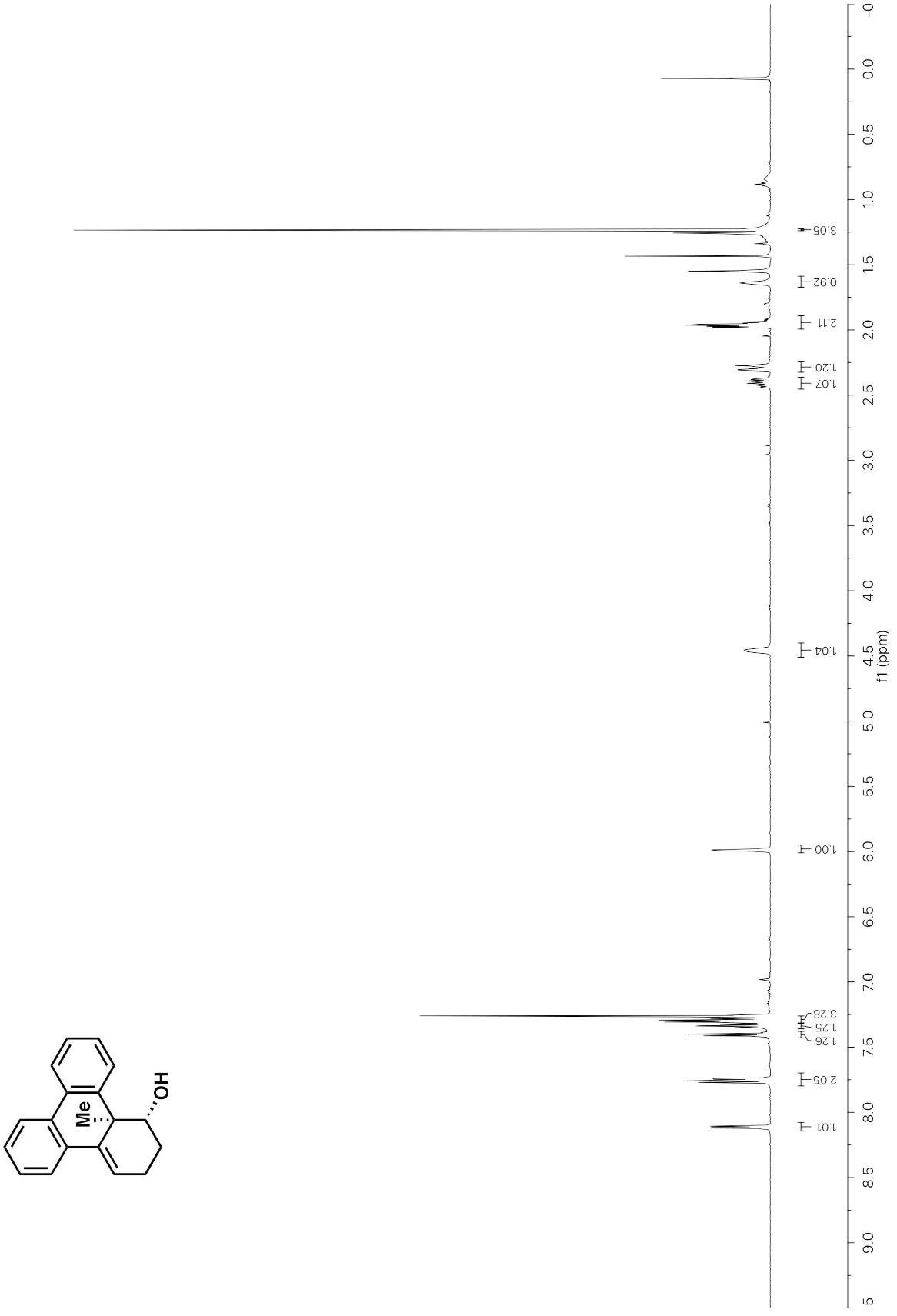
Me
HO
3.05
0.92
2.11
1.20
1.07
1.04
1.00
3.28
1.25
1.26
2.05
1.01
f1 (ppm)

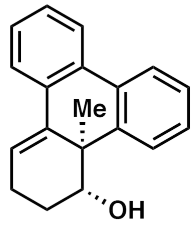
Me
OH

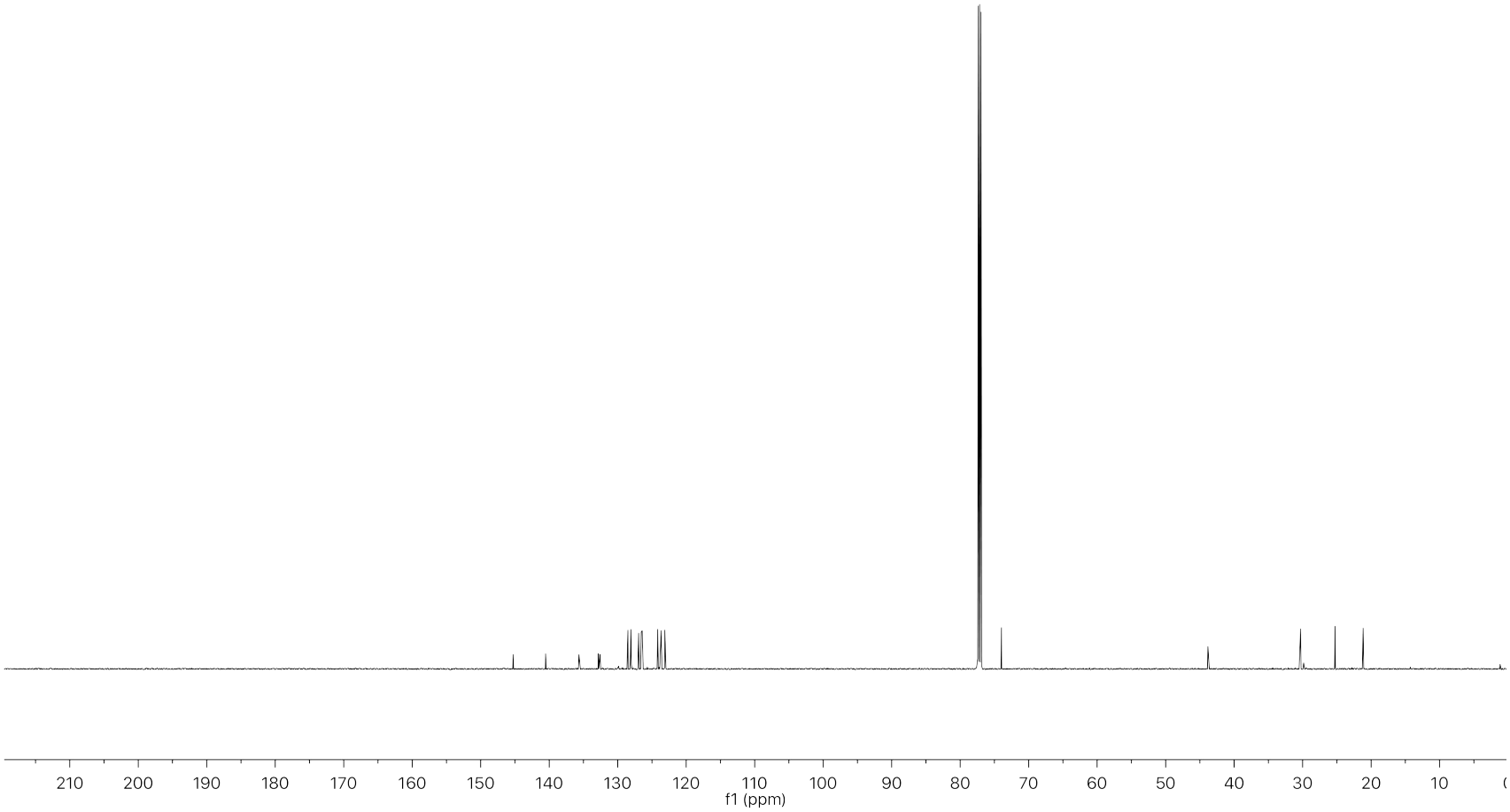
210
200
190
180
170
160
150
140
130
120
110
100
90
80
70
60
50
40
30
20
10
f1 (ppm)

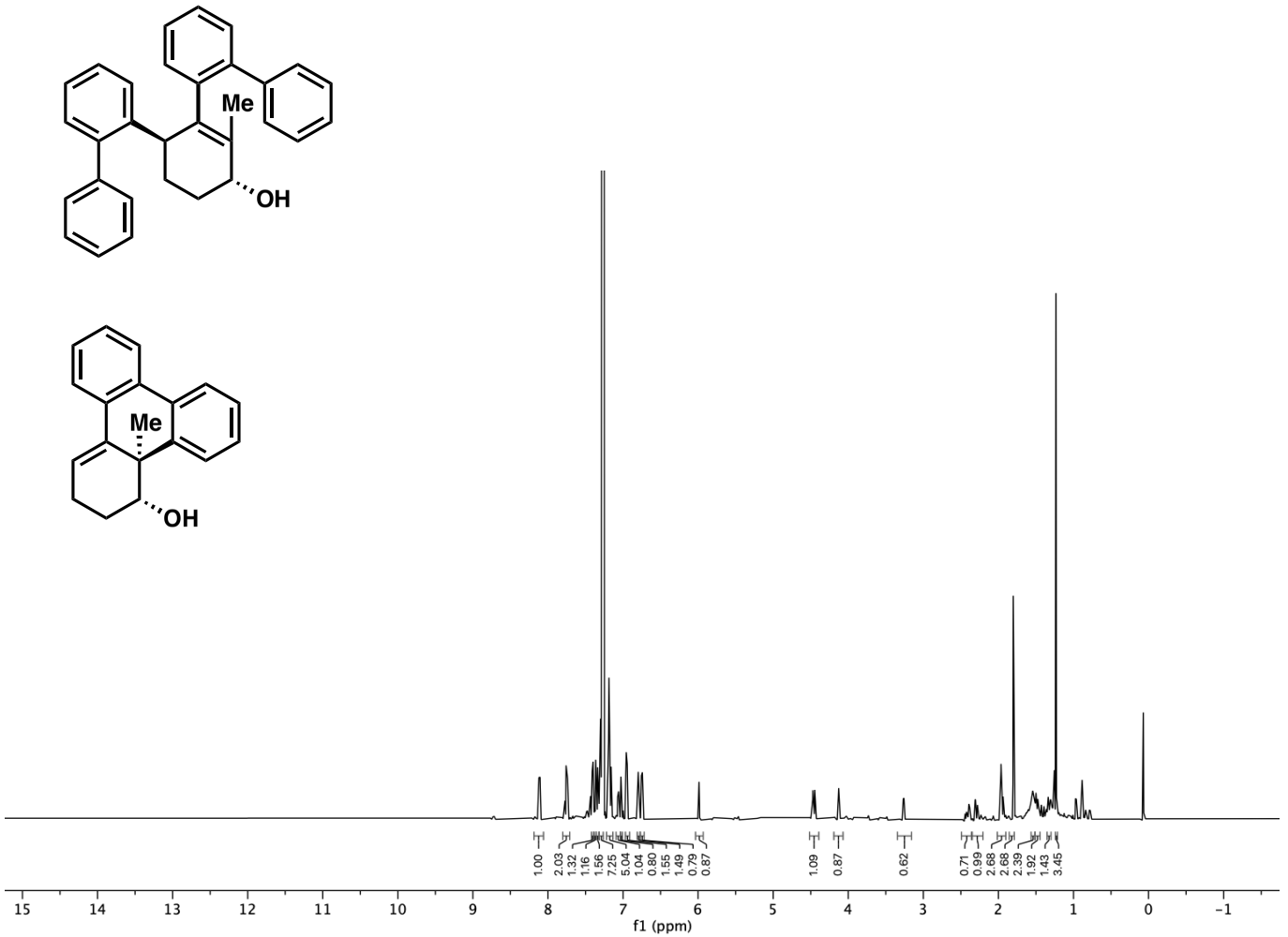
Me
OH
Me
OH
1.00
2.03
1.32
1.16
1.56
7.25
5.04
1.04
0.80
1.55
1.49
0.79
0.87
1.09
0.87
0.62
0.71
0.99
2.68
2.68
2.39
1.92
1.43
3.45
15
14
13
12
11
10
9
8
7
6
5
4
3
2
1
0
−1
f1 (ppm)

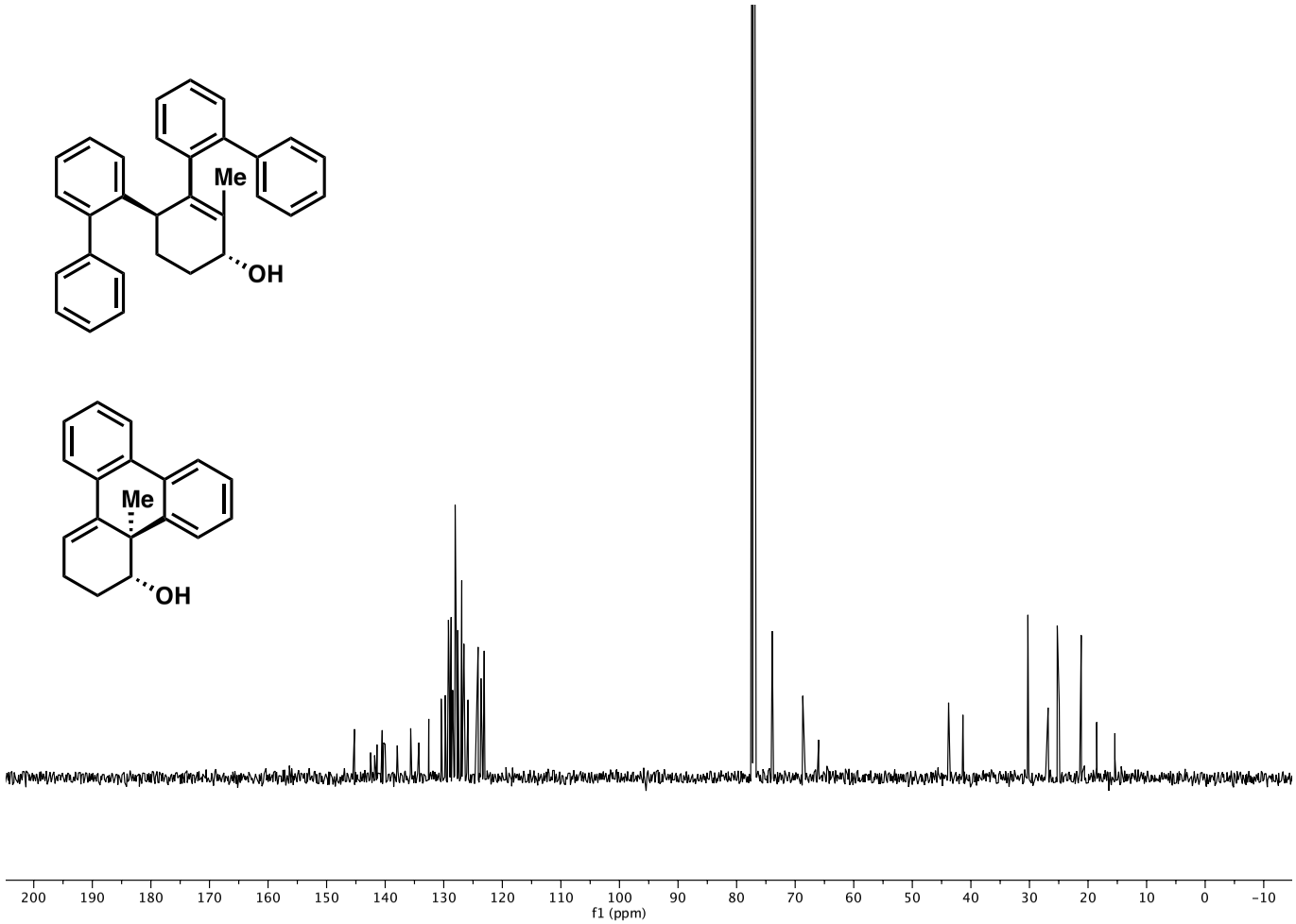
Me
OH
Me
OH
200
190
180
170
160
150
140
130
120
110
100
90
80
70
60
50
40
30
20
10
0
−10
f1 (ppm)

Me
O
2.74
2.16
1.18
3.09
1.09
1.00
1.00
3.83
1.90
f1 (ppm)

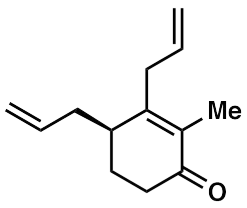
Me
O

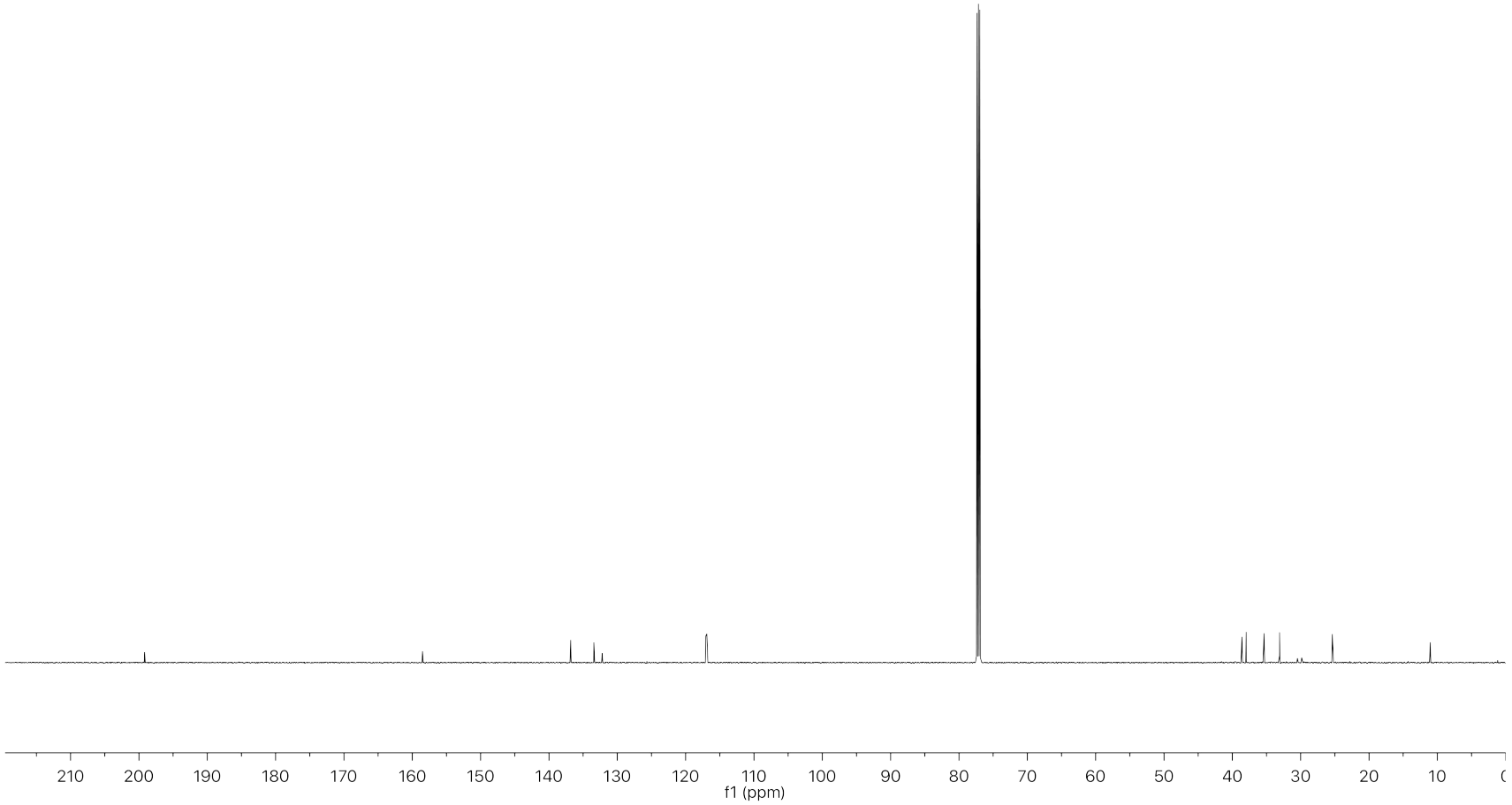
210
200
190
180
170
160
150
140
130
120
110
100
90
80
70
60
50
40
30
20
10
f1 (ppm)

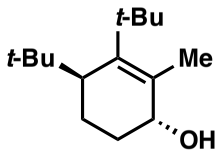
t-Bu
t-Bu
Me
OH

1.13
1.00
1.49
2.62
1.30
1.44
1.89
7.57
7.94
9.5 9.0 8.5 8.0 7.5 7.0 6.5 6.0 5.5 5.0 4.5 4.0 3.5 3.0 2.5 2.0 1.5 1.0 0.5 0.0 -0.5 -1.0 -1.
f1 (ppm)

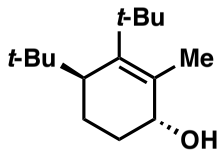
t-Bu
t-Bu
Me
OH

200
190
180
170
160
150
140
130
120
110
100
90
80
70
60
50
40
30
20
10
0
−10
f1 (ppm)

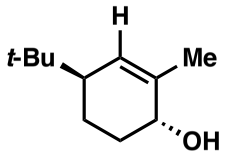
H
t-Bu
Me
OH

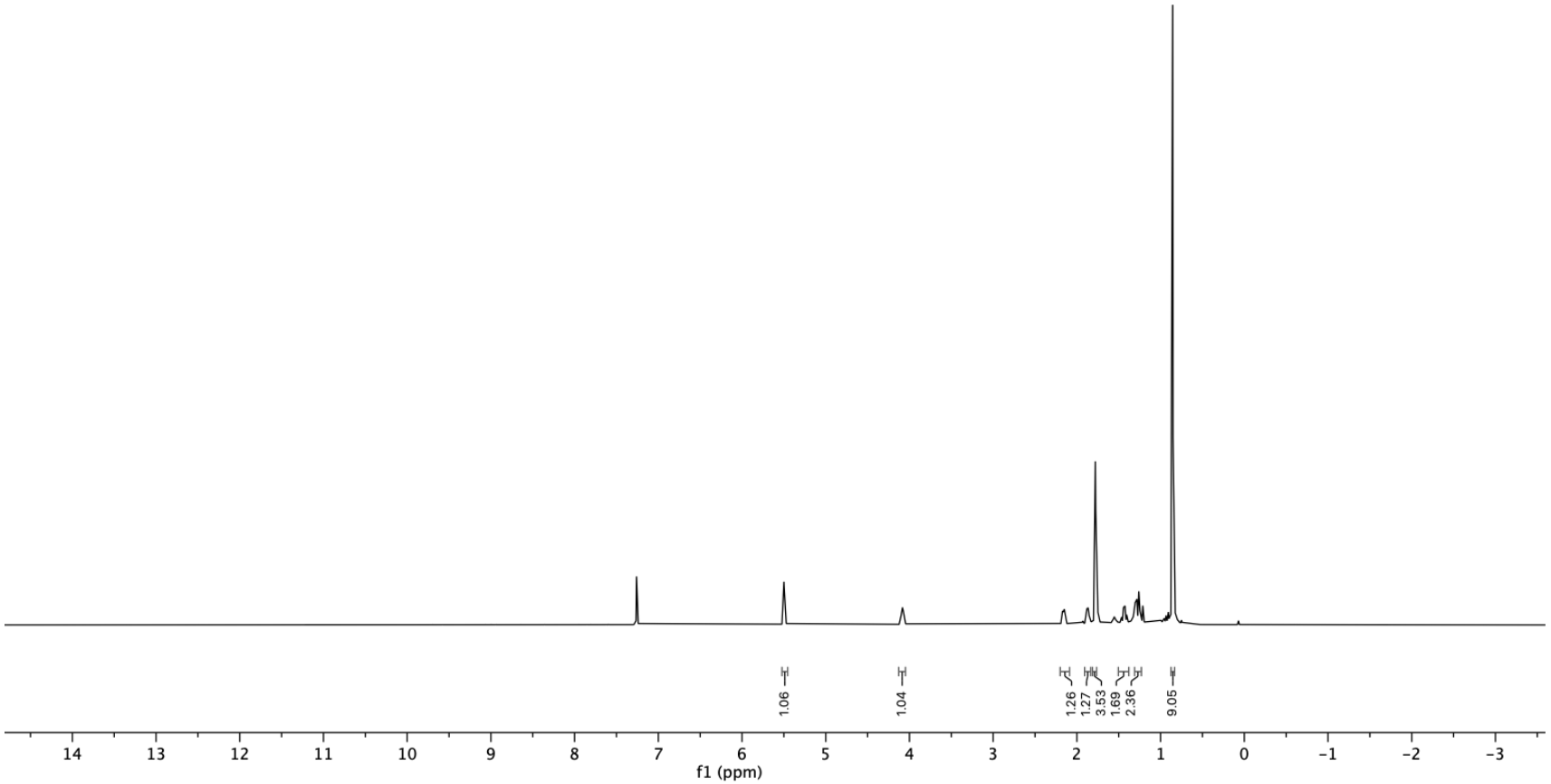
1.06
1.04
1.26
1.27
3.53
1.69
2.36
9.05
14
13
12
11
10
9
8
7
6
5
4
3
2
1
0
−1
−2
−3
f1 (ppm)

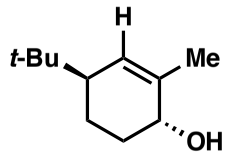
H
t-Bu
Me
OH

90
180
170
160
150
140
130
120
110
100
90
80
70
60
50
40
30
20
10
0
−10
f1 (ppm)

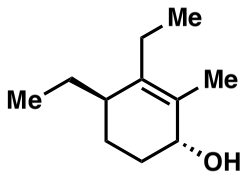
Me
Me
Me
OH

146

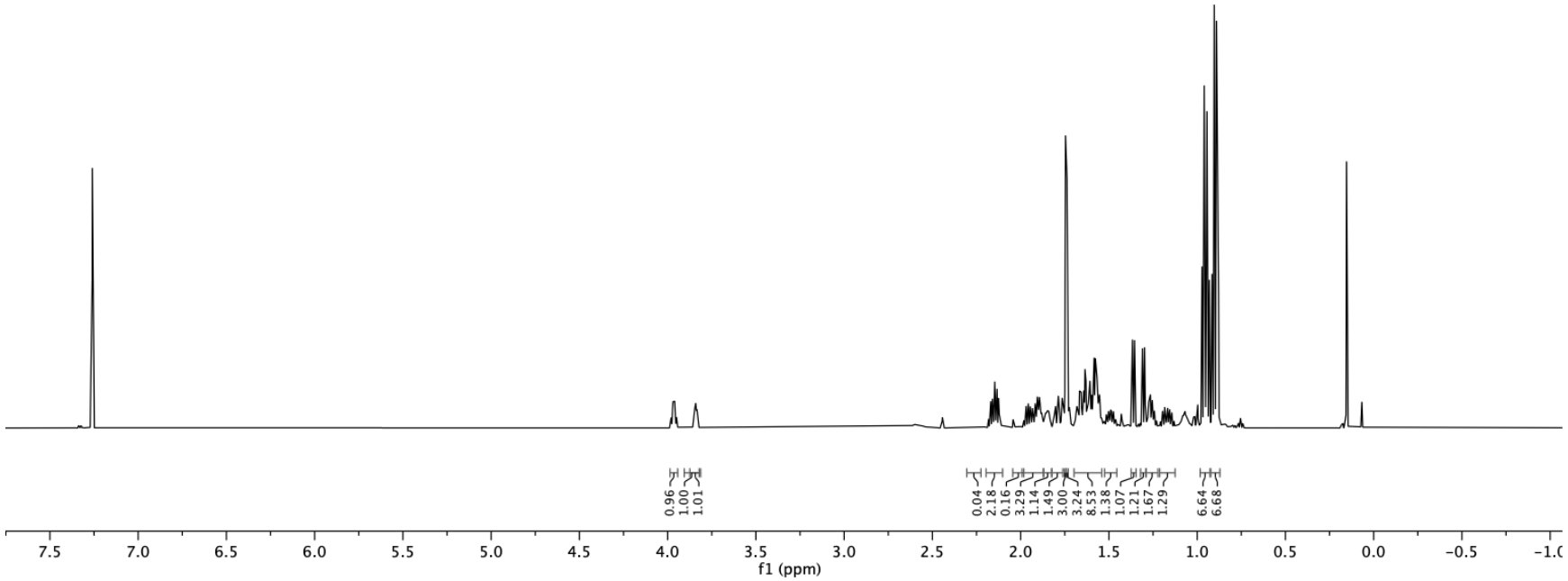
0.96
1.00
1.01
0.04
2.18
0.16
3.29
1.14
1.49
3.00
3.24
8.53
1.38
1.07
1.21
1.67
1.29
6.64
6.68
7.5
7.0
6.5
6.0
5.5
5.0
4.5
4.0
3.5
3.0
2.5
2.0
1.5
1.0
0.5
0.0
−0.5
f1 (ppm)

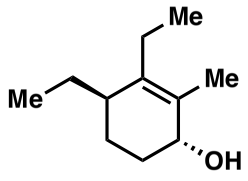
Me
Me
Me
OH

147

190
180
170
160
150
140
130
120
110
100
90
80
70
60
50
40
30
20
10
0
−10
f1 (ppm)

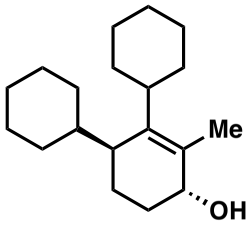
Me
OH

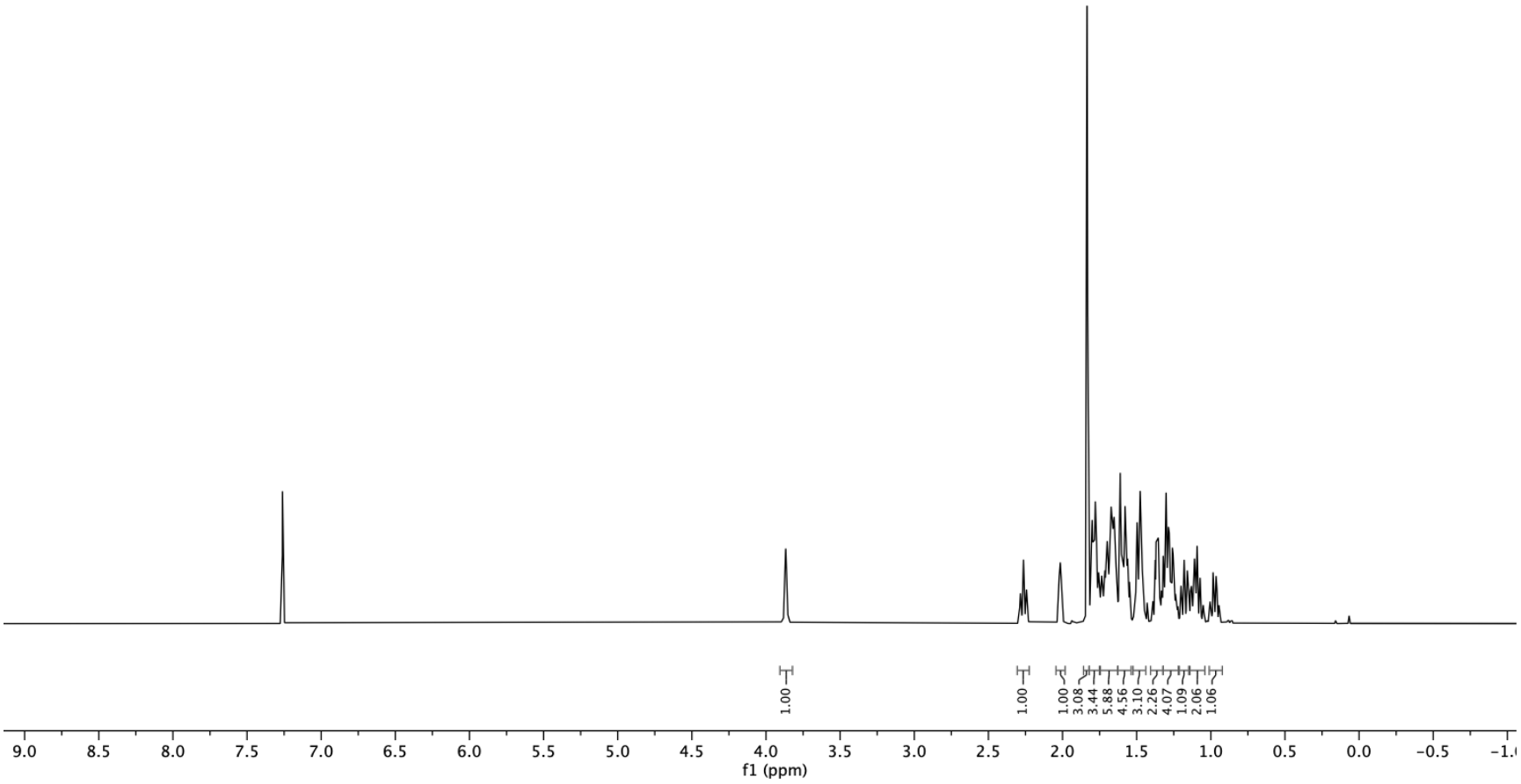
1.00
1.00
1.00
3.08
3.44
5.88
4.56
3.10
2.26
4.07
1.09
2.06
1.06
9.0
8.5
8.0
7.5
7.0
6.5
6.0
5.5
5.0
4.5
4.0
3.5
3.0
2.5
2.0
1.5
1.0
0.5
0.0
-0.5
f1 (ppm)

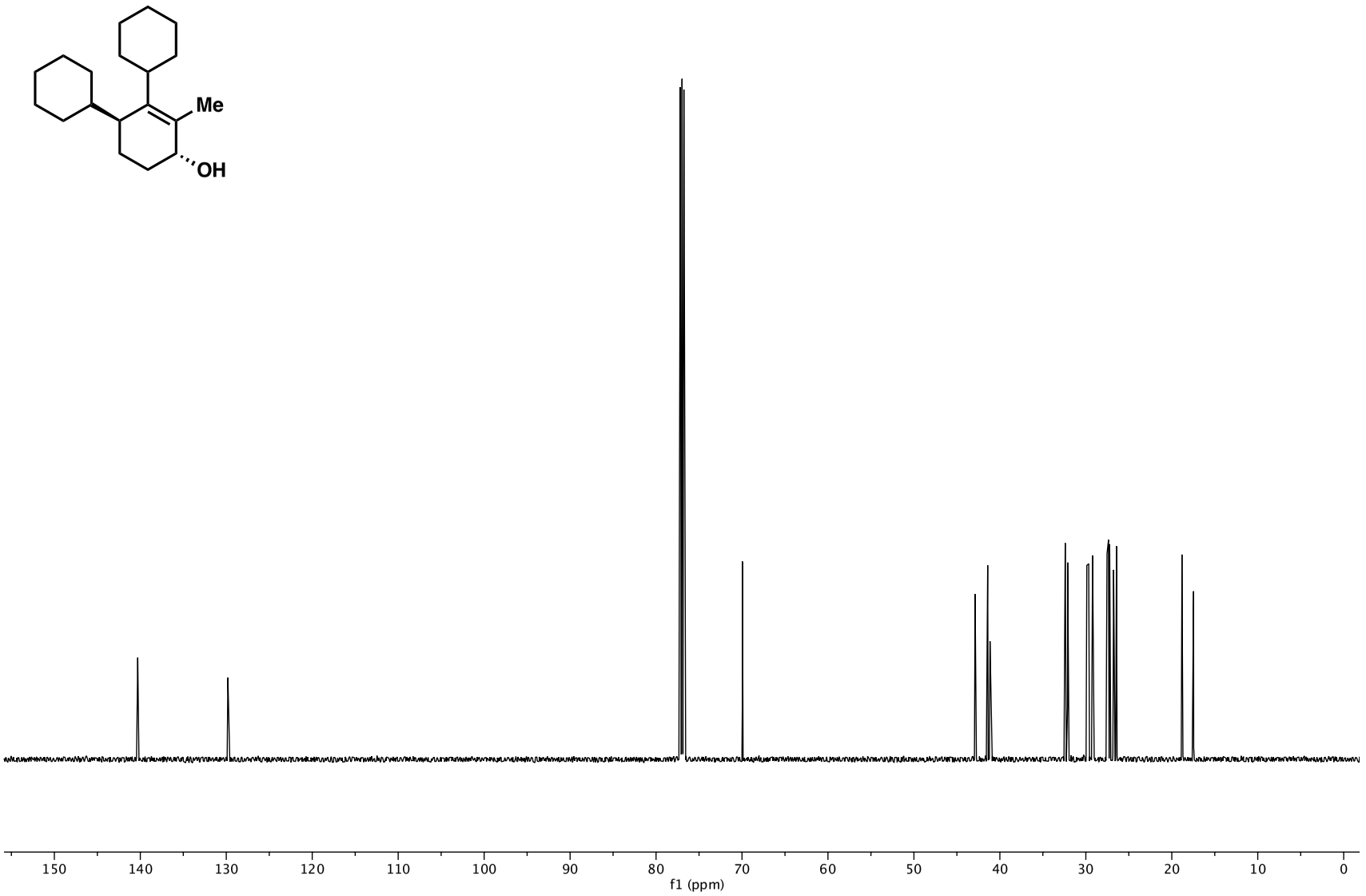
Me
OH
150
140
130
120
110
100
90
80
70
60
50
40
30
20
10
0
f1 (ppm)

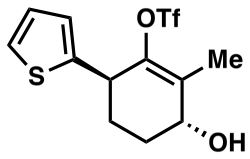
OTf
Me
S
OH

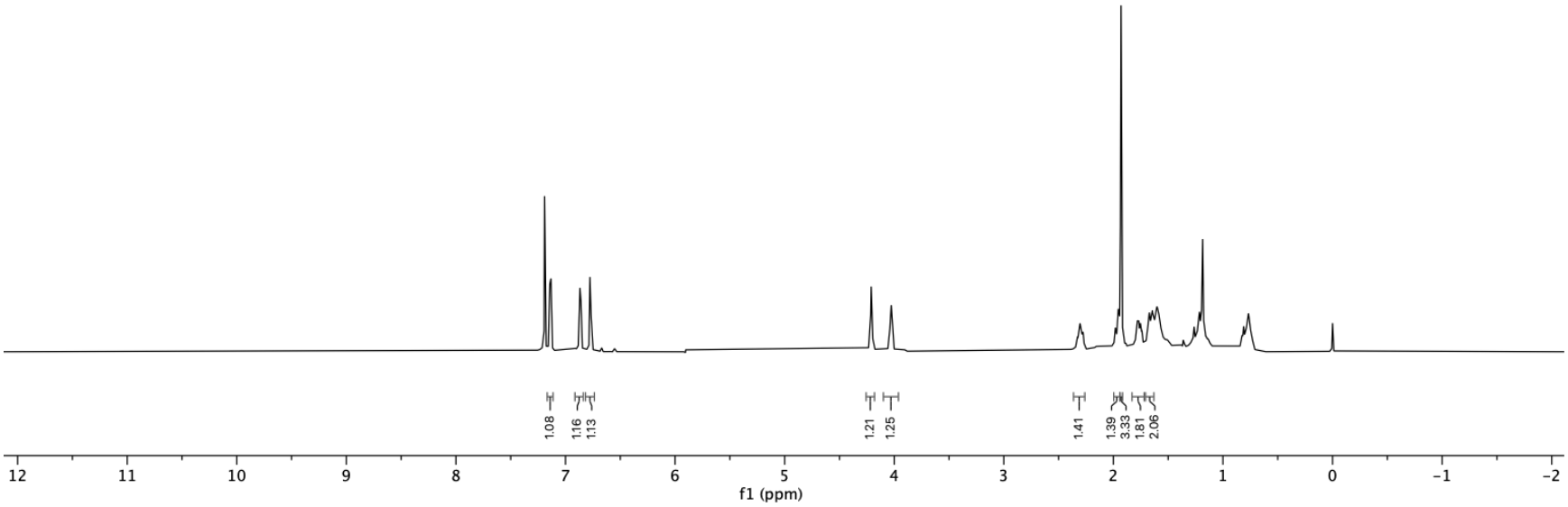
1.08
1.16
1.13
1.21
1.25
1.41
1.39
3.33
1.81
2.06
12
11
10
9
8
7
6
5
4
3
2
1
0
−1
−2
f1 (ppm)

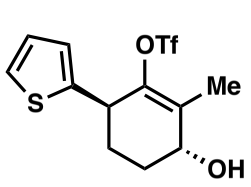
OTf
Me
S
OH

0
180
170
160
150
140
130
120
110
100
90
80
70
60
50
40
30
20
10
0
f1 (ppm)

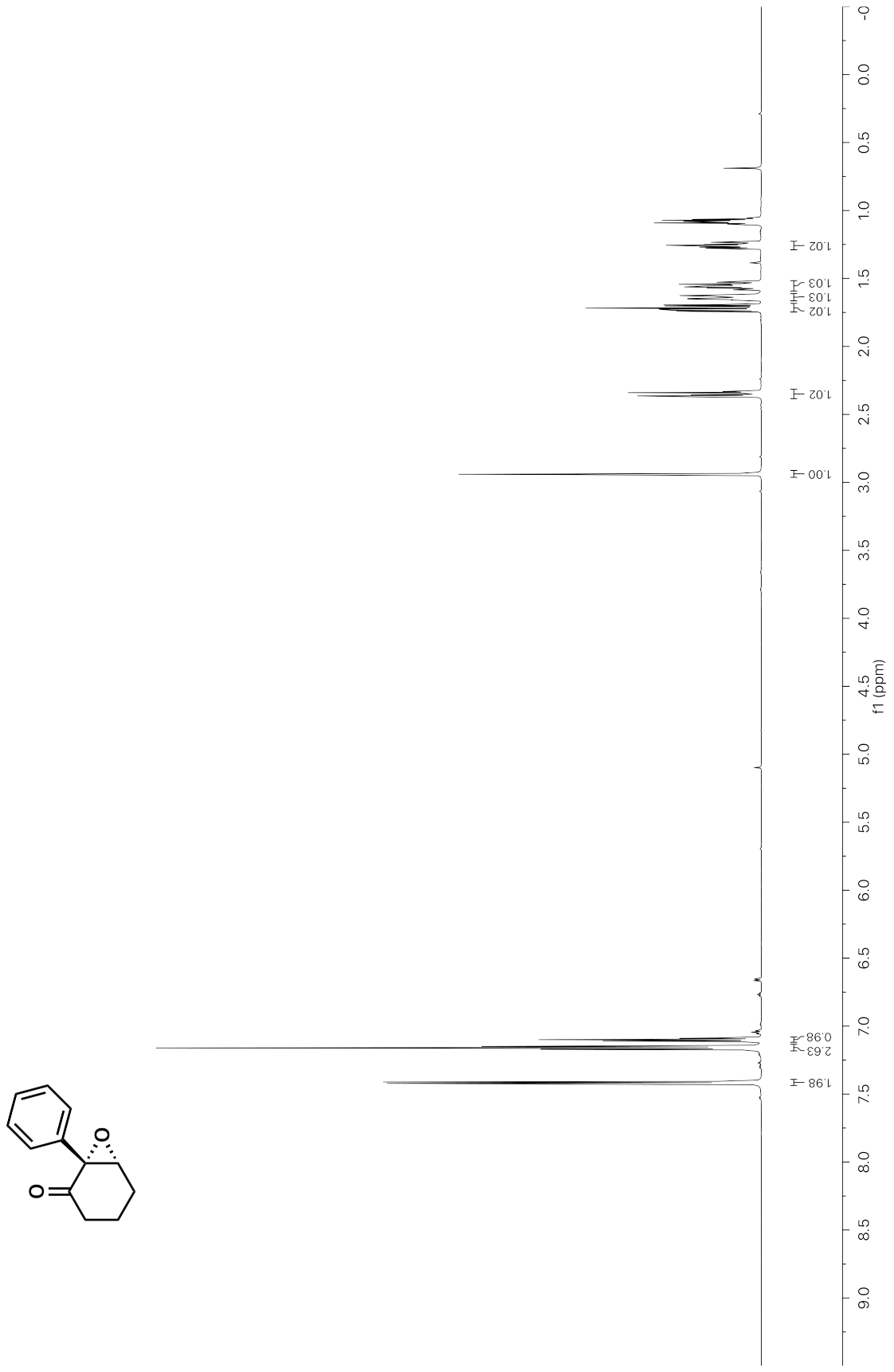
1.98
2.63
0.98
1.02
1.00
1.02
1.03
1.03
1.02
f1 (ppm)

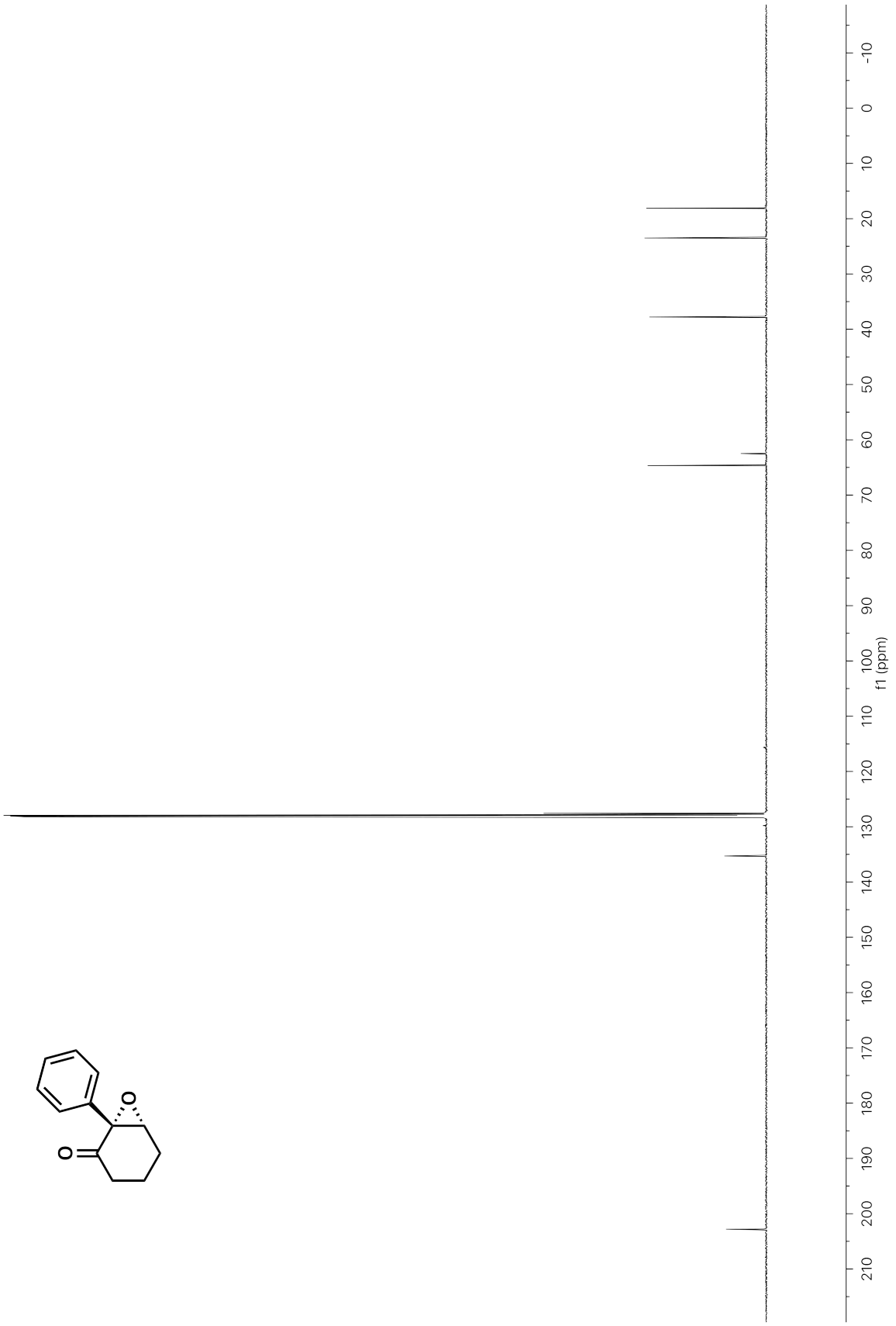
-10
0
10
20
30
40
50
60
70
80
90
100
110
120
130
140
150
160
170
180
190
200
210
f1 (ppm)
O
O

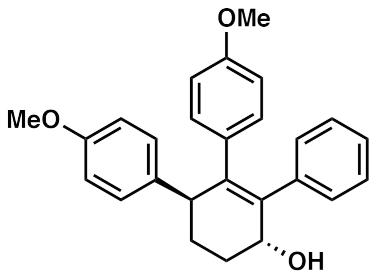
OMe
MeO
OH

2.00
2.05
1.97
2.94
1.85
1.78
1.00
0.99
3.03
2.99
0.99
1.04
1.01
0.99
1.12
9.0
8.5
8.0
7.5
7.0
6.5
6.0
5.5
5.0
4.5
4.0
3.5
3.0
2.5
2.0
1.5
1.0
0.5
0.0
-0
f1 (ppm)

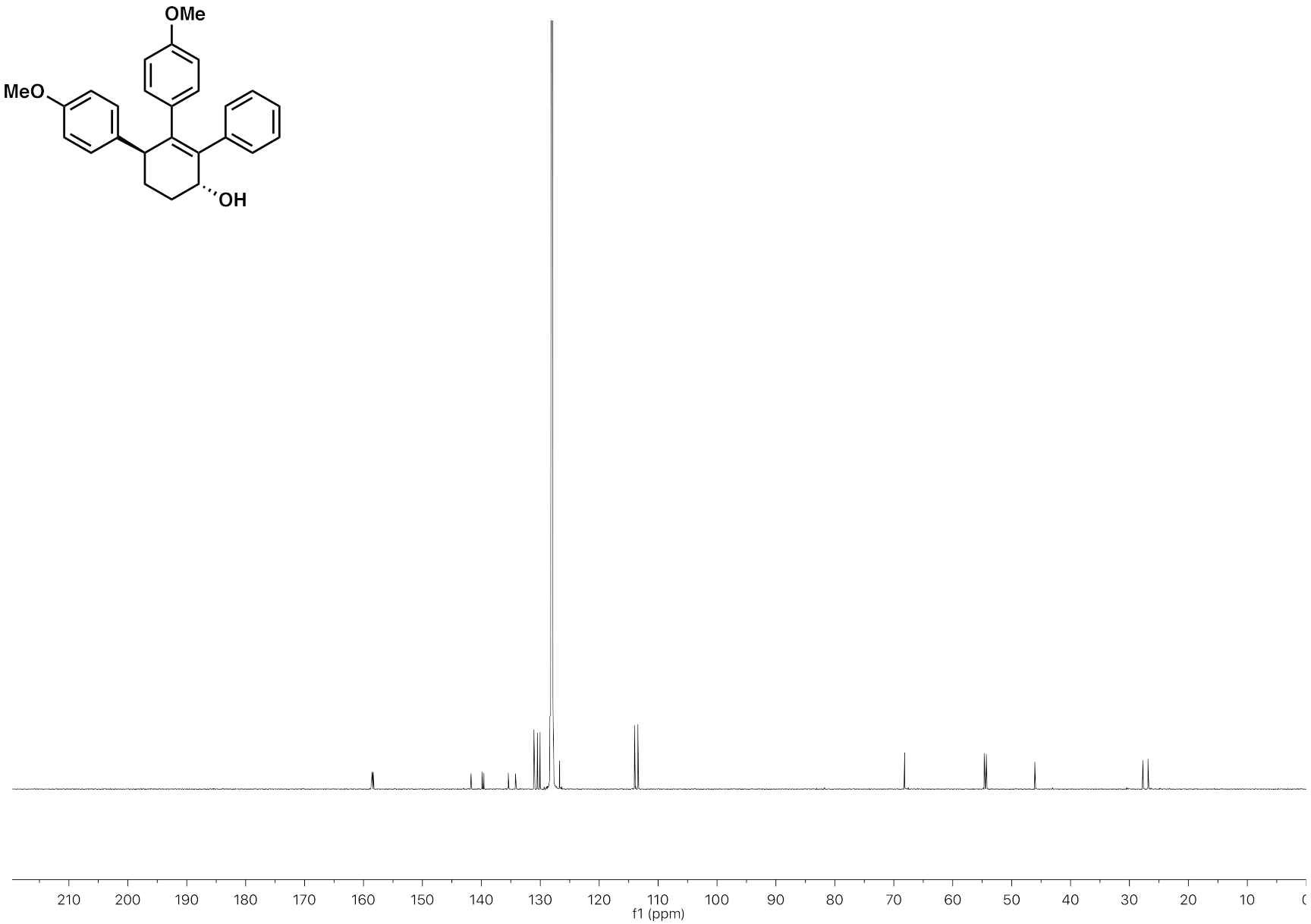
OMe
MeO
OH
210
200
190
180
170
160
150
140
130
120
110
100
90
80
70
60
50
40
30
20
10
f1 (ppm)

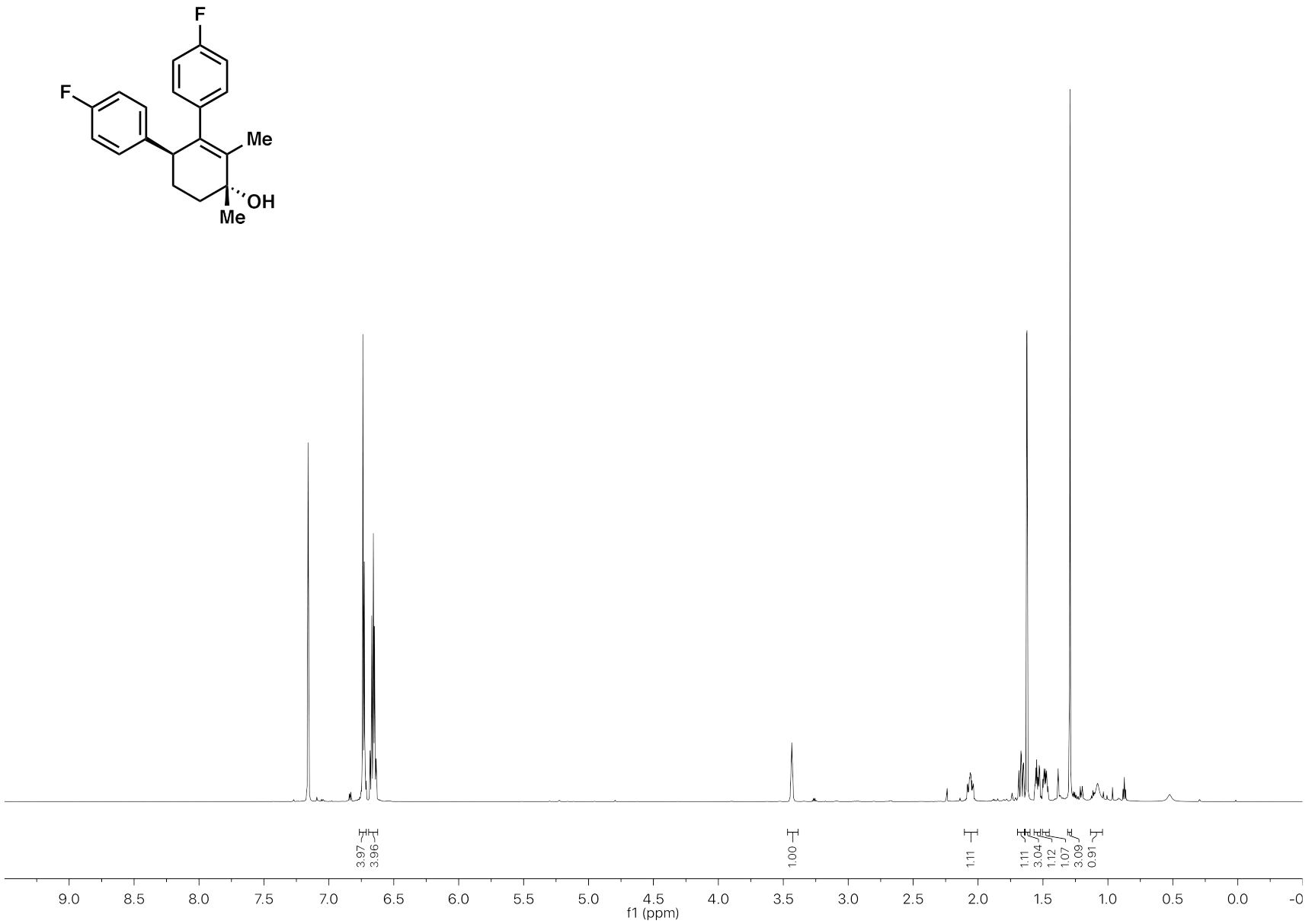
F
F
Me
OH
Me
3.97
3.96
1.00
1.11
1.11
3.04
1.12
1.07
3.09
0.91
9.0
8.5
8.0
7.5
7.0
6.5
6.0
5.5
5.0
4.5
4.0
3.5
3.0
2.5
2.0
1.5
1.0
0.5
0.0
-0
f1 (ppm)

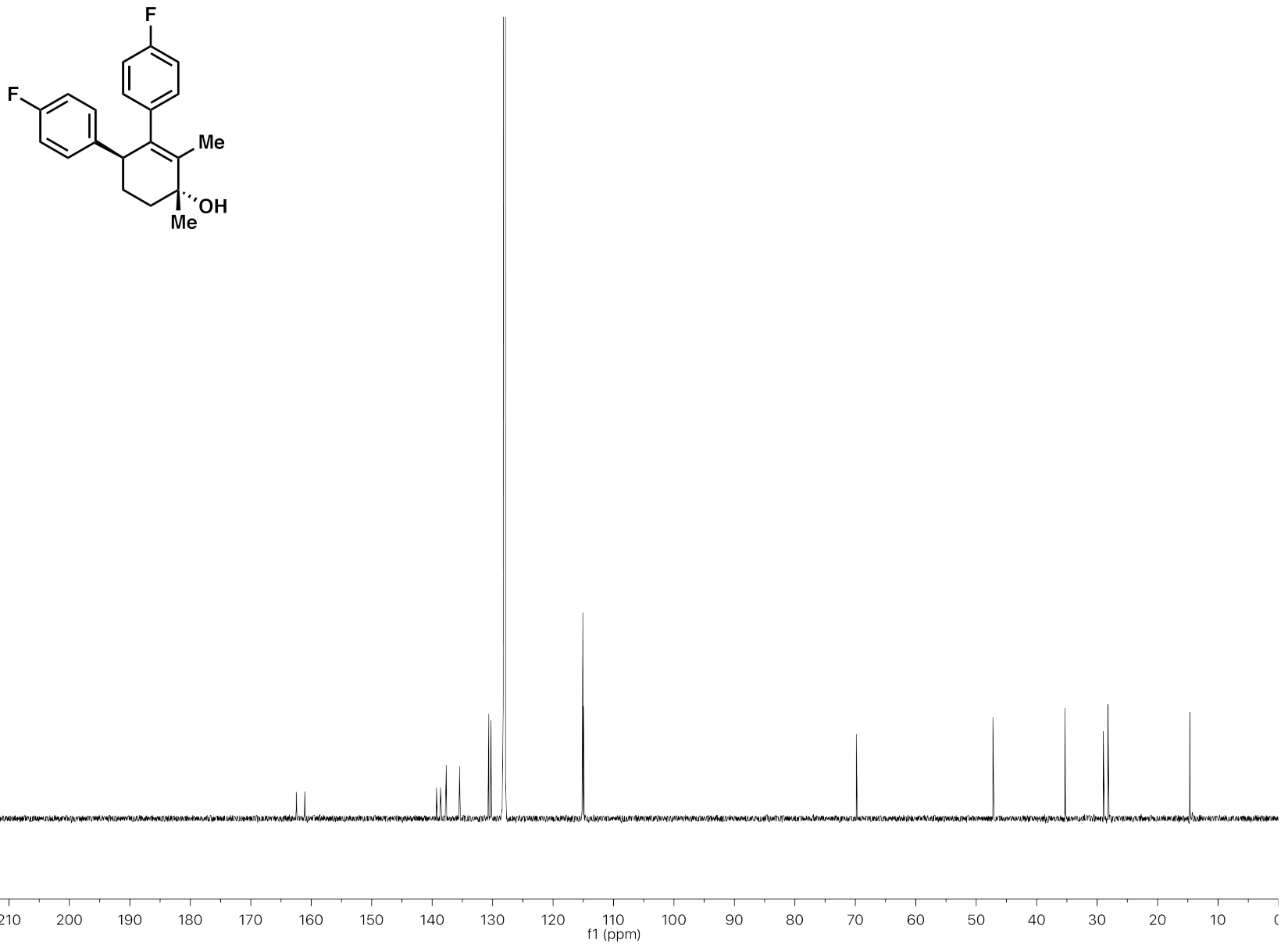
F
F
Me
OH
Me
210
200
190
180
170
160
150
140
130
120
110
100
90
80
70
60
50
40
30
20
10
f1 (ppm)

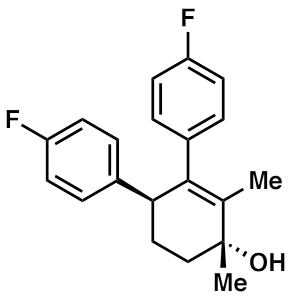
F
F
Me
OH
Me

1.03
1.00
8.0
-108.5
-109.0
-109.5
-110.0
-110.5
-111.0
-111.5
-112.0
-112.5
-113.0
-113.5
-114.0
-114.5
-115.0
-115.5
-116.0
-116.5
-117.0
-117.5
f1 (ppm)

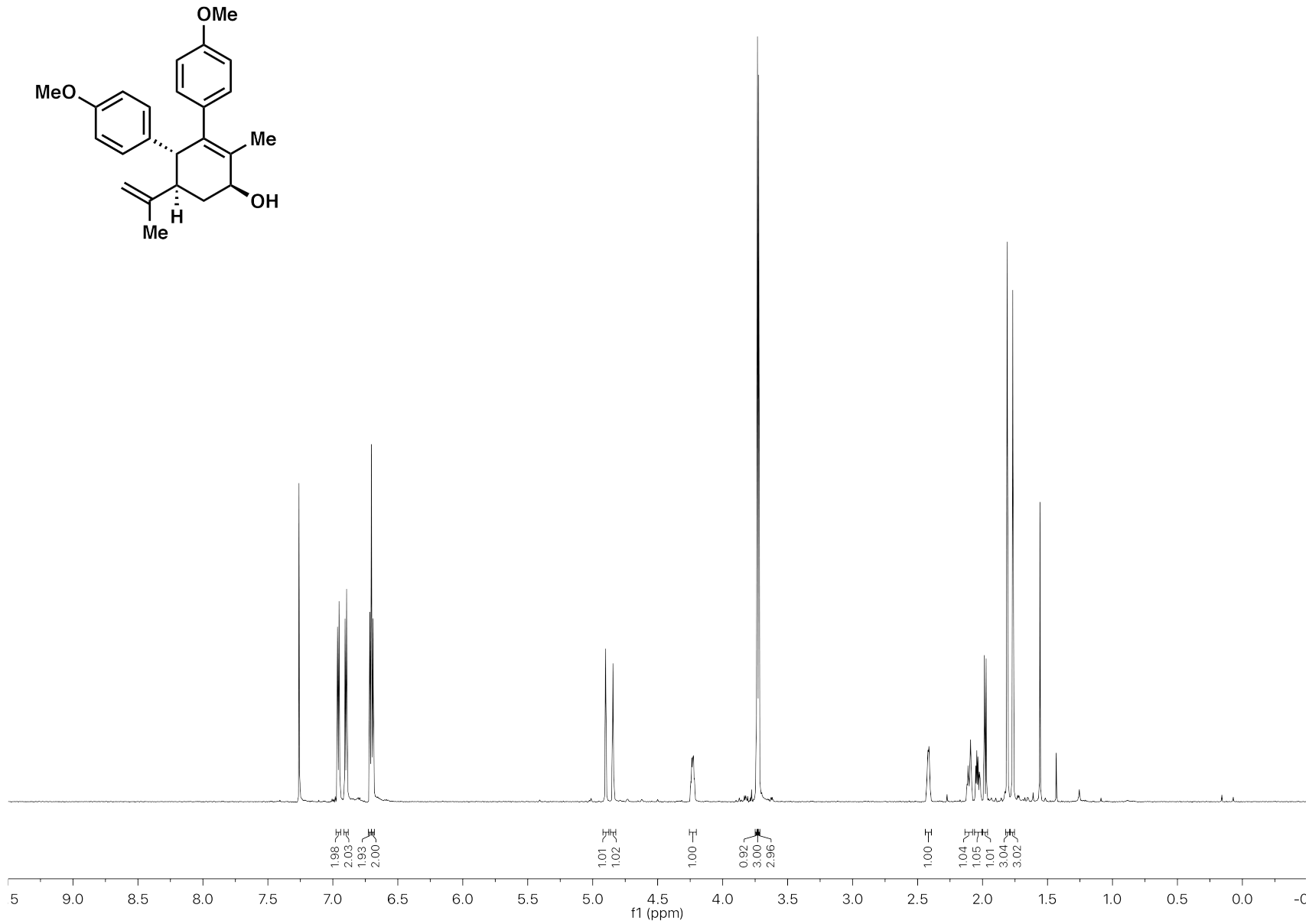
OMe
MeO
Me
OH
H
Me
1.98
2.03
1.93
2.00
1.01
1.02
1.00
0.92
3.00
2.96
1.00
1.04
1.05
1.01
3.04
3.02
9.0
8.5
8.0
7.5
7.0
6.5
6.0
5.5
5.0
4.5
4.0
3.5
3.0
2.5
2.0
1.5
1.0
0.5
0.0
f1 (ppm)

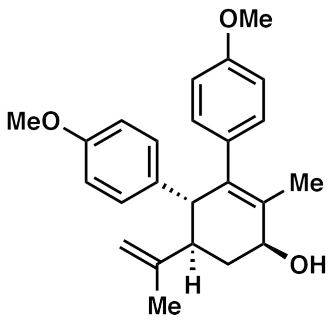
OMe
MeO
Me
OH
H
Me

160

210
200
190
180
170
160
150
140
130
120
110
100
90
80
70
60
50
40
30
20
10
f1 (ppm)

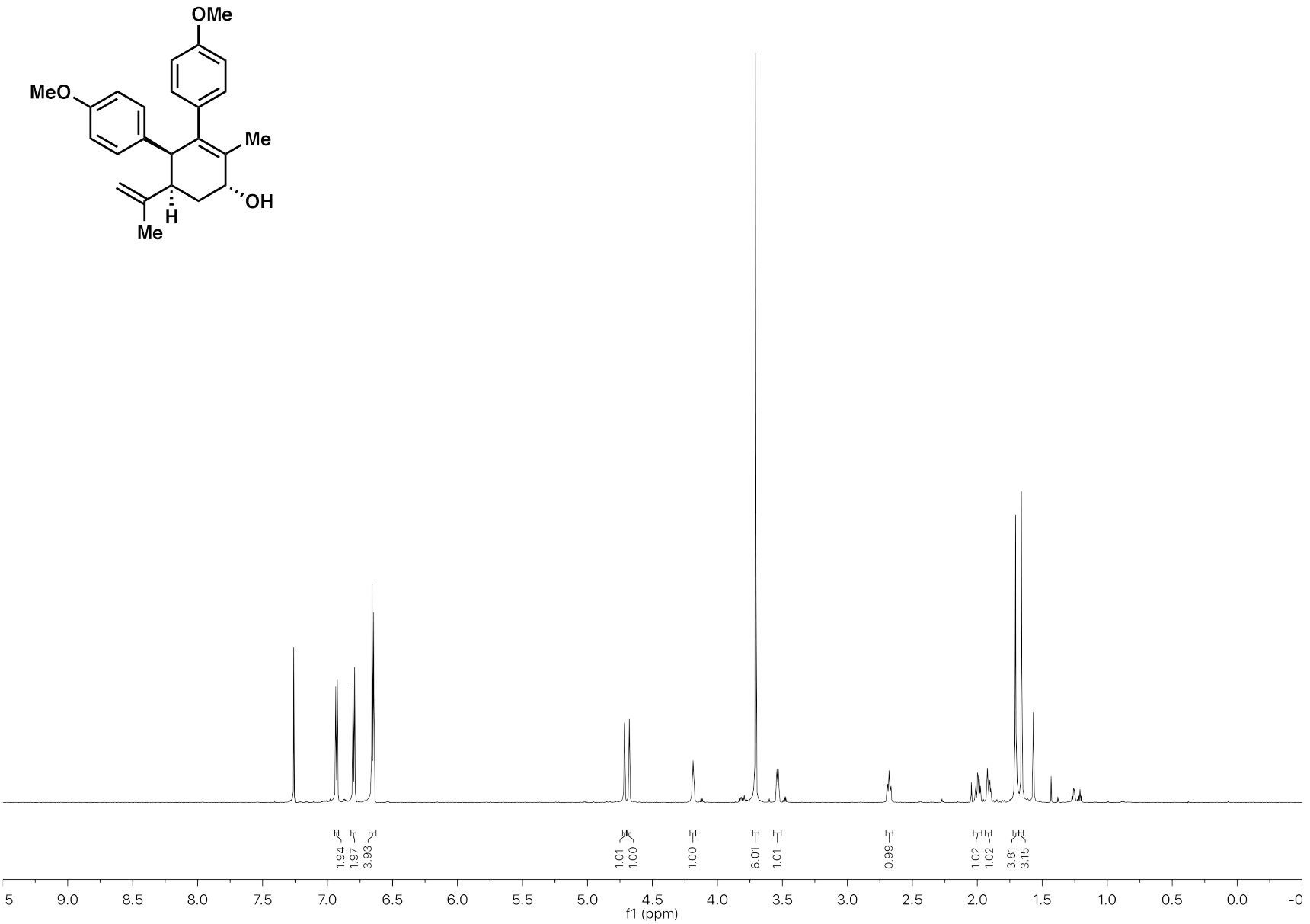
OMe
MeO
Me
OH
H
Me
1.94
1.97
3.93
1.01
1.00
1.00
6.01
1.01
0.99
1.02
1.02
3.81
3.15
5
9.0
8.5
8.0
7.5
7.0
6.5
6.0
5.5
5.0
4.5
4.0
3.5
3.0
2.5
2.0
1.5
1.0
0.5
0.0
-0
f1 (ppm)

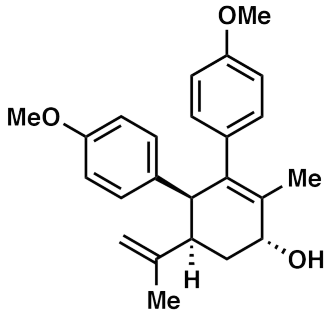
OMe
MeO
Me
OH
H
Me

210
200
190
180
170
160
150
140
130
120
110
100
90
80
70
60
50
40
30
20
10
f1 (ppm)

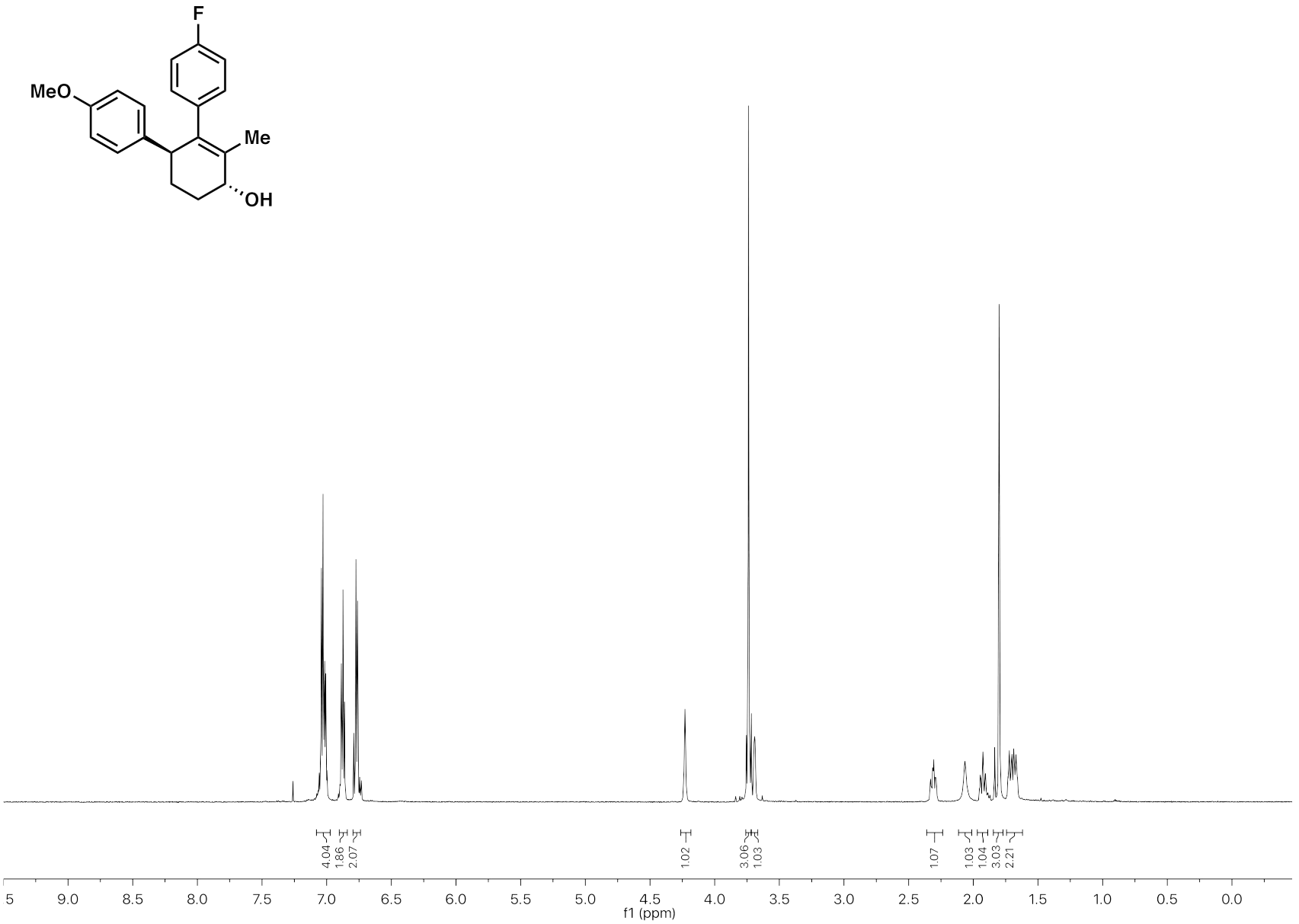
F
MeO
Me
OH
4.04
1.86
2.07
1.02
3.06
1.03
1.07
1.03
1.04
3.03
2.21
f1 (ppm)

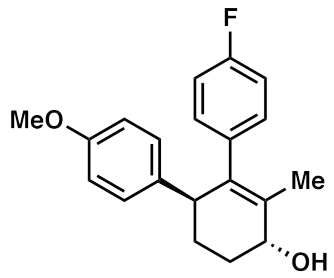
F
MeO
Me
OH

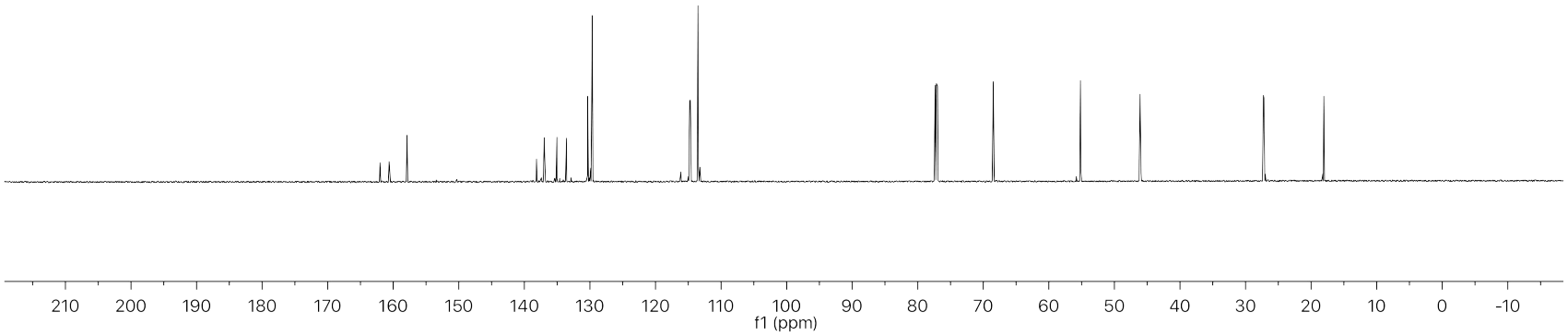
210
200
190
180
170
160
150
140
130
120
110
100
90
80
70
60
50
40
30
20
10
0
-10
f1 (ppm)

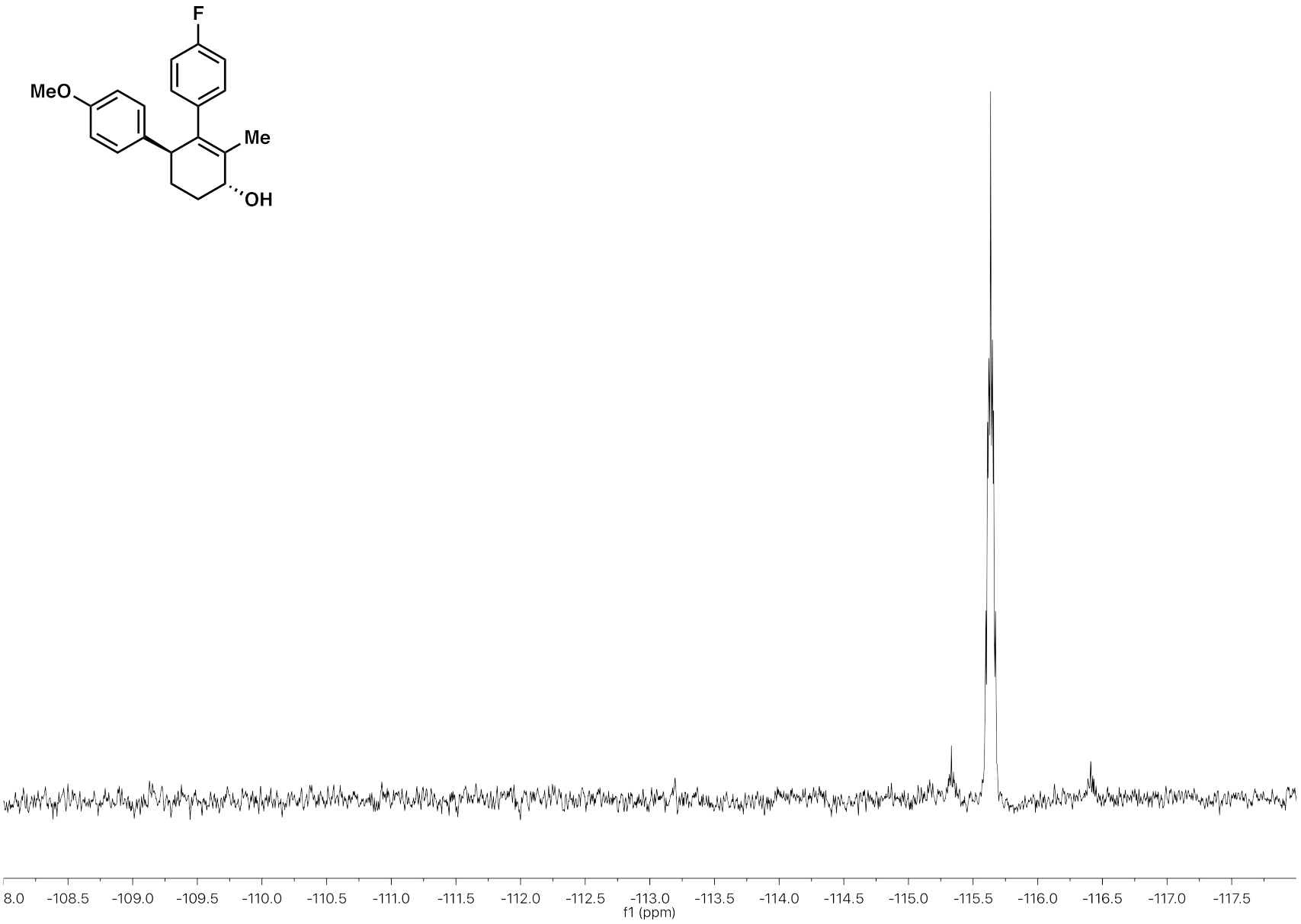
F
MeO
Me
OH
8.0
-108.5
-109.0
-109.5
-110.0
-110.5
-111.0
-111.5
-112.0
-112.5
-113.0
-113.5
-114.0
-114.5
-115.0
-115.5
-116.0
-116.5
-117.0
-117.5
f1 (ppm)

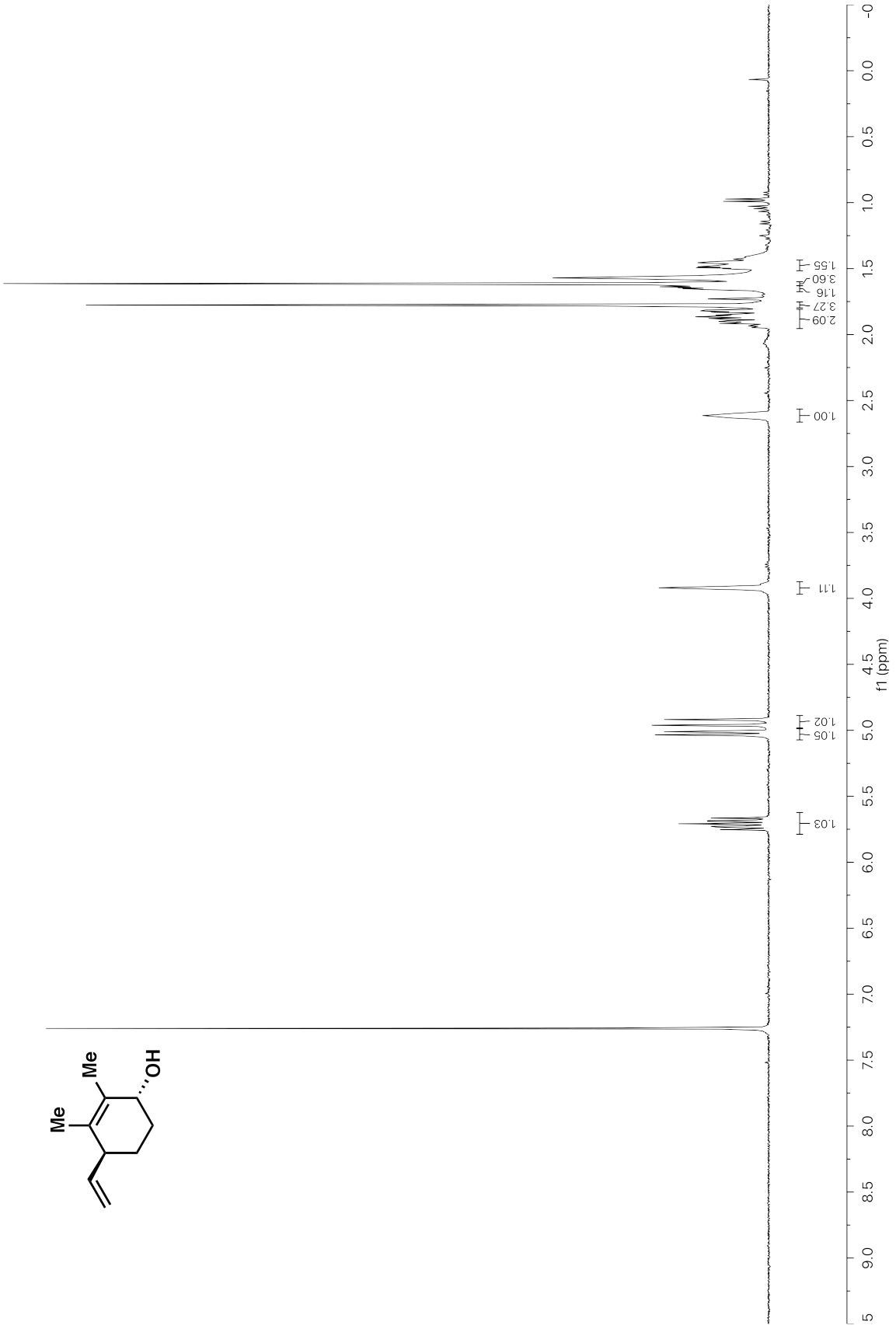
Me
Me
OH
1.03
1.05
1.02
1.11
1.00
2.09
3.27
1.16
3.60
1.55
f1 (ppm)

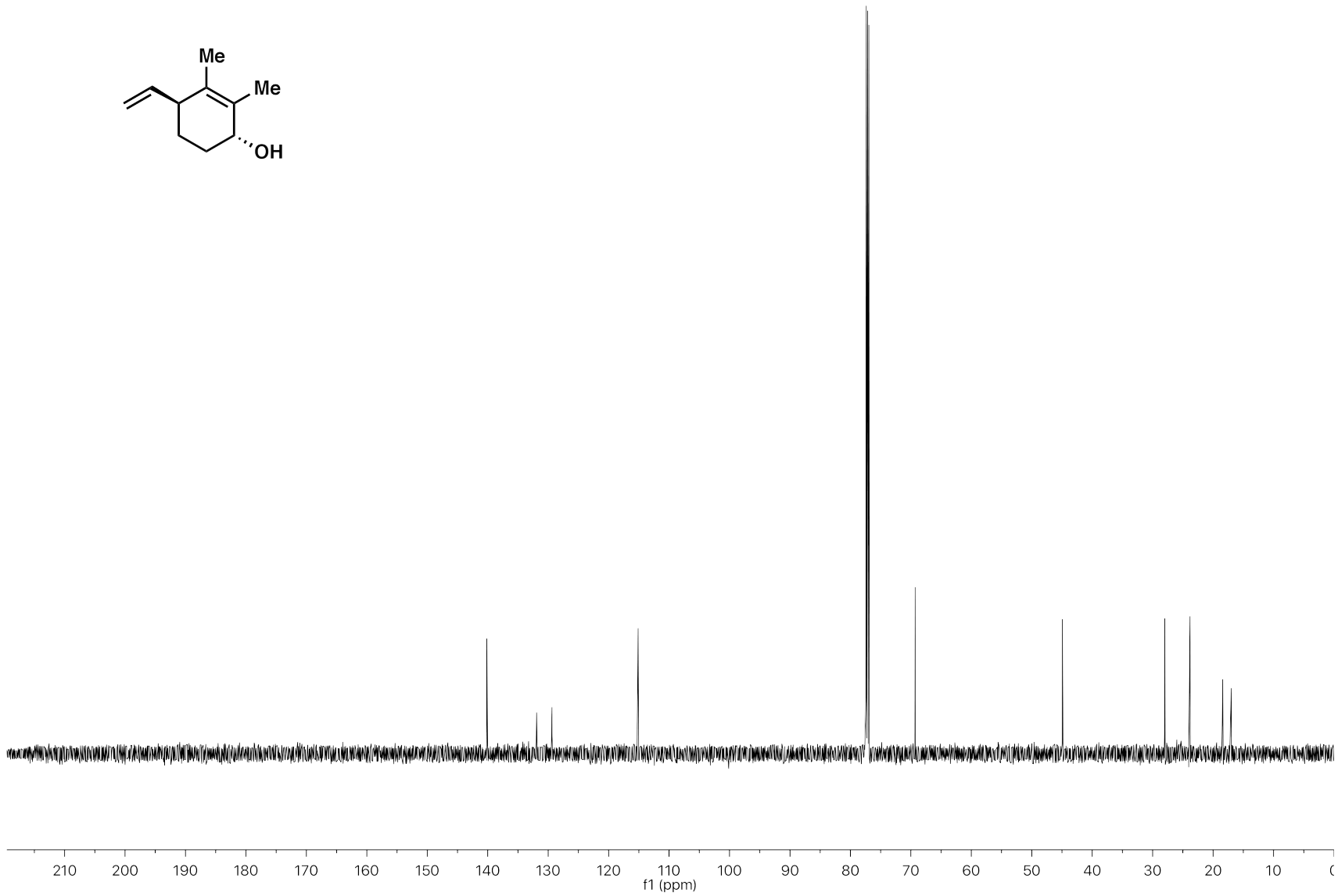
Me
Me
OH
210
200
190
180
170
160
150
140
130
120
110
100
90
80
70
60
50
40
30
20
10
f1 (ppm)

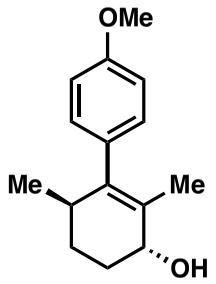
OMe
Me
Me
OH

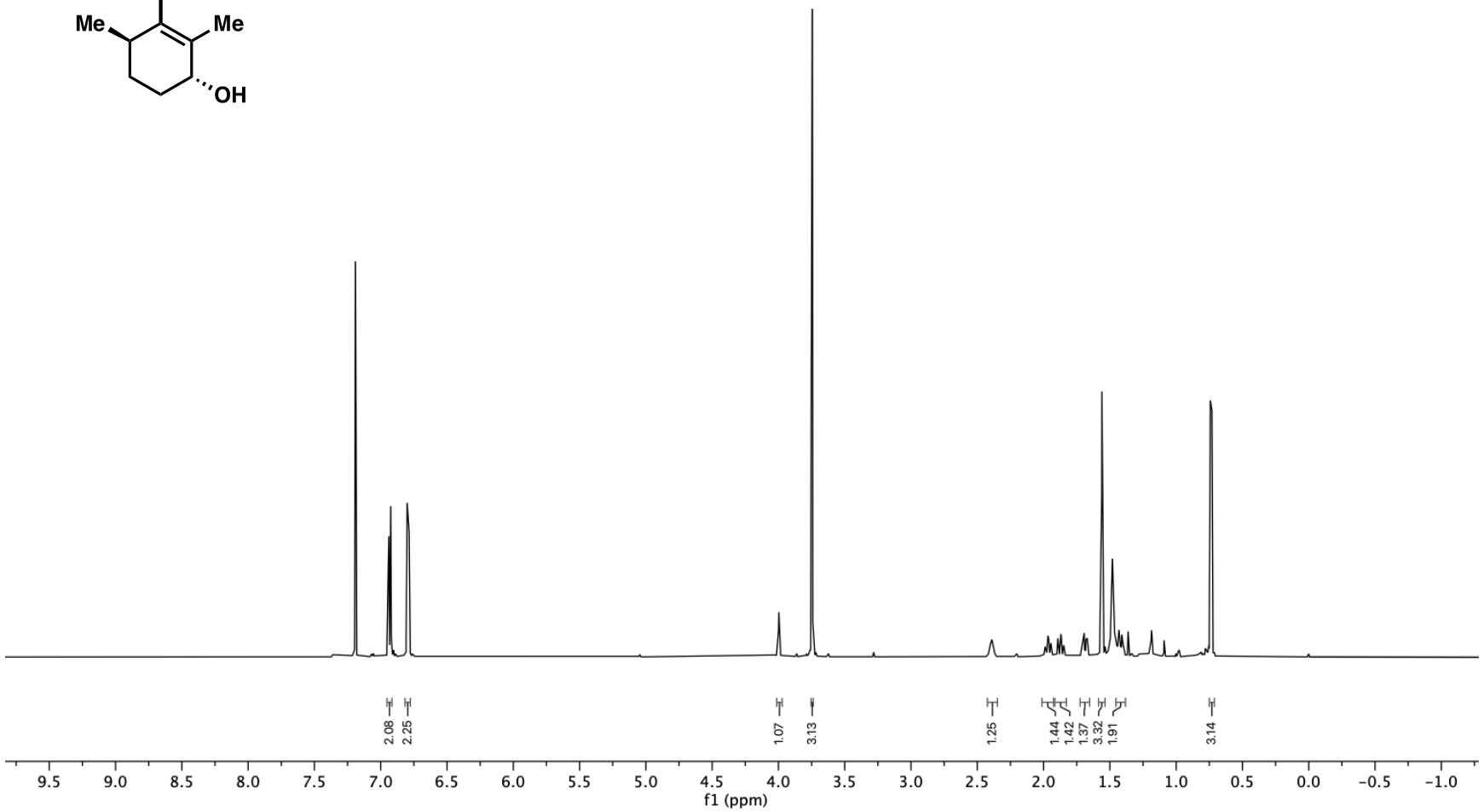
2.08
2.25
1.07
3.13
1.25
1.44
1.42
1.37
3.32
1.91
3.14
9.5
9.0
8.5
8.0
7.5
7.0
6.5
6.0
5.5
5.0
4.5
4.0
3.5
3.0
2.5
2.0
1.5
1.0
0.5
0.0
-0.5
-1.0
f1 (ppm)

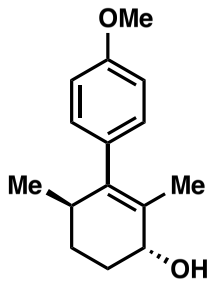
OMe
Me
Me
OH

210
200
190
180
170
160
150
140
130
120
110
100
90
80
70
60
50
40
30
20
10
0
f1 (ppm)

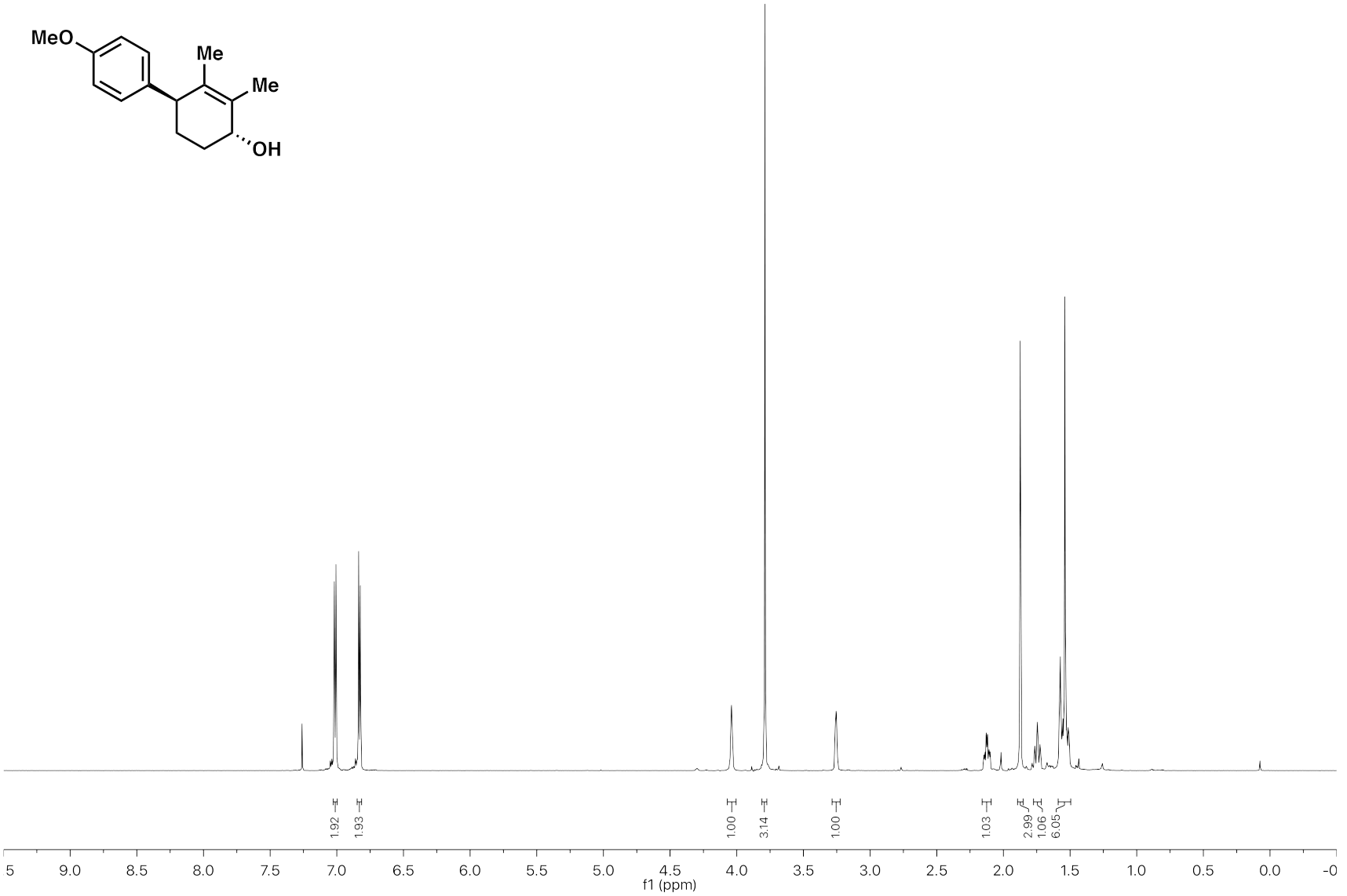
MeO
Me
Me
OH
1.92
1.93
1.00
3.14
1.00
1.03
2.99
1.06
6.05
5
9.0
8.5
8.0
7.5
7.0
6.5
6.0
5.5
5.0
4.5
4.0
3.5
3.0
2.5
2.0
1.5
1.0
0.5
0.0
-0
f1 (ppm)

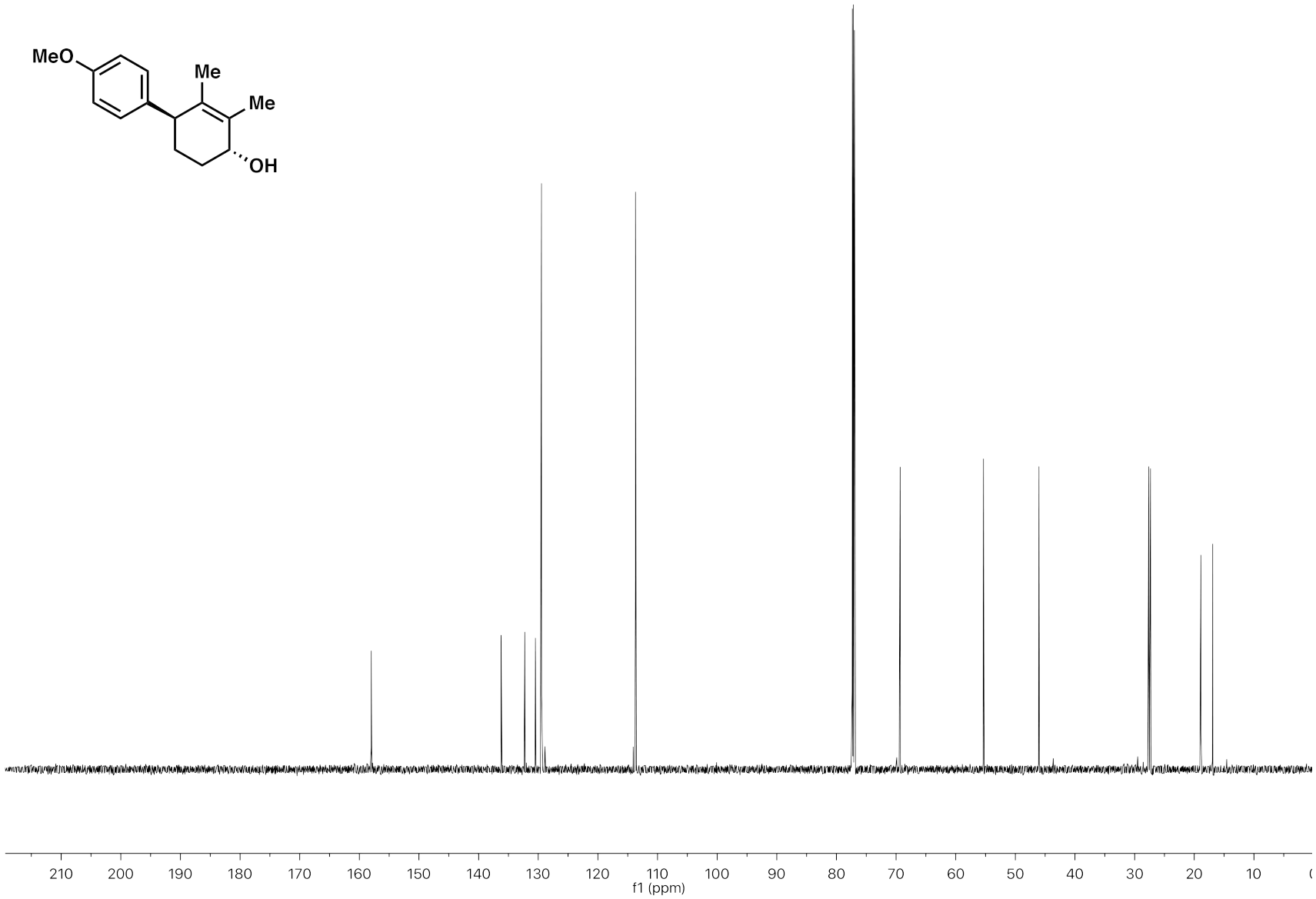
MeO
Me
Me
OH
210
200
190
180
170
160
150
140
130
120
110
100
90
80
70
60
50
40
30
20
10
f1 (ppm)

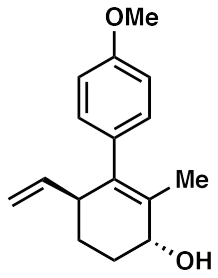
OMe
Me
OH

1.96
2.08
0.97
0.99
0.99
1.00
3.21
1.00
1.11
1.03
1.04
3.01
1.11
0.86
5
9.0
8.5
8.0
7.5
7.0
6.5
6.0
5.5
5.0
4.5
4.0
3.5
3.0
2.5
2.0
1.5
1.0
0.5
0.0
-0
f1 (ppm)

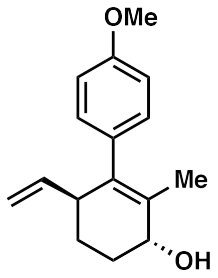
OMe
Me
OH

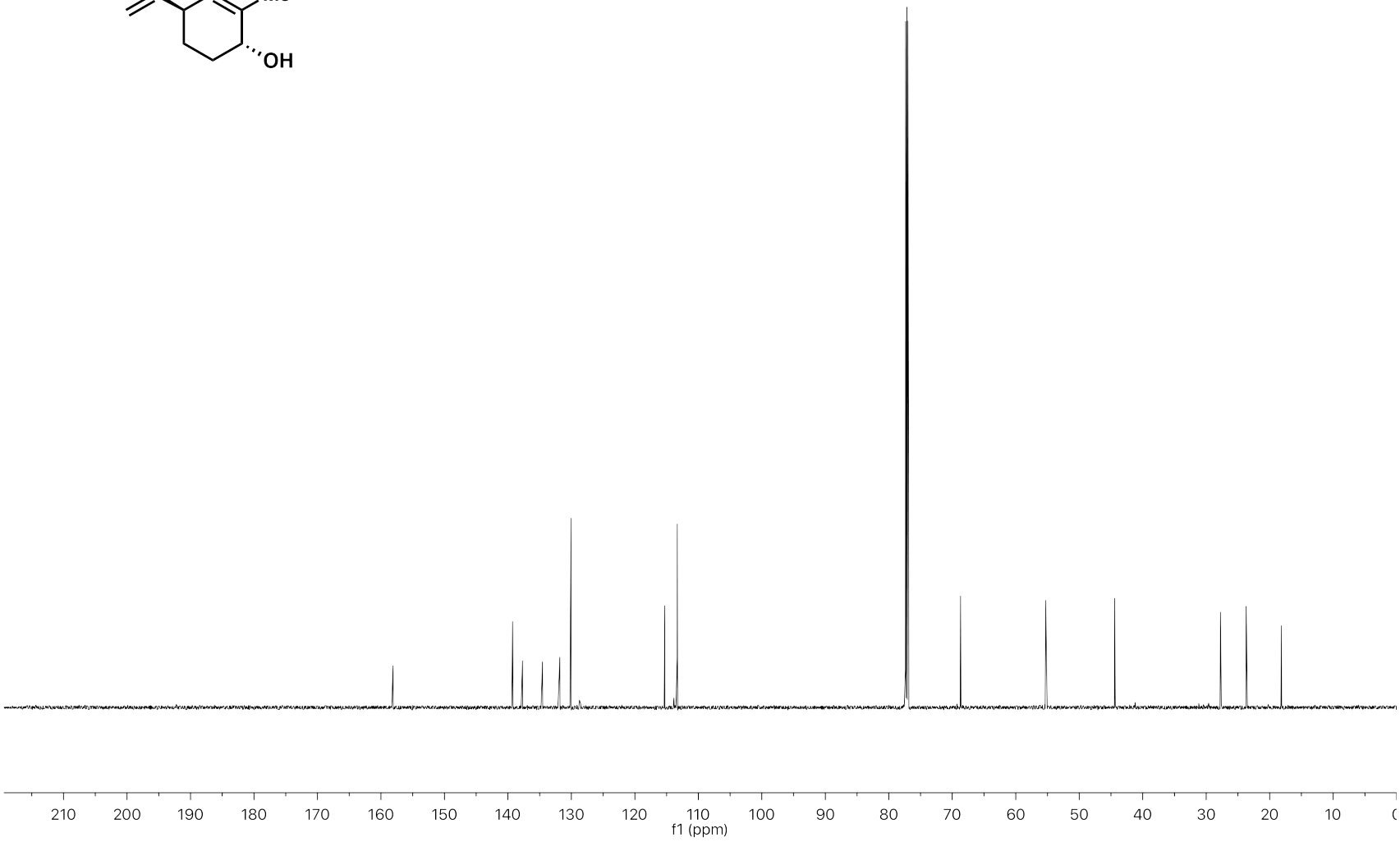
210
200
190
180
170
160
150
140
130
120
110
100
90
80
70
60
50
40
30
20
10
f1 (ppm)

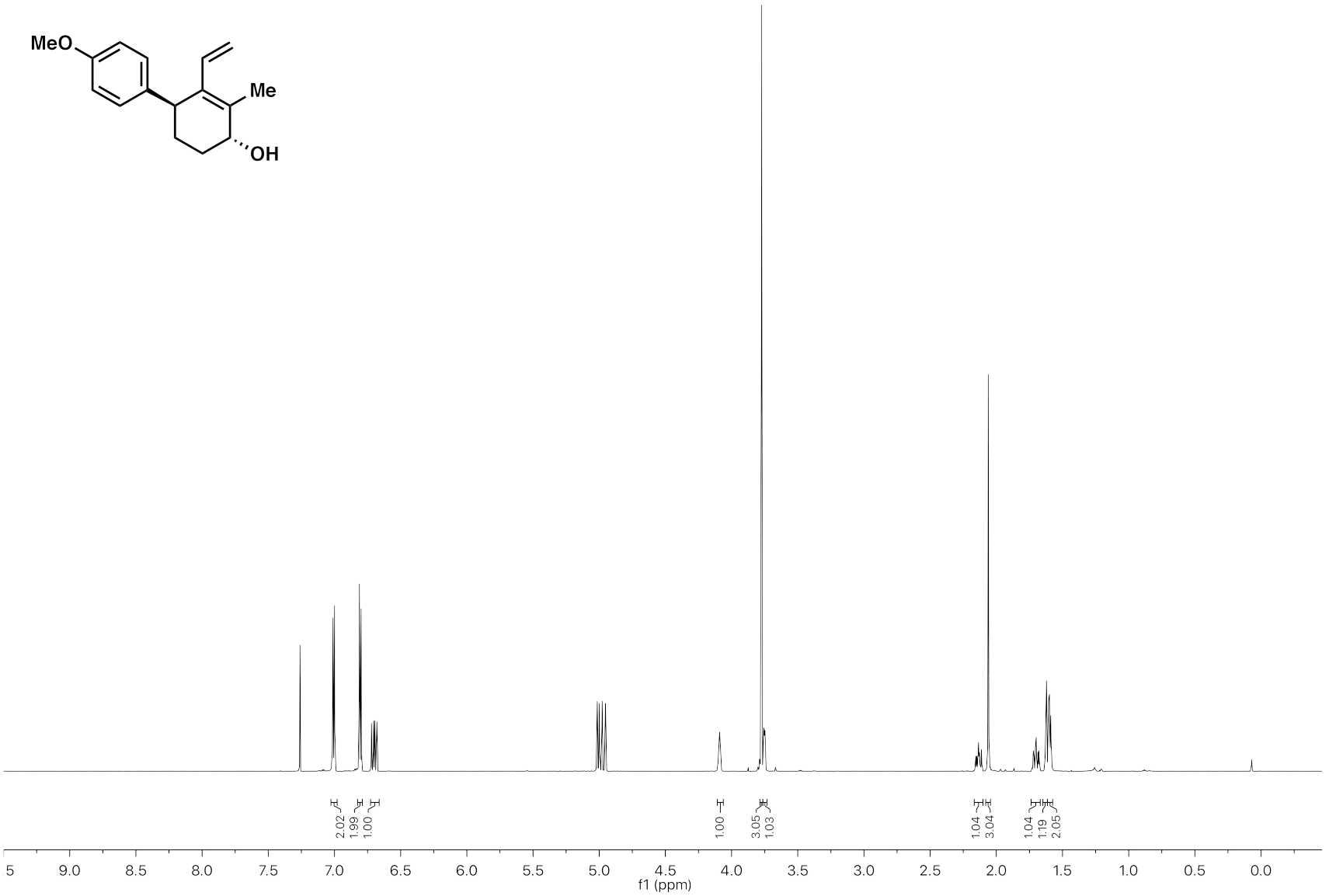
MeO
Me
OH
2.02
1.99
1.00
1.00
3.05
1.03
1.04
3.04
1.04
1.19
2.05
f1 (ppm)

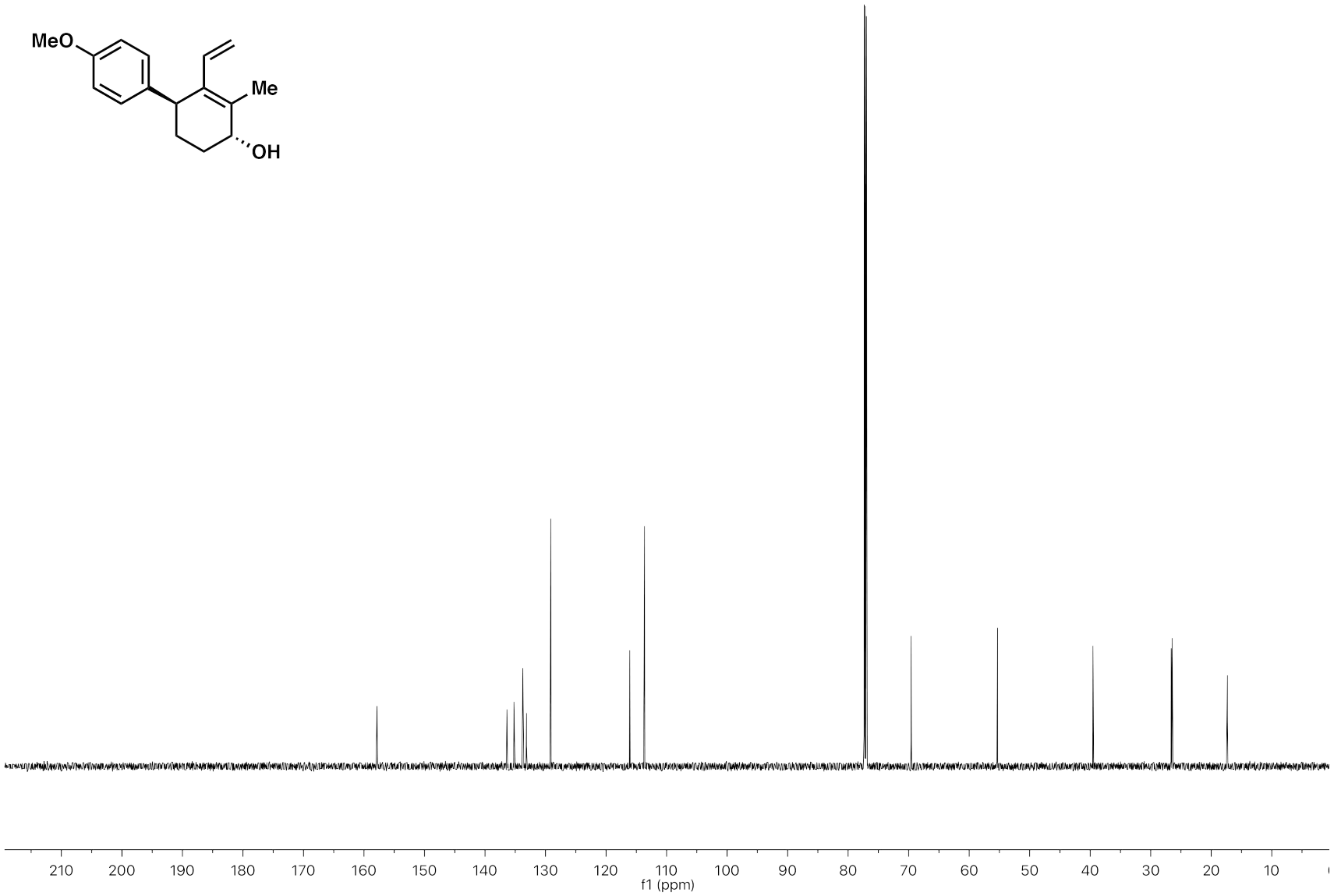
MeO
Me
OH
210
200
190
180
170
160
150
140
130
120
110
100
90
80
70
60
50
40
30
20
10
f1 (ppm)

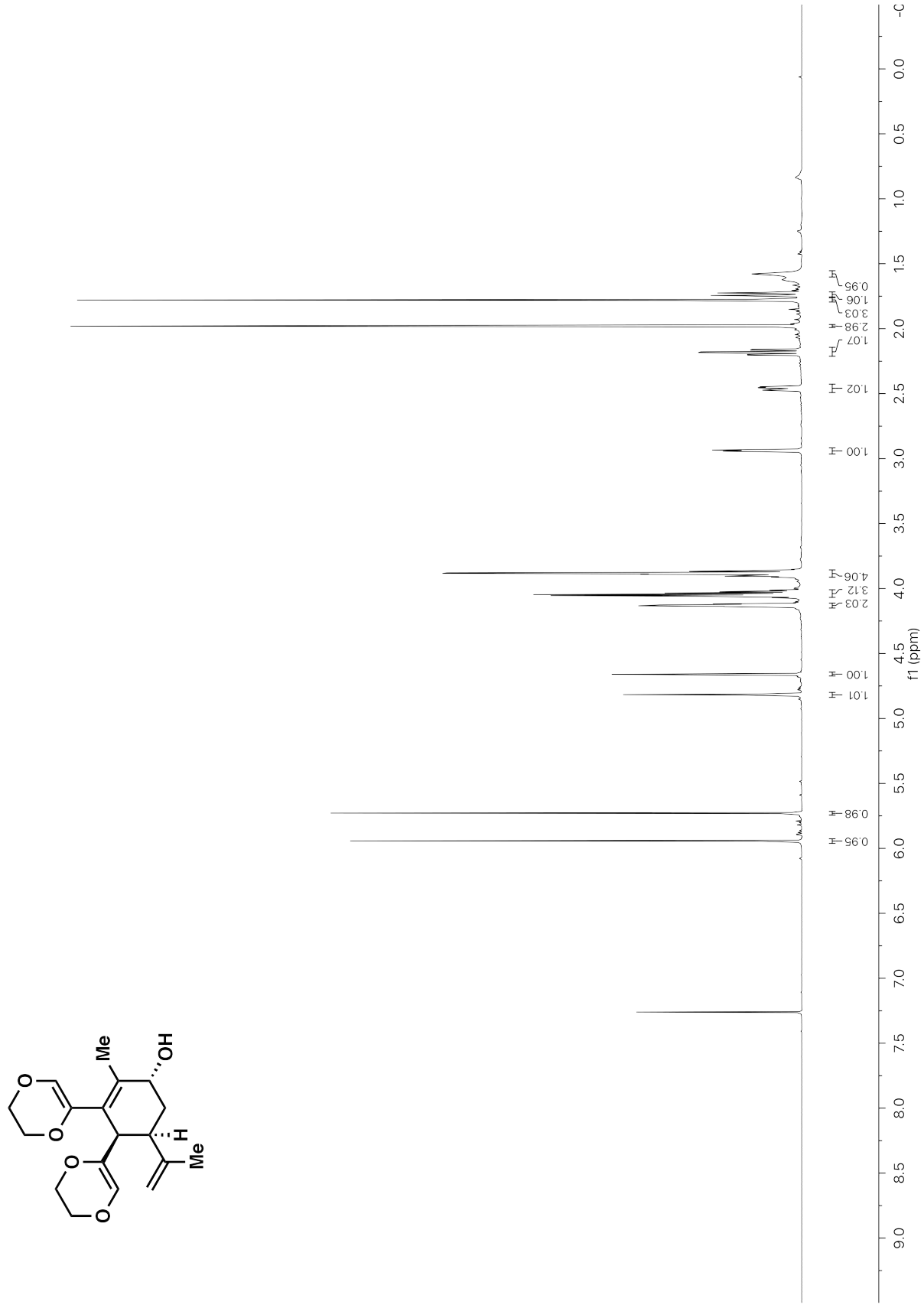
Me
OH
H
Me
O
O
O
O
0.95
0.98
1.01
1.00
2.03
3.12
4.06
1.00
1.02
1.07
2.98
3.03
1.06
0.95
f1 (ppm)

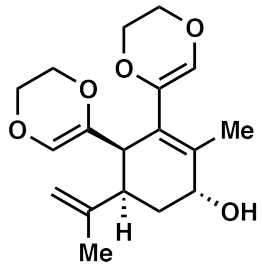
O
O
O
O
Me
OH
H
Me

210
200
190
180
170
160
150
140
130
120
110
100
90
80
70
60
50
40
30
20
10
f1 (ppm)

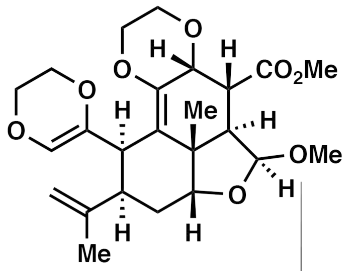
O
H
H
O
CO2Me
O
H
Me
H
O
OMe
H
O
H
H
Me

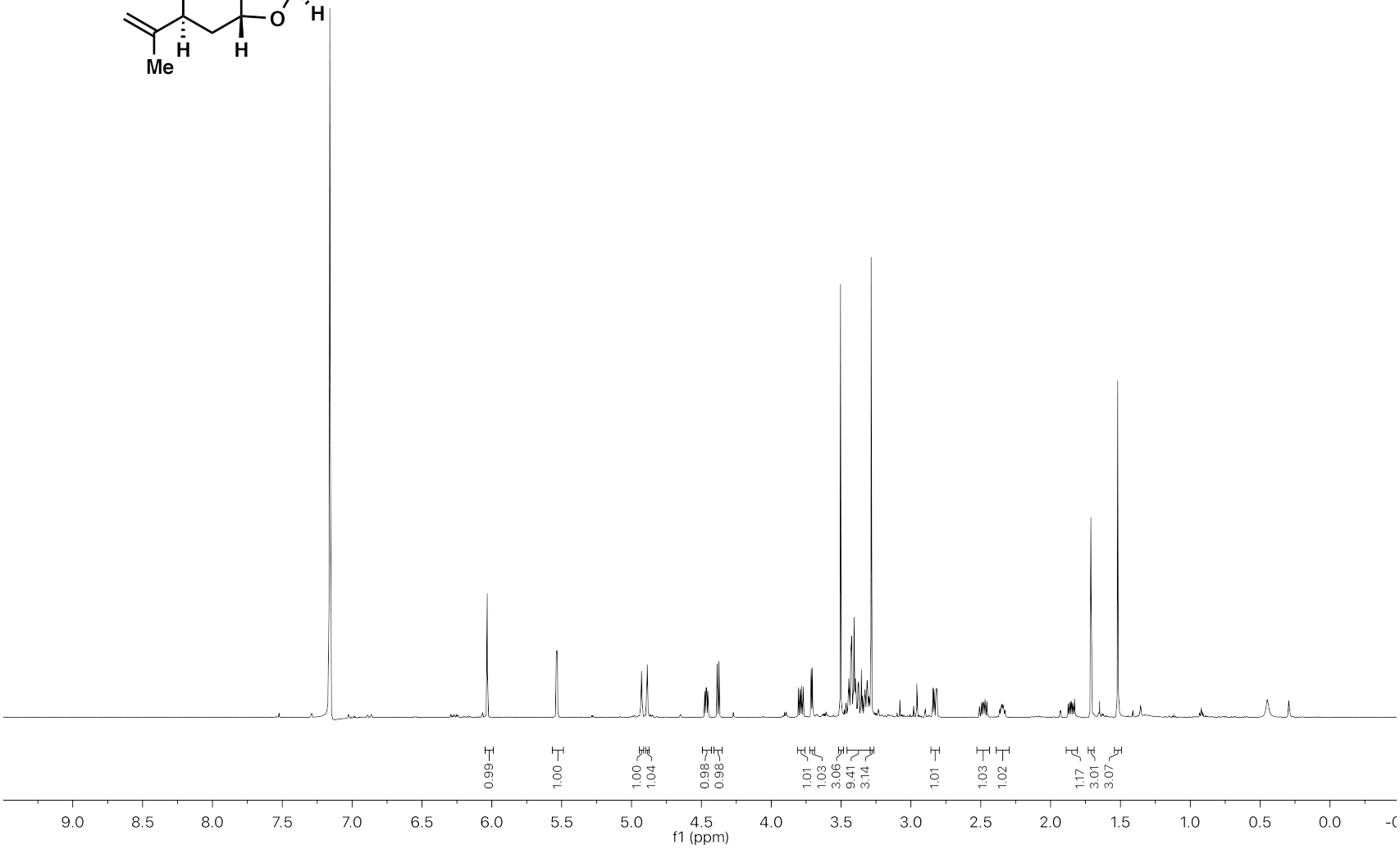
0.99
1.00
1.00
1.04
0.98
0.98
1.01
1.03
3.06
9.41
3.14
1.01
1.03
1.02
1.17
3.01
3.07
9.0
8.5
8.0
7.5
7.0
6.5
6.0
5.5
5.0
4.5
4.0
3.5
3.0
2.5
2.0
1.5
1.0
0.5
0.0
f1 (ppm)

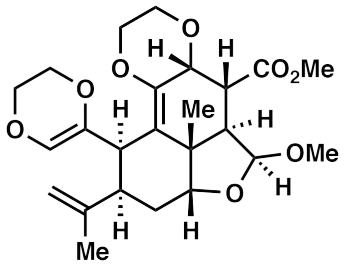
O
H
H
O
CO2Me
O
H
Me
H
O
OMe
O
H
H
H
Me

210
200
190
180
170
160
150
140
130
120
110
100
90
80
70
60
50
40
30
20
10
f1 (ppm)

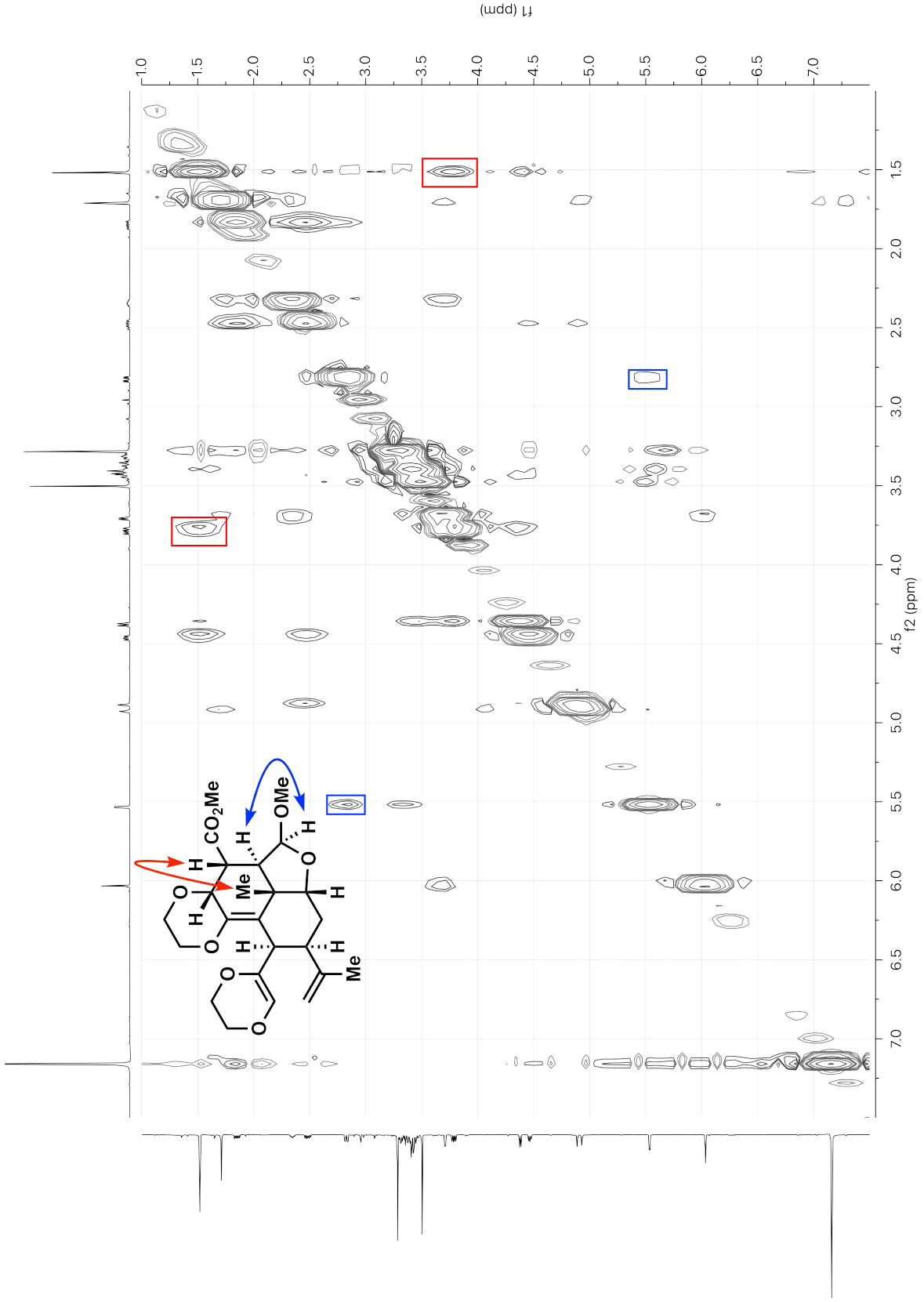
f1 (ppm)
f2 (ppm)
CO2Me
OMe
Me
Me

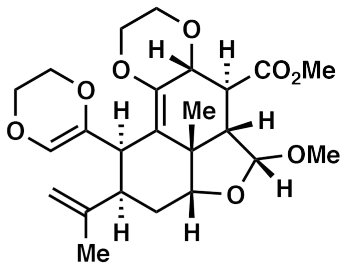
O
H
H
O
CO2Me
O
H
Me
H
O
OMe
O
H
H
H
Me

0.99
2.08
1.06
1.00
8.34
1.12
3.15
1.06
3.17
1.00
3.17
1.00
3.22
3.16
5
9.0
8.5
8.0
7.5
7.0
6.5
6.0
5.5
5.0
4.5
4.0
3.5
3.0
2.5
2.0
1.5
1.0
0.5
0.0
-0
f1 (ppm)

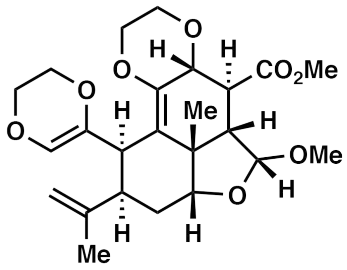
O
H
H
O
CO2Me
O
H
Me
H
O
OMe
H
O
H
H
Me

210
200
190
180
170
160
150
140
130
120
110
100
90
80
70
60
50
40
30
20
10
f1 (ppm)

f1 (ppm)
f2 (ppm)
CO2Me
OMe
Me
Me

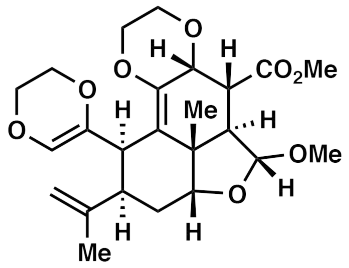
O
H
H
O
CO2Me
O
H
Me
H
OMe
O
H
H
H
Me

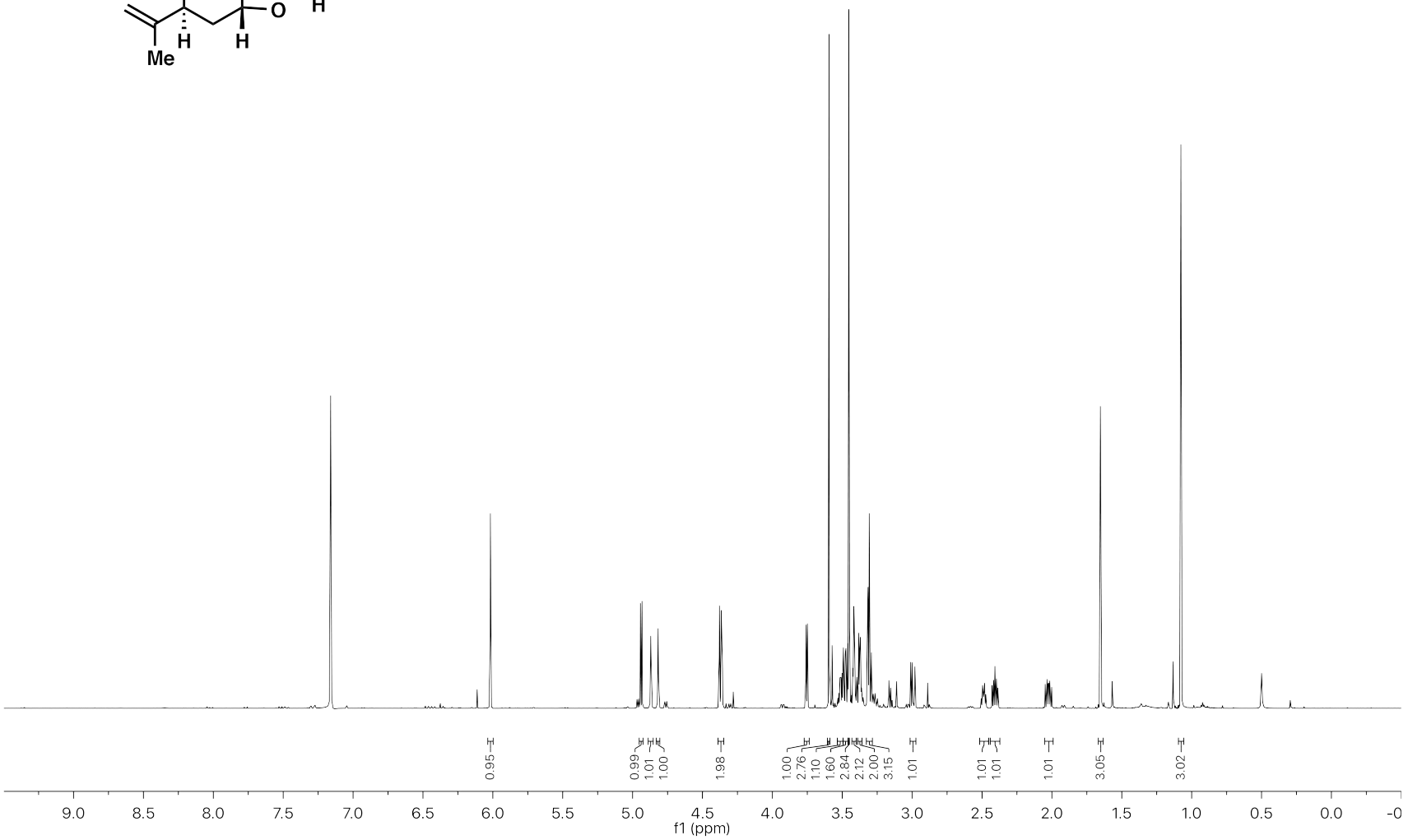
0.95
0.99
1.01
1.00
1.98
1.00
2.76
1.10
1.60
2.84
2.12
2.00
3.15
1.01
1.01
1.01
1.01
3.05
3.02
9.0
8.5
8.0
7.5
7.0
6.5
6.0
5.5
5.0
4.5
4.0
3.5
3.0
2.5
2.0
1.5
1.0
0.5
0.0
-0
f1 (ppm)

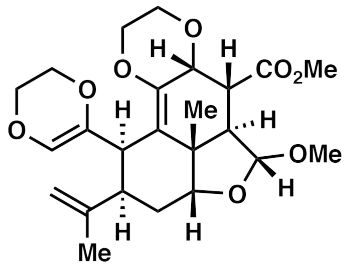
O
H
H
CO2Me
O
O
H
Me
H
OMe
O
H
H
H
Me

210
200
190
180
170
160
150
140
130
120
110
100
90
80
70
60
50
40
30
20
10
f1 (ppm)

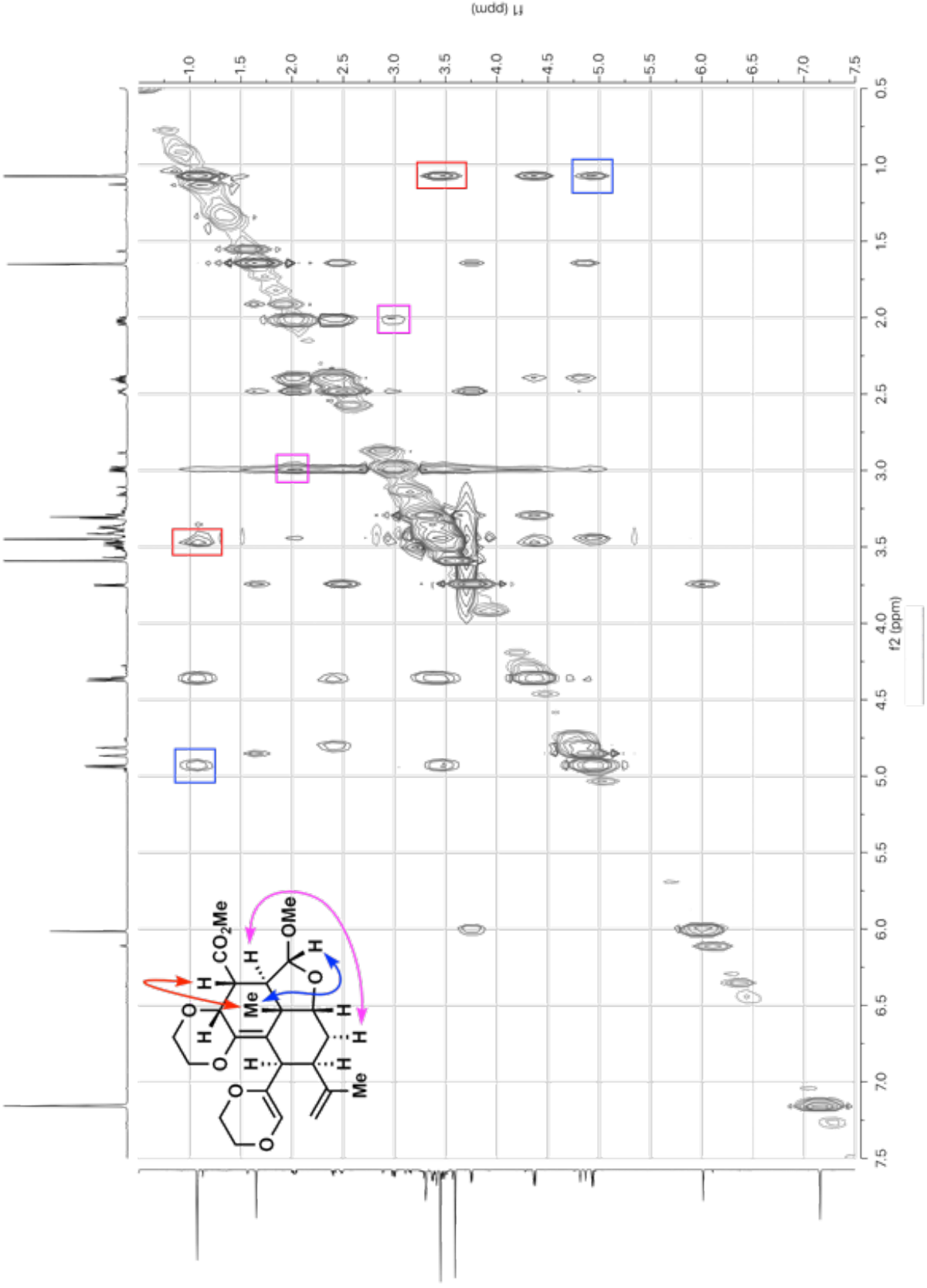
f1 (ppm)
f2 (ppm)
CO2Me
OMe
Me
Me

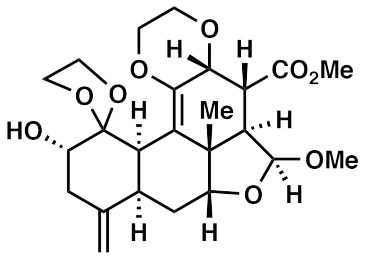
O
H
H
CO2Me
O
O
O
H
Me
H
HO
OMe
O
H
H
H

0.95
0.95
0.95
0.98
1.04
1.07
1.08
1.16
2.17
1.29
1.19
3.74
2.24
1.13
2.93
0.98
1.01
1.04
1.00
1.04
1.06
3.01
5
9.0
8.5
8.0
7.5
7.0
6.5
6.0
5.5
5.0
4.5
4.0
3.5
3.0
2.5
2.0
1.5
1.0
0.5
0.0
f1 (ppm)

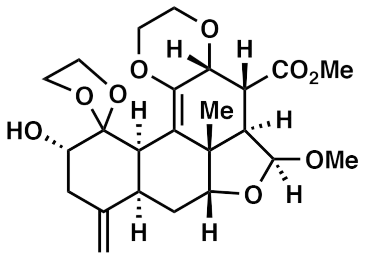
O
H
H
CO2Me
O
O
O
H
Me
H
HO
OMe
O
H
H
H

20
210
200
190
180
170
160
150
140
130
120
110
100
90
80
70
60
50
40
30
20
10
0
-10
f1 (ppm)

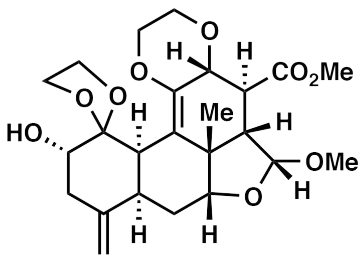
O
H
H
CO2Me
O
O
O
H
Me
H
HO
OMe
H
O
H
H
H

2.00
1.01
1.00
3.43
3.35
2.25
3.06
1.97
1.04
3.07
0.95
1.01
1.04
1.03
1.01
1.11
1.07
3.14
5
9.0
8.5
8.0
7.5
7.0
6.5
6.0
5.5
5.0
4.5
4.0
3.5
3.0
2.5
2.0
1.5
1.0
0.5
0.0
-0
f1 (ppm)

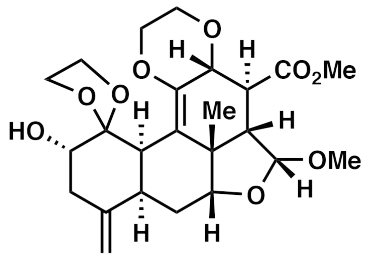
O
H
H
CO2Me
O
O
O
H
Me
H
HO
OMe
H
O
H
H

20
210
200
190
180
170
160
150
140
130
120
110
100
90
80
70
60
50
40
30
20
10
0
-10
f1 (ppm)

Chapter 3

Synthetic Studies Towards Quassin and Other Quassinoid Natural Products

3.1 Application of Copper-Catalyzed Double Coupling Methodology to the generation of Quaternary Centers

Because our methodology gave exclusively the *anti*-selective product, with the methyl group installed we needed the dioxene cuprate to approach from the b-face of the molecule, opposite of the isopropenyl group. We therefore required the *cis* carvone epoxide diastereomer in our desired transformation. Initial attempts to triflate the alkylated carvone species **203** using lithium hexamethyldisilazane (LiHMDS) conditions were very low yielding (< 20%). By switching to sodium or potassium hexamethyldisilazane (NaHMDS and KHMDS respectively) we were able to access the triflate intermediate in much higher yields (~70%). With the desired triflate in hand, we then tested our optimized reaction conditions on the new substrate. Under a variety of copper-mediated conditions, we unfortunately were unable to isolate any double coupled product. Additionally, we did not isolate any cross-coupled or allylic substitution products (**206** and **207** respectively). We then examined several palladium-based conditions using the more sterically accessible 6-methyl *trans*-carvone epoxide (**208**) and eventually discovered Stille conditions[1] that gave a cross-coupled product as a single diastereomer. Upon

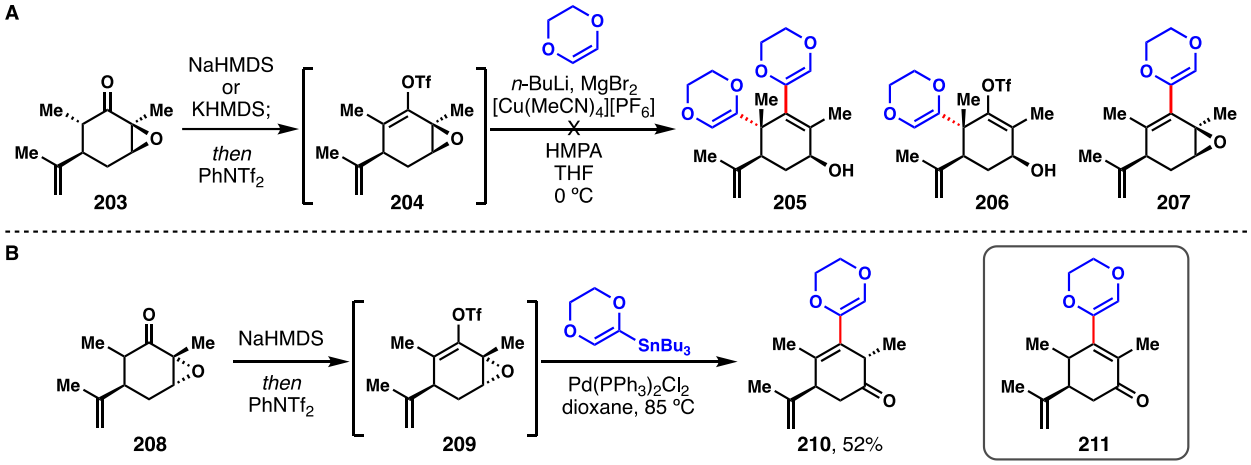

Figure 3.1: (A) Unsuccessful application of the copper-catalyzed double coupling to generate quaternary centers. (B) Stille reaction to cross-couple dioxene to 6-methyl carvone epoxide **208** with concomitant epoxide rearrangement.

characterization, we discovered that our epoxide had undergone rearrangement to ketone **210**. We note that even during extended reaction times, we did not observe any olefin isomerization to the fully conjugated product **211**. Furthermore, we found that at reaction temperatures sufficient for cross-coupling, the epoxide rearrangement proceeded even in the absence of palladium. We, therefore, surmised that any approach moving forward would need to create the quaternary center prior to dioxene cross-coupling.

3.2 Revised Synthetic Strategy and Efforts Towards the Quassinoid Core Architecture

3.2.1 Construction of the Quassinoid A/B-Ring System

Reexamining our synthetic approach, we again pondered small, highly-oxidized two-carbon species that we could incorporate in analogy to dioxene. While dioxene was an exceptional nucleophile, to incorporate the A/B-ring quaternary center we considered that it might be advantageous to have a highly oxidized 2-carbon electrophilic species. Examining the literature, we discovered ethyl glyoxylate (**212**), a small molecule containing both an aldehyde and an ester moiety might serve such a role. We therefore proposed a strategy whereby we would first combine carvone epoxide with **212** to generate the A/B ring system (**213**) followed by triflation and dioxene cross-coupling to access desired Diels-Alder precursor **214**. To incorporate our small electrophilic unit, we thought that a simple Aldol reaction with 6-methyl carvone epoxide could be used. However, efforts to generate the quaternary center (see **216**) with enolate **215** and aldehyde **212** proved unfruitful. We thought a potential issue in this reaction system was the low conversion of the corresponding ketone to the corresponding enolate and switched to Mukaiyama Aldol conditions[2] (see **217**). This way we would be able to more precisely control the equivalents of each species in solution; however, this transformation continued to be low yielding (~13%).

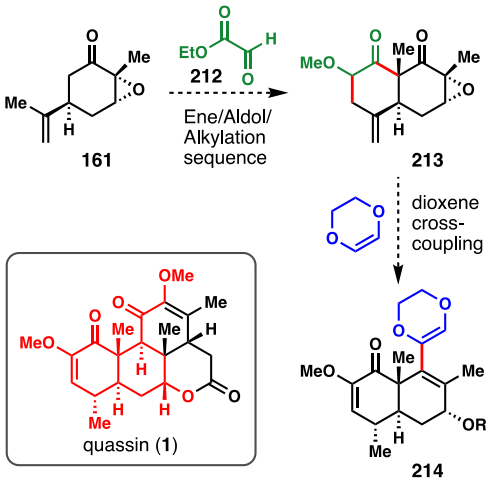

Figure 3.2: Synthetic strategy towards quassin (**1**) utilizing integration of a highly-oxidized 2-carbon electrophile to construct the A-ring and dioxene to install the C-ring oxidation. Insert: Mapping of proposed bicycle **164** onto the quassinoid architecture.

Reconsidering our approach to the desired bicyclic system, we wondered if perhaps an intramolecular approach to our aldol reaction would be more successful. We then sought to first tether our electrophile prior to cyclization through an initial Alder-ene reaction with the pendant, nucleophilic isopropenyl group. Examining the literature, we determined that a number of lewis acids could potentially work for this transformation including those based on both tin and titanium which had previously been employed in glyoxylate-ene reactions.[3] In addition to titanium[4] and tin,[3] other transition metals such as copper,[5] chromium,[6] and scandium[7] have also been employed in asymmetric variants of the glyoxylate-ene reaction. While the stereocenter created from our desired Alder-ene is inconsequential for the synthesis of quassin (**1**), an asymmetric approach to this transformation would be prudent in the construction of other quassinoid A-ring oxidation

patterns. First targeting the non-reagent controlled glyoxylate-ene, we found that in our reaction system, tin tetrachloride ($SnCl_4$) efficiently catalyzed the desired ene-reaction to a produce **218** as an inconsequential 1:1 mixture of alcohol diastereomers in 91% yield.

To realize the synthesis of our bicyclic system, which contains a quaternary methyl stereocenter at the ring junction, we needed to cyclize to the decalin first as alkylation prior to cyclization would likely give the undesired *cis*-fused ring system due to the conformation at C5. By first generating the bicycle, however, the reactive center will first need to planarize before alkylation is possible. With this consideration in mind, we subjected **218** (diastereomeric mixture) to sodium hydride, which rapidly induced cyclization. By using excess sodium hydride, we thought the cyclization intermediate could be directly alkylated in the same reaction mixture and thus added methyl iodide after complete consumption of **218** was noted. While addition of methyl iodide did not afford the C-alkylated product as desired, we found that it reacted with the alcohols to give **219** and **220**. At this point the diastereomers could be separated; however, we chose to carry them forward together in our synthetic efforts as the stereocenter at C2 will be ablated later in the synthesis. With bicycles **219** and **220** in hand, we found that C-

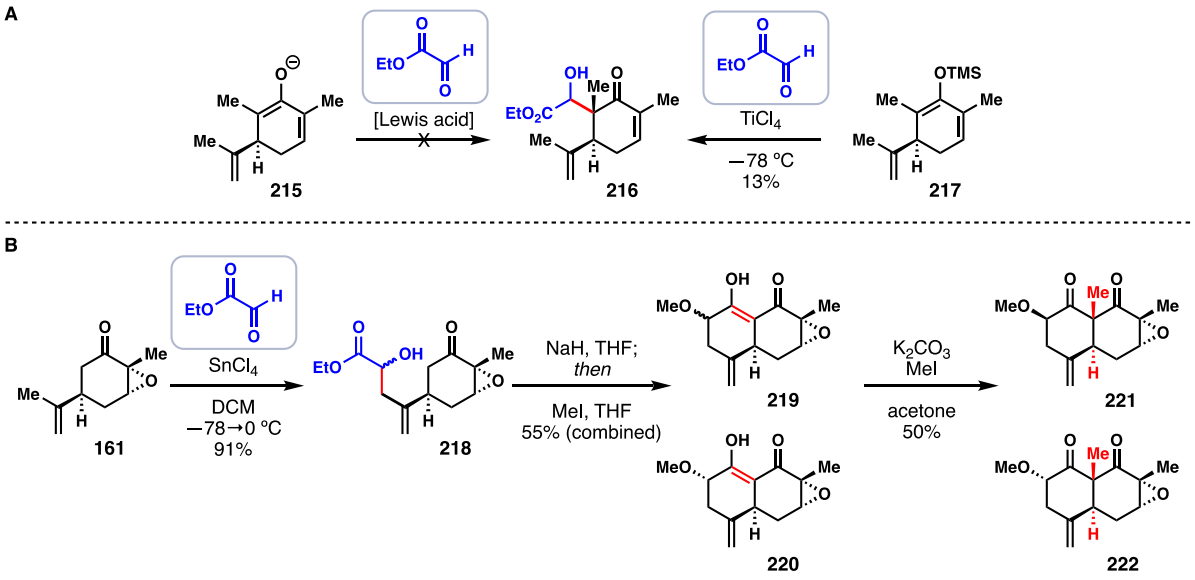

Figure 3.3: (A) Aldol and Mukaiyama-Aldol reactions to construct A-ring precursor **216** containing what would become the C10 quaternary center. (B) Generation of a bicyclic system with the C10 quaternary center installed utilizing and ene reaction/cyclization/alkylation sequence.

alkylation was indeed possible when using potassium carbonate and methyl iodide in acetone giving *trans* decalins **221** and **222**. We were pleased to find that all the transformation up to this point scaled excellently and could be performed on gram scale.

3.2.2 Incorporation of Dioxene

We were now poised to investigate an epoxide-opening/dioxene cross-coupling sequence to arrive at a diene for use in cycloaddition chemistry. A number of variables were considered for determining the ideal substrate to advance. The most challenging aspect to account for was the presence of ketone functionality adjacent to the epoxide. While this oxidation would be necessary for generation of the desired vinyl triflate to cross-couple with dioxene, it also made E1cB type elimination of the β-hydroxy moiety present

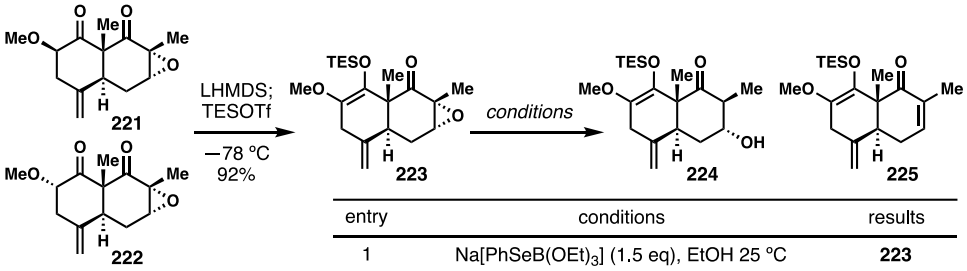

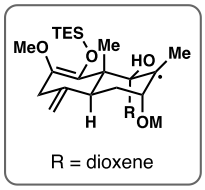

entry	conditions	results
1	$Na[PhSeB(OEt)_3]$ (1.5 eq), EtOH 25 °C	**223**
2	$Na[PhSeB(OEt)_3]$ (3 eq), EtOH 25 °C	**223**
3	$Na[PhSeB(OEt)_3]$ (3 eq), EtOH/AcOH 5→25 °C	**223**
4	NaI, AcOH/NaOAc, acetone	**223**
5	Me_2CuLi (3 eq), Et_2O, −25 °C	**225**
6	Cp_2TiCl_2, Zn, THF, 40 °C	**225**
7	SmI_2, THF, −78 °C	**225**
8	Li-Naphthalenide, THF, −78 °C	**225**

Table 3.1: Conversion of **221** and **222** to **223** and epoxide opening conditions using selenium hydride, acid, and radical-based openings. Insert: proposed transition state for the radical-based openings.

in the desired epoxide opening product (see **225**) possible. We therefore thought first to try acid mediated epoxide openings, which could trap the resulting carbocation with a halogen thereby preventing elimination of the β-hydroxy moiety.[8] However, attempts to harness this reactivity afforded no desired epoxide opened product (Table 3.1, line 4). We next considered selenium hydride-based epoxide openings since these are well precedented in the literature to work on epoxy-ketones including carvone epoxide itself.[9] These efforts on our sterically more challenging system, however, also proved unfruitful (Table 3.1, line 1-3). It was at this point that we turned to radical-based epoxide openings (Table 3.1, line 5-8), which are known to proceed under mild reaction conditions with excellent epoxide opening regioselectivity. To prevent cross reactivity at the A-ring ketone, we first protected it as the silyl enol ether. Using copper,[10] samarium,[11] titanium reagents,[12] we could now observe epoxide opening, but the primary product was the undesired enone **225** instead of the β-hydroxy ketone **224**. Because elimination so readily occurred, we also attempted the epoxide opening with single electron reductant lithium naphthalenolide[13] (Table 3.1, line 8); however, after workup we again isolated the enone species **225**. Although we could not successfully access the desired β-hydroxy ketone, we thought that we could potentially still leverage **225** towards the synthesis of quassin.

It was at this point we wondered if we could perhaps leverage dioxene as a nucleophile and directly add it into our existing ketone. By first performing a 1,2-addition into the B-ring ketone followed by epoxide opening, we could avoid the undesired E1cB elimination pathway that had prevented us from accessing desired intermediate **224**. We considered a number of organometallic species for this transformation including lithium, magnesium, and cerium-based nucleophiles. While there is substantial literature on the use of both lithiates and Grignard reagents in 1,2-additions,[14-15] we were concerned with the basic nature of these reagents. We therefore chose to first explore organocerium reagents in this transformation as they are both highly reactive and non-basic;[16] however, even at elevated temperature and extended reaction times no reaction was observed. Likewise, the dioxene Grignard species also gave no 1,2-addition products. Conversely, the lithiate of dioxene gave the desired product **226** as a single diastereomer. We were pleased to find that the lithiate addition also scaled remarkably well giving significantly higher yields when the reaction system was more concentrated. While we did initially note some silyl deprotection, on larger scales formation of this side product could be almost completely prevented.

Now faced with a new epoxide opening, we reevaluated the literature for the optimal conditions to allow us access to diene **229**. While an acid-based opening could potentially give the desired epoxide-opened product, we thought competing reactivity with the tertiary alcohol in conjugation with the dioxene moiety could be problematic. Selenium hydride openings were also unworkable since our new substrate had no ketone, which is required for this reduction. Thus, we turned again to radical-based epoxide openings. Examining the titanium(III) literature, we found that there were a number of reaction pathways for epoxides based on the substitution pattern of the substrate. Fernández-Mateos and coworkers showed that for epoxy-alcohols they could directly access the epoxide-opened, alcohol elimination product in one step.[17] They also noted that irrespective of leaving group orientation, axial or equatorial, they were able to observe elimination of alcohol and formyl leaving groups. This type of reaction product would be

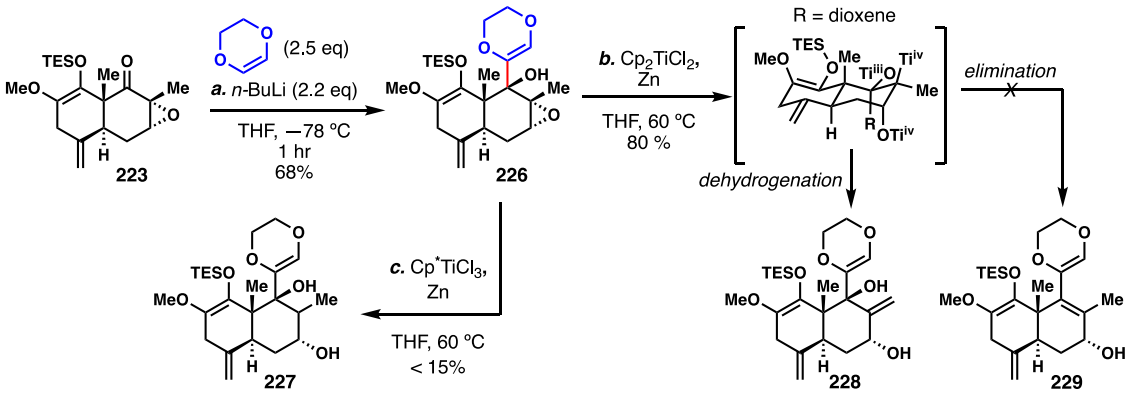

Figure 3.4: Dioxene incorporation via 1,2-addition of the corresponding lithiate into **223** and titanium-catalyzed epoxide opening of **226**. Formation of the epoxide opening products **227** and **228** were dictated by the titanium source used.

extremely valuable since we will eventually need to access the diene for our proposed intramolecular Diels-Alder reaction. Subjecting intermediate **226** to Ti(III) epoxide opening conditions, we found that our system cleanly gave exocyclic olefin **228** instead of desired diene **229**. Increasing either the equivalence of titanium or temperature did not give any desired diene product **229**. We thought there were a couple of reasons this might occur. Either due to our system being unable to adopt a reactive conformation to eliminate or that the dehydrogenation pathway was significantly faster than elimination. Examining other titanocenes, specifically (pentamethylcyclopentadienyl)titanium trichloride (Cp^*TiCl_3), which is known to react reductively with tertiary alcohols,[18] we were unable to isolate any diene **229**. Using this new titanium species, we could now isolate epoxide-opened and reduced product **227**. Due to the low yield of this we decided to proceed with epoxide-opened species **228** and turned our attention to generating the diene **229** through reductive allylic transposition.

3.2.3 Diels-Alder Cycloaddition Strategy and Incorporation of the Dienophile

To gain access to the desired diene moiety, we thought that allylic transposition could be employed. From intermediate **228**, a reductive allylic transposition could lead to intermediate **230** after addition of the side chain, which could then be cyclized to generate a tetracyclic quassinoid scaffold (see **231**) resembling that of quassin (**1**). Alternatively, because we have the tertiary alcohol left over from 1,2-addition into ketone **223** we could transpose the alcohol to arrive at diene **232** after *O*-alkylation. This alternative pathway would allow us to gain entry into higher oxidation state quassinoids such as bruceantin (**3**) from a common intermediate (**228**). We first considered the reductive allylic

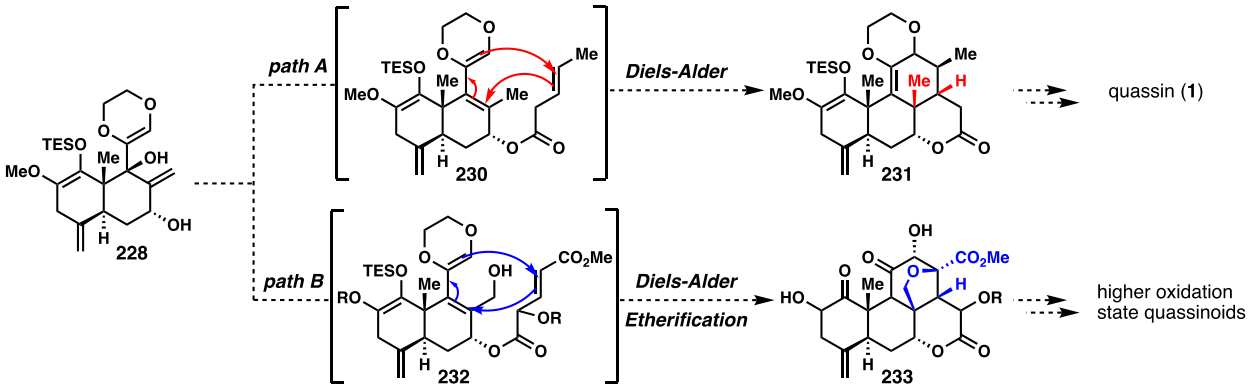

Figure 3.5: Strategy for completion of the quassinoid core either through allylic transposition to construct lowe oxidation state members such as quassin (path A) or higher oxidation state quassinoids (path B).

transposition to access diene **229**. Examining our compound, we thought that a reduction under acidic conditions would be prudent. As our tertiary alcohol is in conjugation with the dioxene moiety, we thought we could leverage its innate reactivity with mildly acidic conditions to selectively reduce the desired allylic alcohol. Using trifluoroacetic acid (TFA)

and triethylsilane we were unable to observe any reduction products. By switching to triethylsilane with borontrifluoride diethyletherate (BF_3•OEt_2)[19] we were able to observe loss of the tertiary alcohol; however, the product was not the desired diene **229**. We instead isolated what we have tentatively assigned as tetracyclic compound **236**, which

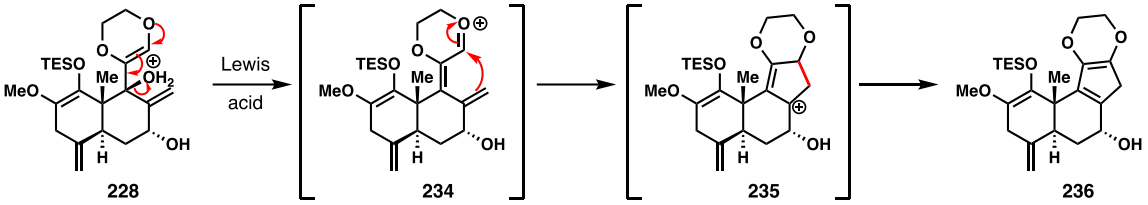

Figure 3.6: Proposed mechanism for unexpected cyclization of **228** when treated with BF_3•OEt_2.

was highly unstable. We believed this intermediate was a result of rapid intramolecular (**234**→**235**) cyclization following dioxene-assisted expulsion of the tertiary alcohol or potentially a Nazarov cyclization. Given the propensity of our system to cyclize, we thought that by first installing the sidechain at the C7 alcohol we could potentially leverage a similar intermediate to cyclize with the side-chain olefin thus generating the C and D rings. We therefore sought to append on the alkyl tether (**202**) to the secondary allylic alcohol.

Analogously to our previous synthetic attempts,[20] we ideally wanted to incorporate **240** as it would form an ester linkage to directly generate the lactone after cyclization. On this new intermediate, however, we now needed to consider the regioselectivity of the O-alkylation. Unlike our previous substrate (see **163**, Section 2.3 Figure 2.5), which contained only one possible location to append on the alkyl tether, **228** contains two allylic alcohols that could potentially be modified. We briefly considered differentiating the alcohols prior to epoxide opening by acylating the tertiary alcohol; however, due to the high steric incumbrance of the reaction site, substitution of the tertiary alcohol prior to epoxide opening proved to be an untenable solution. We therefore thought it would be possible to leverage that sterically challenging environment to distinguish our two alcohols and achieve selective reactivity at the more accessible and

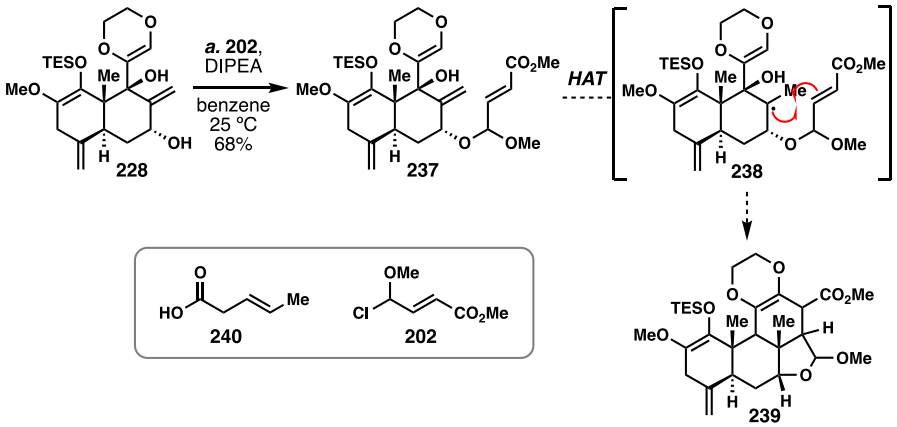

Figure 3.5: O-Alkylation of **228** to install side chain **202** and proposed HAT of **237** to cyclize to quassinoid-like ring system **239**.

desired alcohol. Initial attempts to incorporate alkyl tether **240** using conventional coupling methods with DCC[21] in combination with the carboxylic acid or directly use of the corresponding acid chloride were unfortunately unsuccessful. However, we were able to append on original tether **202** using the same conditions that had been previously employed in our earlier synthetic attempt to generate **237** as a 1:1 mixture of diastereomers.

At this stage we envisioned several pathways forward. The original strategy from intermediate **237** was to perform an allylic reduction of the tertiary alcohol. By doing so, we would be able to access the desired diene precursor for intramolecular Diels-Alder cycloaddition. We wondered, however, if there was a way to directly cyclize from the exocyclic olefin. If we could generate the tertiary radical at C8, we could perform a 5-*exo* cyclization onto the sidechain; whereby, the resulting radical could cyclize onto the dioxene moiety generating the tetracyclic ring system. To gain access to the proposed tertiary radical, we thought metal catalyzed hydrogen atom transfer (MHAT or MH HAT) conditions could be utilized.[22-23] To employ this strategy on intermediate **237**, we needed to determine which olefin the metal hydride species would likely react with. In the literature, there are a multitude of metal hydride conditions that will preferentially react with an electron rich olefin such as a 1,1-disubstituted alkene over an electron poor enone moiety.[24] We therefore thought that for our system we could selectively react a metal hydride with one or both of the exocyclic olefins to generate a productive intermediate for cyclization. Although it is possible for undesired A-ring 1,1-disubstituted olefin to react first, we were not concerned with this side reaction pathway as we would need a methyl group at C4 for completion of the natural product. Thus, we explored a variety of iron and cobalt catalysts using HAT conditions but have thus far been unable to observe any cyclized products. Current efforts are focused on generation of the tetracyclic system through radical and cationic reaction platforms.

3.3 Conclusion

In this chapter, we needed to revise our synthetic strategy to access the quassinoid scaffold after we were unable to extend the previously developed copper-catalyzed double coupling to a substrate containing a quaternary center. Incorporation of a highly oxidized 2-carbon electrophile, ethyl glyoxylate, allowed us to rapidly access the quassinoid A/B-ring system with the critical quaternary center at C10. We were then able to install a highly oxidized 2-carbon nucleophile, dioxene, followed by epoxide opening to generate allylic diol **228**. Up to this point in the synthesis all of the transformations were exceptionally scalable and could be performed on gram scale quantities. Installation of the sidechain **202** and incorporation of all but one of the final carbons then proceeded smoothly. Efforts are ongoing to complete synthesis of quassin (**1**) and other quassinoids.

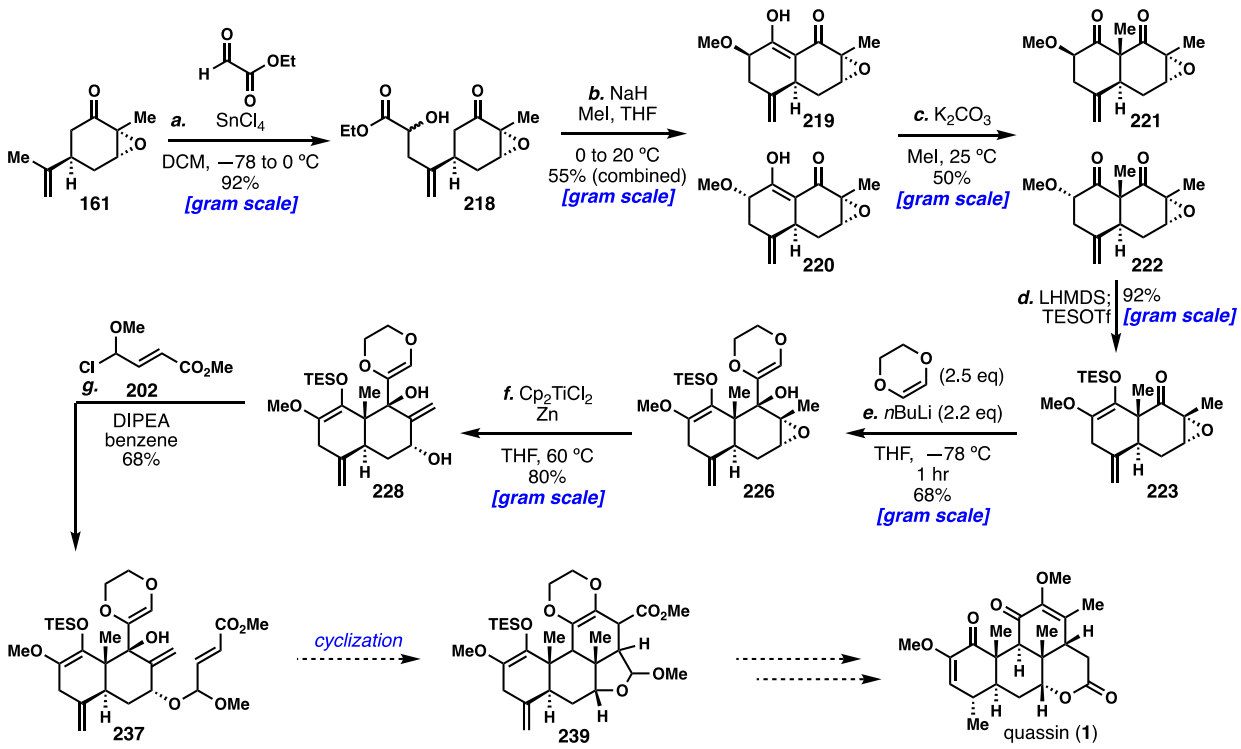

Figure 3.6: Current route towards the synthesis of quassin (**1**) and other quassinoid natural products.

3.4 Distribution of Credit and Acknowledgements.

The route to the quassinoid architecture was conceptualized by R.Z.R and T.J.M. R.Z.R. completed the work presented in the above sections. Zhaodong Zhang (Z.Z) also performed the cross-coupling to generate compound **210** under the tutelage of R.Z.R. Mikiko Okumura (M.O) also executed the first three reactions in the synthesis (**161** →**221/222**) and R.Z.R optimized the conditions.

We are grateful to Hasan Celik for NMR spectroscopic assistance wherein NIH grant GM68933 is acknowledged. N.S.S., Dr. Nick Settineri, X-ray crystallographic analysis wherein support from NIH Shared Instrument Grant (S10-RR027172) is also acknowledged.

3.5 References

1. Kravina, A. G.; Carreira, E. M. *Angew. Chem. Int. Ed.* **2018**, *57*, 13159.
2. Matsuo, J.; Murakami, M. *Angew. Chem. Int. Ed.* **2013**, *52*, 9109.
3. Mikami, K.; Wakabayashi, H.; Nakai, T., *J. Org. Chem.* **1991,** *56*, 4337.
4. Mikami, K.; Terada, M.; Nakai, T., *J. Am. Chem. Soc.* **1990,** *112*, 3949.
5. Evans, D. A.; Burgey, C. S.; Paras, N. A.; Vojkovsky, T.; Tregay, S. W., *J. Am. Chem. Soc.* **1998,** *120*, 5824.
6. Chaladaj, W.; Kwiatkowski, P.; Majer, J.; Jurczak, J., *Tetrahedron Letters* **2007,** *48*, 2405.
7. Evans, D. A.; Wu, J., *J. Am. Chem. Soc.* **2005,** *127*, 8006.

8. Huang, J. W.; Shi, M., *Tetrahedron* **2004,** *60*, 2057.
9. Miyashita, M.; Suzuki, T.; Hoshino, M.; Yoshikoshi, A., *Tetrahedron* **1997,** *53*, 12469.
10. Bell, R. P. L.; Sobolev, A.; Wijnberg, J.; de Groot, A., *J. Org. Chem.* **1998,** *63*, 122-128.
11. Chakraborty, T. K.; Dutta, S., *Tetrahedron Lett.* **1998,** *39*, 101.
12. Hardouin, C.; Chevallier, F.; Rousseau, B.; Doris, E., *J. Org. Chem.* **2001,** *66*, 1046.
13. Jankowska, R.; Mhehe, G. L.; Liu, H. J., *Chem. Commun.* **1999,** 16, 1581.
14. Ashby, E. C.; Laemmle, J. T., *Chem. Rev.* **1975,** *75*, 521.
15. Lecomte, V.; Stephan, E.; Le Bideau, F.; Jaouen, G., *Tetrahedron* **2003,** *59*, 2169.
16. Liu, H. J.; Shia, K. S.; Shang, X.; Zhu, B. Y., *Tetrahedron* **1999,** *55*, 3803.
17. Fernandez-Mateos, A.; Teijon, P. H.; Gonzalez, R. R., *Tetrahedron* **2013,** *69*, 1611.
18. Xie, H.; Guo, J. D.; Wang, Y. Q.; Wang, K.; Guo, P.; Su, P. F.; Wang, X. T.; Shu, X. Z., *J. Am. Chem. Soc.* **2020,** *142*, 16787-.
19. Kraus, G. A.; Molina, M. T.; Walling, J. A., *J. Chem. Soc., Chem. Commun.* **1986,** 21, 1568.
20. Condakes, M.; Rosen, R. Z.; Harwood, S. J.; Maimone, T. J., *Chem. Sci.* **2019,** *10*, 768.
21. Spino, C.; Hill, B.; Dube, P.; Gingras, S., *Can. J. Chem.* **2003,** *81*, 81.
22. Chen, P. Q.; Wang, C.; Yang, R.; Xu, H. J.; Wu, J. H.; Jiang, H. F.; Chen, K.; Ma, Z. Q., *Angew. Chem. Int. Ed.* **2021,** *60*, 5512.
23. Crossley, S. W. M.; Obradors, C.; Martinez, R. M.; Shenvi, R. A., *Chem. Rev.* **2016,** *116*, 8912.
24. Lo, J. C. L.; Gui, J. H.; Yabe, Y. K.; Pan, C. M.; Baran, P. S., *Nature* **2014,** *516*, 343.

Supporting Information for

Chapter 3

Efforts Towards the Quassinoid Core Architecture

SI2.1 General Procedures:

All reactions were performed in flame- or oven-dried glassware under a positive pressure of nitrogen or argon, unless otherwise noted. Air- and moisture-sensitive liquids were transferred via syringe. Volatile solvents were removed under reduced pressure rotary evaporation below 35 °C. Analytical and preparative thin-layer chromatography (TLC) were performed using glass plates pre-coated with silica gel (250 μm thickness, 10 μm particle size, Millipore Sigma) impregnated with a fluorescent indicator (254 nm). TLC plates were visualized by exposure to ultraviolet light (UV) and then were stained by submersion in an ethanolic anisaldehyde solution, followed by brief heating on a hot plate. Flash column chromatography was performed employing silica gel purchased from Fisher (60 Å, 230-400 mesh, 40-63 μm).

Anhydrous tetrahydrofuran (THF), diethyl ether (Et_2O), toluene (PhMe), and dichloromethane (DCM) were obtained by passing these previously degassed solvents through activated alumina columns. Hexamethylphosphoramide (HMPA) was distilled over calcium hydride and stored under inert atmosphere. Though commercially available, *cis*-carvone epoxide could also be prepared according to the literature procedure.[1] Additional epoxide substrates were prepared following established literature protocols.[2] Lithium bis(trimethylsilyl)amide was purchased as a 1.0 M solution in THF from Millipore Sigma and used as received. N-Phenyl-bis(trifluoromethanesulfonamide) was purchased from Oakwood Chemicals and used as received. $[Cu(MeCN)_4][PF_6]$ was purchased from Millipore Sigma and used as received. Ethyl glyoxylate was purchased from Sigma-Aldrich as a 50% solution in toluene and used as received. All other solvents and reagents were purchased at the highest commercial grade and used as received, without additional purification.

Proton nuclear magnetic resonance (^{1}H NMR) spectra and carbon nuclear magnetic resonance (^{13}C NMR) spectra were recorded on Bruker DRX 500 (500 MHz/126 MHz), Bruker AV 500 (500 MHz/126 MHz), Bruker AV 600 (600 MHz/151 MHz), or Bruker AV 700 (700 MHz/176 MHz) spectrometers at 23 °C. Fluorine nuclear magnetic resonance (^{1}F NMR) spectra were recorded on a Bruker AVQ 400 (376 MHz) spectrometer at 23 ºC. Proton chemical shifts are expressed as parts per million (ppm, δ scale) and are referenced to residual protium in the NMR solvent ($CHCl_3$: δ 7.26, C_6D_5H: δ 7.16, CD_2HOD: δ 3.31). Carbon chemical shifts are expressed as parts per million (ppm, δ scale) and are referenced to the carbon resonance of the NMR solvent ($CDCl_3$: δ 77.16, C_6D_6: 128.06, CD_3OD: δ 49.00). Fluorine chemical shifts are expressed as parts per million (ppm, δ scale) and are not additionally referenced. Data are represented as follows: chemical shift, multiplicity (s = singlet, d = doublet, t = triplet, q = quartet, m = multiplet, br = broad), coupling constant (*J*) in Hertz (Hz), and integration. Infrared (IR) spectra were recorded on a Bruker Alpha FT-IR spectrometer as thin films and are reported in frequency of absorption (cm^{-1}). Optical rotations were recorded on a Perkin Elmer polarimeter, model 241. High-resolution mass spectra were obtained at the QB3/Chemistry Mass Spectrometry Facility at University of California, Berkeley using a Thermo LTQ-FT mass spectrometer, and at the Lawrence Berkeley National Laboratory Catalysis Center using a Perkin Elmer AxION 2 TOF mass spectrometer. X-ray diffraction data for compounds **10**, **13**, **24**, **25**, **26**, **27**, and **SI-7** were collected at the Small Molecule

X-ray Crystallography Facility (CheXray) at University of California, Berkeley using a Bruker MicroSTAR-H APEX II QUAZAR X-ray source.

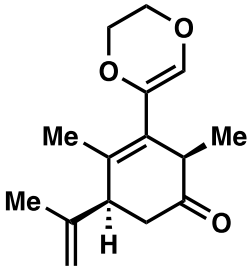

Substrate 210: A solution of epoxy ketone (**208**, 50 mg, 0.28 mmol, 1.0 equiv) in THF (0.3 mL) was cooled to –78 ºC. NaHMDS (1.0 M in THF, 0.28 mL, 0.28 mmol, 1.0 equiv) was added dropwise and the resulting solution was stirred for 2 h. *N*-Phenyl-bis(trifluoromethanesulfonamide) (104 mg, 0.29 mmol, 1.05 equiv) was then added as a solid and the solution was warmed to 25 ºC and stirred for 15 min. The reaction was quenched with NH_4Cl and extracted with Et_2O. The organic layers were collected, dried over Na_2SO_4, and concentrated. The crude triflate mixture **209** (~70% yield) was used directly in the next step. Crude Triflate **209** (assumed: 0.2 mmol, 1 equiv) Dioxene-$SnBu_3$ (375 mg, 1.0 mmol, 5 equiv),[1] and $Cl_2Pd(PPh_3)_2$ (35 mg, 0.5 mmol, 0.25 equiv) were dissolved in dioxane (5.4 mL) and the system purged and refilled with N_2 three times. The reaction mixture was heated to 85 ºC for 1 h, then cooled, filtered through celite, and concentrated. The crude residue was purified using silica gel column chromatography (1:4:1 DCM/hexanes/Et_2O) to afford **210** (38.9 mg, 0.16 mmol, 56% over 2 steps) as a white solid.^{1}H NMR (700 MHz, C_6D_6) δ 5.91 (s, 1H), 4.69 (d, *J* = 2.3 Hz, 1H), 4.68 (s, 1H), 3.59 – 3.47 (m, 4H), 3.11 (q, *J* = 7.6 Hz, 1H), 2.73 (d, *J* = 7.4 Hz, 1H), 2.42 (dd, *J* = 14.0, 7.6 Hz, 1H), 2.27 (dd, *J* = 14.0, 2.5 Hz, 1H), 1.74 (s, 3H), 1.48 (s, 3H), 1.25 (d, *J* = 7.4 Hz, 3H). ^{13}C NMR (151 MHz, C_6D_6) δ 210.48, 145.32, 134.46, 134.38, 130.86, 127.14, 112.70, 64.38, 64.15, 50.79, 45.28, 41.12, 20.23, 19.88, 18.38.

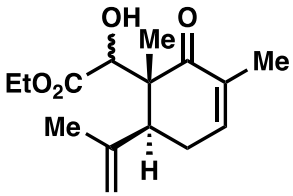

Substrate 216: A solution of TMS silyl enol ether **217** (118 mg, 0.5 mmol, 1 equiv)[2] in DCM (0.5 mL) was cooled to –78 ºC. Ethyl glyoxylate (50% in toluene, 0.15 mL, 1 mmol, 2 equiv) was added followed by $TiCl_4$ (1M in DCM, 0.5 mL, 0.5 mmol, 1 equiv). The reaction was stirred for 4 h at –78 ºC before diluting with Et_2O and quenching with $NaHCO_3$. The layers were separated, and the aqueous layer was extracted with Et_2O. The combined organic layers were dried over Na_2SO_4, filtered, and concentrated. The crude residue was purified by silica gel column chromatography (20→50% EtOAc in hexanes) to give **216** (17 mg, 0.065 mmol, 13%) as a mixture of diastereomers (5:1 dr). ^{1}H NMR (600 MHz, C_6D_6) δ 6.05 (dddq, *J* = 6.3, 4.8, 3.0, 1.4 Hz, 1H)**, 5.02 (s, 1H)*, 5.00 – 4.95 (m, 1H), 4.81 (s, 1H), 4.79 (s, 1H)*, 4.08 (ddd, *J* = 7.8, 5.3, 4.0 Hz, 1H), 3.96 – 3.83 (m, 2H)**, 3.82 – 3.75 (m, 2H)*, 2.86 (d, *J* = 4.1 Hz, 1H)*, 2.67 – 2.63 (m, 1H), 2.54 (dq, *J* = 11.3, 6.8 Hz, 1H)*, 2.49 (dd, *J* = 8.9, 5.7 Hz, 1H), 2.46 – 2.42 (m, 1H)*, 2.39 (ddd, *J* = 14.5, 3.9, 1.2 Hz, 1H), 2.29 – 2.25 (m, 1H)*, 2.26 – 2.19 (m, 1H), 2.15 (ddd, *J* = 14.3, 7.4, 0.9 Hz, 1H)*, 1.91 (dd, *J* = 2.3, 1.4 Hz, 3H)*, 1.81 (dq, *J* = 3.8, 1.8 Hz, 3H), 1.15 (s, 3H), 1.13 (s, 3H)*, 0.97 (s, 3H), 0.96 (s, 3H)*, 0.87 (t, *J* = 7.2 Hz, 3H), 0.80 (t, *J* = 7.2 Hz, 3H)*.

* indicates peaks for minor diastereomer

** indicates overlapping peaks for diastereomers

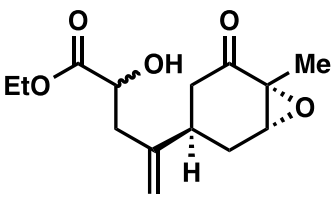

Substrate 218: (R)-carvone epoxide (**161**, 6.0 g, 1.10 g/mL, 36 mmol, 1 equiv) was dissolved in DCM (360 mL), cooled to –78 ºC, and ethyl glyoxylate (50% in toluene, 72 mmol, 10.7 mL, 1.5 equiv) was added. A 1M solution of $SnCl_4$ in DCM (72 mL, 72 mmol, 1.5 equiv) was then added dropwise and the mixture allowed to slowly warm to 0ºC over 3h. The reaction mixture was then diluted with 200 mL DCM and carefully quenched with $NaHCO_3$. The organic layer was collected, and the aqueous layer extracted with DCM (200 mL x 3). The combined organic layers were dried over Na_2SO_4, filtered, and concentrated. The crude residue was purified by silica gel chromatography (20→50% EtOAc in hexanes) to afford **218** (8.9 g, 33.5 mmol, 92%) as a clear oil (~ 5:1 d.r.).
^{1}H NMR (600 MHz, C_6D_6) δ 4.98 (dd, *J* = 4.5, 1.2 Hz, 1H), 4.74 – 4.70 (m, 1H), 4.14 (p, *J* = 3.5 Hz, 1H), 4.08 (s, 0H)*, 3.98 – 3.84 (m, 2H)*, 2.91 (dd, *J* = 10.7, 5.0 Hz, 1H), 2.82 (d *J* = 3.4 Hz, 1H), 2.81 (d, *J* = 3.4 Hz, 0H)*, 2.47 (td, *J* = 11.9, 4.2 Hz, 1H), 2.44 – 2.38 (m, 0H)*, 2.36 (ddd, *J* = 15.2, 4.2, 1.3 Hz, 0H)*, 2.33 – 2.28 (m, 1H), 2.11 (ddd, *J* = 15.1, 8.1, 1.0 Hz, 1H), 2.06 (ddd, *J* = 15.1, 8.1, 1.1 Hz, 0H)*, 2.01 (dt, *J* = 14.9, 3.7 Hz, 1H), 1.96 (dt, *J* = 14.8, 3.7 Hz, 0H)*, 1.68 (dt, *J* = 11.5, 6.9 Hz, 1H), 1.36 (s, 3H), 1.36 (s, 1H)*, 1.35 – 1.30 (m, 1H)*, 1.14 (d, *J* = 6.9 Hz, 0H)*, 1.11 (d, *J* = 6.9 Hz, 2H), 0.91 (dt, *J* = 8.8, 7.1 Hz, 3H)*.^{13}C NMR (151 MHz, C_6D_6) δ 206.2*, 206.1, 174.4*, 174.3, 146.3*, 146.0, 128.2*, 128.0, 113.5*, 113.4, 69.6*, 69.4, 61.2*, 61.2, 61.1*, 59.9, 59.9*, 58.2, 45.9, 45.8*, 41.0*, 40.8, 39.2, 38.9*, 30.0, 29.8*, 15.7, 13.8*, 13.72. $C_{14}H_{20}O_5Na$ $[M+Na]^+$: 291.1201, found: 291.1203. Note: Products isolated as a 5:1 mixture. *indicates minor diastereomer peaks.

Cyclization and methyl protection: Sodium hydride (30% dispersion in mineral oil,1.72 g, 49.8 mmol, 3 equiv) was suspended in THF (148 mL) and cooled to 0 ºC. Compound **218** (4.4 g, 16.6 mmol, 1 equiv) was added dropwise and the mixture stirred 5 min at 0 ºC before methyl iodide (4.06mL, 83 mmol, 5 equiv) was added. The reaction was stirred an additional hour warming to room temperature before diluting with 100 mL EtOAc and quenching with NH_4Cl and H_2O. The layers were separated and the aqueous layer was extracted with EtOAc (100 mL x 2). The combined organic layers were dried over Na_2SO_4, filtered, and concentrated. The crude residue was purified by silica gel chromatography (5%→30% EtOAc in hexanes) to afford a mixture of **219** and **220** (2.2 g, 9.1 mmol, 55%) as a clear oil (~ 5:1 d.r.).

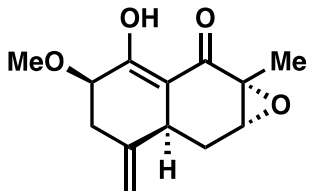

Substrate 219: ^{1}H NMR (600 MHz, C_6D_6) δ 15.75 (s, 1H), 4.78 – 4.74 (m, 1H), 4.63 (dd, *J* = 2.2, 1.2 Hz, 1H), 3.44 (dd, *J* = 4.6, 3.5 Hz, 1H), 3.31 (s, 3H), 3.14 – 3.07 (m, 1H), 2.84 (t, *J* = 2.9 Hz, 1H)*, 2.29 (dd, *J* = 13.6, 3.5 Hz, 1H), 1.95 (ddd, *J* = 14.1, 4.6, 2.7 Hz, 2H), 1.37 (s, 3H), 1.16 (dd, *J* = 14.1, 12.2 Hz, 1H). ^{13}C NMR (151 MHz, C_6D_6) δ 197.39, 176.98, 142.05, 128.21, 109.24, 106.42, 76.46, 61.16, 58.25, 57.68, 37.39, 32.39, 26.49, 15.33. $C_{13}H_{16}O_4Na$ $[M+Na]^+$: 259.0946, found: 259.0941.

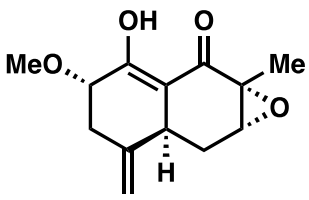

Substrate 220:^{1}H NMR (600 MHz, C_6D_6) δ 15.95 (s, 1H), 4.69 (t, *J* = 1.6 Hz, 1H), 4.58 (t, *J* = 1.5 Hz, 1H), 3.66 (ddd, *J* = 8.5, 5.6, 1.2 Hz, 1H), 3.33 (s, 3H), 3.24 – 3.19 (m, 1H), 2.84 (t, *J* = 2.9 Hz, 1H)*, 2.27 – 2.21 (m, 1H), 1.88 (ddd, *J* = 14.1, 5.0, 3.4 Hz, 1H), 1.38 (s, 4H), 1.12 – 1.07 (m, 1H). ^{13}C NMR (151 MHz, C_6D_6) δ 196.37, 179.33, 143.14, 127.97, 109.81, 106.36, 60.59, 58.03, 57.35, 37.41, 32.27, 27.78, 15.31. $C_{13}H_{16}O_4Na$ $[M+Na]^+$: 259.0946, found: 259.0941.*overlapping diastereomer peaks

Quaternary methylation: MeI (2.65 mL, 21.1 mmol 10 equiv) and **219**+**220** mixture (1.0 g, 4.2 mmol, 1 equiv) were added to a suspended solution K_2CO_3 (2.95 g, 42.4 mmol, 5 equiv) in 43 mL of acetone then stirred overnight at 25 ºC. The mixture was filtered, diluted with EtOAc (100 mL), and washed with H_2O (50 mL x 2). The organic layer was then dried over Na_2SO_4, filtered, and concentrated. The crude residue was purified by silica gel chromatography (10%→50% EtOAc in hexanes) to afford a mixture of **221** and **222** (547 mg, 2.2 mmol, 52%) as a white solid (~ 5:1 d.r.). Recrystallization of the purified mixture in Et_2O epimerizes the stereocenter to give exclusively **222**.

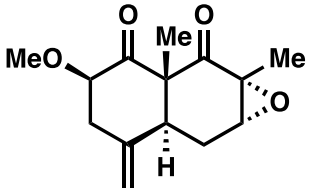

Substrate 221: ^{1}H NMR (600 MHz, C_6D_6) δ 4.62 (q, *J* = 1.9 Hz, 1H), 4.45 (q, *J* = 2.0 Hz, 1H), 3.66 (t, *J* = 9.0 Hz, 1H), 3.21 (s, 3H), 3.13 – 3.07 (m, 1H), 2.67 (d, *J* = 2.4 Hz, 1H), 2.54 (ddt, *J* = 15.7, 8.6, 2.4 Hz, 1H), 2.17 (ddt, *J* = 16.4, 9.8, 1.6 Hz, 1H), 1.72 (dt, *J* = 14.9, 3.3 Hz, 1H), 1.35 – 1.26 (m, 1H), 1.24 (s, 3H), 0.93 (s, 3H).^{13}C NMR (151 MHz, C_6D_6) δ 204.22, 199.93, 140.55, 110.94, 81.25, 59.16, 58.61, 58.14, 57.33, 36.83, 36.14, 23.14, 16.57, 13.83. $C_{14}H_{18}O_4Na$ $[M+Na]^+$: 273.1096, found: 273.1097.

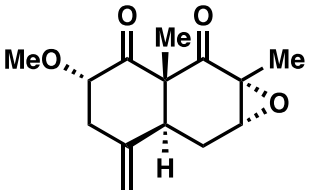

Substrate 222: ^{1}H NMR (600 MHz, $CDCl_3$) δ 5.07 (q, *J* = 1.8 Hz, 1H), 4.92 (q, *J* = 2.0 Hz, 1H), 4.13 (dd, *J* = 9.6, 8.3 Hz, 1H), 3.43 (s, 4H), 3.35 – 3.29 (m, 1H), 3.02 (ddtd, *J* = 16.5, 8.3, 2.5, 1.6 Hz, 1H), 2.46 – 2.29 (m, 2H), 2.07 (ddd, *J* = 15.0, 12.1, 1.3 Hz, 1H), 1.46 (s, 3H), 1.19 (s, 3H). ^{13}C NMR (126 MHz, $CDCl_3$) δ 205.19, 200.03, 139.62, 112.07, 81.44, 59.52, 58.54, 58.45, 57.55, 36.41, 35.95, 23.22, 16.60, 14.85. $C_{14}H_{18}O_4Na$ $[M+Na]^+$: 273.1096, found: 273.1097.

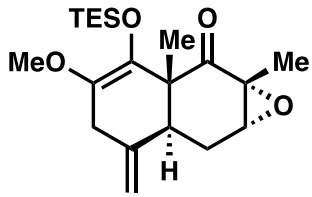

Substrate 223: A mixture of **221** and **222** (1.0 g, 4.0 mmol, 1 equiv) was dissolved in 8.0 mL THF and cooled to –78 ºC. LHMDS (1M in THF, 4.2 mL, 4.2 mmol, 1.05 equiv) was added dropwise and the reaction mixture stirred 30 min. TESOTf (1.0 mL, 4.4 mmol,1.1 equiv) was then added and stirred an additional hour at –78 ºC. The reaction was quenched with $NaHCO_3$, warmed to room temperature, diluted with Et_2O, and washed with cold water. The organic layer was then collected, dried over Na_2SO_4, filtered, and concentrated. The crude residue was purified by silica gel chromatography, and due to the instability of the product to acid, chromatographic eluents were buffered with triethylamine

(typically 5→30% Et_2O in hexanes + 3% Et_3N). Residence time of the compounds on the column was likewise minimized. The product **223** was isolated as a clear oil (1.3 g, 3.7 mmol, 92%). ^{1}H NMR (600 MHz, $CDCl_3$) δ 4.81 – 4.77 (m, 1H), 4.55 (d, *J* = 2.1 Hz, 1H), 3.26 (d, *J* = 0.5 Hz, 3H), 3.16 (d, *J* = 2.0 Hz, 1H), 2.84 (dq, *J* = 16.9, 2.0 Hz, 1H), 2.54 (d, *J* = 16.9 Hz, 1H), 2.38 (ddd, *J* = 12.5, 4.2, 1.7 Hz, 1H), 1.99 (ddd, *J* = 15.0, 4.2, 2.0 Hz, 1H), 1.92 (ddd, *J* = 14.8, 12.4, 1.9 Hz, 1H), 1.24 (s, 3H), 0.92 (s, 3H), 0.81 – 0.69 (m, 9H), 0.61 – 0.44 (m, 6H). ^{13}C NMR (126 MHz, $CDCl_3$) δ 203.20, 140.69, 134.54, 134.37, 109.09, 77.28, 77.02, 76.77, 59.54, 57.18, 55.21, 51.33, 36.59, 33.86, 23.69, 16.68, 14.44, 7.13, 5.67.

Epoxide opening: Cp_2TiCl_2 (62 mg, 0.25 mmol, 2.5 equiv) and Zn (33 mg, 0.50 mmol, 5 equiv) were suspended in THF (0.76 mL) and stirred until the color changed to green (approximately 30 min). A mixture of **223** (36 mg, 0.10 mmol, 1 equiv) in THF (0.2 mL) and MeOH (0.1 mL) was then added and the reaction stirred 15 min at 25 ºC. The reaction mixture quenched with a solution of 10% K_2CO_3 in water and filtered. The aqueous layer was extracted with Et_2O (x2) and DCM. The combined organic layers were dried over Na_2SO_4, filtered, and concentrated. The crude residue was purified by silica gel column chromatography to afford **225** (25 mg, 0.7 mmol, 71%) and **SI3-1** (2 mg, 0.01 mmol, 10%).

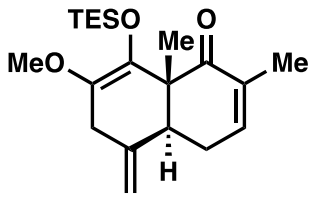

Substrates 225: ^{1}H NMR (600 MHz, C_6D_6) δ 5.88 (dt, *J* = 5.7, 1.9 Hz, 1H), 4.80 (q, *J* = 1.5 Hz, 1H), 4.53 (q, *J* = 1.7 Hz, 1H), 3.17 (s, 3H), 2.80 (dq, *J* = 16.9, 2.0 Hz, 1H), 2.56 (d, *J* = 16.9 Hz, 1H), 2.46 (ddd, *J* = 11.4, 4.0, 1.7 Hz, 1H), 2.01 (ddq, *J* = 16.4, 8.7, 2.5 Hz, 1H), 1.74 (dt, *J* = 2.7, 1.5 Hz, 3H), 1.71 – 1.62 (m, 1H), 1.32 – 1.20 (m, 11H), 1.20 – 1.00 (m, 9H). ^{13}C NMR (126 MHz, C_6D_6) δ 200.06, 142.70, 138.39, 136.76, 133.96, 133.30, 128.23, 127.99, 127.89, 127.79, 127.70, 127.60, 127.50, 108.13, 54.63, 52.95, 49.87, 45.20, 33.45, 25.19, 16.51, 15.36, 7.40, 6.92, 6.13, 5.79.

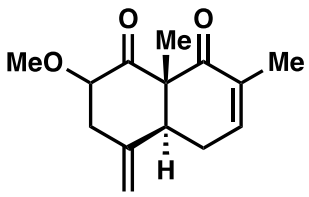

Substrate SI3-1: ^{1}H NMR (600 MHz, C_6D_6) δ 5.89 (dt, *J* = 5.5, 1.8 Hz, 1H), 4.63 (q, *J* = 2.0 Hz, 1H), 4.47 (q, *J* = 2.3 Hz, 1H), 3.80 (dd, *J* = 10.9, 8.7 Hz, 1H), 3.36 (s, 3H), 2.81 – 2.75 (m, 1H), 2.71 (ddq, *J* = 16.8, 8.8, 2.4 Hz, 1H), 2.24 (ddq, *J* = 16.8, 10.8, 1.6 Hz, 1H), 1.79 – 1.73 (m, 0H), 1.71 (h, *J* = 1.8 Hz, 3H), 1.69 – 1.59 (m, 1H), 1.06 (s, 3H). ^{13}C NMR (151 MHz, C_6D_6) δ 204.55, 195.80, 141.28, 140.41, 132.90, 110.25, 80.26, 57.96, 57.80, 43.93, 35.51, 25.08, 16.23, 13.58.

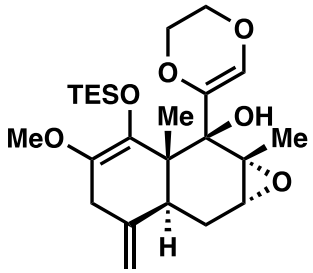

Substrates 226: Dioxene (0.65 M in THF, 14.6 mL, 9.5 mmol, 2.5 equiv) was cooled to 0 ºC then *n*BuLi (2.5 M in hexanes, 3.3 mL, 8.4 mmol, 2.2 equiv) was added and the pale yellow solution was stirred at 0 ºC for 1 h. In a separate flask **223** (1.4 g, 3.8 mmol, 1.0 equiv) was dissolved in 3.0 mL THF and cooled to –78 ºC. The dioxene-lithiate solution was then added dropwise and stirred at –78 ºC for 1h. The reaction was quenched with NH_4Cl and diluted with EtOAc. The layers were separated and the organic layer was further washed with cold water, dried over Na_2SO_4, filtered, and concentrated. The crude residue was purified by silica gel chromatography neutralized with Et_3N (typically 5→40% EtOAc in hexanes) to give **226** (1.2 g, 2.6 mmol, 68%) as a white solid. ^{1}H NMR (600 MHz, $CDCl_3$) δ 6.51 (s, 1H), 4.88 (q, *J* = 1.7 Hz, 1H), 4.64 (q, *J* = 1.8 Hz, 1H), 4.10 – 4.05 (m, 1H), 4.05 – 3.98 (m, 2H), 3.94 (ddd, *J* = 10.8, 6.4, 2.3 Hz, 1H), 3.62 (s, 1H), 3.45 (s, 3H), 3.16 – 3.10 (m, 2H), 3.09 – 3.02 (m, 1H), 2.68 (d, *J* = 16.6 Hz, 1H), 1.99 (ddd, *J* = 14.8, 4.2, 2.0 Hz, 1H), 1.90 (ddd, *J* = 14.6, 12.2, 2.0 Hz, 1H), 1.33 (s, 3H), 0.96 (t, *J* = 8.0 Hz, 9H), 0.88 (s, 3H), 0.75 – 0.61 (m, 6H).^{13}C NMR (151 MHz, $CDCl_3$) δ 143.27, 140.93, 137.51, 131.77, 125.40, 107.69, 77.24, 77.03, 76.81, 75.36, 64.02, 63.75, 61.81, 60.47, 55.10, 44.70, 35.19, 33.79, 24.19, 18.74, 15.76, 6.91, 5.71. $C_{24}H_{38}O_6NaSi$ $[M+Na]^+$: 473.2330, found: 473.2330.

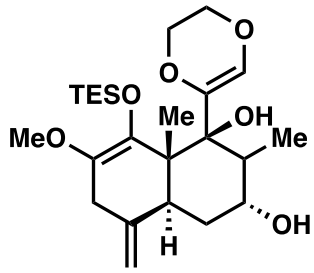

Substrate 227: Cp*$TiCl_3$ (73 g, 0.33 mmol, 3.0 equiv) and Zn (47.9 mg, 0.73 mmol, 6.6 equiv) were dissolved in 1.5 mL THF and stirred at 25 ºC until the mixture was a dark green (approximately 20-30 min). In a separate flask **226** (50 mg, 0.11 mmol, 1 equiv) was dissolved in 22 mL THF to which the Ti(III) solution was added. The mixture was heated to 60 ºC and stirred for 1h before cooling to 25 ºC. The reaction was filtered, and partially concentrated then directly added onto the silica gel column for chromatography. The crude residue was purified by silica gel chromatography neutralized with Et_3N (typically 10→60% EtOAc in hexanes) to give white solid **227** (6.5 mg, 0.015 mmol, 13%) as a single diastereomer.^{1}H NMR (600 MHz, C_6D_6) δ 6.63 (s, 1H), 4.83 (q, *J* = 1.6 Hz, 1H), 4.67 (q, *J* = 1.9 Hz, 1H), 3.88 (dq, *J* = 11.0, 3.5 Hz, 1H), 3.50 – 3.42 (m, 3H), 3.34 (ddd, *J* = 10.3, 7.9, 3.7 Hz, 1H), 3.31 – 3.26 (m, 1H), 3.00 – 2.93 (m, 1H), 2.52 (d, *J* = 17.0 Hz, 1H), 2.15 (qd, *J* = 7.0, 4.2 Hz, 1H), 1.92 (dt, *J* = 13.7, 2.6 Hz, 1H), 1.74 – 1.66 (m, 1H), 1.39 (d, *J* = 7.0 Hz, 3H), 1.20 (s, 3H), 1.00 (t, *J* = 8.0 Hz, 9H), 0.79 – 0.63 (m, 6H).^{13}C NMR (151 MHz, C_6D_6) δ 144.92, 140.51, 138.20, 132.22, 128.59, 128.43, 108.10, 79.09, 70.11, 64.24, 63.36, 55.32, 47.19, 40.98, 38.40, 34.34, 32.18, 15.76, 12.67, 7.21, 6.19.

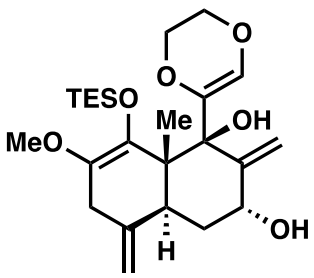

Substrate 228: Cp_2TiCl_2 (1.2 g, 4.8 mmol, 2.2 equiv) and Zn (949 mg, 14.5 mmol, 6.6 equiv) were dissolved in 22 mL THF and stirred at 25 ºC until the mixture was a dark green (approximately 20-30 min). In a separate flask **226** (1.0 g, 2.2 mmol, 1 equiv) was dissolved in 22 mL THF to which the Ti(III) solution was added. The mixture was heated to 60 ºC and stirred for 1h before cooling to 25 ºC and quenching with a saturated solution of NaH_2PO_4. The biphasic suspension was stirred vigorously for 30 min then filtered and rinsed with EtOAc. The layers were separated and the organic layer was further washed with $NaHCO_3$ and brine, dried over Na_2SO_4, filtered, and concentrated. The crude residue was purified by silica gel chromatography neutralized with Et_3N (typically 10→60% EtOAc in hexanes) to give **228** (811 mg, 1.8 mmol, 80%) as a white solid.^{1}H NMR (700 MHz, C_6D_6) δ 7.00 (s, 1H), 6.02 (d, *J* = 2.5 Hz, 1H), 5.41 (d, *J* = 2.5 Hz, 1H), 4.81 (d, *J* = 2.0 Hz, 1H), 4.63 (t, *J* = 2.0 Hz, 1H), 4.58 (d, *J* = 10.7 Hz, 2H), 3.54 – 3.48 (m, 4H), 3.44 – 3.41 (m, 2H), 3.04 (t, *J* = 1.1 Hz, 3H), 2.88 – 2.82 (m, 1H), 2.50 (d, *J* = 17.0 Hz, 1H), 1.97 (dt, *J* = 13.7, 2.7 Hz, 1H), 1.75 (td, *J* = 13.4, 3.8 Hz, 1H), 1.16 (s, 3H), 1.02 (t, *J* = 8.0 Hz, 11H), 0.74 (ddt, *J* = 35.1, 15.0, 7.6 Hz, 7H). ^{13}C NMR (176 MHz, C_6D_6) δ 148.48, 144.28, 141.19, 139.36, 132.52, 126.10, 117.69, 108.62, 79.08, 72.87, 64.64, 63.52, 54.73, 46.74, 38.76, 33.89, 32.20, 16.31, 7.22, 6.16. $C_{24}H_{38}O_6NaSi$ $[M+Na]^+$: 473.2330, found: 473.2330.

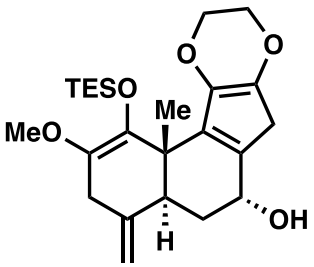

Compound 236: Compound **228** (10 mg, 0.9 mmol, 1 equiv) and Et_3SiH (0.01 mL, 0.9 mmol, 1 equiv) were dissolved in THF and cool to 0 ºC. BF_3OEt_2 (0.01 mL, 0.09 mmol, 1 equiv) was added and the reaction slowly warmed to 25 ºC. The reaction mixture was diluted with Et_2O and quenched the NH_4Cl. The layers were separated and the organic layer washed with brine then dried over Na_2SO_4, filtered, and concentrated. The crude residue was purified by silica gel column chromatography (10%→40% EtOAc in hexanes) to give tentatively compound **236**. Due to the instability of this compound we were unable to obtain a carbon spectra prior to decomposition. ^{1}H NMR (700 MHz, C_6D_6) δ 4.88 – 4.85 (m, 1H), 4.64 (d, *J* = 2.9 Hz, 1H), 3.92 (dd, *J* = 7.5, 4.2 Hz, 1H), 3.77 – 3.68 (m, 4H), 3.51 (s, 1H)*, 3.07 (s, 3H), 2.92 (dq, *J* = 19.0, 2.5 Hz, 1H), 2.81 (dd, *J* = 13.4, 2.5 Hz, 1H), 2.75 (d, *J* = 19.0 Hz, 1H), 2.71 (dd, *J* = 17.1, 7.5 Hz, 1H), 1.97 (dd, *J* = 17.1, 4.2 Hz, 1H), 1.58 (dt, *J* = 14.1, 2.0 Hz, 1H), 1.25 (s, 3H), 1.16 (t, *J* = 8.0 Hz, 9H), 0.94 (q, *J* = 8.0 Hz, 6H).

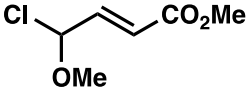

Dienophile 202: (*E*)-4,4-dimethoxybut-2-enoic acid methyl ester (480 mg, 3.0 mmol, 1.0 equiv)[5] and acetyl chloride (430 µL, 6.0 mmol, 2.0 equiv) were combined with a crystal of iodine (8 mg, 0.03 mmol, 0.01 equiv). The mixture was stirred at rt for 6 h. The crude residue was directly concentrated and then azeotroped from benzene (3 x 5 mL). The dienophile was used immediately in the next step without further purification (*ca.* 480 mg, near quantitative mass recovery). This crude product typically contained *ca.* 5% recovered

starting material and *ca*. 5% (2E)-4-oxo-2-butenoic acid, along with some decomposition products; a purity of 80% was conservatively assumed by ^{1}H NMR analysis for the subsequent step. Tabulated ^{1}H and ^{13}C NMR data of this unpurified material were obtained: ^{1}H NMR (600 MHz, C_6D_6) δ 7.00 (dd, *J* = 15.6, 4.7 Hz, 1H), 6.11 (dd, *J* = 15.6, 1.3 Hz, 1H), 5.34 (ddq, *J* = 4.7, 1.3, 1.1 Hz, 1H), 3.30 (s, 3H), 2.97 (d, *J* = 1.1 Hz, 3H); ^{13}C NMR (151 MHz, C_6D_6) δ 165.6, 142.6, 122.4, 95.3, 57.2, 51.4.

Substrate 236: Substrate **228** (320 mg, 1.0 mmol, 1.0 equiv) was dissolved in PhMe (10 mL) and N,N-diisopropylethylamine (0.67 mL, 4.0 mmol, 4.0 equiv) was added at room temperature. Dienophile **202** (crude from previous operation, 328 mg, 2.0 mmol, 2.0 equiv) was dissolved in PhMe (5 mL) and added dropwise to the solution. The reaction mixture was stirred at room temperature for 12 h. The reaction was diluted quenched with NH_4Cl and extracted with EtOAc. The organic layers were combined and the was further washed with brine, dried over Na_2SO_4, filtered, and concentrated. The crude residue was purified by silica gel chromatography neutralized with Et_3N (typically 10→60% EtOAc in hexanes) to give **236** (811 mg, 1.8 mmol, 80%) as a white solid. ^{1}H NMR (700 MHz, C_6D_6) δ 4.88 – 4.85 (m, 1H), 4.64 (d, *J* = 2.9 Hz, 1H), 3.92 (dd, *J* = 7.5, 4.2 Hz, 1H), 3.77 – 3.68 (m, 4H), 3.51 (s, 1H), 3.07 (s, 3H), 2.92 (dq, *J* = 19.0, 2.5 Hz, 1H), 2.81 (dd, *J* = 13.4, 2.6 Hz, 1H), 2.75 (d, *J* = 19.0 Hz, 1H), 2.71 (dd, *J* = 17.1, 7.5 Hz, 1H), 1.97 (dd, *J* = 17.2, 4.2 Hz, 1H), 1.58 (dt, *J* = 14.1, 2.0 Hz, 1H), 1.28 – 1.20 (m, 4H), 1.16 (t, *J* = 8.0 Hz, 9H), 0.94 (q, *J* = 8.0 Hz, 6H), 0.89 (d, *J* = 6.1 Hz, 1H). ^{13}C NMR (176 MHz, C_6D_6) δ 165.9, 164.5, 145.8, 143.2, 145.7, 143.4, 144.3, 144.3, 140.5, 140.3, 139.2, 139.0, 131.2, 130.7, 125.2, 124.6, 125.2, 124.9, 119.9, 117.4, 108.2, 107.8, 98.1, 95.1, 78.6, 78.2, 63.3, 63.4, 54.3, 54.1, 51.1, 51.0, 50.8, 49.7, 45.4, 45.4, 38.8, 38.7, 33.3, 33.4, 29.6, 28.8, 16.4, 6.82, 6.72, 6.1, 5.8.

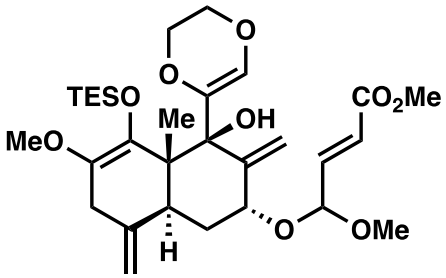

References

1. Prepared using the procedure from: Kravina, A. G., Carreira, E. M. *Angew. Chem. Int. Ed.* **2018**, 57, 13159.
2. Pavlova, A. V.; Il'ina, I. V.; Morozova, E. A.; Korchagina, D. V.; Karpova, E. V.; Volcho, K. P.; Tolstikova, T. G.; Salakhutdinov, N. F. *J. Med. Chem.* **2011**, 54, 3866.

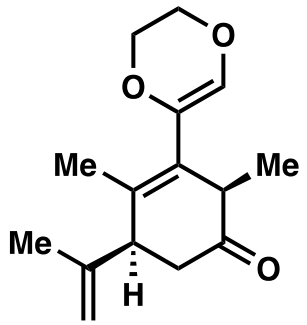
O
O
Me
Me
Me
O
H

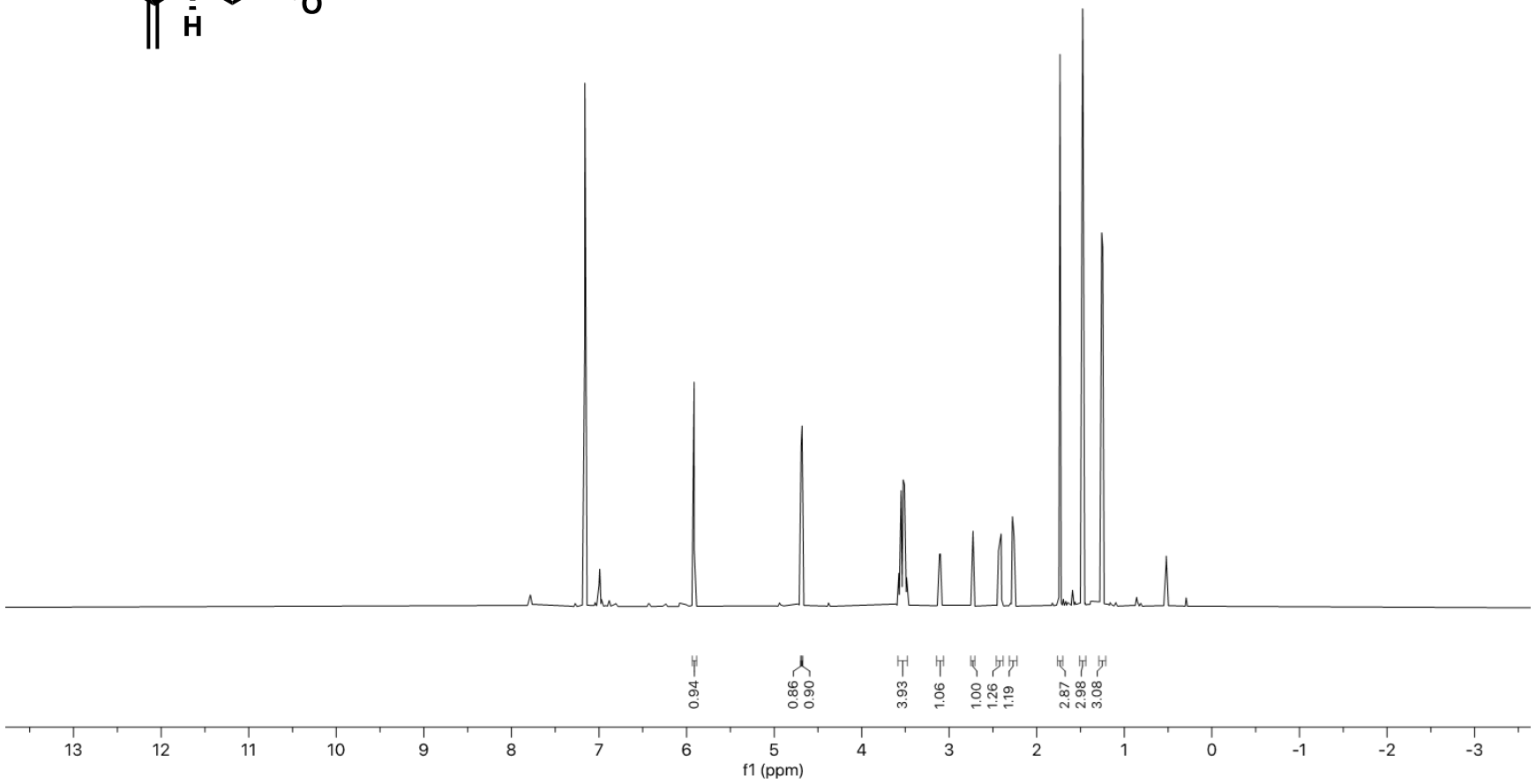
0.94
0.86
0.90
3.93
1.06
1.00
1.26
1.19
2.87
2.98
3.08
13
12
11
10
9
8
7
6
5
4
3
2
1
0
-1
-2
-3
f1 (ppm)

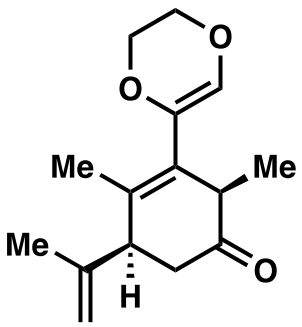
O
O
Me
Me
Me
O
H

212

20
210
200
190
180
170
160
150
140
130
120
110
100
90
80
70
60
50
40
30
20
10
0
-10
f1 (ppm)

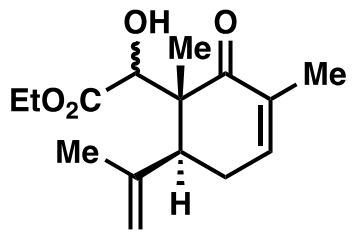
OH
O
Me
Me
EtO2C
Me
H

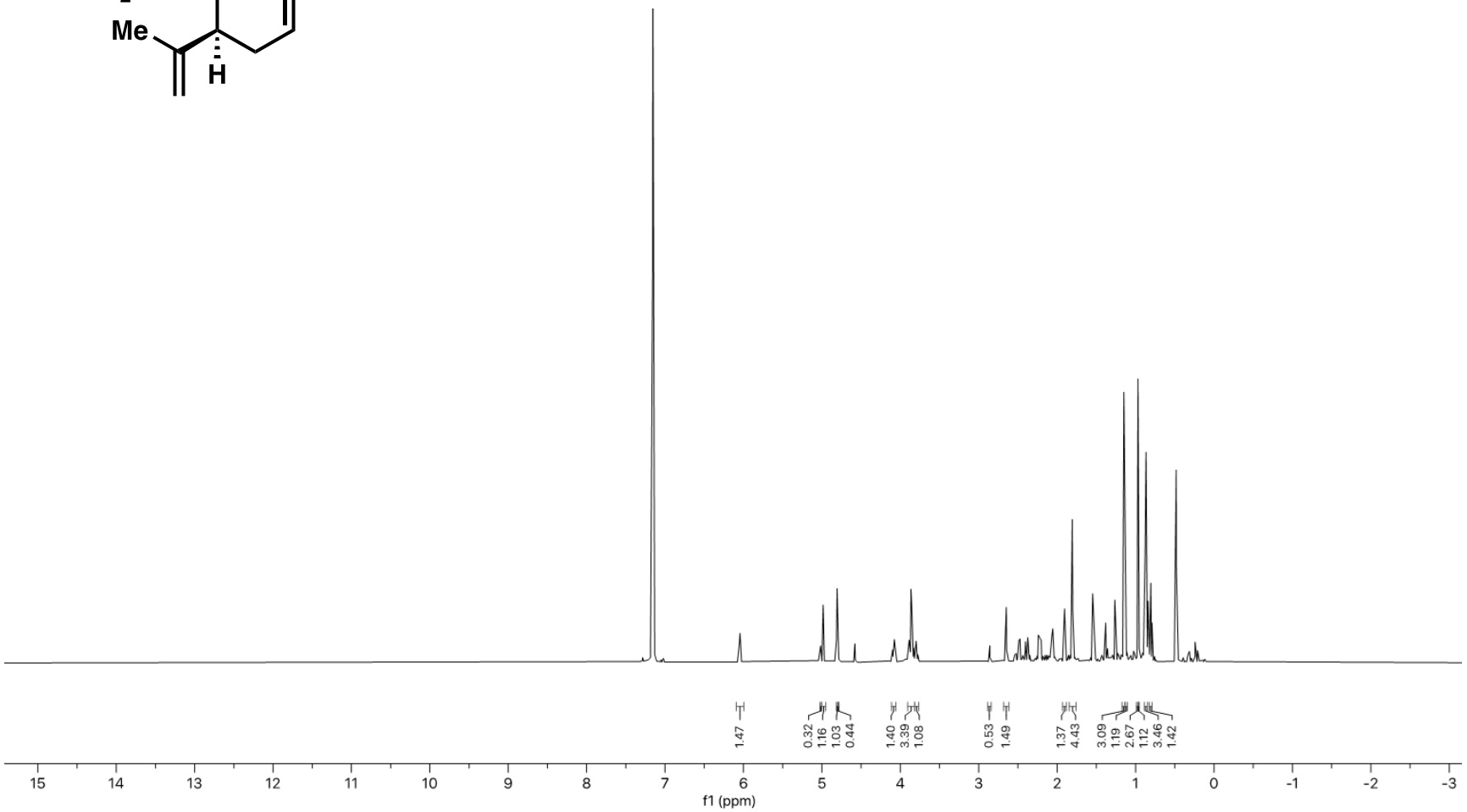
1.47
0.32
1.16
1.03
0.44
1.40
3.39
1.08
0.53
1.49
1.37
4.43
3.09
1.19
2.67
1.12
3.46
1.42
15
14
13
12
11
10
9
8
7
6
5
4
3
2
1
0
-1
-2
-3
f1 (ppm)

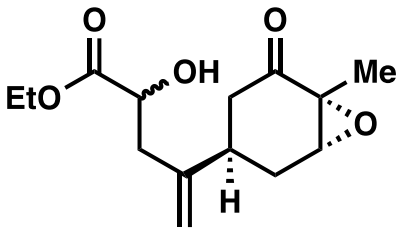
O
O
OH
Me
EtO
O
H

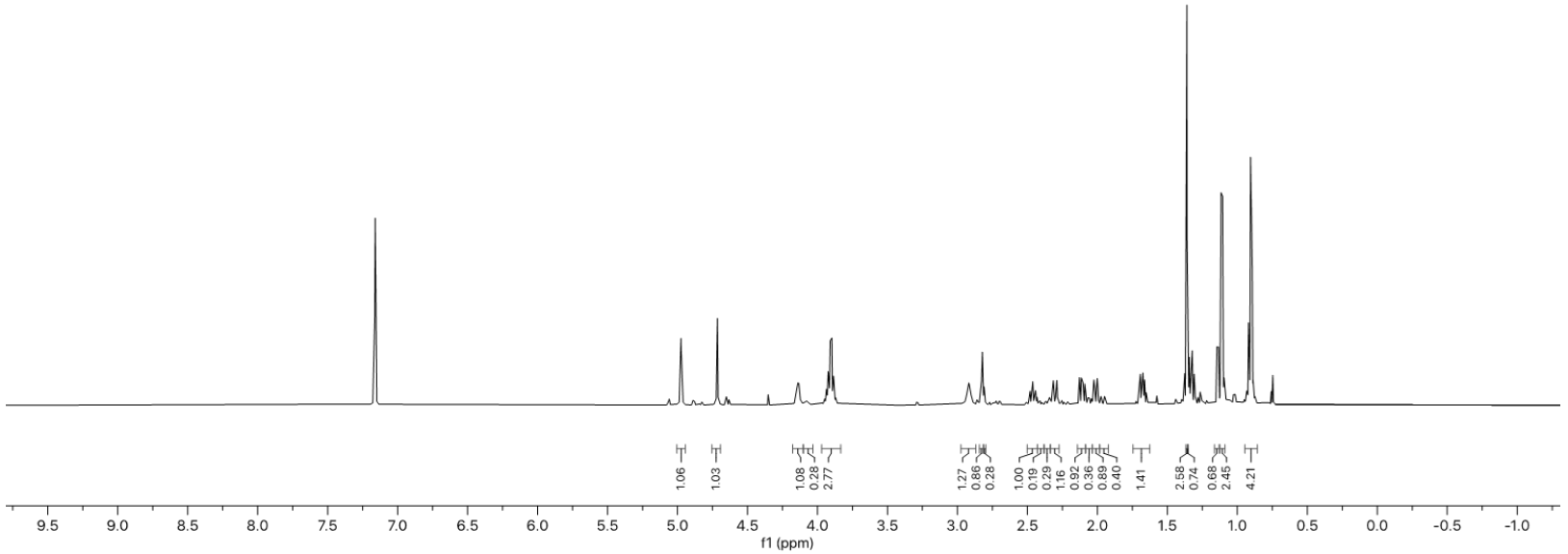
1.06
1.03
1.08
0.28
2.77
1.27
0.86
0.28
1.00
0.19
0.29
1.16
0.92
0.36
0.89
0.40
1.41
2.58
0.74
0.68
2.45
4.21
9.5
9.0
8.5
8.0
7.5
7.0
6.5
6.0
5.5
5.0
4.5
4.0
3.5
3.0
2.5
2.0
1.5
1.0
0.5
0.0
-0.5
-1.0
f1 (ppm)

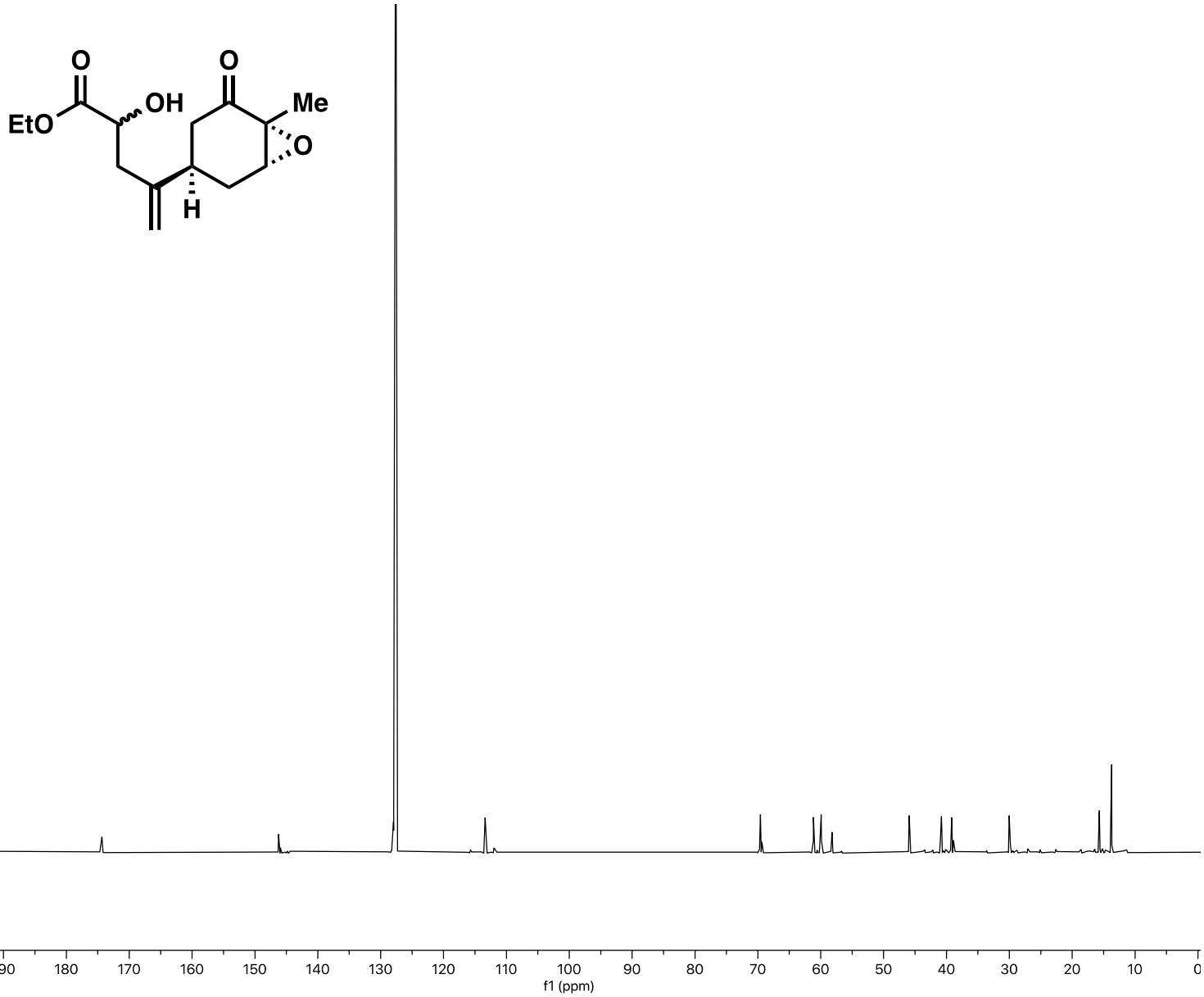
O
O
OH
Me
EtO
O
H
f1 (ppm)

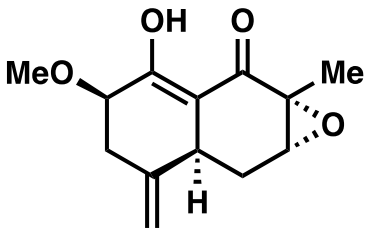
OH
O
MeO
Me
O
H

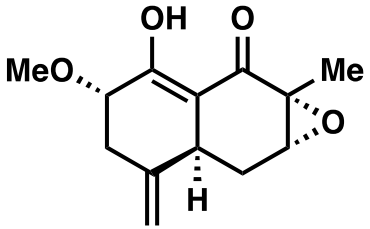
OH
O
MeO
Me
O
H

0.24
1.00
1.04
0.25
1.05
0.26
0.24
1.03
0.73
3.03
0.27
1.03
1.25
1.57
2.10
0.28
0.77
2.99
1.13
0.22
16
15
14
13
12
11
10
9
8
7
6
5
4
3
2
1
0
-1
-2
-3
f1 (ppm)

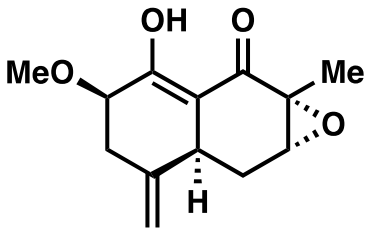
OH
O
MeO
Me
O
H

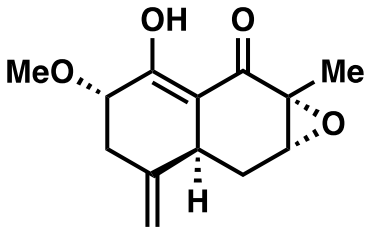
OH
O
MeO
Me
O
H

210
200
190
180
170
160
150
140
130
120
110
100
90
80
70
60
50
40
30
20
10
0
f1 (ppm)

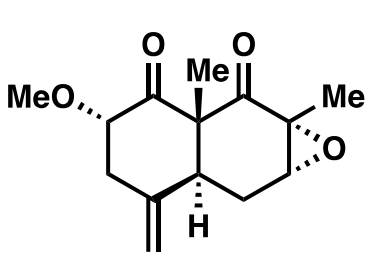
O
Me
O
MeO
Me
O
H

1.00
1.07
1.03
3.76
1.04
1.11
2.11
1.17
2.71
2.67
11
10
9
8
7
6
5
4
3
2
1
0
-1
-2
f1 (ppm)

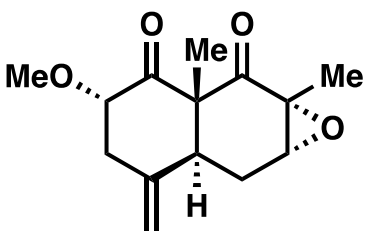
O
O
Me
MeO
Me
O
H

210
200
190
180
170
160
150
140
130
120
110
100
90
80
70
60
50
40
30
20
10
0
-10
f1 (ppm)

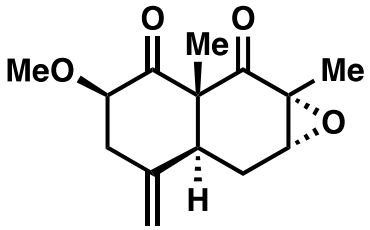
O
O
Me
MeO
Me
O
H

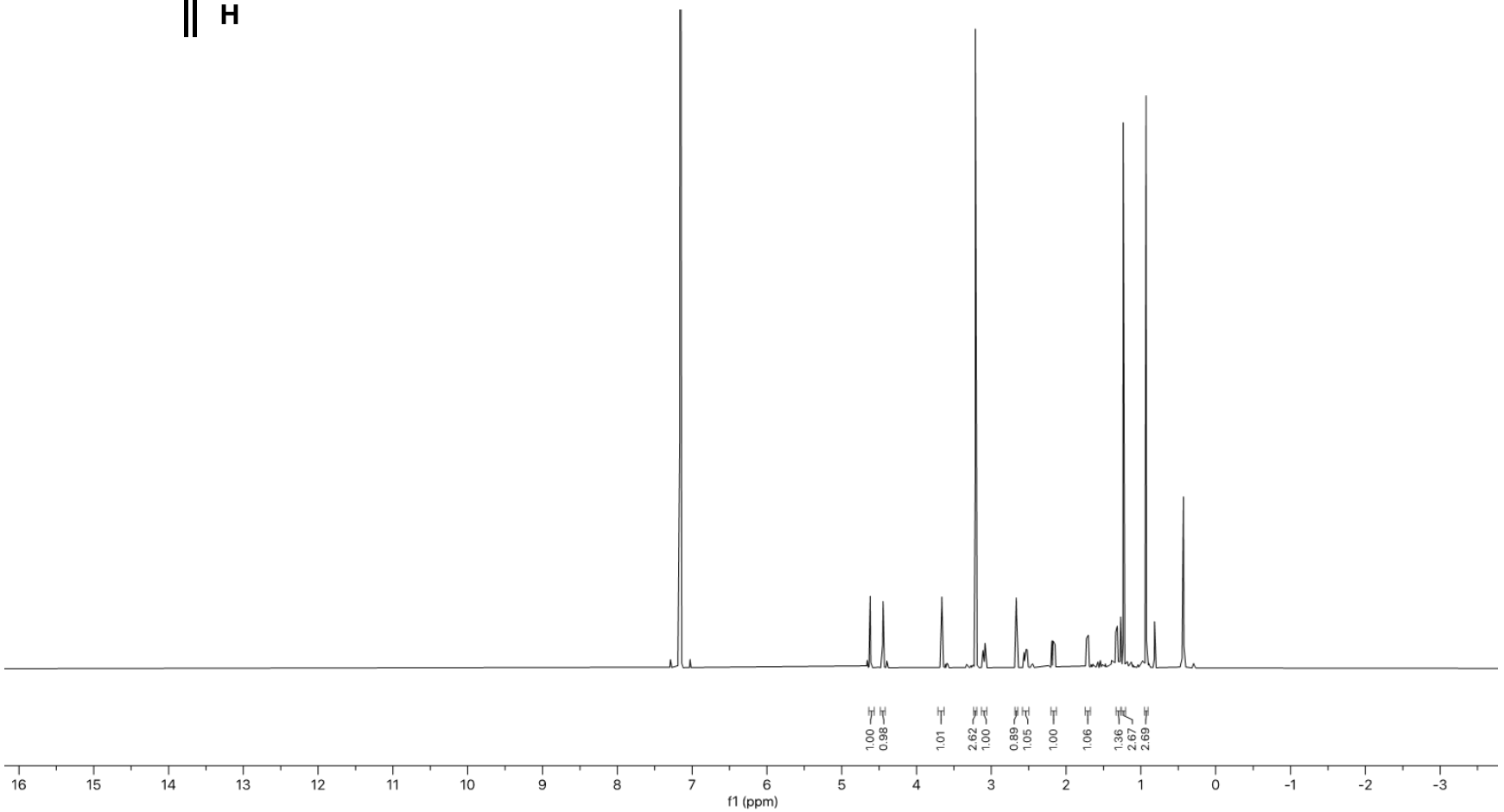
1.00
0.98
1.01
2.62
1.00
0.89
1.05
1.00
1.06
1.36
2.67
2.69
16
15
14
13
12
11
10
9
8
7
6
5
4
3
2
1
0
-1
-2
-3
f1 (ppm)

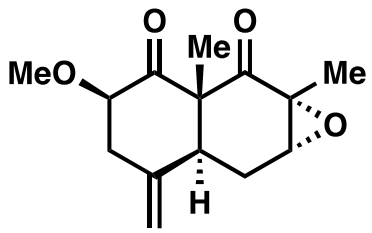
O
O
Me
MeO
Me
O
H

220
210
200
190
180
170
160
150
140
130
120
110
100
90
80
70
60
50
40
30
20
10
0
-10
f1 (ppm)

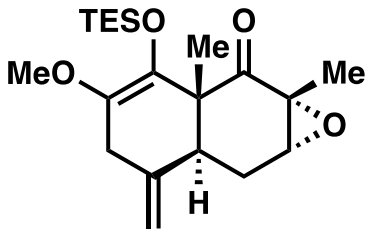
TESO
O
Me
MeO
Me
O
H

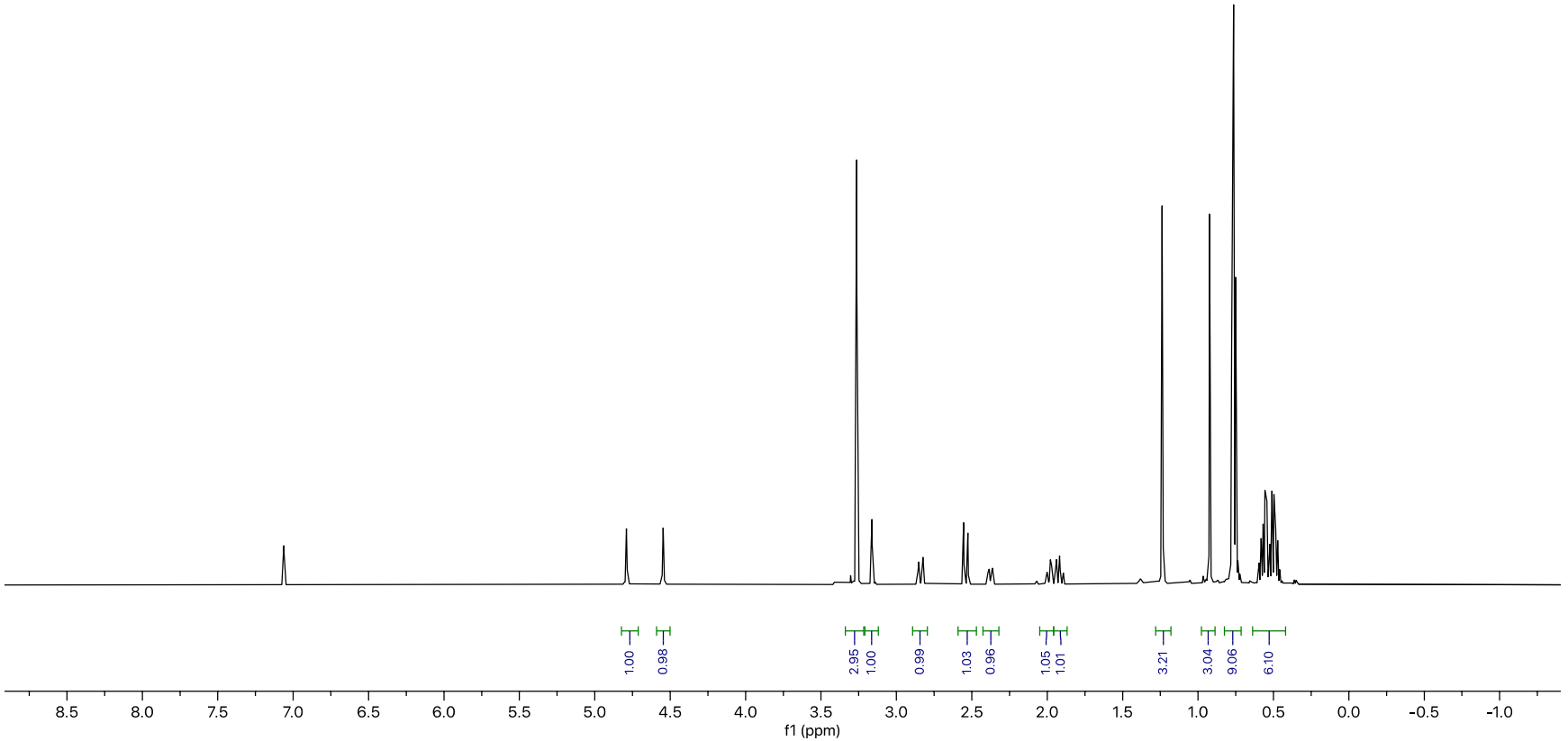
1.00
0.98
2.95
1.00
0.99
1.03
0.96
1.05
1.01
3.21
3.04
9.06
6.10
8.5
8.0
7.5
7.0
6.5
6.0
5.5
5.0
4.5
4.0
3.5
3.0
2.5
2.0
1.5
1.0
0.5
0.0
-0.5
-1.0
f1 (ppm)

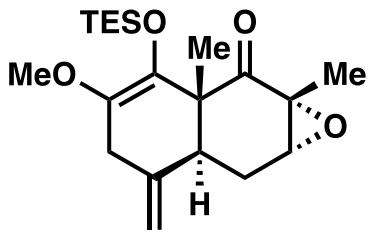
TESO
O
Me
MeO
Me
O
H

223

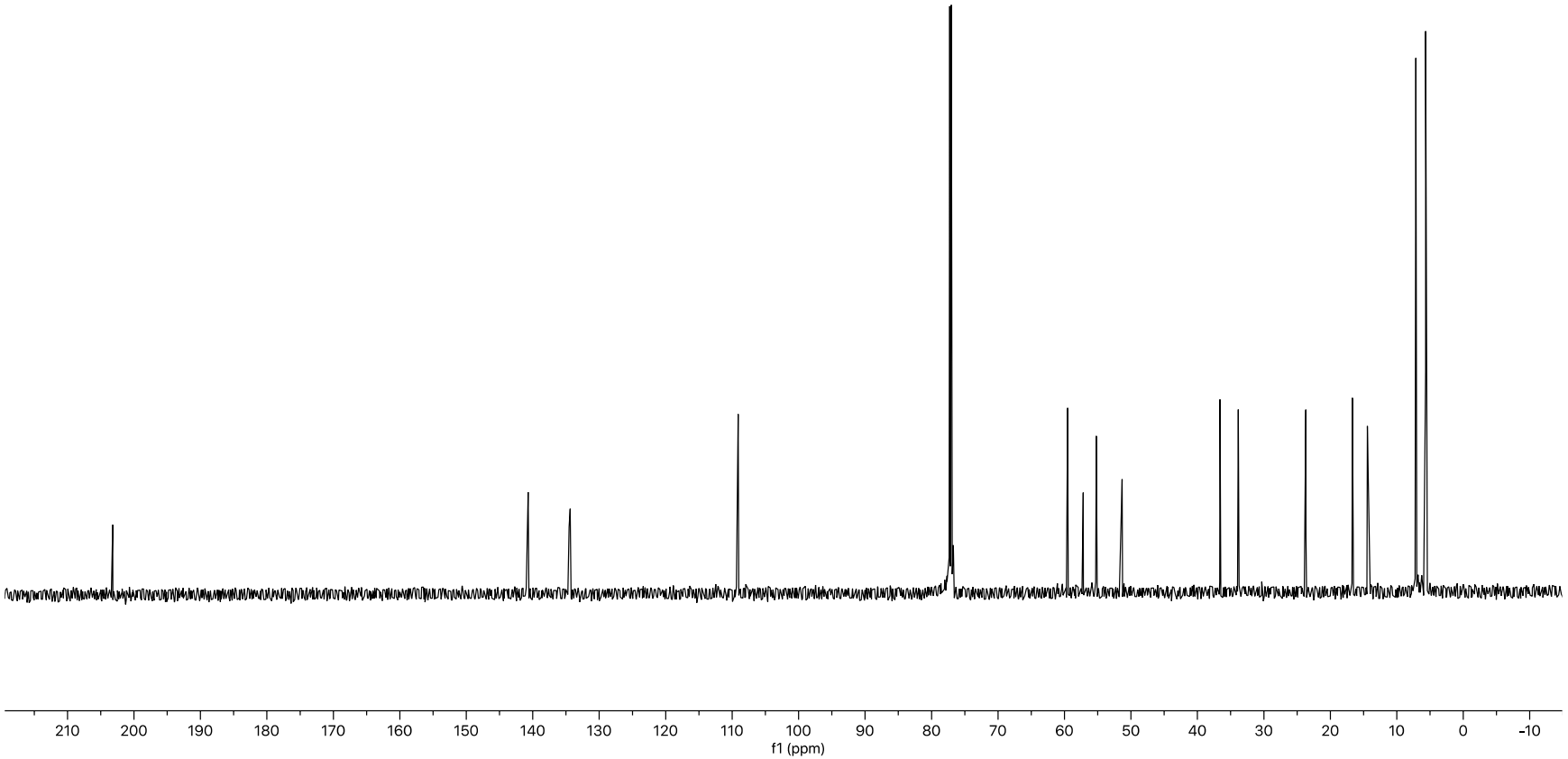
210
200
190
180
170
160
150
140
130
120
110
100
90
80
70
60
50
40
30
20
10
0
-10
f1 (ppm)

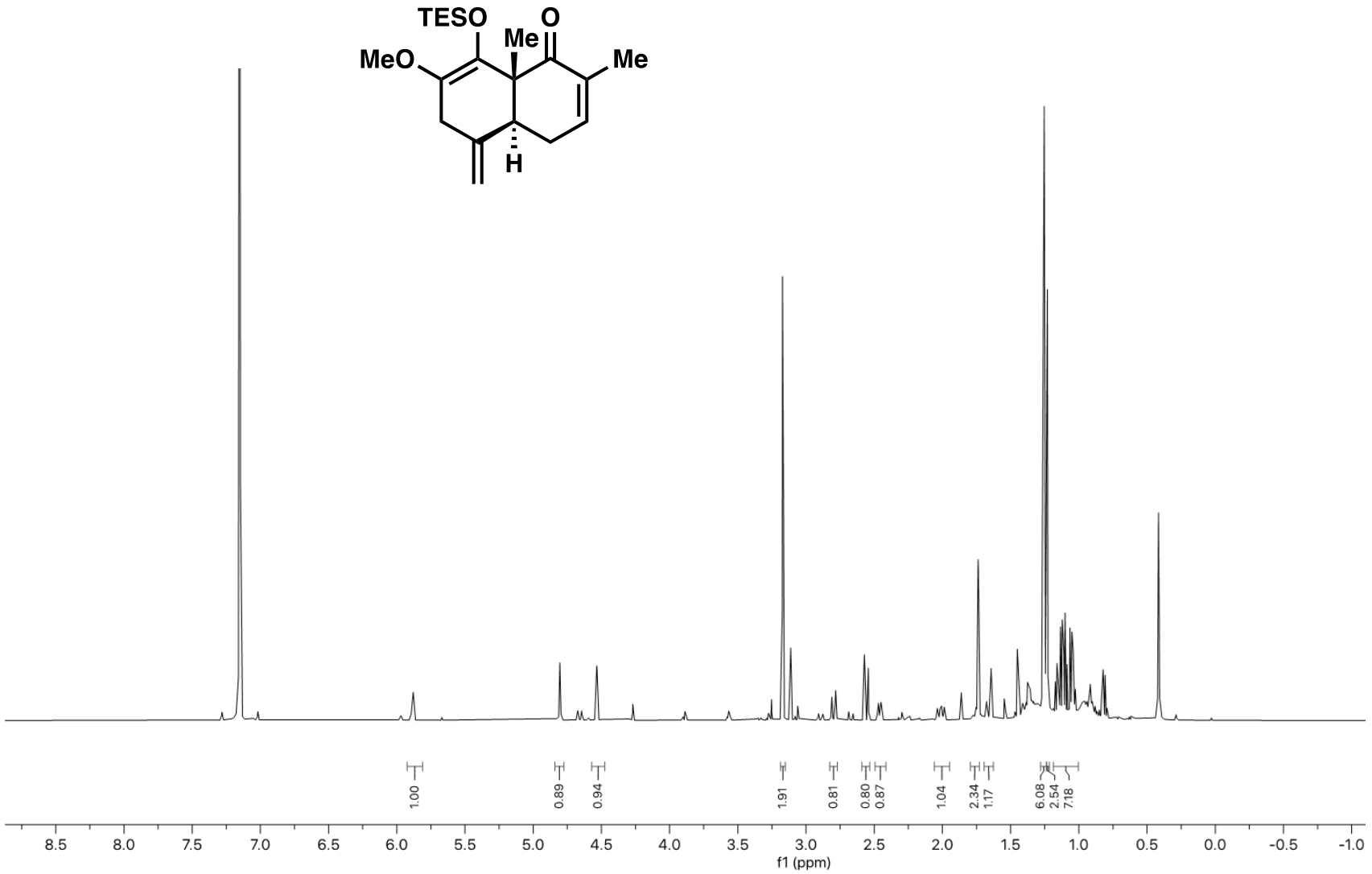
TESO
O
Me
MeO
Me
H
1.00
0.89
0.94
1.91
0.81
0.80
0.87
1.04
2.34
1.17
6.08
2.54
7.18
8.5
8.0
7.5
7.0
6.5
6.0
5.5
5.0
4.5
4.0
3.5
3.0
2.5
2.0
1.5
1.0
0.5
0.0
-0.5
-1.0
f1 (ppm)

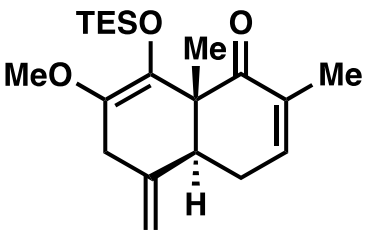
TESO
O
Me
MeO
Me
H

225

210
200
190
180
170
160
150
140
130
120
110
100
90
80
70
60
50
40
30
20
10
0
-10
f1 (ppm)

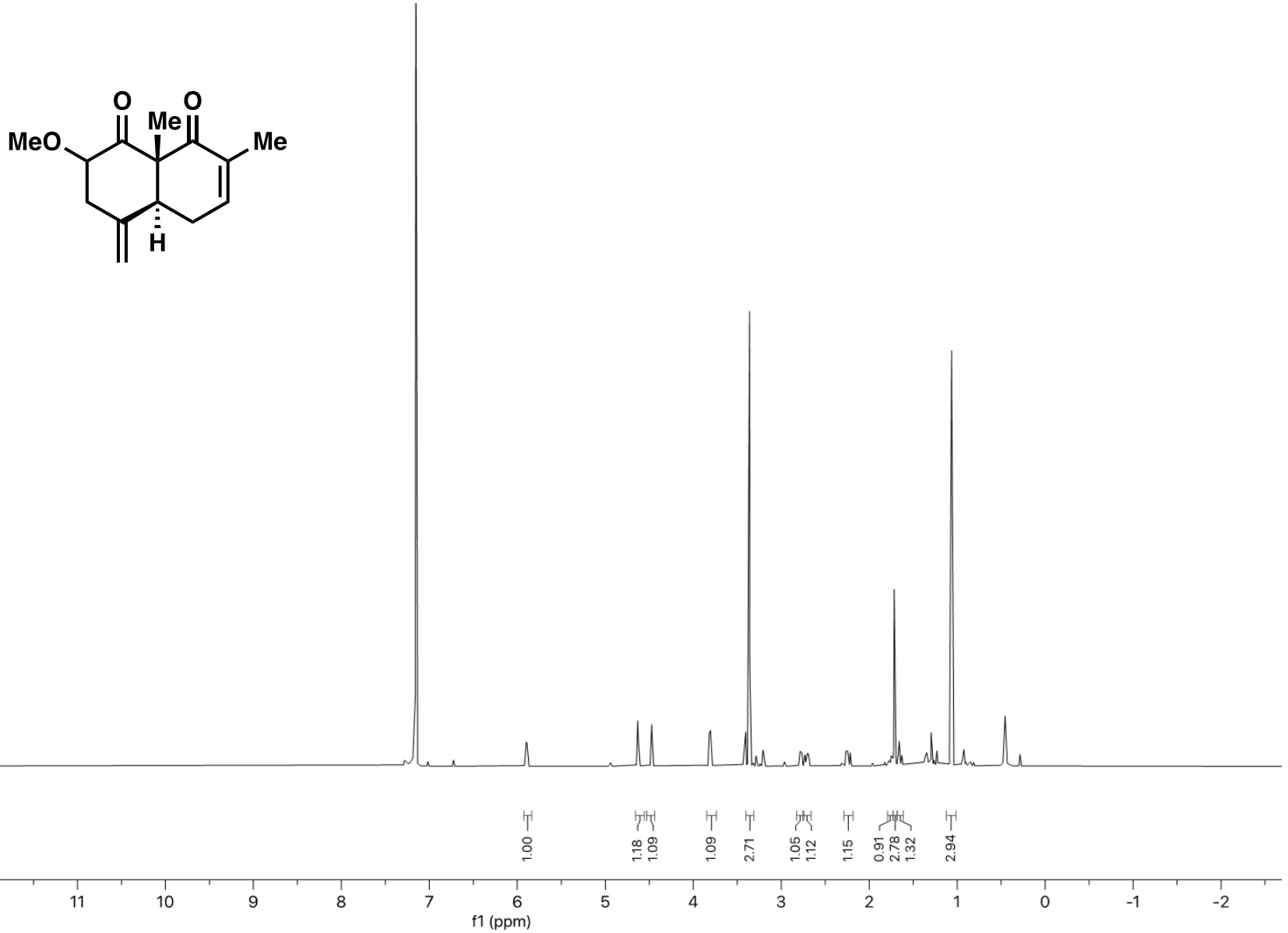
O
Me
O
MeO
Me
H
1.00
1.18
1.09
1.09
2.71
1.05
1.12
1.15
0.91
2.78
1.32
2.94
12
11
10
9
8
7
6
5
4
3
2
1
0
-1
-2
f1 (ppm)

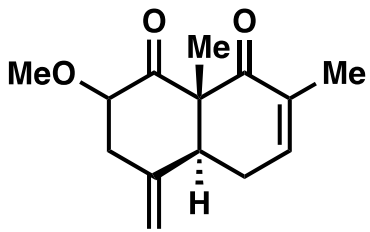
O
O
Me
MeO
Me
H

227

210
200
190
180
170
160
150
140
130
120
110
100
90
80
70
60
50
40
30
20
10
0
-10
f1 (ppm)

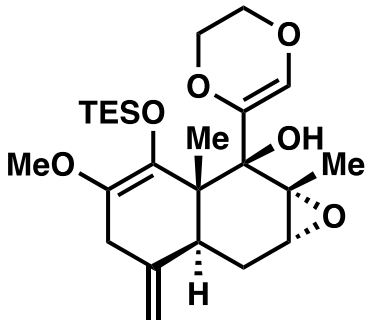
O
O
TESO
Me
OH
MeO
Me
O
H

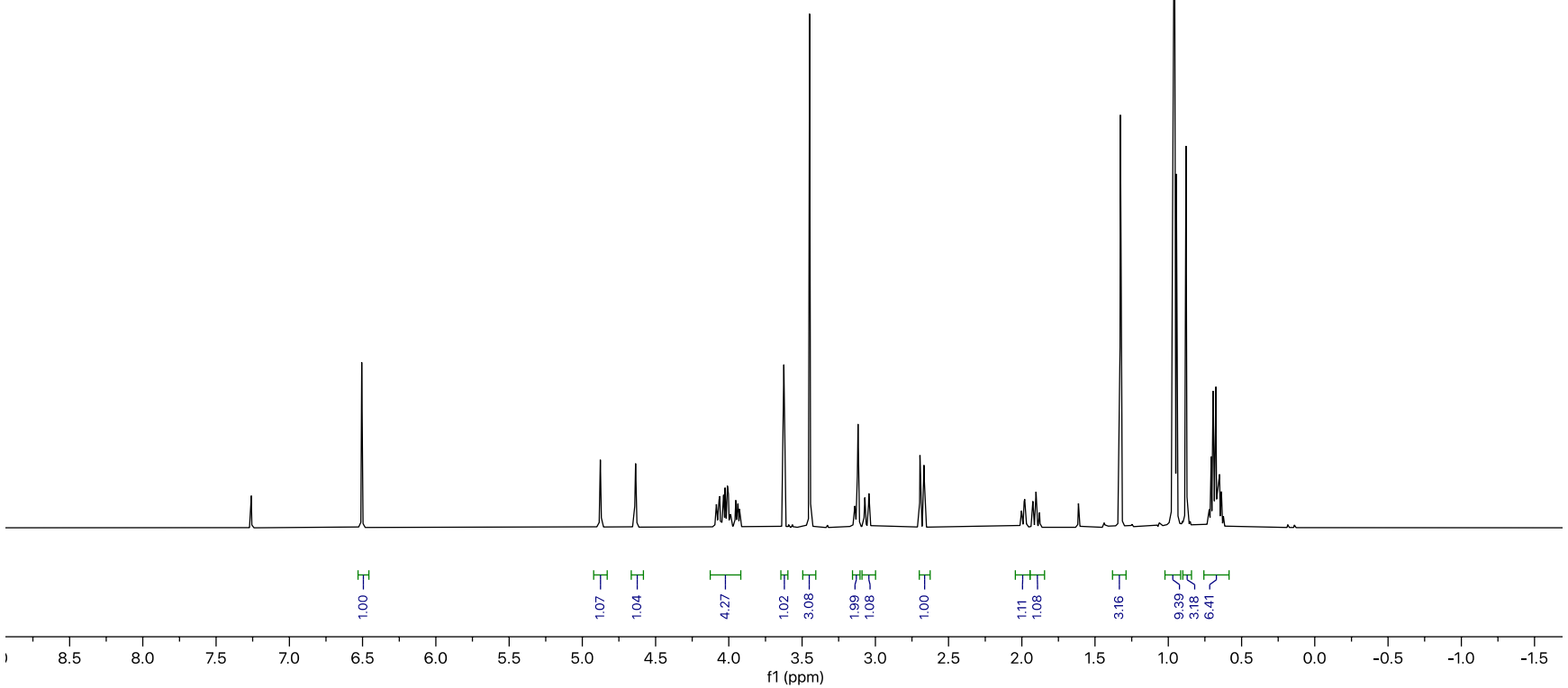
1.00
1.07
1.04
4.27
1.02
3.08
1.99
1.08
1.00
1.11
1.08
3.16
9.39
3.18
6.41
8.5
8.0
7.5
7.0
6.5
6.0
5.5
5.0
4.5
4.0
3.5
3.0
2.5
2.0
1.5
1.0
0.5
0.0
-0.5
-1.0
-1.5
f1 (ppm)

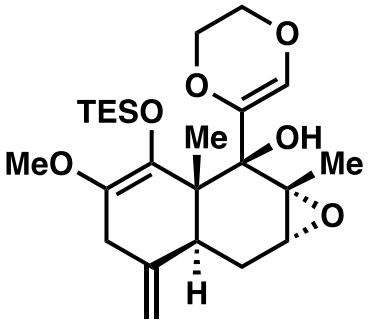
O
O
TESO
Me
OH
MeO
Me
O
H

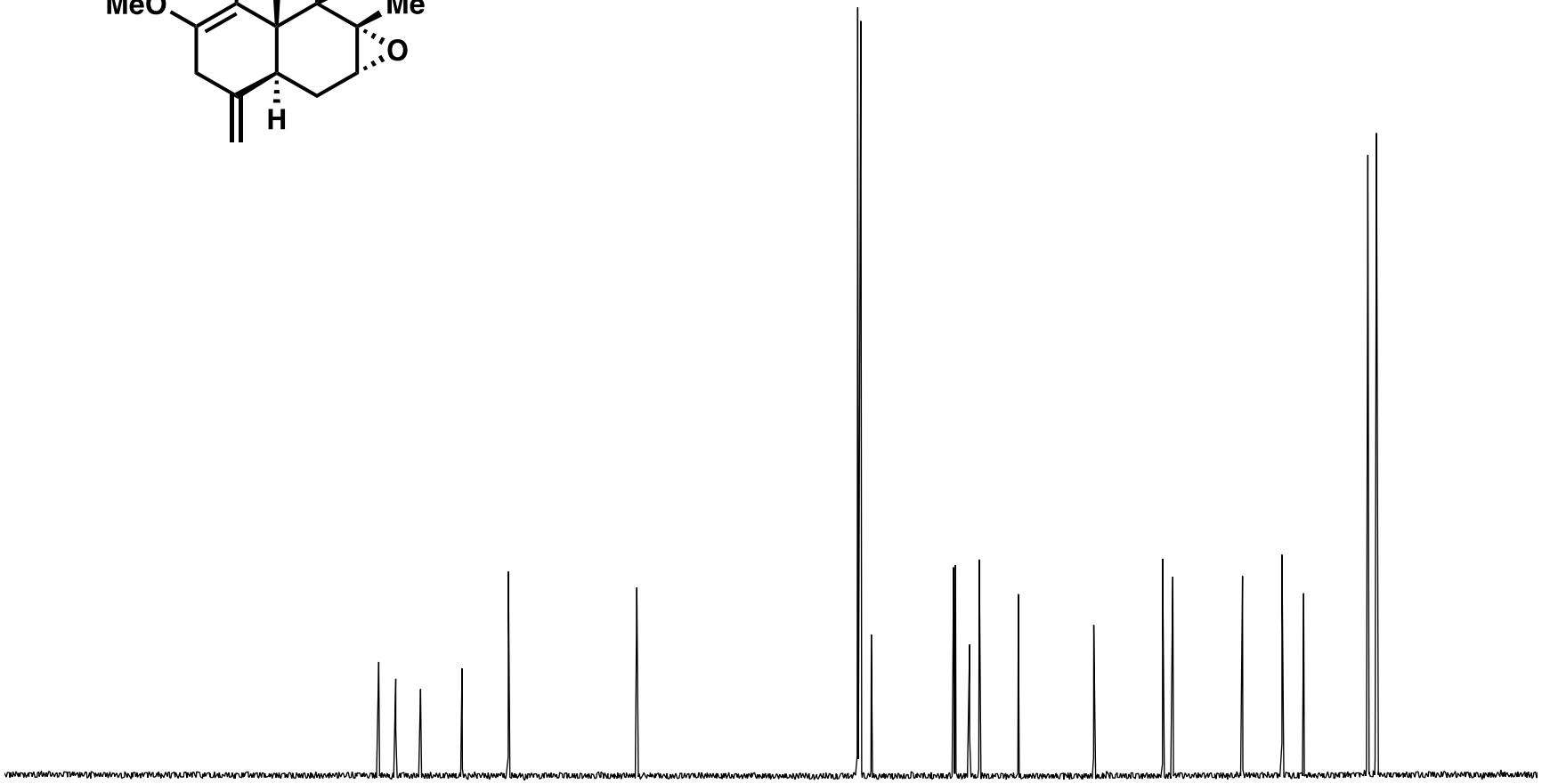

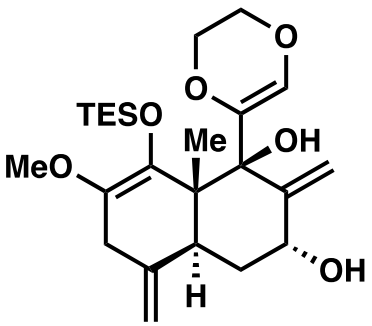
O
O
TESO
Me
OH
MeO
OH
H

1.26
1.07
1.05
1.22
0.93
1.83
5.19
3.04
1.01
0.99
1.00
0.99
3.17
8.40
6.32
13
12
11
10
9
8
7
6
5
4
3
2
1
0
-1
-2
-3
-4
-5
f1 (ppm)

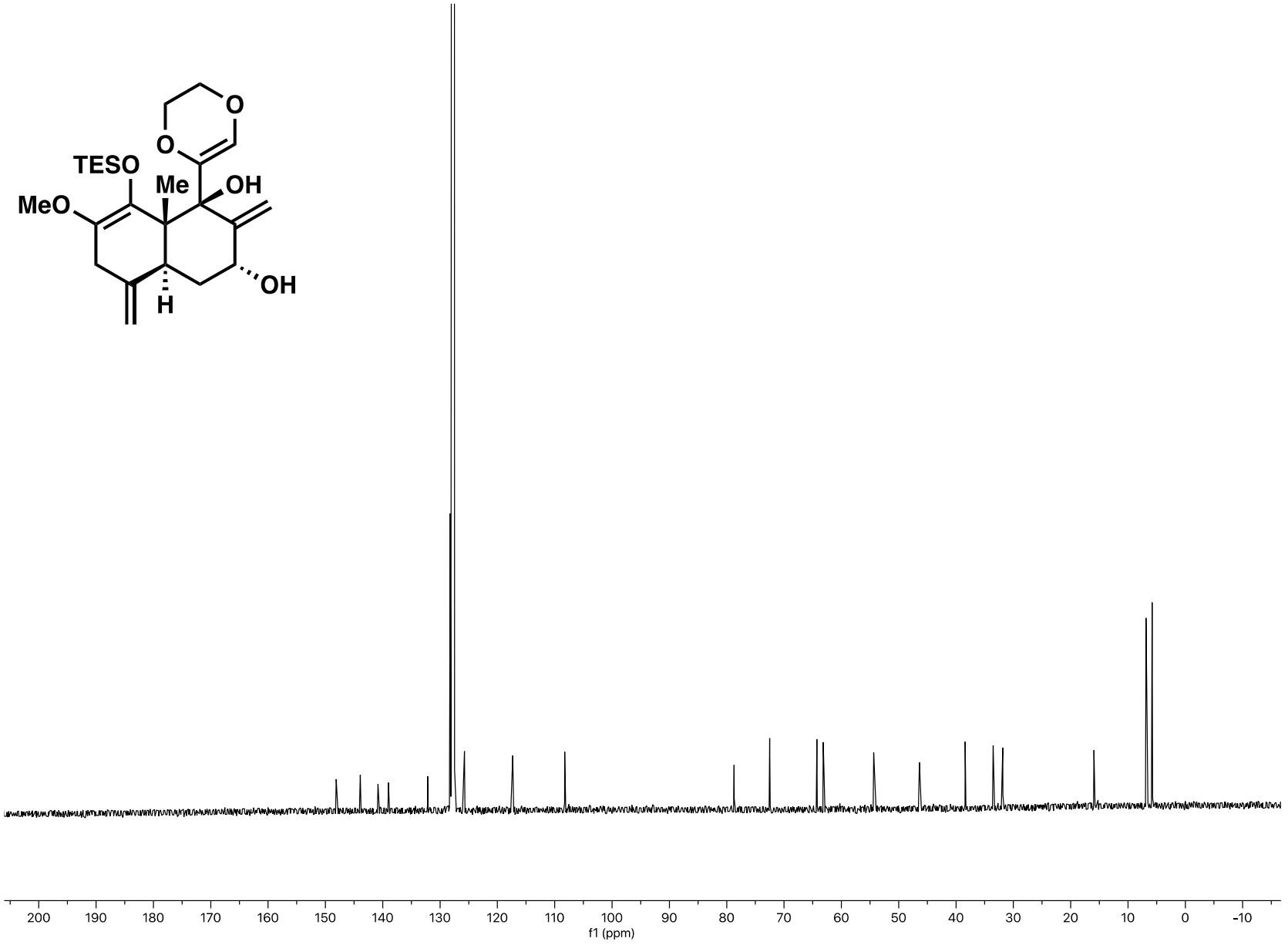
O
O
TESO
Me
OH
MeO
OH
H
200
190
180
170
160
150
140
130
120
110
100
90
80
70
60
50
40
30
20
10
0
-10
f1 (ppm)

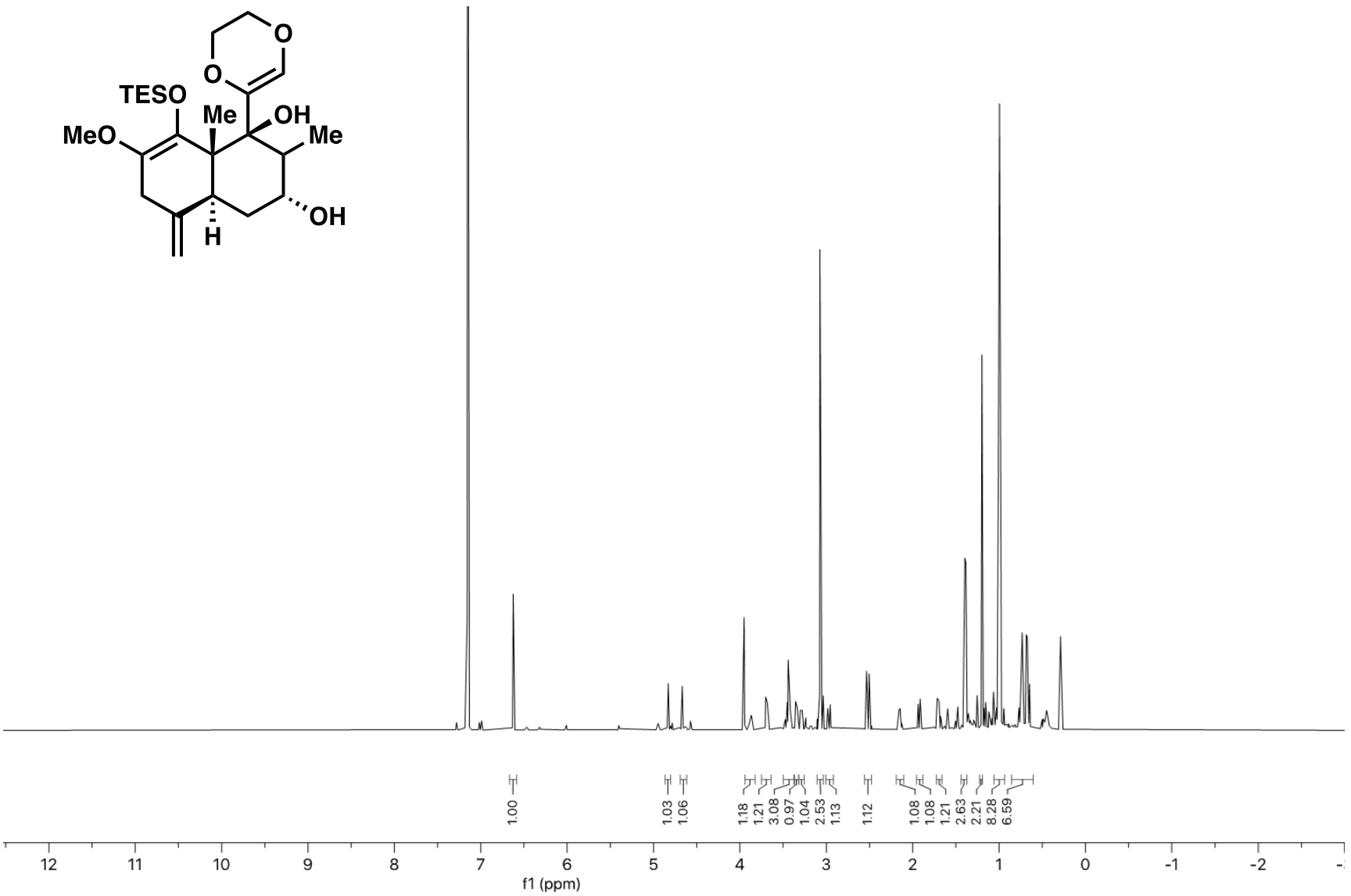
TESO
MeO
Me
OH
Me
O
O
OH
H
1.00
1.03
1.06
1.18
1.21
3.08
0.97
1.04
2.53
1.13
1.12
1.08
1.08
1.21
2.63
2.21
8.28
6.59
12
11
10
9
8
7
6
5
4
3
2
1
0
-1
-2
f1 (ppm)

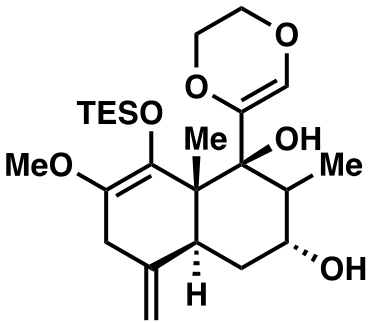
O
O
TESO
Me
OH
MeO
Me
OH
H

200
190
180
170
160
150
140
130
120
110
100
90
80
70
60
50
40
30
20
10
0
-10
f1 (ppm)

234

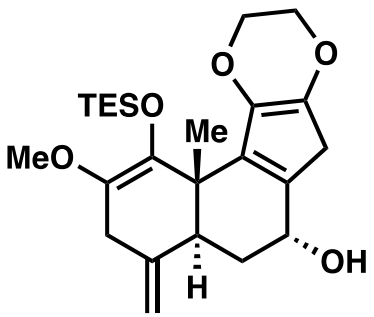
TESO
Me
MeO
O
O
OH
H

1.00
1.01
0.93
3.72
1.15
2.96
0.99
0.98
1.05
1.01
0.93
1.04
4.53
1.34
10.06
8.48
12
11
10
9
8
7
6
5
4
3
2
1
0
-1
-2
-3
-4
f1 (ppm)

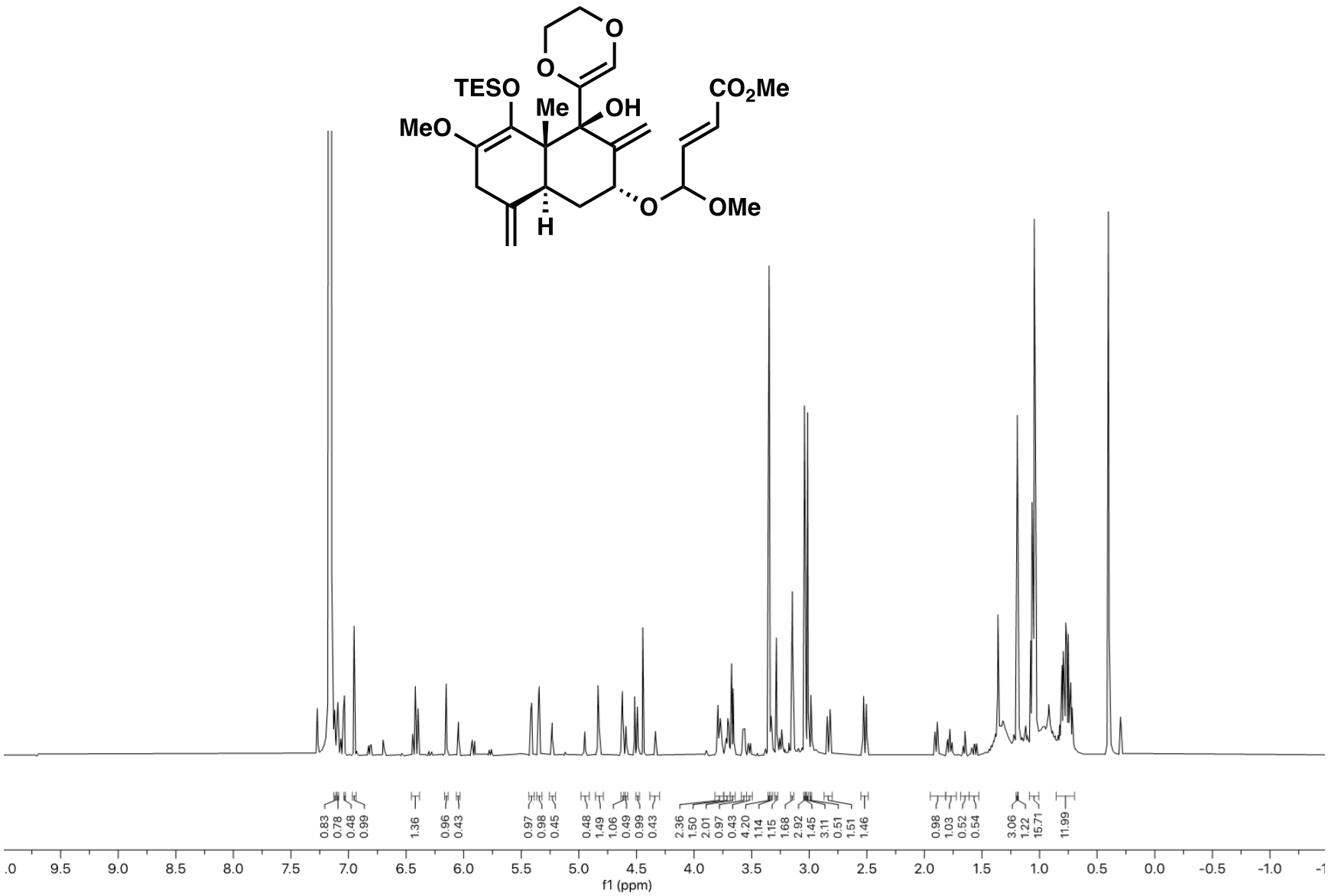
TESO
MeO
Me
OH
CO2Me
O
O
O
O
OMe
H
0.83
0.78
0.48
0.99
1.36
0.96
0.43
0.97
0.98
0.45
0.48
1.49
1.06
0.49
0.99
0.43
2.36
1.50
2.01
0.97
0.43
4.20
1.14
1.15
1.68
2.92
1.45
3.11
0.51
1.51
1.46
0.98
1.03
0.52
0.54
3.06
1.22
15.71
11.99
f1 (ppm)